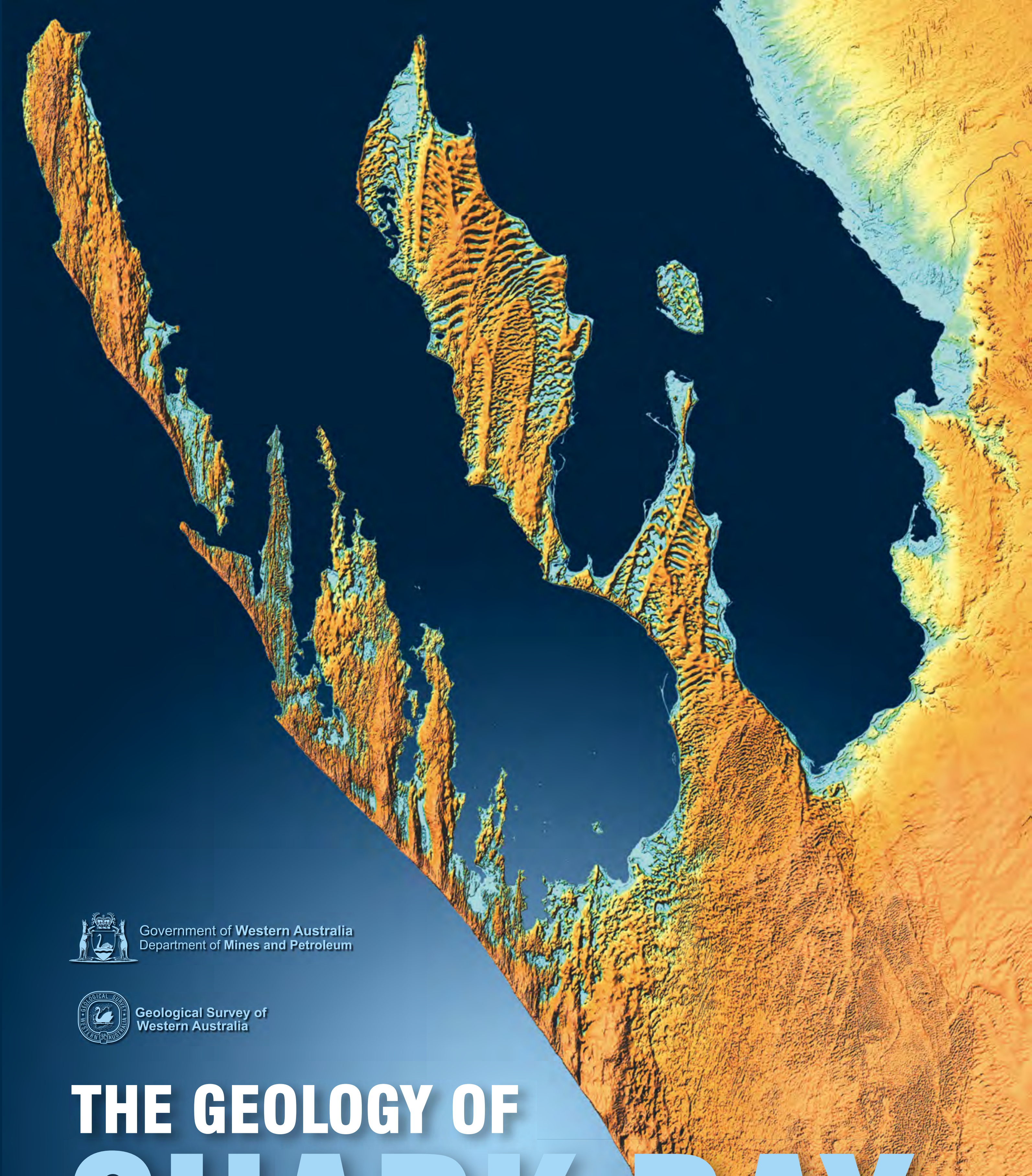

Government of Western Australia
Department of Mines and Petroleum

Geological Survey of Western Australia

THE GEOLOGY OF SHARK BAY

Geological Survey of Western Australia: Bulletin 146

Phillip E Playford, Anthony E Cockbain, Patrick F Berry, Anthony P Roberts, Peter W Haines, and Brendan P Brooke

THE GEOLOGY OF SHARK BAY

Phillip E Playford, Anthony E Cockbain, Patrick F Berry,
Anthony P Roberts, Peter W Haines, and Brendan P Brooke

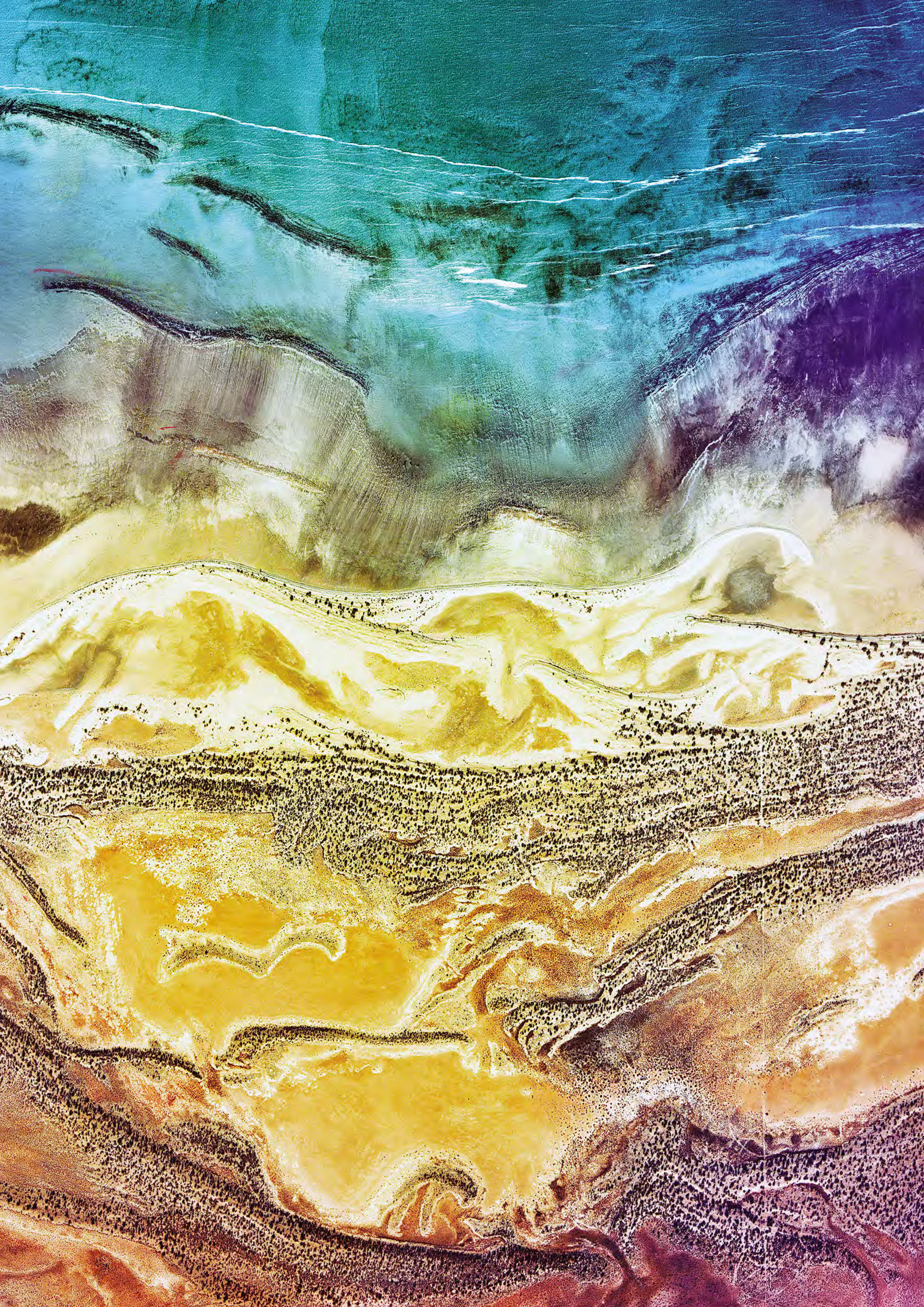

Government of **Western Australia**
Department of **Mines and Petroleum**

BULLETIN 146

THE GEOLOGY OF SHARK BAY

by
Phillip E Playford, Anthony E Cockbain, Patrick F Berry, Anthony P Roberts, Peter W Haines, and Brendan P Brooke

Geological Survey of Western Australia

MINISTER FOR MINES AND PETROLEUM
Hon. Bill Marmion MLA

DIRECTOR GENERAL, DEPARTMENT OF MINES AND PETROLEUM
Richard Sellers

EXECUTIVE DIRECTOR, GEOLOGICAL SURVEY OF WESTERN AUSTRALIA
Rick Rogerson

REFERENCE
The recommended reference for this publication is:
Playford, PE, Cockbain, AE, Berry, PF, Roberts, AP, Haines, PW and Brooke, BP 2013, The geology of Shark Bay: Geological Survey of Western Australia, Bulletin 146, 281p.

National Library of Australia Cataloguing-in-publication entry

Author:	Playford, Phillip E.
Title:	The geology of Shark Bay / Phillip E. Playford, Anthony E. Cockbain, Patrick F. Berry, Anthony P. Roberts, Peter W. Haines, Brendan P. Brooke.
ISBN:	9781741685039 (hardback)
Series:	Bulletin (Geological Survey of Western Australia) ; 146.
Notes:	Includes bibliographical references and index.
Subjects:	Geology--Western Australia--Shark Bay Region.
Other Authors:	Cockbain, Anthony E.
	Berry, Patrick F.
	Roberts, Anthony P.
	Haines, Peter W.
	Brooke, Brendan P.
Dewey Number:	559.413

ISSN 0508–4741

Grid references in this publication refer to the Australian Geodetic Datum (AGD84). Locations mentioned in the text are referenced using Australian Map Grid (AMG) coordinates, Zones 51 and 52, because maps accompanying the Bulletin use that datum. All locations are quoted to at least the nearest 100 m.

Copy editor: AE Cockbain
Cartography: M Prause
Desktop publishing: RL Hitchings
Printed by Quality Press

Published 2013 by Geological Survey of Western Australia

Further details of geological publications and maps produced by the Geological Survey of Western Australia are available from:
Information Centre
Department of Mines and Petroleum
100 Plain Street
EAST PERTH, WESTERN AUSTRALIA 6004
Telephone: +61 8 9222 3459 Facsimile: +61 8 9222 3444
www.dmp.wa.gov.au/GSWApublications

Front cover: Digital elevation model (DEM) image of the Shark Bay area

Frontispiece: Vertical airphoto near Kopke Point, showing beach ridges, linear mounds of Hamelin Coquina, yellow marsh deposits, and successive lines of stromatolite reefs, grown over Pleistocene beach ridges

Back cover: Intertidal stromatolites, south of Flagpole Landing, Hamelin Pool

Contents

Figures

Tables

THE GEOLOGY OF SHARK BAY

by

Phillip E Playford[1], Anthony E Cockbain[1], Peter W Haines[1], Patrick F Berry[2], Anthony P Roberts[3], Brendan P Brooke[4]

Summary

The Shark Bay area has been home to Aboriginal people for more than 40 000 years, and became the first part of Western Australia known to Europeans, beginning with the visit of Dirk Hartog, skipper of the Dutch East India Company's ship *Eendracht* in 1616. He landed at Cape Inscription on Dirk Hartog Island and was followed there or nearby by a succession of famous Dutch, British, and French navigators — Willem de Vlamingh (1697), William Dampier (1699), Louis de St Aloüarn (1772), Emmanuel Hamelin (1802), Louis de Freycinet (1818), and Phillip Parker King (1822). The *Zuytdorp*, a great ship of the Dutch East India Company, was wrecked south of Shark Bay in 1712. Survivors of that wreck may have become the first long-term European inhabitants of Australia.

British colonial settlement in the Shark Bay area began in the 1850s, with the establishment of a short-lived guano industry and a pearling industry that peaked in the 1870s and continued on a diminishing scale up to the 1930s. The pastoral industry began in the 1860s, and has continued since then in various parts of the area. The present economy of Shark Bay is based largely on tourism, fishing, a cultured-pearl industry, and a major solar-salt industry (at Useless Loop). In 1991 Shark Bay was proclaimed a World Heritage Area, because of its outstanding natural values.

The first geologists to study the Shark Bay area were Daryl Johnstone, Phillip Playford, and Richard Chase, for West Australian Petroleum Pty Ltd (WAPET) in 1954–55. Detailed research on aspects of the geology and marine sedimentation in Shark Bay, directed by Brian Logan of The University of Western Australia (UWA), was conducted from the late 1950s to the mid-1970s. The Geological Survey of Western Australia (GSWA) commenced work in the area in 1968, with a study of the modern stromatolites at Hamelin Pool, followed by 1:250 000 mapping and detailed research on various aspects of the geology.

Shark Bay is bounded to the west by Dirk Hartog Island, Dorre Island, Bernier Island, and the Zuytdorp Cliffs, and is divided by the Peron and Nanga Peninsulas into two arms of the sea: the western arm includes Henri Freycinet Harbour, and the eastern arm includes L'Haridon Bight and Hamelin Pool. Drilling on Dirk Hartog Island has shown that it is underlain by an anticline in Cenozoic rocks, and the peninsulas are similarly thought to be localized by underlying anticlinal structures.

The Zuytdorp Cliffs are a striking geomorphological feature that defines the southwestern margin of the Shark Bay area. These cliffs are interpreted to be a fault-line scarp, thought to have resulted from normal faulting during the late Pleistocene and perhaps early Holocene. Most of the land surface in the Shark Bay area is occupied by Holocene sand dunes — of the massive, seif, parabolic, transverse, barchan, and undulating dune types — which are well defined using digital elevation models (DEMs). Evaporite pans, filled with gypsum and known locally as birridas, are unique features of the Shark Bay area. They are mainly developed between transverse sand dunes.

The seawater in Shark Bay can be divided into three main salinity realms: oceanic (in the western and northern parts of the bay), metahaline (north of Hamelin Pool), and hypersaline (in Hamelin Pool and L'Haridon Bight). Henri Freycinet Harbour varies, seasonally, from hypersaline to metahaline.

1 Geological Survey of Western Australia, East Perth WA 6004
2 Western Australian Museum, Welshpool WA 6106
3 University of Queensland, St Lucia Qld 4072
4 Geoscience Australia, Canberra ACT 2601

The northern margin of Hamelin Pool is defined by a shallow sand and seagrass bank, known as Faure Sill, which restricts circulation between Hamelin Pool and the open-marine part of Shark Bay. A similar barrier, L'Haridon Sill, defines the northern margin of L'Haridon Bight.

As a result of its hypersaline water, Hamelin Pool lacks most of the gastropods, bivalves, thallophytic algae, and seaweeds that grow in the oceanic parts of Shark Bay. However, one small bivalve, *Fragum erugatum*, flourishes in Hamelin Pool, L'Haridon Bight, and parts of Henri Freycinet Harbour. This species is able to thrive in the low-nutrient, high-salinity conditions because of the presence in its tissues of zooxanthellae — symbiotic photosynthetic organisms that provide their host with energy through the products of photosynthesis. Enormous numbers of *Fragum erugatum* are cast ashore by storms and cyclones crossing Hamelin Pool and L'Haridon Bight, forming successive beach ridges and mounds, known as the Hamelin Coquina. The oldest of these deposits is about 5300 years old, marking the onset of hypersaline conditions in Hamelin Pool. Successive lithified ridges dip towards the sea and show pronounced cyclicity. The base of each cycle is marked by 'mass-transport' coquina, with haphazard or 'nested' shells, and the upper part is composed of sandy coquina. Convex-up shells, testifying to wind transport, often occur in the upper parts of these cycles. The thicknesses of major cycles in the Hamelin Coquina range from about 0.3 to 1.5 m, with intervening smaller cycles about 0.1 to 0.3 m thick. It is estimated that at least 50 major cycles are present in the type section of the Hamelin Coquina near Flagpole Landing, with an average frequency of about 100 years.

A series of linear and isolated mounds of coquina and sandy coquina occur in parts of the Hamelin Coquina around Hamelin Pool, overlying planed-off cyclic beds. These mounds are thought to have been built by strong winds and waves associated with very large tropical cyclones. The linear mounds in the type locality of the formation near Flagpole Landing have an average frequency of about 400 years.

A characteristic feature of the west coasts of Dirk Hartog, Dorre, Bernier, and Koks Islands, and the coastline at Point Quobba, is the occurrence there of huge blocks of calcrete (calcretized limestone), weighing up to at least 700 t, on the tops of low coastal cliffs. Similar blocks occur along the northwest coastlines of Legendre and Barrow Islands off the Pilbara coast.

These boulder deposits are thought to have resulted from mega-tsunami impacts on the coast a few thousand years ago. The oldest and highest of the linear mounds of Hamelin Coquina near Flagpole Landing may also have been thrown up by a tsunami, which could have resulted from submarine slumping on the continental slope, local faulting, or asteroid impacts on the Indian ocean off the Pilbara and Shark Bay coasts. Similar tsunami deposits occur in the Kimberley, but those are more likely to have resulted from tectonic activity along the eastern Sunda Arc and the Banda Arc of eastern Indonesia.

Tides at Shark Bay consist of two components — astronomical and meteorological. The meteorological component, resulting from the effects of changing winds and air pressures, is commonly larger than the astronomical component. The tidal zone in Shark Bay is defined here as being between extreme high-water and extreme low-water levels. It is subdivided into the supratidal zone (between mean high-water and extreme high-water levels), the intertidal zone (between mean low-water and mean high-water levels), the shallow-subtidal zone (between mean low-water and extreme low-water levels), and the deep-subtidal zone, below extreme low-water level.

Stromatolites, structures built by microbe communities with positive relief above the sea floor, are able to thrive in the hypersaline conditions of Hamelin Pool, because the hypersalinity there results in the lack of most grazing animals, seagrasses, and seaweeds. The stromatolites of Hamelin Pool are the most diverse and abundant marine stromatolites known anywhere in the world. They mainly grow on hard and irregular substrates beside headlands, whereas flat microbial mats are commonly developed in bays, where suitable rocky substrates are absent. L'Haridon Bight is similarly hypersaline, and although flat microbial mats are widespread there, stromatolites are absent, presumably because of the lack of suitable rocky substrates.

The stromatolites at Hamelin Pool occur over wide areas of the tidal zone and sublittoral shelf, extending to maximum depths of about 4 m below mean sea level. Pustular-mat, smooth-mat, colloform-mat, and composite stromatolites are the main types of stromatolites, growing in progressively deeper water, from intertidal to deep subtidal. Dead stromatolites occur especially in the supratidal zone, extending up to about 90 cm above mean sea level. They testify to a relative fall in sea level, amounting to about 1 m, during the recent past. However, dead or dormant stromatolites also occur in many parts of the shallow- and deep-subtidal zones. Some have died or become dormant after being overwhelmed by submarine waves of ooid or pelloidal sands, re-emerging when those waves move on.

The morphology of Hamelin Pool stromatolites is governed by both biological and environmental factors. The species of cyanobacteria and diatoms that construct these stromatolites largely control their external and internal characteristics. The principal environmental controls on stromatolite morphology are the direction of wave translation, the prevailing wind direction, and the nature of the substrate. Some lines of stromatolites are localized by underlying Pleistocene beach ridges, others are elongate in the direction of wave translation, and seif stromatolites have formed in response to the prevailing southerly winds that induce Langmuir circulation in shallow water.

The greatest damage to Hamelin Pool stromatolites as a result of human activities has been at places where camel-drawn drays were used, prior to the mid-1930s, to load bales of wool onto dinghies, for transport to lighters and from them to ships. The tracks made by the camels and drays travelling over and through the stromatolites and over flat microbial mats have remained almost unchanged over about the past 80 years. This testifies to the extremely slow growth rates of the stromatolites, commonly less than 0.5 mm per year.

The Tamala Limestone is a distinctive formation that is well developed on the west side of Edel Land Peninsula. It is composed of limestone eolianite, largely of middle Pleistocene age, originally blown up as dunes behind the coast, largely during the glacial period MIS 8, about 250 000 years ago. At the type section below Womerangee Hill the formation is 250 m thick, consisting of sandy limestone (eolianite) with thin soil and calcrete layers. The base of the formation is below sea level. The top of the type section is marked by a thick layer of calcrete, once overlain by residual quartz sand that resulted from leaching of the eolianite in a Quaternary soil profile. The former dune at this locality must have been more than 300 m high.

The structural geology of the Shark Bay area is marked by both compression and tension during the Cenozoic, leading to folding and both reverse and normal faulting. Prominent structural features are anticlines that are interpreted to underlie Peron, Nanga, and Edel Land Peninsulas, Dorre and Bernier Islands, and Yaringa and Kopke Promontories, and have been proved by drilling to underlie Dirk Hartog Island. The bays between the peninsulas are thought to be underlain by synclines. The compression that resulted in these folds seemingly occurred during the Paleogene, Neogene, and Pleistocene, and may be continuing today. The Zuytdorp Fault is thought to have had normal displacement of up to 300 m since the early Pleistocene, in response to regional tension. On the other hand, there is also evidence of compression in the Shark Bay area during late Holocene times, resulting in uplift of about 14.5 m at Faure Island over the past 3500 years. There is also evidence on that island of alternating tension and compression in very recent times, resulting in the tensional opening of joints following compressive extrusion of sand along older joints. In addition, the Hardabut Fault (east of Kalbarri) has operated as a reverse fault in recent times, whereas it had previously experienced much greater normal movement.

Mineral commodities that are being exploited, or have been exploited, in the Shark Bay area, are solar salt, gypsum, shell deposits, building stone, guano, pearls, pearl shell, and cultured pearls. Mineral-sand deposits are known in the area south of Hamelin Pool and are expected to be developed in future. Of these deposits, solar salt, mineral sands, and cultured pearls have the largest economic values. Further potentially economic deposits of gypsum and heavy mineral sands are known in the area. However, as these prospects are within the World Heritage Area it seems unlikely that they will be developed in the near future.

KEYWORDS: Aboriginals, clay pans, dunes, faulting, fault line, folding, geomorphology, guano, gypsum deposits, islands, mangroves, pearls, salinity, salt production, stromatolites, tides, tsunamis

Introduction

History

Prior to colonization, the Shark Bay area (Fig. 1) was inhabited by nomadic Aborigines of the Malgana, Nanda, and Yinggarda tribes, probably for more than 40 000 years (Bowdler, 1990, 1995; Playford, 1996; Fig. 2). Evidence of the past presence of these people is shown by the many stone artefacts, mainly chips of Cretaceous chert used as knives, that are now scattered through much of the area. Grinding stones have also been found around some Aboriginal wells and soaks, notably at Wale Well on Tamala Station (Fig. 3). Heavy boulders of Tumblagooda Sandstone and Precambrian metamorphic rocks, used as grinding stones, were carried there by Aborigines from the Murchison River area, more than 100 km to the south, upstream of the Murchison River mouth (Fig. 4; Van de Graaff 1980; Playford 1996).

Aborigines obtained much of their drinking water from ‘beach wells’ (Fig. 5), dug by hand close to the shoreline. These wells tapped into the thin layer of potable water, up to about 100 cm thick, that is commonly present above salt water near the coast. In some places kangaroos dig holes to obtain water from this thin freshwater layer (Fig. 6).

Some of the Aboriginal wells were appropriated and enlarged by early European pastoralists, who also dug many more, in order to provide water for their livestock. Most were abandoned during the early part of the 20th century, when artesian and subartesian bores were drilled to exploit groundwater from the Cretaceous Birdrong Sandstone. The shallow watertable beside the coast rises and falls with the tides, and consequently the windmills installed over beach wells used a floating foot-valve to ensure that the water was produced from the thin freshwater layer rather than the underlying saltwater.

Figure 1. Locality map of Shark Bay and surrounding areas, showing some of the principal places mentioned in the text.

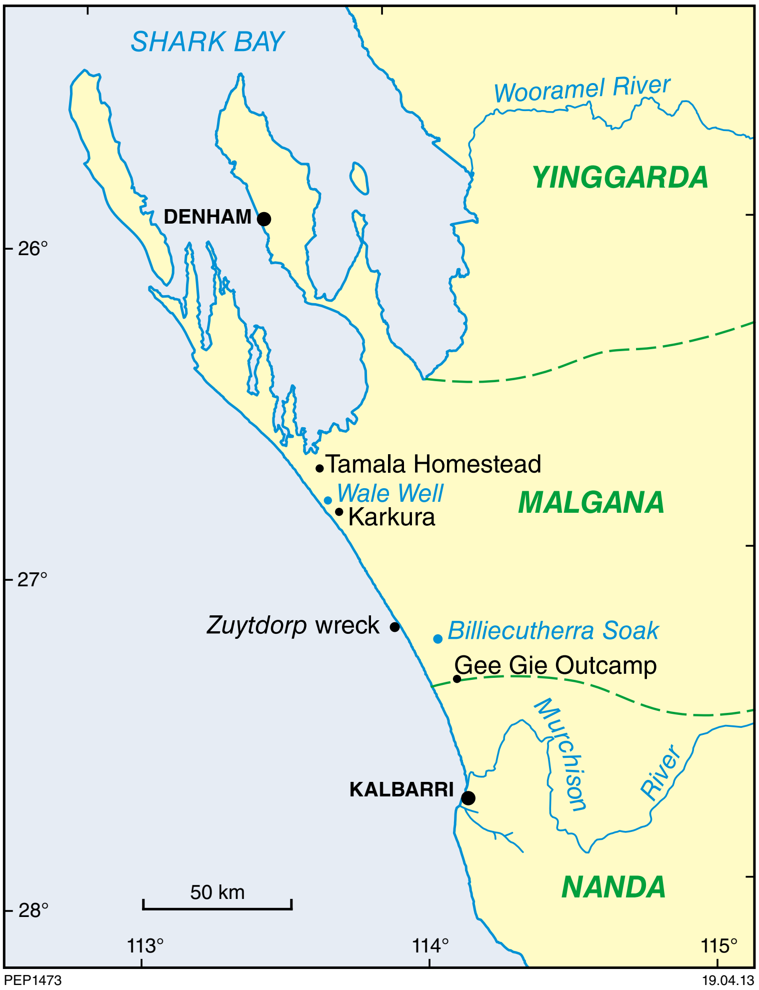

Figure 2. Aboriginal tribal territories in the Shark Bay area prior to European settlement.

Figure 3. Malgana Aboriginal site known as 'Wale', looking south. The name refers to the white areas on the floor of the valley, consisting of calcrete precipitated from groundwater where it seeps out at the surface. Wale Well is in the background of the cleared area.

Figure 4. Aboriginal grindstones, composed of Ordovician Tumblagooda Sandstone and Precambrian metamorphic rocks, near Wale Well on Tamala Station. These stones were carried from the Murchison River area, more than 100 km south of this well.

Figure 5. Depressions marking the sites of former Aboriginal beach wells in Hamelin Coquina north of Flagpole Landing.

Figure 6. Holes dug by kangaroos, in the floor of a shell quarry near Flagpole Landing, seeking to drink from the thin layer of freshwater that overlies hypersaline groundwater.

Shark Bay has had a long history of early European contact (Playford, 1996, 1998; Edwards, 1999). It was the first part of Western Australia to be discovered by Europeans, beginning with a visit in 1616 by Dirk Hartog, skipper of the Dutch East India Company's ship the *Eendracht*, and continuing during the 17th, 18th, and 19th centuries with visits by other Dutch, French, and British navigators. Most of the European seamen went ashore at Cape Inscription, at the north end of Dirk Hartog Island (Fig. 7).

The long history of exploration makes the Cape Inscription area one of the most significant historic sites in Australia, and it was added to the Australian National Heritage List in 2006. A commemorative event is planned for 25 October 2016 to celebrate the 400th anniversary of Dirk Hartog's landing.

Dirk Hartog landed on 25 October 1616 at the north end of the island that now bears his name, at what is now known as Cape Inscription. He had been following the newly authorized Brower route to the Indies, which directed skippers of the company's ships to sail east from the Cape of Good Hope across the Indian Ocean, driven by the prevailing westerly winds (the 'Roaring Forties'), for 1000 Dutch miles (about 7400 km). Then they were to head north to Sunda Strait, between Sumatra and Java. However, because of the impossibility of accurately measuring longitude at that time, it was inevitable that one of the Dutch skippers would eventually sail too far east and encounter the coast of Australia.

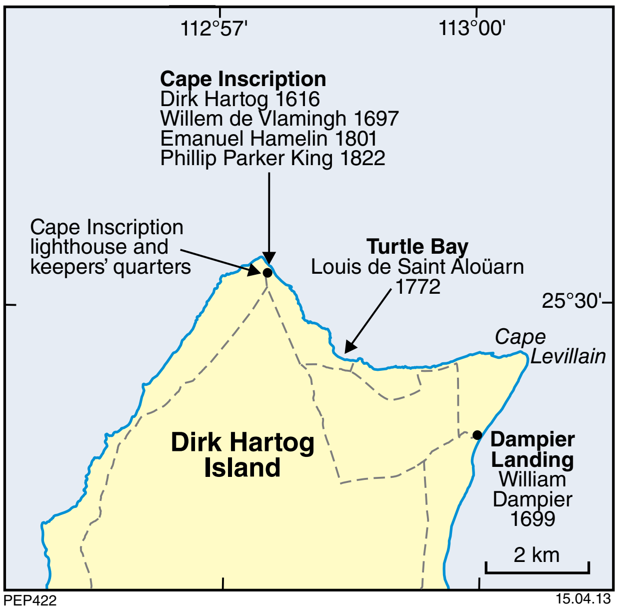

Figure 7. Map of the Cape Inscription area on Dirk Hartog Island, showing sites visited by Dutch, French, and British seamen during the 17th, 18th, and 19th centuries.

Dirk Hartog was the first to do so. He left behind a flattened pewter plate inscribed with a record of his visit (Figs 8–10), nailed to a post standing upright in a rock cleft on top of the cliff (Figs. 9, 10). That plate is the oldest extant record of a European landing in Australia, and is now preserved in the Rijksmuseum in Amsterdam (Heeres, 1899, Playford, 1998, 2005). Hartog's visit resulted in the newly discovered continent becoming known as 'The land of Eendracht' (*t lant van Eendracht*, meaning 'The land of Unity') or 'The land of the Eendracht' (*t landt van de Eendracht*) (Figs 11, 12). It had previously been depicted on maps as a hypothetical southern continent *Terra Australis Incognita* ('Unknown South Land'). Its name became 'New Holland' later in the 17th century, and eventually 'Australia' in the early 19th century.

As a result of Hartog's discovery, the sailing instructions for Dutch skippers were changed to allow them to sail within sight of the Land of the Eendracht at 27°S, or further north, before heading north-northwest to Sunda Strait.

In 1697, Willem de Vlamingh circumnavigated Dirk Hartog Island during his voyage of discovery along the coast of Western Australia between the Swan River and North West Cape, and gave the island its name after finding Dirk Hartog's plate (Playford, 1998; Fig. 13). Vlamingh took the historic plate to Batavia (now Jakarta) and from there it was sent on to Amsterdam. In its place, he left a pewter plate inscribed with a copy of Dirk Hartog's original inscription and a record of his own visit, nailed to a post of cypress pine he had collected on Rottnest Island. This post was placed upright in the rock cleft on top of the cliff, beside Dirk Hartog's decayed post. It is now in the collection of the Western Australian Maritime Museum, Fremantle.

The plate left by Willem de Vlamingh was in turn found in 1801 by members of Nicolas Baudin's French expedition. Jacques Félix Emmanuel Hamelin, skipper of the *Naturaliste* (one of Baudin's two ships) decided that it would be sacrilege to remove this plate from the place where it had remained for more than a century. He nailed it to a new post, placing it upright in the same rock cleft.

Louis de Freycinet, one of Hamelin's junior officers, was dismayed by his commander's decision to leave the plate, believing that its proper place would be in a French institute. Consequently, 17 years later, after he had gained command of his own ship, Freycinet sailed across the Indian Ocean to Cape Inscription, where he recovered the plate and took it to Paris. That famous plate was eventually returned by the French Government to Australia in 1947, in recognition of the part played by Australian soldiers in the defence of France during two world wars. It is now in the collection of the Western Australian Maritime Museum, Fremantle.

Another person to land near Cape Inscription was William Dampier, the famous British navigator, naturalist, and privateer (Figs 7, 14). Naming the large bay 'Sharks Bay' due to the large numbers of sharks seen and caught there by his crew (Fig. 14), Dampier went ashore in 1699 at what is now known as Dampier Landing (Fig. 7; Dampier, 1703). There he gathered the first-ever collection of Australian plants, which is still held in the University of Oxford.

In June 1712 the Dutch East India Company's ship *Zuytdorp* (meaning 'south village' and pronounced 'Zowt-dorp') was wrecked about 65 km south-southeast of Shark Bay (near the southern boundary of the Shark Bay World Heritage Area) at the base of a line of coastal cliffs named the Zuytdorp Cliffs (Playford, 1959, 1996). The *Zuytdorp* was the first of four early Dutch shipwrecks to be discovered and identified in Western Australia (Fig. 15). In the report of the Select Committee on Ancient Shipwrecks of the Western Australian Legislative Assembly (Pendal, 1994), Playford was named as one of two primary discoverers of this wreck, the other being a stockman, Tom Pepper, who had first visited the site in 1927 and who told Playford about it in 1954.

The *Zuytdorp* is the only one of four early Dutch shipwrecks known on the Western Australian coast where no survivors ever returned to European civilization to tell their story. Of some 200 people on board the *Zuytdorp* when it left the Cape of Good Hope, there is evidence that a number of people (perhaps less than 50) managed to survive and scramble ashore. Evidence, in the form of a well-preserved brass tobacco-box lid made in Leiden, suggests that some of the survivors reached Wale Well, a major campsite for the Aboriginal people of the Malgana Tribe, 50 km north of the wreck (Fig. 2). Their eventual fate is unknown, but it seems possible that a few cohabited with the Aboriginal people of the area, perhaps to become Australia's first long-term European inhabitants (Playford, 1996).

The French navigator Louis de Saint Aloüarn landed at Turtle Bay, close to Cape Inscription, in 1772 (Godard and de Kerros 2002; Edwards, 1999, Green 2007; Fig. 7). He climbed the cliff there, burying two bottles, one containing a parchment with a written statement claiming this part of New Holland in the name of the King of France. A silver coin under a lead seal was placed on top of each bottle. The two coins and lead seals, one with an intact bottle, were discovered in 1998, but there was no sign of any parchment.

Phillip Parker King, the famous Australian-born navigator, landed at Cape Inscription in 1822, expecting to find the Vlamingh plate. He was unaware that it had already been retrieved four years earlier by Louis de Freycinet. King left his name spelled out with nails driven into Hamelin's post (Hordern, 1997).

In 1858 Henry Mangles Denham, skipper of HMS *Herald*, charted the whole of Shark Bay and left his name and the date of his visit carved on a limestone cliff at Eagle Bluff (David, 1995, Edwards, 1999). That part of the cliff has since collapsed, but the rock with the inscription was recovered and is now in the Pioneer Park in Denham.

European settlement in the Shark Bay area began in the 1850s, with the establishment of a guano industry, centred on the many small islands in the area where sea birds had nested for thousands of years, leaving behind their phosphate-rich excrement. The first island to be mined was Egg Island, beside the east coast of Dirk Hartog Island.

Figure 8. Aerial view of Cape Inscription looking northwest. The arrow points to an open joint in calcrete at the cliff top, where Dirk Hartog in 1616 and Willem de Vlamingh in 1697 placed posts with engraved plates that recorded their visits, and Emmanuel Hamelin added another post in 1802. A thick layer of calcrete at the top of the cliff has broken away in places, yielding the large tabular blocks that lie on the slope and at its base.

Figure 9. The cliff top at Cape Inscription looking southeast, showing the open joint in calcrete where Dirk Hartog and Willem de Vlamingh placed their posts and inscribed plates in 1616 and 1697 respectively. The two posts mark the approximate sites of those posts.

Figure 10. Dirk Hartog's inscribed plate, which he left at Cape Inscription on 25 October 1616, and a facsimile of the inscription.

Figure 11. Part of an atlas by Gerard Mercator (1632) showing the recently discovered *t lant van Eendracht* ('The land of Unity'), named after Dirk Hartog's ship. Reproduced from Heeres (1899).

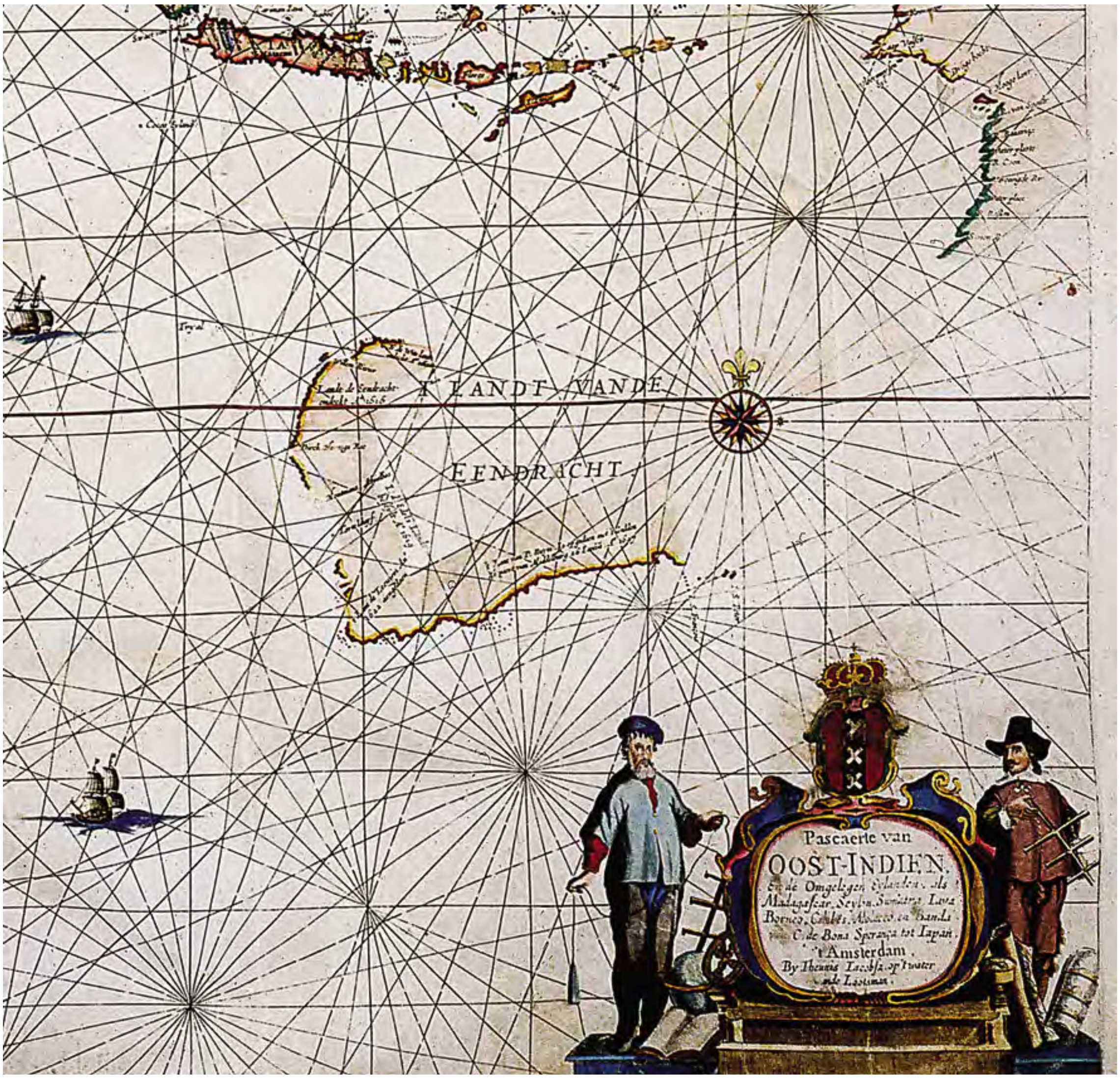

Figure 12. Part of a map by Theunis Jacobsz (c. 1630), based on charts of the Dutch East India Company. This map shows the Australian continent as *t landt van de Eendracht*. Courtesy of Badische Landesbibliothek, Karlsruhe, Germany.

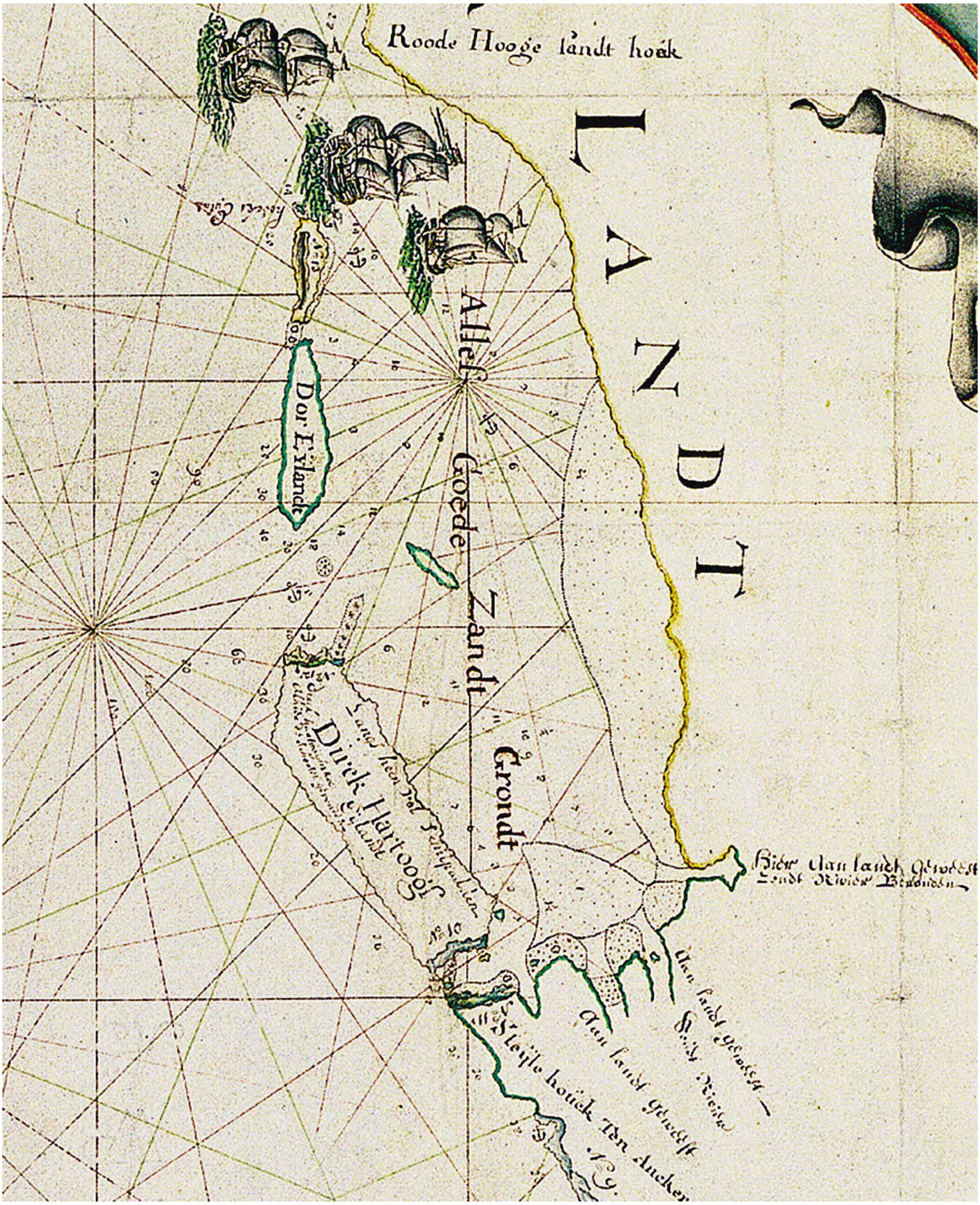

Figure 13. Map of the Shark Bay area by Willem de Vlamingh (1697). This explorer was responsible for naming Dirk Hartog Island ('Dirck Hartoogs Eylandt'), and Dorre Island ('Dor Eylandt').

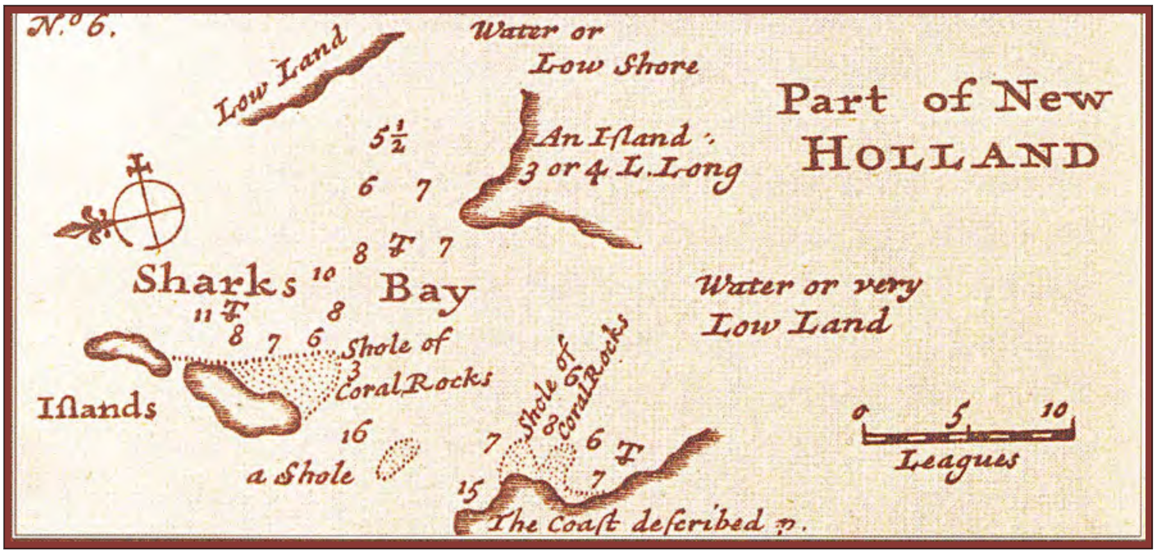

Figure 14. Map of 'Sharks Bay', published by William Dampier in 1703.

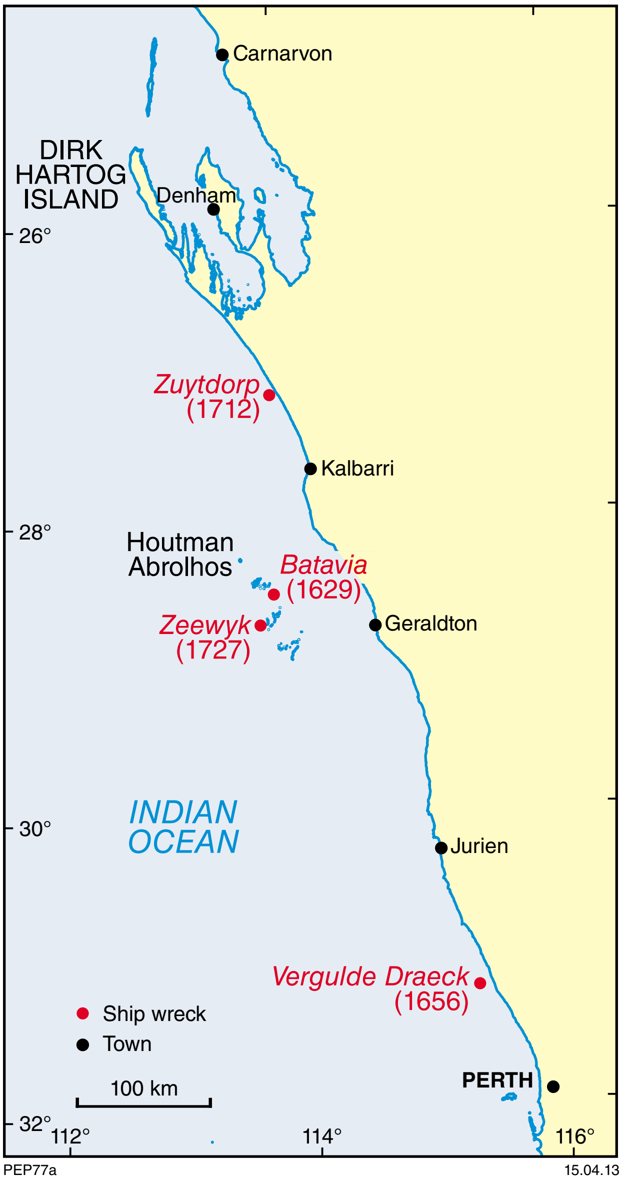

Figure 15. Map showing the locations of four shipwrecks of vessels owned by the Dutch East India Company that are known to have been lost on the coast of Western Australia during the 17th and 18th centuries.

The upper surfaces of the islands were stripped bare to remove the guano, which was mostly exported to Europe for use as a fertilizer. Many of the small islands in Shark Bay show evidence of guano mining, in the form of their flat tops, bare of vegetation (Fig. 16). A military garrison was briefly established in 1851 on Dirk Hartog Island at Quoin Bluff South to protect this valuable industry and collect colonial revenue (Edwards, 1999; Fig.17).

The Shark Bay pearling industry, which also began during the 1850s, was based on the Shark Bay oyster (*Pinctada albino*, known colloquially as 'the bastard pearl shell'), which had first been observed by Dampier (1703) during his visit to the area in 1699 (Hancock, 1989). This relatively small pearl shell was gathered by dragging wire-mesh baskets over the shallow banks, behind small single-mast sailing boats. Economic returns came mainly from pearls, and, to a lesser extent, from pearl shell, although both pearls and shell were less valuable than those of the much larger *Pinctada maxima*, which became the source of pearling industries based further north, at Broome and Cossack (Edwards, 1999).

The main centre for the Shark Bay pearling industry was at Freshwater Camp (later renamed Denham), where the main street, Knight Terrace, was once paved with pearl shell (Saville-Kent, 1897). When Playford first visited the town in 1954 it had changed little since the early 1900s; Figs 18–20). Another pearling base, Wilya Mia, near the north end of Heirisson Prong, was destroyed by a cyclone in 1921.

The peak of the pearling industry in Shark Bay was achieved during the 1870s, when up to 80 boats were dredging the shallow banks, especially around Useless Inlet, Freycinet Reach, and Disappointment Reach. However, the dredging method of collecting shells disturbed the biological environment of the sea floor and led to the near collapse of the industry in 1891 (Hancock, 1989). Thereafter, pearling in Shark Bay was more closely controlled by the government, and continued on a reduced scale until the late 1930s. After the demise of pearling, the economy of Shark Bay became dependent on the fishing industry, and, more recently, on tourism, the solar-salt industry, and a cultured-pearl venture.

Figure 21 shows a sketch made in 1883 by Government Geologist ET Hardman, of a typical pearler's camp, probably at Freshwater Camp (now Denham), with its odious barrels known as 'pogey pots'. It was the practice to scrape oyster flesh into these barrels and leave it to rot, allowing any pearls to sink to the bottom. The rotting flesh was later boiled in water to yield any remaining pearls. At the time, it was said that Denham could be smelled from more than 30 km away! Another of Hardman's paintings showed the first homestead on Dirk Hartog Island, then occupied by Aubrey Brown, near the southern end of the island (Fig. 22).

The pastoral industry in the Shark Bay area began when a sheep station was established on Dirk Hartog Island in 1868, by Francis Louis Von Bibra and his partner Aubrey Brown (Graham-Taylor, 2012). Other stations were established in the area from the 1870s to the 1950s. All were sheep stations, but Tamala disposed of its sheep and converted to cattle in 1984 (it has since been destocked, but has retained many feral goats and camels). Many former stations in the area (Peron, Nanga, Nilemah, Carrarang, and Dirk Hartog Island) have been purchased by the State Government, and are now incorporated in national parks.

The stock route that was used in travelling and droving sheep from the Shark Bay area until 1963 is shown in Figure 23. The only source of water along most of that route came from rainwater catchment sheds, the largest of which was Willy's Shed, said to have been the largest catchment shed in Western Australia. It remained almost intact when photographed in 1993 (Fig. 24). The stock route is now abandoned and is hard to detect on the ground. Some of the vehicle tracks shown on Figure 23 are now disused and overgrown.

In 1991 Shark Bay was proclaimed as a World Heritage Area, the first in Western Australia (Fig. 25). It met all the natural-heritage listing criteria. The most important of the natural features are the living stromatolites at Hamelin Pool. In view of the area's remarkable history, which is of both national and international significance, the area would seemingly also meet the criteria for cultural-heritage listing.

Today, Shark Bay is best known to the public as a tourist destination and a recreational fishing centre. The other principal attractions to tourists are the natural beauty of the area, the bottle-nose dolphins at Monkey Mia (Fig. 26), the Discovery Centre in Denham, the stromatolites at Hamelin Pool, and the coquina (shell) deposits at Hamelin Pool and L'Haridon Bight.

Figure 16. Small, flat-topped island north of Useless Loop, one of the many islands stripped bare by guano miners during the 1850s.

Figure 17. The site of a military encampment established in 1851 on the east side of Dirk Hartog Island, immediately west of Quoin Bluff South. The purpose of the line of boulders projecting out into the water is unknown.

Figure 18. Old Denham, photographed in 1958, which at the time had changed little since the 1920s. Note the long jetty, constructed in 1956 and destroyed by Cyclone Hazel in 1979.

Figure 19. Knight Terrace, the main street in Denham, in 1954, with Denham Hotel in the foreground. The road, previously paved with pearl shell, had only recently been bituminized.

Figure 20. Knight Terrace, the main street in Denham, 1954, showing the lighter *Will Succeed* pulled up on the shore in the left background. At that time, nearly all buildings in town were in a state of rust and decay.

Figure 21. Sketch by Government Geologist Edward Hardman (in his field book) of a pearler's camp at Shark Bay, 3 April 1883.

Figure 22. Painting by Government Geologist Edward Hardman (in his field book) of the south end of Dirk Hartog Island and the location of Aubrey Brown's homestead, 3 April 1883.

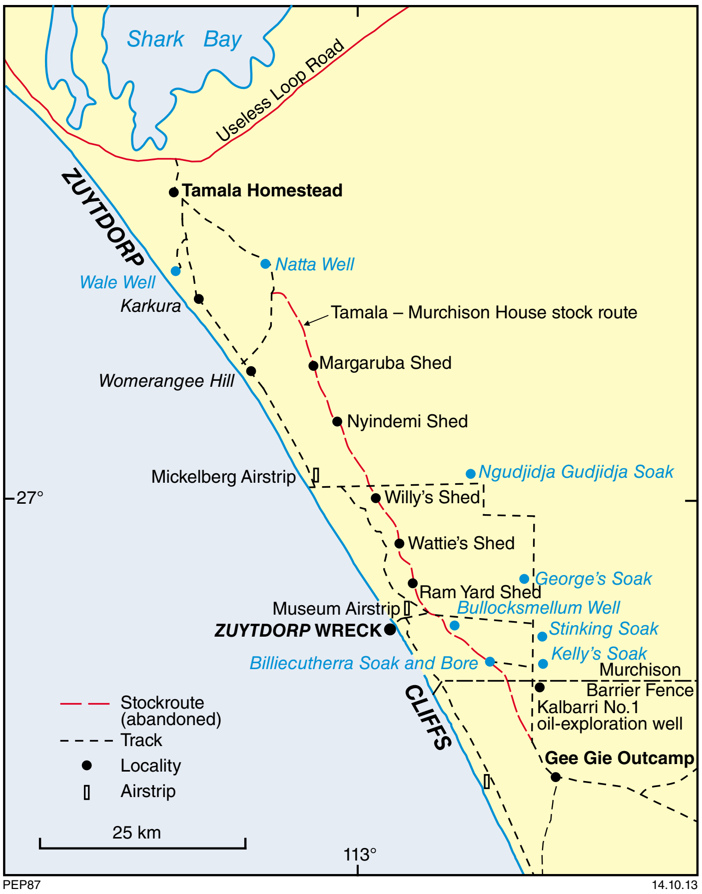

Figure 23. **Map of part of the Zuytdorp Cliffs area indicating the site of the *Zuytdorp* wreck, the abandoned stock route, vehicle tracks, and the sites of rain-catchment sheds.**

Figure 24. **Willy's rain-catchment shed on the stock route between Murchison House and Tamala Station, photographed in 1993. This shed had been used to water sheep being driven along the stock route from Tamala to Murchison House.**

Figure 25. Map showing the extent of the Shark Bay World Heritage Area.

Figure 26. Bottle-nose dolphins at Monkey Mia. The photo was taken in 1979, a few days after Cyclone Hazel had passed over the area.

Geological investigations

The first geologist to visit Shark Bay was Government Geologist ET Hardman in 1883, who sketched some features of the area and made a few broad geological observations. Little was known of the geology of Shark Bay until 1954–55, when West Australian Petroleum Pty Ltd (WAPET) conducted a geological reconnaissance over the area (Johnstone and Playford, 1955; Playford and Chase, 1955).

A program of detailed geological and sedimentological research by (or led by) Brian Logan of UWA, was carried out in the area from the late 1950s to the mid-1970s (Logan, 1959, 1961, Logan et al., 1964, Logan et al., 1970a, Logan et al., 1974b). The publications by Logan et al. (1970a) and Logan et al. (1974b) are fundamental sources of information on the geology and sedimentology of the area.

The Baas Becking Geobiological Laboratory began studying the modern stromatolites in Hamelin Pool in 1979, and expanded this into a detailed sedimentological study of the area (Bauld et al., 1979; Bauld, 1984; Burne and James, 1986; Walter and Bauld, 1986, Skyring and Bauld, 1990). The Baas Becking Laboratory was disbanded in 1987, prior to completion of the research program, but some details of the information obtained through that program were recorded by Burne and Hunt (1990) and Burne and Johnson (2012).

Studies of the Hamelin Pool stromatolites and Hamelin Coquina by GSWA began in 1968 (Playford, 1972, 1979, 1980a, 1980b, 1990; Playford and Cockbain, 1976). GSWA also mapped the 1:250 000 sheets that cover the Shark Bay area as a whole (Van de Graaff et al., 1983; Butcher et al., 1984; Denman et al., 1985). Hocking et al. (1987) described the geology of the Carnarvon Basin, including Shark Bay.

Recent papers on the Hamelin Pool area have been published by Reid et al. (2003) and Jahnert and Collins (2011, 2012) on stromatolites, and O'Leary et al. (2008) on coral-reef development during the Late Pleistocene. Berry and Playford (1997) described the life cycle of *Fragum erugatum*, the shells of which form the Hamelin Coquina. Subsequent field studies were conducted in the area from 2009 to 2013; among the most important new discoveries being that of mega-tsunami deposits on the outer islands of Shark Bay (Playford, 2012).

The text and most illustrations for this Bulletin were prepared by Playford, with input from the other authors: Cockbain participated in studies of stromatolites at Hamelin Pool and assisted with the editing, Berry undertook research on living *Fragum erugatum* and participated in fieldwork on Faure Island, Roberts was responsible for mathematical studies and illustrations of tides, and Haines and Brooke measured and documented the type section of the Tamala Limestone.

This Bulletin focuses on the main features of our research, dealing especially with stromatolites, dunes, eolianites, birridas, coquinas, tsunamis, and tectonism. Many photographs are included, as this is deemed to be the most effective way of presenting the geology, geomorphology, sedimentology, and history of the area. The photographs were taken by Playford, unless otherwise acknowledged.

Geomorphology

General

Shark Bay is a region of shallow sea in the Southern Carnarvon Basin, bounded to the west by Edel Land Peninsula, and Dirk Hartog, Dorre, and Bernier Islands (Fig. 1). It is divided into two major arms of the sea by Peron and Nanga Peninsulas.

The peninsulas and islands are covered by Holocene and Pleistocene dune sands, eolianites, and marine deposits. These sedimentary rocks are here considered to have accumulated over anticlines (and perhaps some fault blocks) in Pleistocene and older sedimentary rocks.

The Zuytdorp Cliffs, which are 180 km long and up to 260 m high, mark the western boundary of the Edel Land Peninsula, extending south to the mouth of the Murchison River at Kalbarri (Playford, 1990; Brooke et al., 2012). They form one of the most prominent features of the Shark Bay area; indeed, this line of precipitous cliffs, some 200 km long, is one of the most remarkable geomorphological features of the Australian coast. François Pelsaert, commodore of the *Batavia*, wrecked on the Houtman Abrolhos in 1629, was the first person to describe these cliffs (Godard, 1993). During his voyage in the longboat, while seeking to sail to Batavia (Jakarta), he recorded that at 27°S:

> They had no possibility of nearing the land with the boat, for the breakers were too strong and the coast too steep and jagged, without any foreland or inlet as is usually found on other coasts, so that it seemed to them a bare and cursed country, devoid of green or grass.

In 1697 Willem de Vlamingh, while on board the *Geelvink*, vividly described these cliffs as follows (Playford, 1998):

> The land here appears very bleak, and so abrupt as if the coast has been chopped off with an axe, which makes it almost impossible to land. The waves break here with so great a fury that one should say that everything around must shake and become dismembered, which appears to us a truly terrible sight. Nevertheless, we found it rather difficult to drag ourselves away from this evil place.

Indeed, anyone seeing this awe-inspiring line of cliffs must come away similarly impressed.

The cliffs were first examined geologically in 1954 (Johnstone and Playford, 1955) and at that time were among the least-known parts of the Australian coast, being shown on some maps of the continent as a dotted or dashed line.

These cliffs are interpreted to be a fault-line scarp, formed through early Holocene or late Pleistocene movement along the Zuytdorp Fault (see the section on 'Structure' later in this Bulletin). Since then, the steep cliffs have been subjected to relatively small amounts of marine and subaerial erosion.

Another striking feature of the Shark Bay area are the flat-floored claypans, known locally as 'birridas', after their Aboriginal (*Malgana*) name. Most are subcircular and sparsely covered with low samphire shrubs. They typically occur in interdune valleys, and are floored by gypsum up to 5 m thick (Jones, 1994).

Marine realm

Shark Bay can be broadly divided into three main salinity regimes (Fig. 27): oceanic (salinity 35–40‰), metahaline (salinity 40–55‰), and hypersaline (salinity 55–>70‰; Logan and Cebulski, 1970; Logan, 1974; Fig. 27).

These highly saline bodies of water result from the restricted interchange with water of the open ocean, combined with strong winds, low rainfall (average 210 mm/yr), and high rates of evaporation (average 2200 mm/yr). Hamelin Pool and L'Haridon Bight are hypersaline throughout, and parts of Henri Freycinet Harbour at different times of the year range from just above to just below the hypersaline–metahaline boundary. Thus, the water in Henri Freycinet Harbour at Nanga was hypersaline (salinity 57.25 and 58.1‰) in October and December 1994, respectively, whereas in February and April 1995 it was metahaline (salinity 52.05 and 52.65‰; Table 1).

The restricted-circulation regime in Hamelin Pool produces anoxic conditions on much of the sea floor, resulting in the deposition of black muds in the deeper parts of the basin, and gypsum in parts of the supratidal zone.

The prevailing wind directions over most of Shark Bay are overwhelmingly from the south, but in the southeastern end of Hamelin Pool they are from the south to southeast (Fig. 28). Southerly winds are especially strong and persistent during the summer months.

Bierwirth et al. (1992, 1993) described a method, using multispectral imagery, of mapping the sea floor at Useless Inlet (between Bellefin and Heirisson Prongs) and Hamelin Pool. This innovative method has yet to be applied to other areas of Shark Bay.

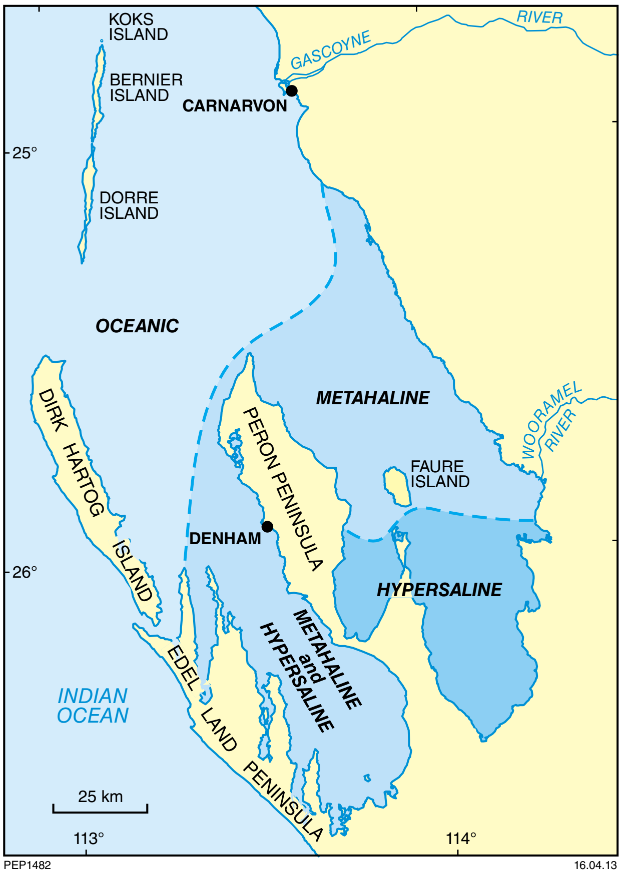

Figure 27. Map showing the salinity realms in waters of the Shark Bay area (after Logan and Cebulski, 1970).

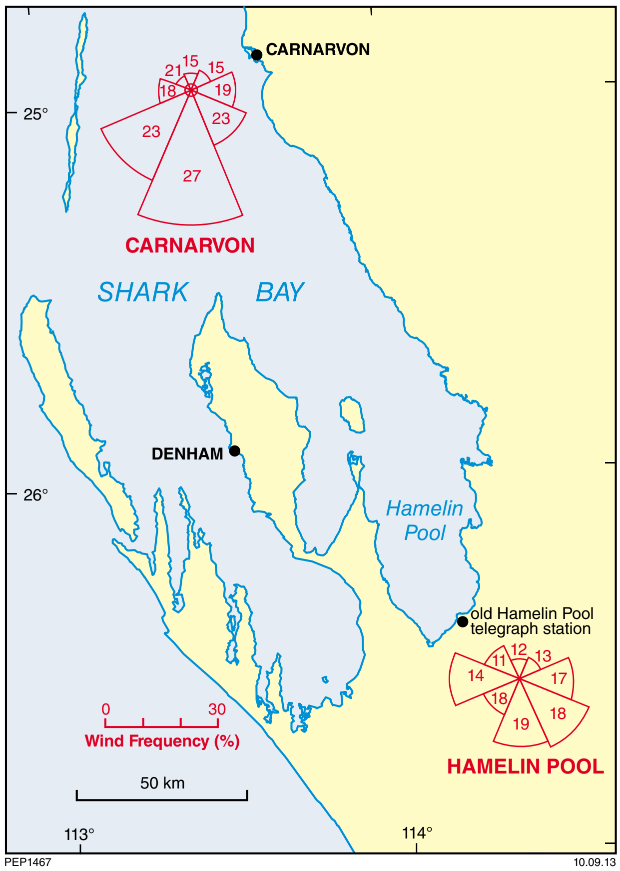

Figure 28. Annual wind-rose diagrams for the Carnarvon and Hamelin Pool weather stations (after Playford, 1980a). Numbers show average wind velocities (in kilometres per hour). The circle in the centre of the wind rose for Carnarvon illustrates the percentage of calms reported: 1.5%. For Hamelin Pool calms were only 0.2%.

Table 1. Water analyses from Henri Freycinet Harbour, L'Haridon Bight, and Hamelin Pool (Flagpole Landing and Carbla Point) showing seasonal variations in total dissolved solids as reported by the Government Chemical Laboratories

Locality	*Sample date*	*Total dissolved solids (mg/L)*
Nanga, Henri Freycinet Harbour		
	October 1994	57 250
	December 1994	58 100
	February 1995	52 050
	April 1995	52 650
South-southwestern side of L'Haridon Bight		
	August 1994	61 300
	October 1994	62 300
	December 1994	61 250
	February 1995	61 250
	April 1994	62 550
Carbla Point, Hamelin Pool		
	August 1994	69 450
	October 1994	69 250
	February 1995	72 500
	April 1995	70 200
Flagpole Landing, Hamelin Pool		
	August 1994	68 750
	October 1994	72 350
	December 1994	75 800
	February 1995	73 200
	April 1995	74 300

Peninsulas

Three main peninsulas, Peron, Nanga, and Edel Land Peninsulas, are striking features of the Shark Bay area (Figs 29–32). All are interpreted as having been localized by anticlines, perhaps associated with reverse faulting, in the underlying Neogene, Paleogene, and Cretaceous deposits. The bays between the peninsulas are thought to mark synclines.

Bellefin, Heirisson, and Boorabuggatta Prongs, and Carrarang Peninsula, are a series of elongate, north–south trending promontories on the east side of Edel Land Peninsula (Fig. 29). These promontories, separated by narrow inlets, mark the sites of massive dunes formed during the last Pleistocene ice age, when sea level and rainfall were lower (Shulmeister et al., 2004), and the prevailing southerly winds were much stronger than now.

Peron Peninsula

Peron Peninsula is about 75 km long, extending from Cape Peron to Taillefer Isthmus. It is almost entirely covered by dune sands of the Denham Sand (Fig. 30), which are regarded as mid-Pleistocene to early Holocene in age. The topography of the peninsula is defined by parabolic and transverse sand dunes that are not readily discerned at the surface or on airphotos, but are clearly displayed in DEM images (Figs 31, 32).

Pleistocene Peron Sandstone outcrops sporadically around the coast of the peninsula, especially at headlands such as Cape Peron (the Peron Sandstone type locality; Figs 33, 34) and Cape Lesueur. Small outcrops of Dampier Limestone and Bibra Limestone also occur at a few localities along the coast (Butcher et al., 1984).

Birridas are extensively developed on Peron Peninsula, in interdune depressions between transverse dunes (Fig. 32).

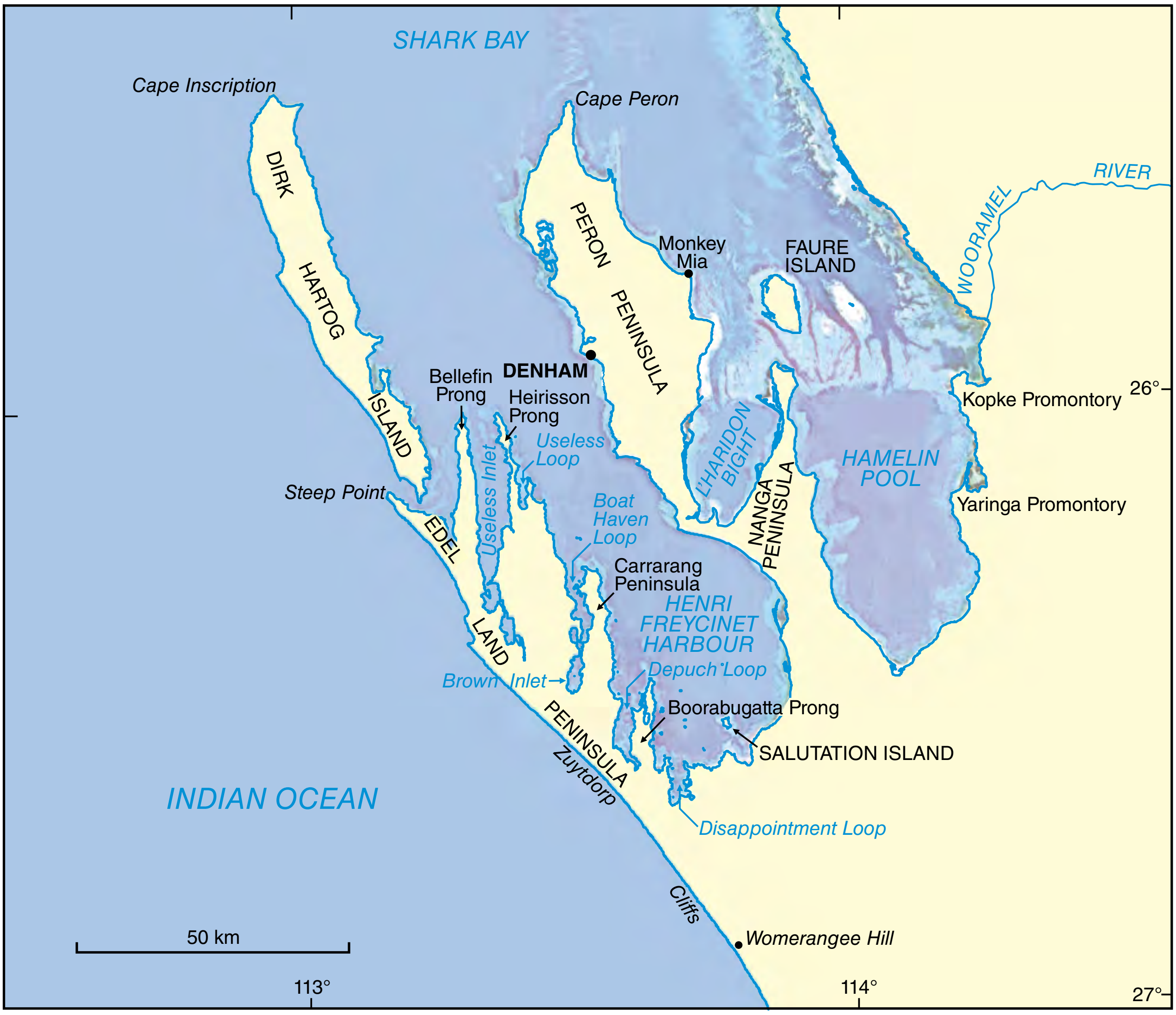

Figure 29. Peninsulas, prongs, and promontories in the Shark Bay area.

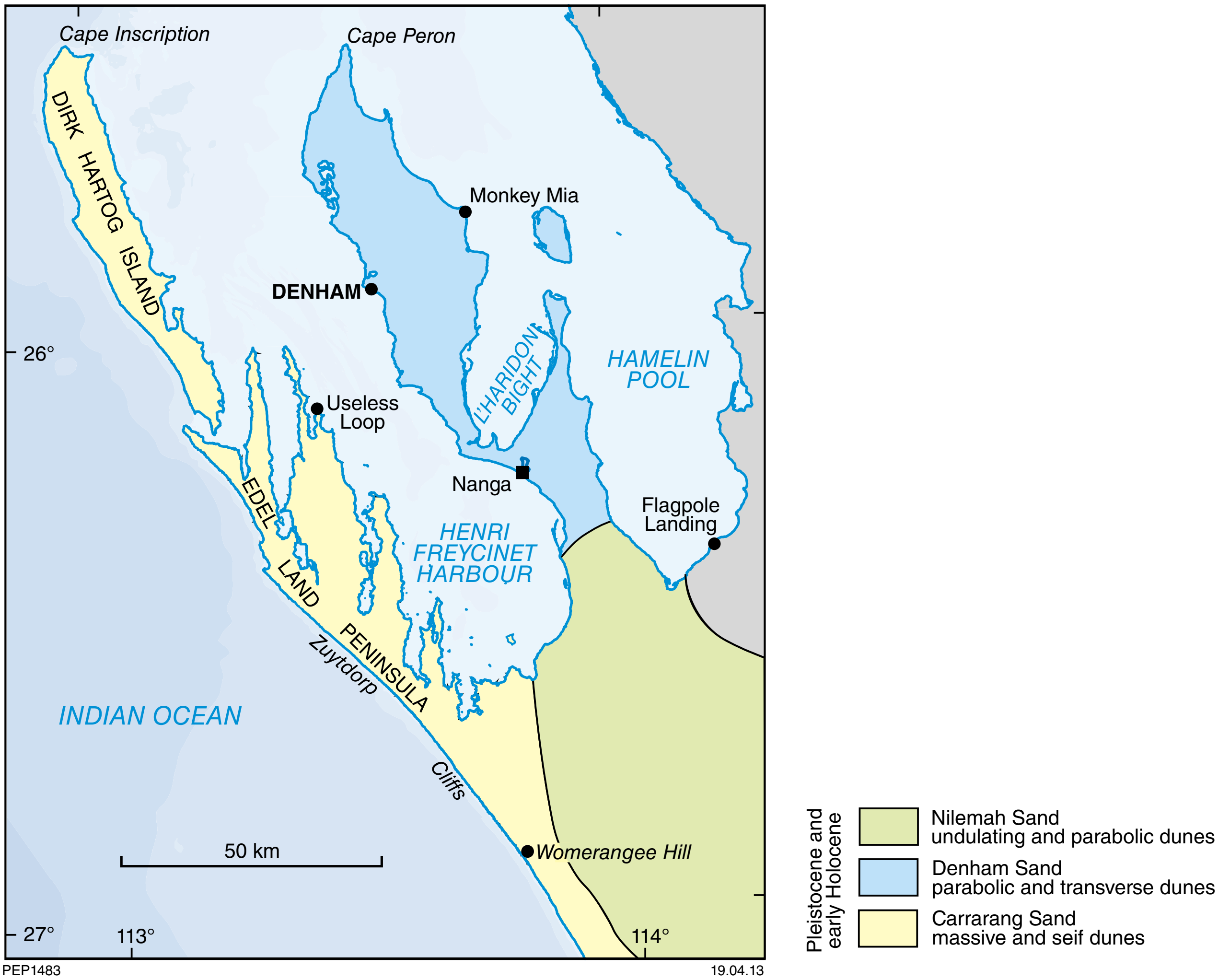

Figure 30. Map showing the distribution of sand-dune formations in the Shark Bay area.

In many places, a broad band of pale-red to white ooid or pelloidal sand, commonly ripple marked, can be observed in shallow waters between the shoreline and swathes of dark seagrass that cover the sea floor in deeper water (Fig. 35). At Denham, this band of sand is exposed not more than two or three times a year, during exceptionally low tides (Fig. 36; L Moss and D Matthews, 2010, 2011, pers. comm.).

Nanga Peninsula

Nanga Peninsula extends for about 60 km in a north–south direction from Petit Point to near Nanga. The northern part of this peninsula is covered by red transverse and parabolic sand dunes of the Denham Sand, together with parabolic and undulating dunes of the Nilemah Sand in the southern part (Figs 30–32). Birridas are present in north–south trending belts between transverse dunes (Fig. 37). Pleistocene Dampier Limestone and Bibra Limestone are exposed at a few localities along the coast of the peninsula (Butcher et al., 1984).

Extensive narrow belts of the Holocene Hamelin Coquina are exposed along the east and west coasts of Nanga Peninsula adjacent to Hamelin Pool and L'Haridon Bight, and they also occur to a lesser extent along parts of the Henri Freycinet Harbour shoreline. Living, dead, and dormant stromatolites are well developed in Hamelin Pool beside the east coast of Nanga Peninsula, where they extend between the supratidal and subtidal zones.

Edel Land Peninsula

The name Edel Land Peninsula is applied to the peninsula on the west side of Shark Bay, extending for about 80 km from Steep Point to Tamala Station. It is bounded to the

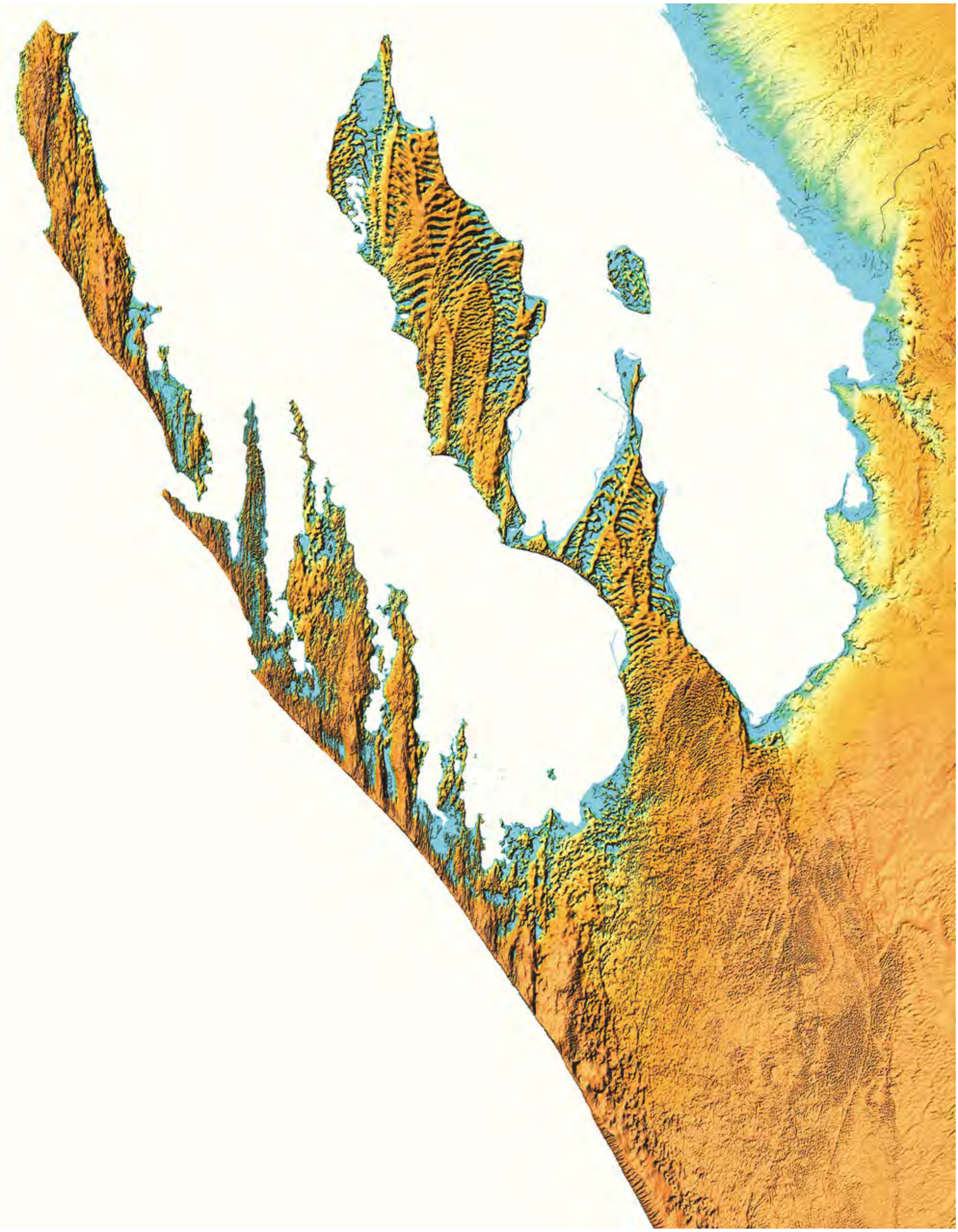

Figure 31. Digital elevation model (DEM) image of part of the Shark Bay area, illustrating the geomorphology of the area and the various types of sand dunes shown in Figure 30.

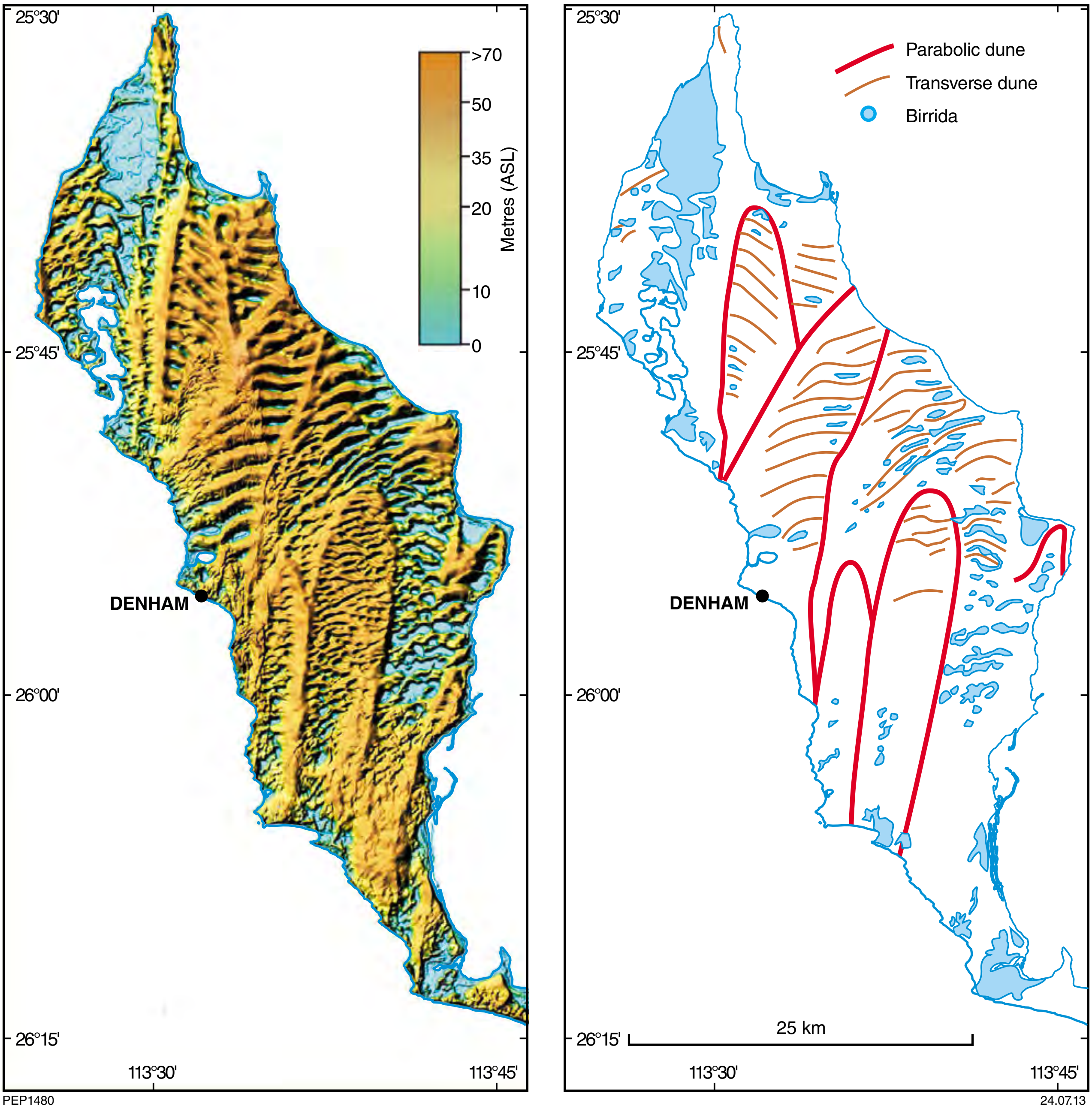

Figure 32. **DEM image and map of Peron Peninsula, showing the development of parabolic and transverse dunes in the Denham Sand. Birridas are located between the transverse dunes. Note that the dunes are truncated along the shoreline.**

southwest by the Zuytdorp Cliffs fault-line scarp. The topography of the peninsula is marked by a series of north–south seif and massive dunes, and lesser parabolic dunes, of the Carrarang Sand (Figs 30, 31, 38). The height of the seif dunes above the interdune valleys is generally 10–15 m. Those dunes were formed by very strong prevailing southerly winds during the late Pleistocene and early Holocene.

Smaller peninsulas and promontories

A number of small peninsulas, prongs, and promontories with intervening inlets and loops are developed beside Edel Land Peninsula and on the east side of Hamelin Pool (Figs 29, 38–46).

Small prongs and peninsulas with intervening inlets are developed on the northeastern side of the Edel Land Peninsula — from north to south they are named the Bellefin Prong, Heirisson Prong, Carrarang Peninsula, and Boorabuggatta Prong (Fig. 29). These features are 20–50 km long, and are occupied by seif dunes of the Carrarang Sand (Figs 30, 31). Birridas are developed in some interdune depressions and have been mined for gypsum south of Useless Loop.

On the eastern coast of Shark Bay, the Yaringa and Kopke Promontories, each about 5 km long, project into Hamelin Pool (Fig. 29). Hutchison Embayment (Figs 47, 48) and Gladstone Embayment are on the north sides of those promontories. Cretaceous Toolonga Calcilutite, Neogene Lamont Sandstone, Quaternary calcrete, and various non-marine Quaternary deposits outcrop on the surface of the promontories (Van de Graaff et al., 1983; Denman et al., 1985).

Descriptions of the geology of Gladstone Embayment were given by Davies (1970b) and of the Hutchison Embayment by Hagan and Logan (1974b). Nilemah Embayment, at the southern end of Hamelin Pool, was described by Brown and Woods (1974).

Based on interpretations of water-bore logs in the area of Kopke and Yaringa Promontories, Playford and Chase (1955) concluded that the peninsulas are developed over anticlinal folds in underlying Cretaceous rocks, and further deduced that Hamelin Pool overlies a syncline. Furthermore, they suggested that Dirk Hartog Island was controlled by an anticlinal fold, a conclusion subsequently confirmed by drilling (Fig. 49; Butcher et al., 1984).

Figure 33. Aerial view of Cape Peron looking northeast, showing red Peron Sandstone exposed along the coast.

Figure 34. Red sandstone of the Peron Sandstone at its type locality, Cape Peron.

Figure 35. Aerial view of Denham township and its environs looking north, showing ooid and pelloid sand below shallow water (the pale-green areas), and dark seagrass below deeper water.

Figure 36. Ripple-marked ooid sand exposed in front of Denham township, when the tide was extremely low, on 24 January 2010. Such low tides occur rarely, not more than two or three times a year, during summer. Photo courtesy of Des Matthews.

Figure 37. Aerial view looking north over Nanga Peninsula, with Hamelin Pool on the right and L'Haridon Bight on the left. Shell Beach is at the south end of L'Haridon Bight. Note the lines of birridas in interdune depressions on the peninsula, and spits of coquina along the east coast of L'Haridon Bight.

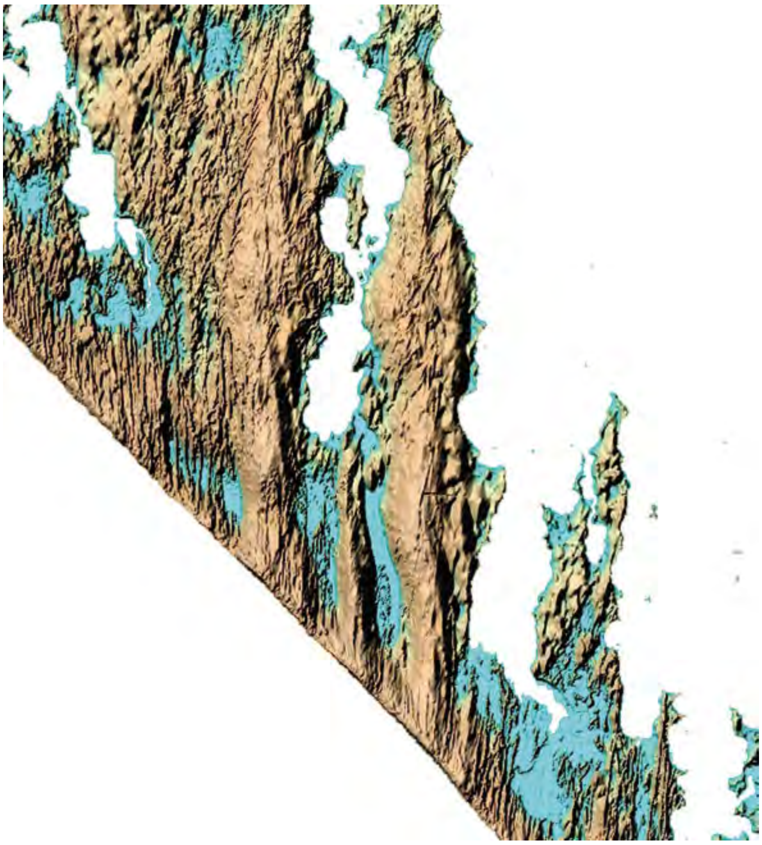

Figure 38. Vertical DEM image of part of the Edel Land Peninsula area, showing broad, massive, linear dunes and narrow seif dunes, oriented north–south (up the page) and abruptly truncated by the Zuytdorp Cliffs fault-line scarp. Inlets seen on the north side of the peninsula (from west to east, left to right) are: Useless Inlet, Brown Inlet, Depuch Loop, and part of Disappointment Loop.

Figure 39. Oblique aerial view of Bellefin Prong looking south, showing seif dunes in the Carrarang Sand, parallel to the prevailing southerly winds. Note the truncation of dunes along the present shoreline, showing that they developed when sea level was lower than it is today.

Figure 40. Aerial view of Heirisson Prong, looking south, showing seif dunes in the Carrarang Sand, truncated at the shoreline. The dunes trend northeast to north-northeast, oblique to the prevailing southerly winds.

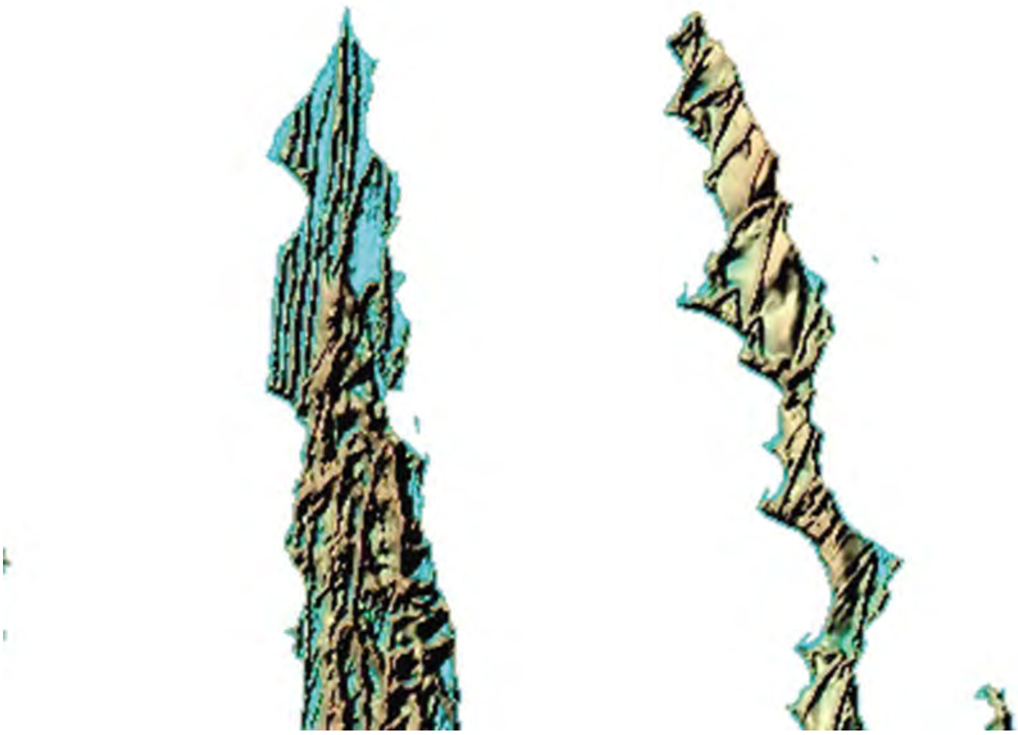

Figure 41. DEM image of the north ends of Bellefin Prong (left) and Heirisson Prong (right), showing seif dunes of the Carrarang Sand truncated along the present shorelines. The seif dunes on Bellefin Prong are oriented north–south, parallel to the prevailing southerly winds, whereas those on Heirisson Prong are oblique to that direction (the reason is unknown). The dunes (now stabilized by vegetation) were formed when sea level was lower and the prevailing winds were stronger than they are today.

Figure 42. Aerial view looking south along Boat Haven Loop, with Carrarang Peninsula on the left and Heirisson Peninsula on the right. Note the well-developed tidal channel in the front part of Boat Haven Loop, with curved bands of seagrass on either side.

Figure 43. Aerial view looking west over Boat Haven Loop, towards Heirisson Peninsula, showing curved bands of seagrass (black) alternating with mega-ripples of ooid or pelloid sand, on either side of the tidal channel. The sand is probably exposed during extremely low tides.

Figure 44. Aerial view looking south along Carrarang Peninsula, showing seif and undulating dunes of the Carrarang Sand. Note the enigmatic, partly rectilinear, feature on the sea floor in the foreground, with mega-ripples of white ooid or pelloid sand adjoining its right side. The black areas on the sea floor are occupied by dense seagrass.

Figure 45. Aerial view looking south over Boorabuggatta Prong, showing long seif dunes of the Carrarang Sand. The top of the Zuytdorp Cliffs fault-line scarp can be seen in the background. The small island (bottom, left) was stripped of guano during the 1850s.

Figure 46. Aerial view looking southwest over the southern part of Henri Freycinet Harbour and Disappointment Loop. The straight line marking the top of the Zuytdorp Cliffs fault-line scarp can be seen in the background.

Figure 47. Aerial view, looking south over Hutchison Embayment and Kopke Promontory, on the east side of Hamelin Pool. The promontory is thought to be controlled by an anticline, and the embayment by a syncline, in underlying Cretaceous rocks.

Figure 48. Aerial view, looking south over Hutchison Embayment, illustrating the complex sedimentological relationships described by Hagan and Logan (1974b).

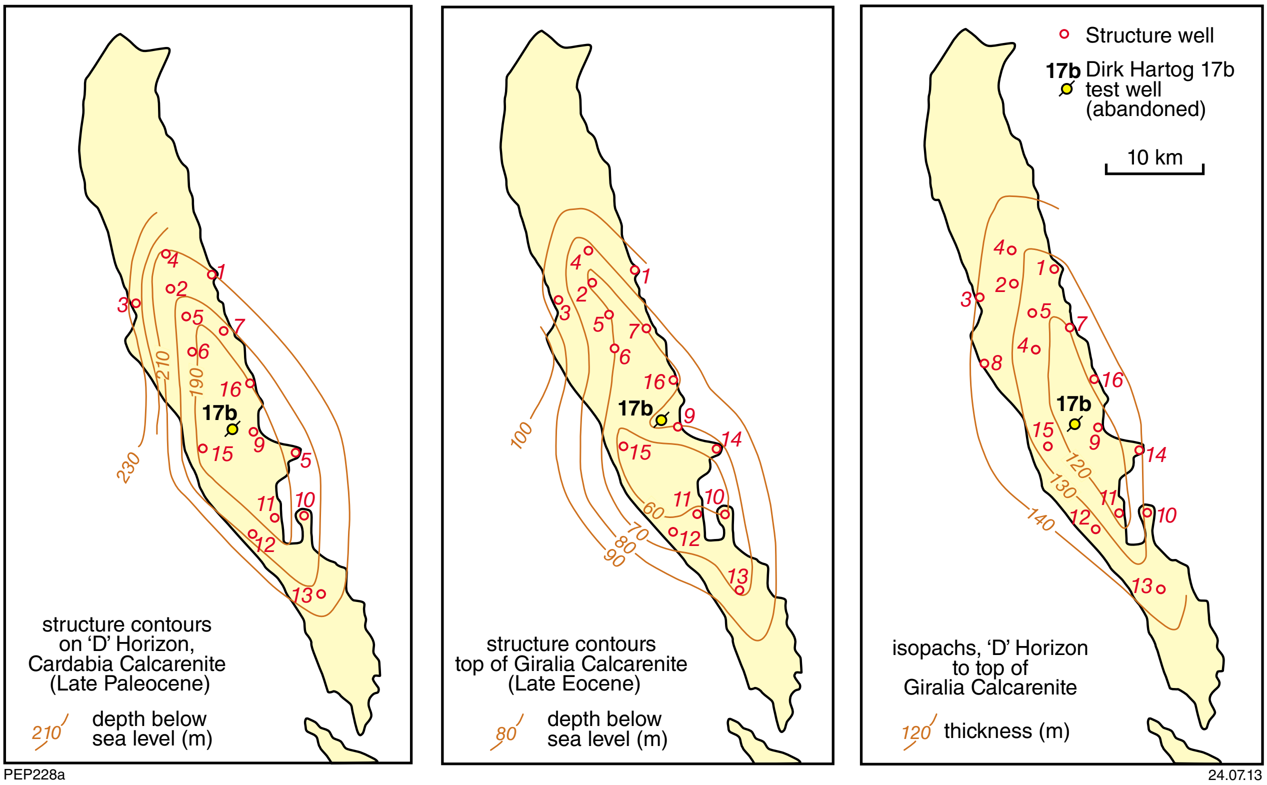

Figure 49. Maps showing structure contours in late Paleocene and late Eocene horizons below Dirk Hartog Island, and isopachs between those horizons. The structure was defined by a series of 16 scout bores and tested for petroleum in one bore (Dirk Hartog 17b), which proved to be dry. The deposition of Pleistocene dunes forming the island was localized by the underlying anticlinal structure. Folding occurred during the Paleocene and Eocene, and may have continued throughout the Pleistocene, perhaps continuing into the Holocene. After Butcher et al. (1984).

Hamelin Pool

Hamelin Pool occupies the southeastern part of Shark Bay. It is a barred from the rest of Shark Bay by Faure Sill, a shallow sand and seagrass bank (Figs 50–52). This sill restricts the interchange with water of the open ocean, so that Hamelin Pool is hypersaline. It is rimmed by intertidal flats, which pass into shallow shelves up to 2 km wide and 6 m deep. The maximum water depth in the basin is about 11 m (Fig. 51).

Hamelin Pool is regarded as a classic example of a barred basin. Because of the restricted circulation, combined with low annual rainfall (average 210 mm) and high annual evaporation (average 2200 mm), the water in Hamelin Pool is hypersaline, with salinity ranging from 55‰ to 70‰, about double that of the open ocean. Hypersalinity is the main reason why stromatolites and the small bivalve *Fragum erugatum* are able to thrive in Hamelin Pool — because of the hypersalinity there is a general lack of animals, especially gastropods, that would otherwise graze on microbes that build stromatolites, and fish that would consume *Fragum erugatum*.

L'Haridon Bight

L'Haridon Bight, like Hamelin Pool, is a hypersaline barred basin. It is bounded on its north side by L'Haridon Sill, which (like Faure Sill) is a sand and seagrass bank cut by a number of tidal channels (Fig. 53).

Tides

A tide gauge was installed at Hamelin Pool 2.75 km northeast of Flagpole Landing (218575E 7078795N) on behalf of GSWA by the then Department of Marine and Harbours (now Department of Transport), from June 1979 to August 1980 (15 months, 416 days; Playford, 1990). Tide data for Hamelin Pool was then compared to that for Denham over the same period (Fig. 54). These readings were continuous, apart from a six-day gap in Hamelin Pool records in April 1980, and a 12-day gap at Denham in July–August 1979. The tide levels at both locations were recorded every 15 minutes.

Another tide gauge was installed by the Baas Becking Geobiological Laboratory at a site near Flint Cliff, between October 1983 and April 1985, with water levels recorded every two hours. The resulting records from this site, compared with those at Carnarvon and Geraldton, were discussed by Burne and Johnson (2012). Their analysis divides the meteorological tides into a seasonal component and a 'short-term irregular cycle' with an average duration of 11 days. Some differences between their interpretations of the astronomical tides and those described here are due to the long recording interval at the Flint Cliff site (two hours) when compared with the much shorter interval at the gauge north of Flagpole Landing (15 minutes).

The term 'tide' is generally understood to refer to water-level changes caused by the gravitational forces exerted by the moon and the sun. However, the term is used here to include changes in water level due to the combined effects of astronomical forces (controlled by the moon and the sun) and meteorological forces (controlled by wind strength and direction, atmospheric pressure, and changes in water temperature). These two components of the tide are referred to here as astronomical tides and meteorological tides, respectively.

Astronomical tides at Shark Bay are classed as mixed diurnal and semidiurnal, and are predominantly semidiurnal (Figs 54, 55; Playford, 1990). The greatest range in water levels during 1979–80, caused by a combination of meteorological and astronomical tides, was 1.59 m at Hamelin Pool and 1.88 m at Denham. An analysis of the astronomical tide component in the Shark Bay area is given by Burling et al. (2003), but without discussion of the much larger meteorological tide component.

At Hamelin Pool and Denham the periodicity of meteorological tides is very variable, and in 1979–80 it was commonly between 10 and 20 days, compared with 12 and 24 hours for astronomical tides. Astronomical tides at Hamelin Pool during the recording period had amplitudes of 15–90 cm, with an average of 45 cm.

The astronomical components of tides are larger at Denham than at Hamelin Pool, whereas the meteorological components are larger at Hamelin Pool (Figs 56, 57). The astronomical tides at Hamelin Pool lagged behind those at Denham by 12 minutes (Fig. 58). This is because of the dampening effects of the Faure Sill, which restricts the flow of seawater into and out of Hamelin Pool. Sea levels along the coast of southwestern Australia are known to rise significantly with low-pressure systems and fall with high-pressure systems (Hodgkin and Di Lolo, 1958). The Shark Bay area is subjected to very strong prevailing southerly winds, and changes in the occurrence and strength of those winds have considerably larger effects on tides than changing atmospheric pressures.

Weekly averages of high-water levels were higher, and of low-water level were lower, at Hamelin Pool than Denham (Fig. 59). The daily changes in water levels during the periods covered in 1979 and 1980 show that the mean tidal range (combined astronomical and meteorological) was greater at Denham (77 cm) than at Hamelin Pool (45 cm; Fig. 60).

The meteorological components of tides in the Shark Bay area commonly exceed the astronomical components, which raises the issue of how best to define the terms 'subtidal', 'intertidal', and 'supratidal' in this area. That question is particularly important in relation to tidal controls on the growth and desiccation of stromatolites in Hamelin Pool. Most authors have not differentiated between the astronomical and meteorological controls of tides in this area, and have used the terms 'intertidal', 'subtidal', and 'supratidal' rather arbitrarily, without quantifying their limits. The 'intertidal zone' has generally been assumed to be that part of the shoreline that is exposed between high-water levels and low-water levels in response to astronomical controls. However, in the Shark Bay area, and especially in Hamelin Pool, the magnitude of the meteorological components of tides is normally greater than that of astronomical tides.

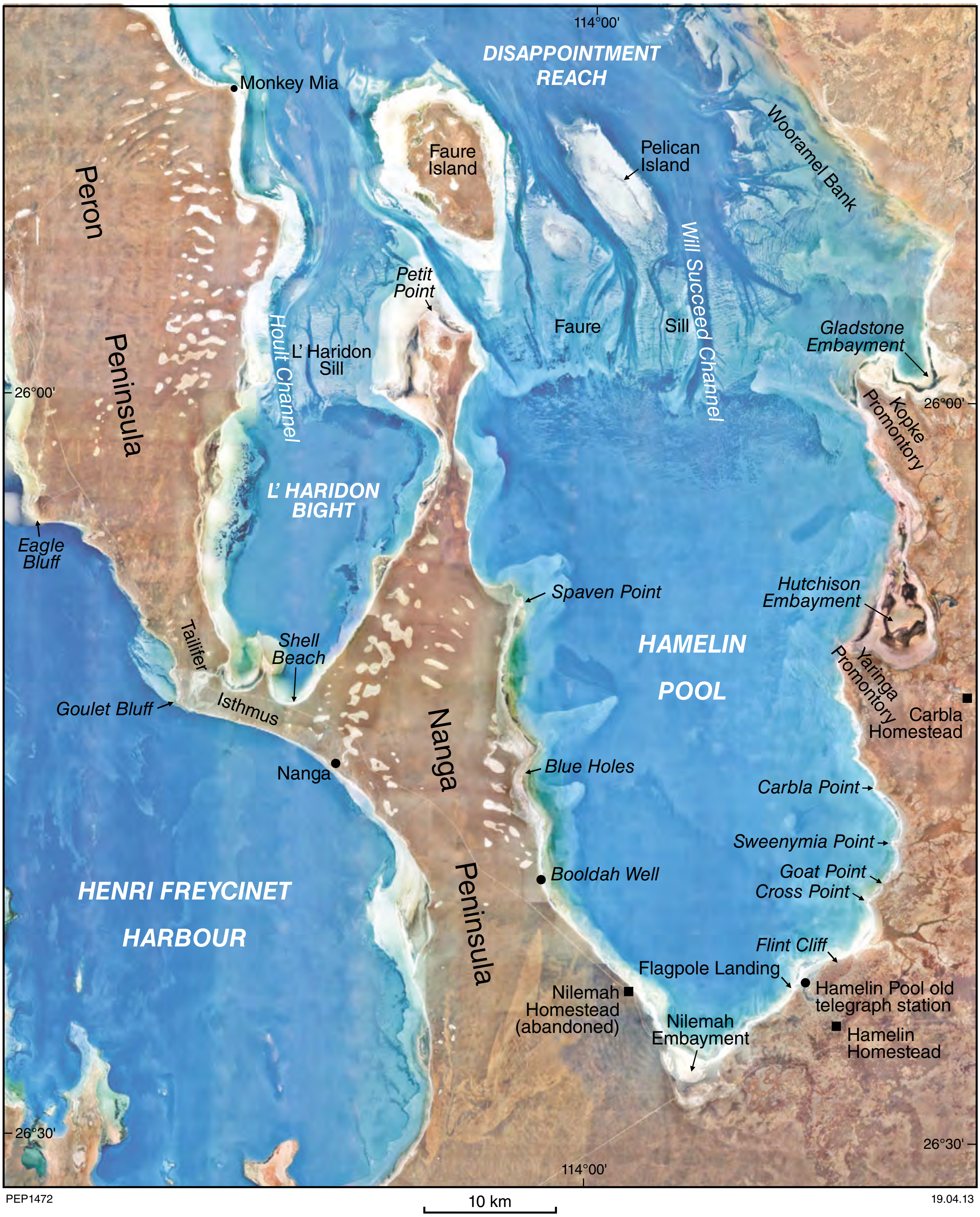

Figure 50. Airphoto mosaic of Hamelin Pool, L'Haridon Bight, Faure Island, Nanga Peninsula, and parts of Peron Peninsula and Henri Freycinet Harbour, collated from photos supplied by Landgate, Western Australia. Note the shallow sand and seagrass banks that form Faure and L'Haridon Sills, and the birridas on the peninsulas.

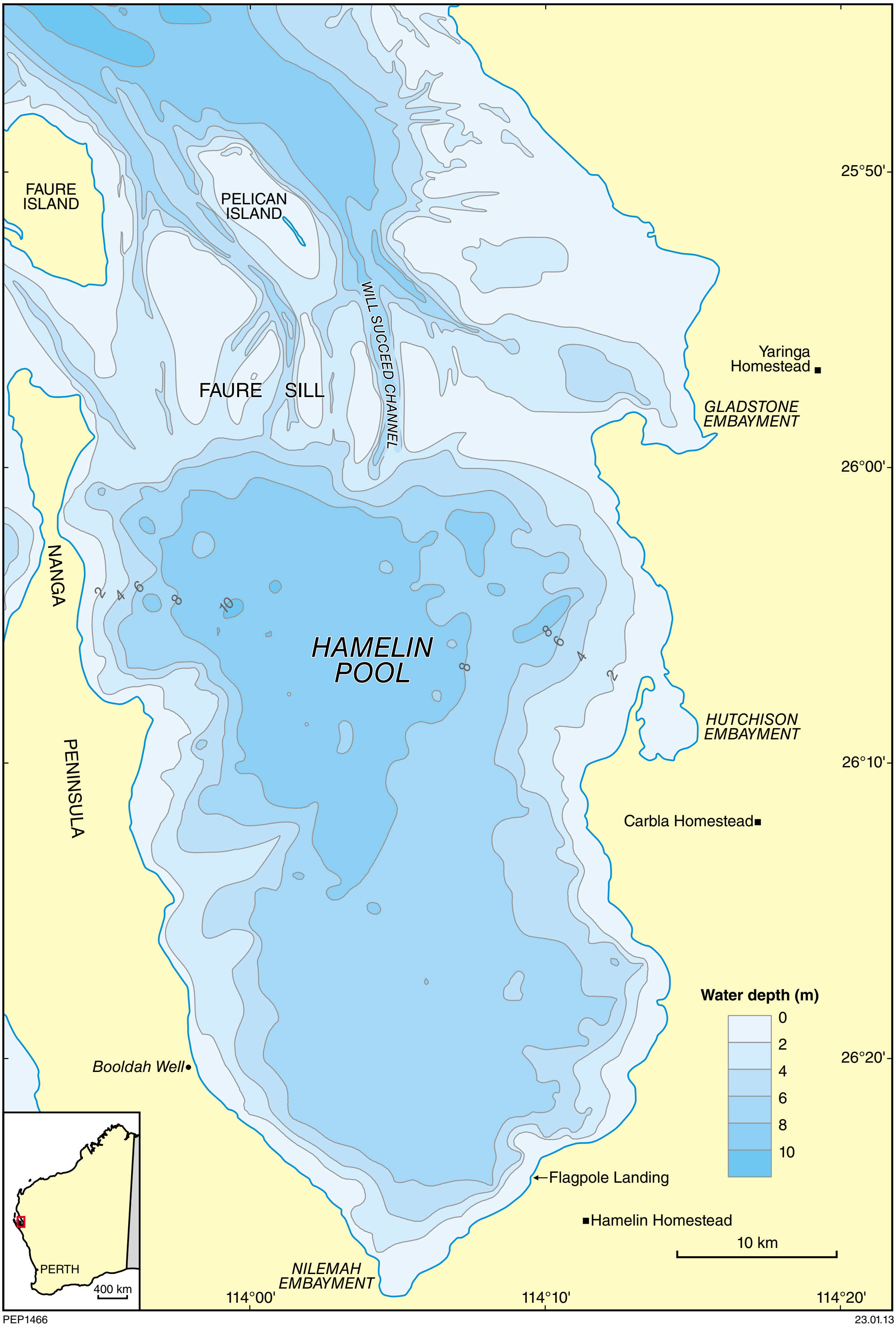

Figure 51. **Bathymetric map of Hamelin Pool and Faure Sill, from a map supplied by Tanya Whiteway of Geoscience Australia (GA), modified from airphotos by GSWA.**

Figure 52. Airphoto mosaic of Faure Sill (between Kopke Point and Faure Island) and L'Haridon Sill (between Faure Island and the east side of Carbla Peninsula), showing localities mentioned in the text. Collated from photos provided by Landgate, Western Australia.

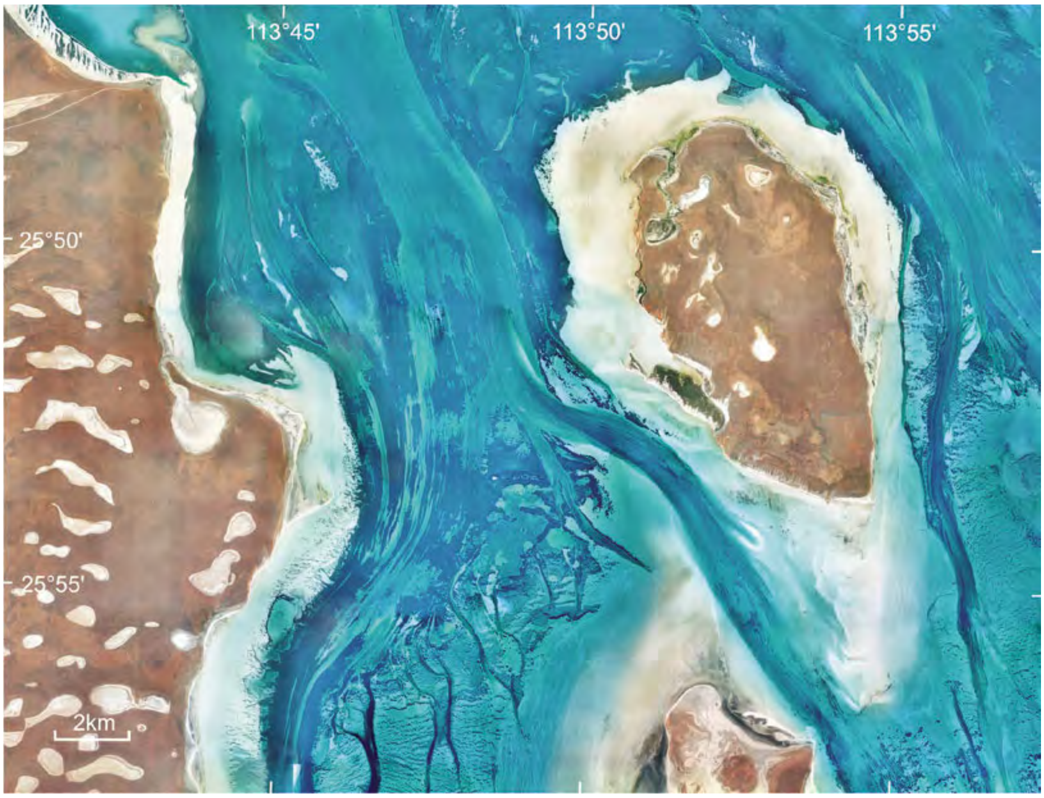

Figure 53. Airphoto mosaic of Faure Island, the eastern part of Peron Peninsula (with many birridas), Petit Point at the north end of Nanga Peninsula, and L'Haridon Sill between Faure Island and Nanga Peninsula. The sill is cut by Hoult Channel on the left, which flows into L'Haridon Bight, and by another major channel on the centre right, that flows into Hamelin Pool. Note also the many smaller channels cutting through the sill, and another large channel to the right (east) of Faure Island cutting through the western margin of Faure Sill. Collated from photos provided by Landgate, Western Australia.

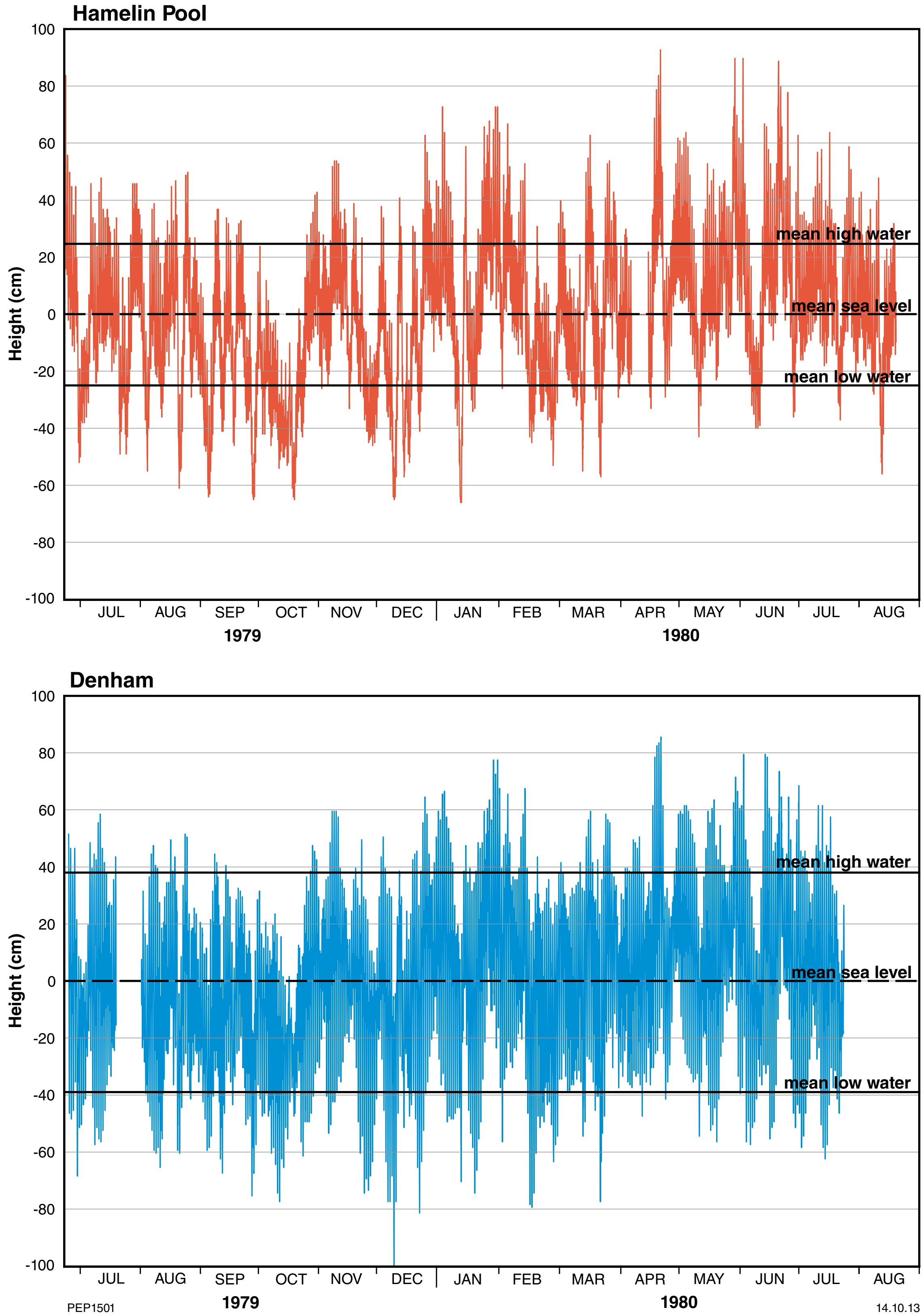

Figure 54. Graphs of tide data from June 1979 to August 1980 for Hamelin Pool, and June 1979 to July 1980 for Denham. These data were obtained by the Western Australian Department of Marine and Harbours (now the Department of Transport) from tide gauges at Hamelin Pool and Denham.

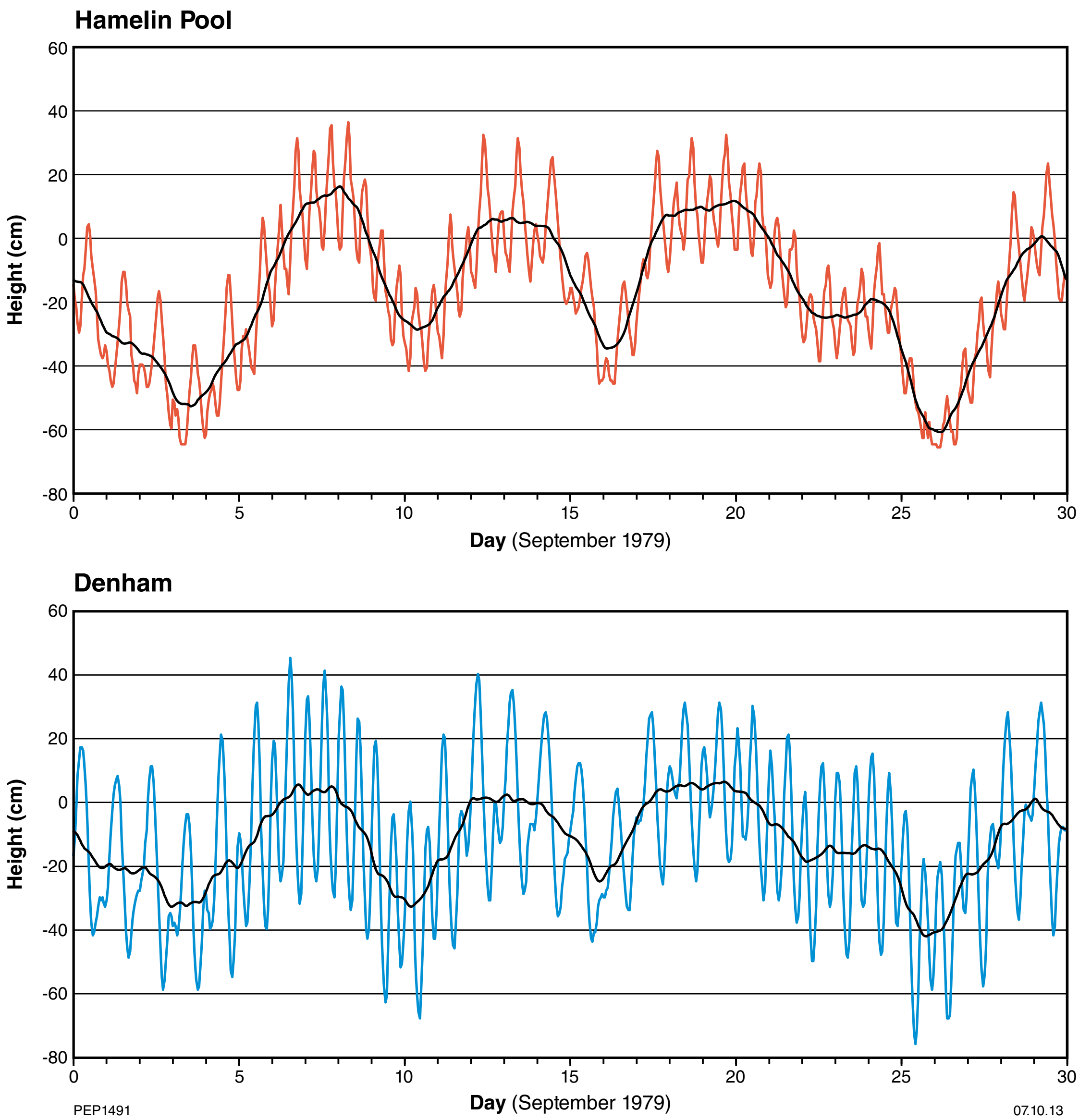

Figure 55. Tide profiles for Hamelin Pool and Denham for September 1979, illustrating the combined effects of astronomical tide components, and inferred meteorological tide components (black lines) at each locality. The astronomical tides are classed as mixed diurnal and semidiurnal. At Hamelin Pool, astronomical tides are smaller, and meteorological tides are larger, than at Denham.

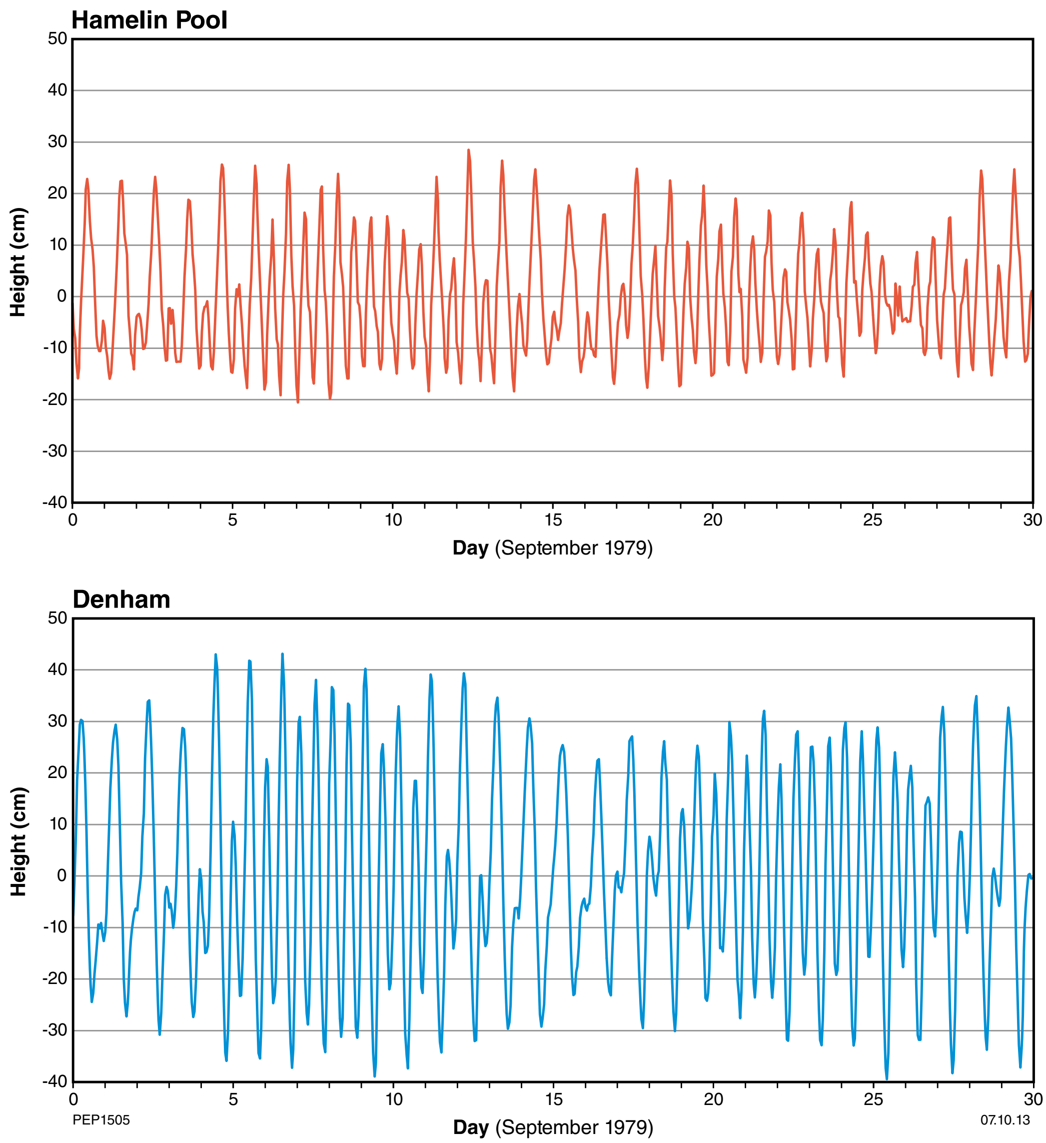

Figure 56. The astronomical components of tides at Hamelin Pool and Denham during September 1979. The astronomical tides are significantly larger at Denham than at Hamelin Pool, because the dampening effect of the Faure Sill restricts the flow of seawater into and out of Hamelin Pool.

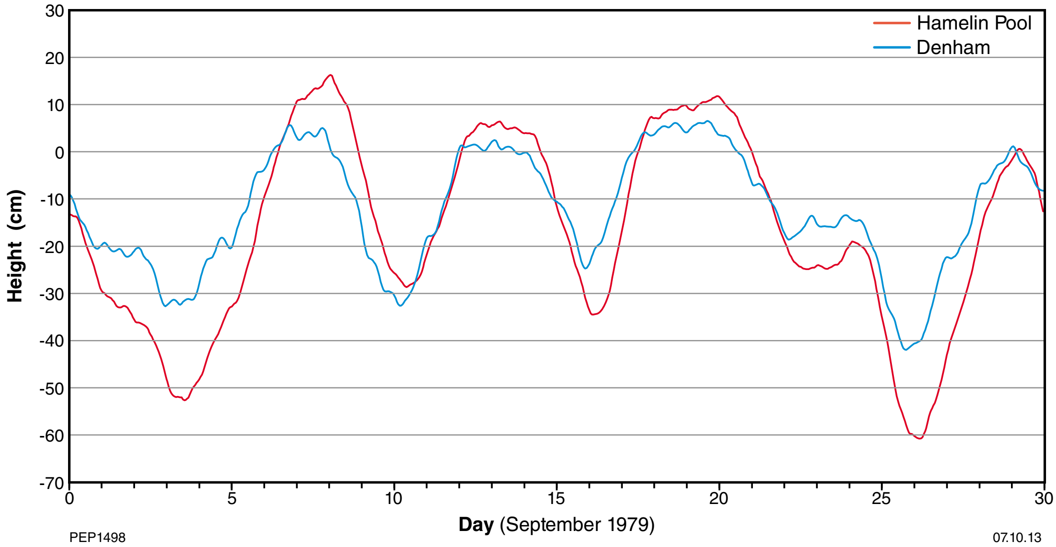

Figure 57. **Inferred meteorological components of tides at Hamelin Pool and Denham during September 1979, showing how these are larger at Hamelin Pool than at Denham.**

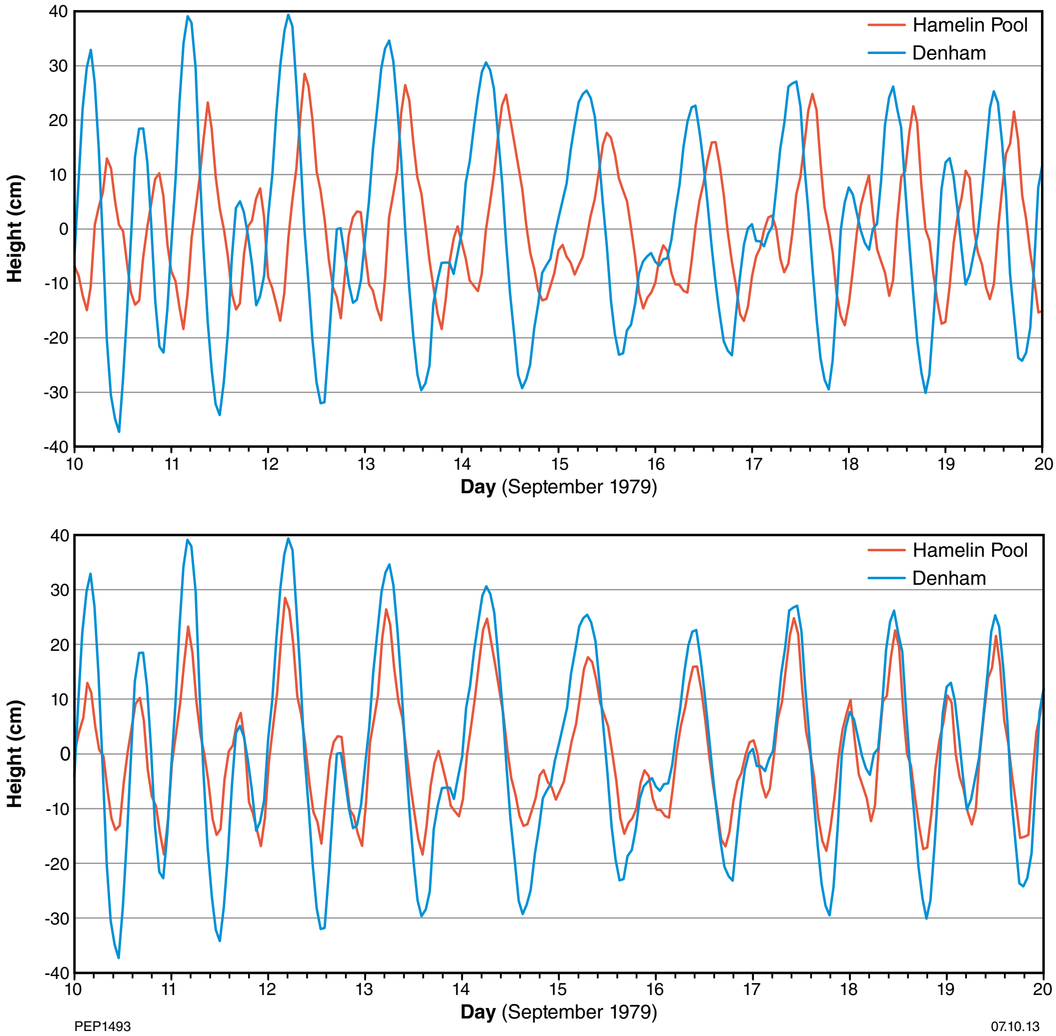

Figure 58. **Astronomical components of tides at Hamelin Pool and Denham during part of September 1979, showing that the astronomical tides in Hamelin Pool lag behind those at Denham. The lower graph shows the coincidence of the records when the Hamelin Pool data are delayed by 12 minutes. Note that astronomical tides at Hamelin Pool are significantly less than those at Denham.**

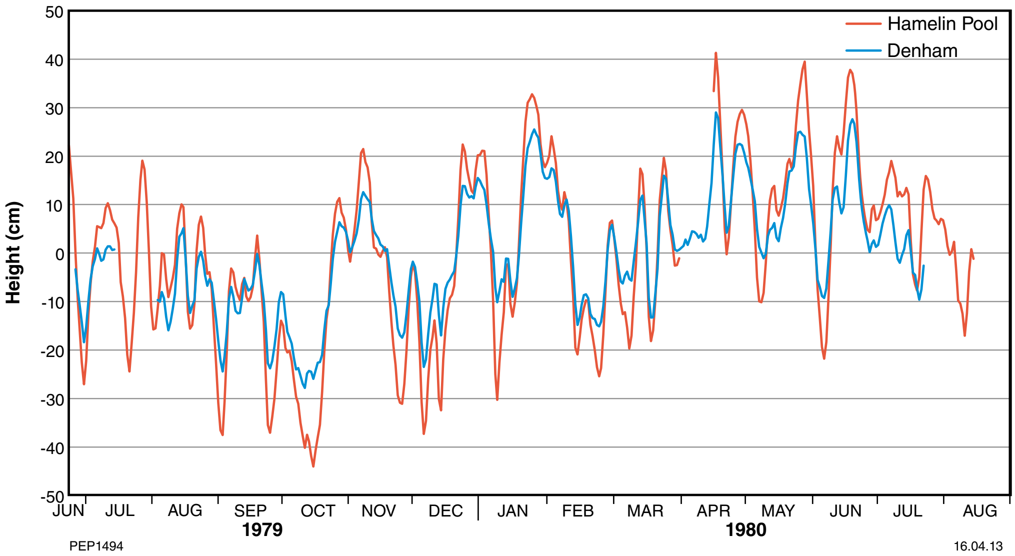

Figure 59 **A comparison between weekly average sea levels at Hamelin Pool and Denham in 1979–80. The weekly average range in sea level is greater at Hamelin Pool than at Denham because the larger meteorological components at Hamelin Pool outweigh its smaller astronomical components. The astronomical components (which are stronger at Denham) are smoothed out by the weekly averaging process.**

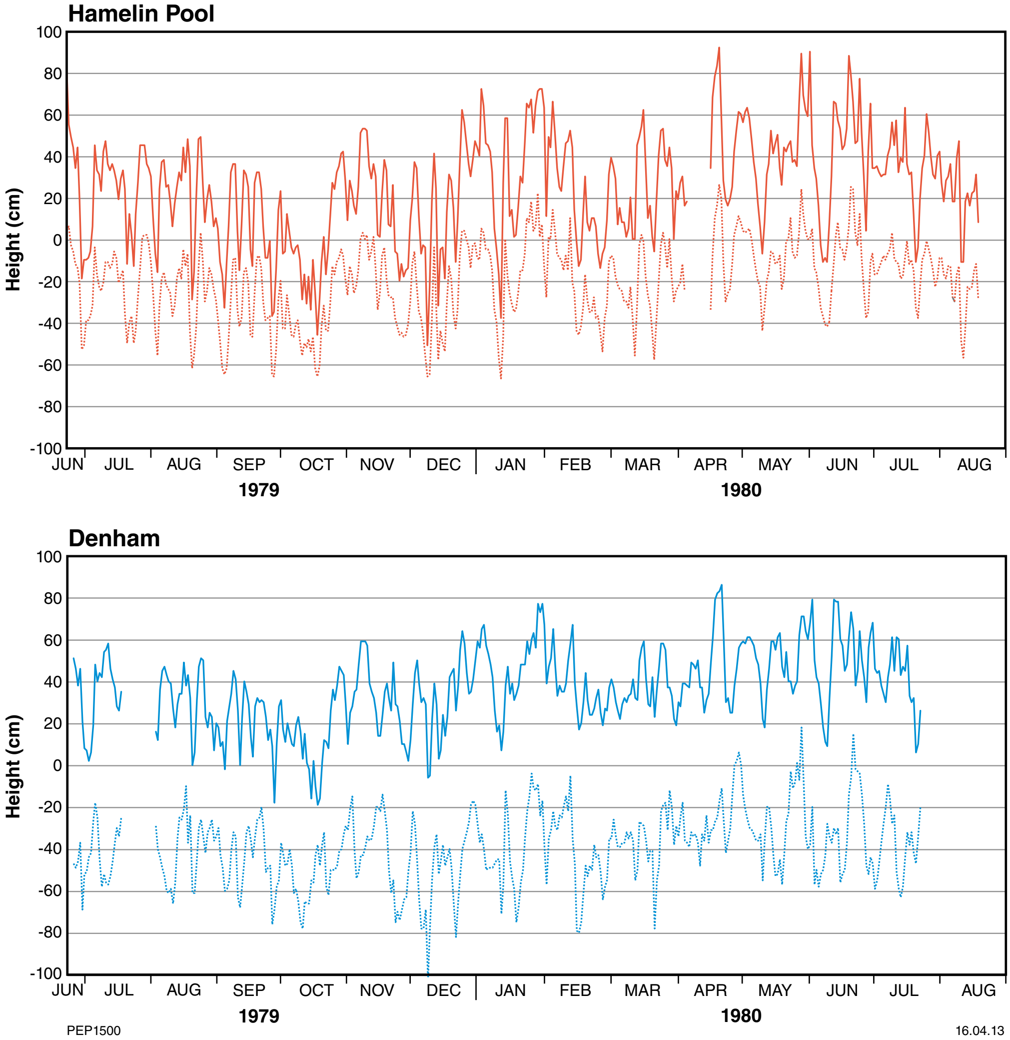

Figure 60. **Graphs showing daily high-water level (solid line) and low-water level (dotted line) at Hamelin Pool and Denham. The mean tidal range (combined astronomical and meteorological) is greater at Denham (77 cm) than at Hamelin Pool (45 cm)**

In this Bulletin the term 'tidal zone' is applied to the part of the coast between extreme highest and extreme lowest tides. In 1979–80 this was from 93 cm above to 66 cm below mean sea level at Hamelin Pool and 85 cm above to 103 cm below mean sea level at Denham (Fig. 61).

The term 'intertidal zone' is defined as that part of the coast extending between mean high-water levels and mean low-water levels, in response to the combined effects of astronomical and meteorological components of the tides. The part of the tidal zone that is above mean high-water level is termed the 'supratidal zone'. Using the 1979–80 data, the supratidal zone extends from 25 to 93 cm above mean sea level at Hamelin Pool and from 38 to 85 cm above mean sea level at Denham. The 'shallow-subtidal zone' is between mean low-water level and the lowest tide level, from –20 to –66 cm at Hamelin Pool and –39 to –103 cm at Denham. The term 'deep-subtidal zone' is used for areas of the sea floor that are deeper than 66 cm below mean sea level at Hamelin Pool and more than 103 cm below mean sea level at Denham (Fig. 61).

A biologically important consequence of the exceptionally large meteorological component of tides at Shark Bay is that life forms in the higher parts of the tidal zone have to endure long periods of continuous exposure on the one hand and continuous submergence on the other. For example, at Hamelin Pool between June 1979 and August 1980 the part of the shoreline at mean sea level was continuously exposed for seven periods of five days and four periods of more than six days, and was continuously submerged for four periods of five days and three periods of more than six days. The periods of continuous exposure/submergence at mean sea level were significantly shorter during the same observation period at Denham. There was only one five-day period of continuous submergence and one five-day period of continuous exposure at mean sea level at Denham during that same period. This contrasts with what could be expected to result from semidiurnal (six hours) and diurnal (12 hours) factors alone.

The cyclones that occasionally pass over Hamelin Pool result in very high water levels. For example, when Cyclone Hazel passed just west of Hamelin Pool on 13 March 1979, sea level along the south coast of Hamelin Pool is deduced to have risen to about 2.8 m, and waves to about 4 m, above mean sea level (observations made on 27 March 1979). It was notable that this cyclone caused very little damage to living stromatolites, because they were protected by becoming deeply submerged as a result of the cyclone-induced surge in water level.

Water levels throughout Shark Bay are usually lower in summer than winter, because the prevailing southerly winds are stronger and atmospheric pressures are higher during the summer months. On the other hand, sea-surface temperatures are hotter in summer (Fig. 62), which tends to raise sea level, although not enough to counter the wind and air-pressure effects.

Sea-surface temperatures in Hamelin Pool generally have a maximum range of some 15ºC, from about 35ºC in summer to 20ºC in winter. Those temperatures are considerably higher and lower respectively than in the open ocean off Shark Bay (Fig. 62).

It was observed during the winter of 2012 that tide levels were higher than in some previous winters, but the reasons for this are unknown. It is clear that more tide, wind, atmospheric-pressure, and water-temperature observations are needed to more fully understand the annual tide fluctuations in Hamelin Pool. Another factor that must partly control water levels and temperatures in Hamelin Pool is the variation in the strength of the Leeuwin Current, which brings warm water down from the north along the southwest coast of Western Australia, although it largely bypasses Shark Bay. The prevailing state of El Niño/La Niña conditions is another factor likely to affect sea levels in Shark Bay.

Faure Sill

Faure Sill is a sand and seagrass bank that extends from Faure Island to Kopke Point. It is 10–20 km wide and is mostly covered by water between 0.5 m and 1 m deep (Figs 50–52, 63–65). North of Kopke Point the sill merges into an extensive seagrass bank, known as the Wooramel Bank, which extends northwest for more than 120 km along the east coast of Shark Bay (Davies, 1970a). Faure Sill is cut by a series of tidal-exchange channels up to 18 km long, 1.5 km wide, and 8 m deep (Figs 63, 64). The largest of these, once used by lighters when transporting wool from local stations, is named the 'Will Succeed Channel' after the lighter '*Will Succeed*' (Fig. 20), once owned by Henry J (Joe) Spaven. This lighter sailed through that channel, into and out of Hamelin Pool, until the mid-1930s.

The seagrasses of the Faure Sill are dominated by *Amphibolis antarctica* and *Posidonia australis*, which grow in bands 20–50 m wide, about 100 m apart, and up to 750 m long (Figs 63–65). The seagrass bands are generally oriented almost east–west, at right angles to the tidal-exchange channels that cut through the sill. They must be controlled by tidal currents, although details of the mechanisms involved have yet to be explained. South of Pelican Island, the sill has some narrow, bifurcating bands of *Amphibolis antarctica*, 1–2 m wide, up to 750 m long, 4–5 m apart, and typically oriented west-southwest to east-northeast (Fig. 65; GA Kendrick, email communication, 2011).

A considerable amount of biological research has been conducted on these seagrass banks (Aires et al., 2011). The seagrass areas support large numbers of dugongs, together with a rich fauna that includes encrusting foraminifers, gastropods, bivalves, scaphopods, and coralline algae (Kendrick et al., 1988). The calcium-carbonate remains of these organisms make major contributions to the sediments of the sill. Those sediments also contain quartz sand, which is subordinate to the organic contributions over most of the sill (Davies, 1970a).

L'Haridon Sill

L'Haridon Sill is a sand and seagrass bank, 10.5 km long and 7 km wide, at the northern end of L'Haridon Bight. It extends west from Petit Point to the coast of Peron Peninsula, and is similar to Faure Sill (Figs 53, 66). The

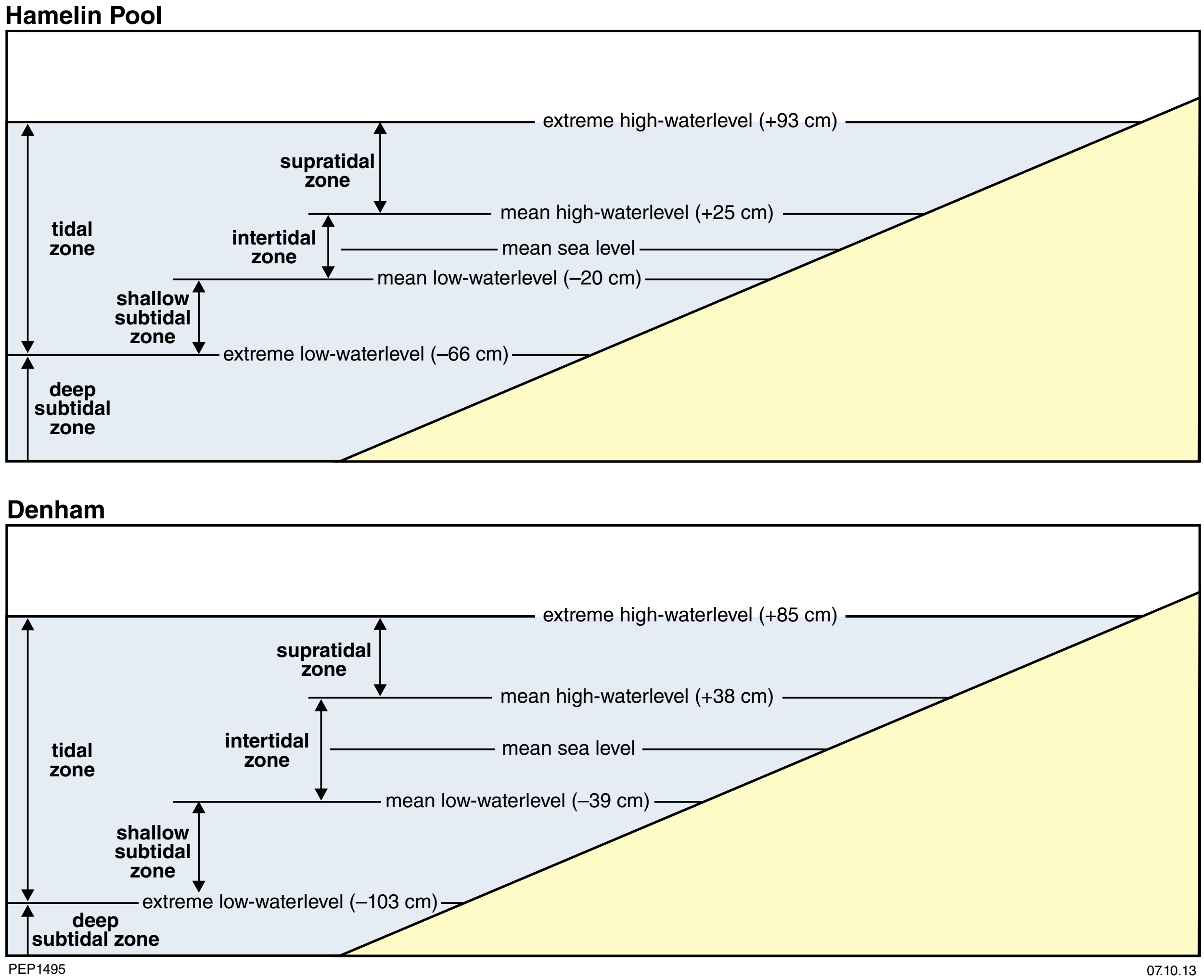

Figure 61. Diagram to illustrate terms used to denote the tidal ranges at Hamelin Pool and Denham, with elevations (based on the 1979–80 data) shown in brackets.

water depth over the sill ranges from less than 1 m to about 2 m. The sill is cut on its western side by a large tidal-exchange channel, up to 8 m deep (Fig. 66), here named the Hoult Channel after the late Mac Hoult, a prominent pearler and pastoralist of Shark Bay whose family once owned Faure Island Station.

Birridas

Birridas (evaporite pans) are conspicuous features of the Peron, Nanga, and Edel Land Peninsulas and parts of Dirk Hartog and Faure Islands. They are filled with gypsum and are commonly subcircular in shape. On Peron Peninsula, Nanga Peninsula, and Faure Island, birridas typically form on the floors of interdune depressions, especially between transverse dunes (Figs 32, 67–71). They are less common on Edel Land Peninsula, where they occupy interdune depressions between north–south-trending seif dunes.

The flat upper surfaces of birridas are commonly close to mean sea level, but some are as much as 5 m above that level. Birridas commonly have a central ‘plateau’ covered with sparse samphire bushes of an undescribed species, surrounded by a shallow circular depression or ‘moat’, about a metre below the top of the plateau (Figs 67, 68). A larger and darker coloured samphire species (also undescribed) commonly grows around the side of each plateau, adjacent to the moat. Moats commonly fill with water after heavy rain.

Little Lagoon, near Denham townsite, is a former birrida now inundated by the sea and connected to Denham Sound by a narrow channel (Figs 72, 73). Similar flooded birridas are known in several other areas near the coast. Big Lagoon, in the northwest part of Peron Peninsula, formed where a chain of birridas was invaded by the sea in Holocene times, possibly as a result of tilting on the west flank of the anticline below Peron Peninsula (Figs 74, 75).

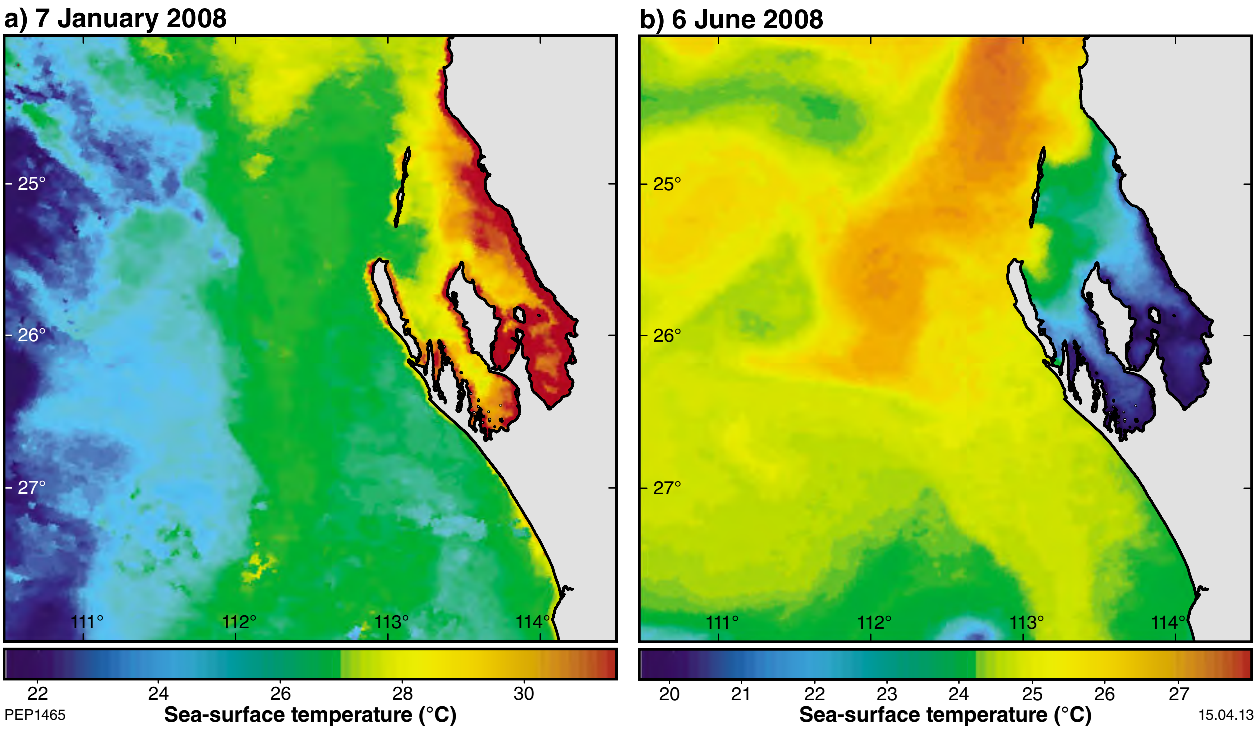

Figure 62. Satellite-derived sea-surface temperatures for Hamelin Pool and adjoining areas on 7 January (left) and 6 June 2008 (right), illustrating how those temperatures are warmer in summer and colder in winter than in the adjoining open ocean. Images provided by CSIRO, Hobart.

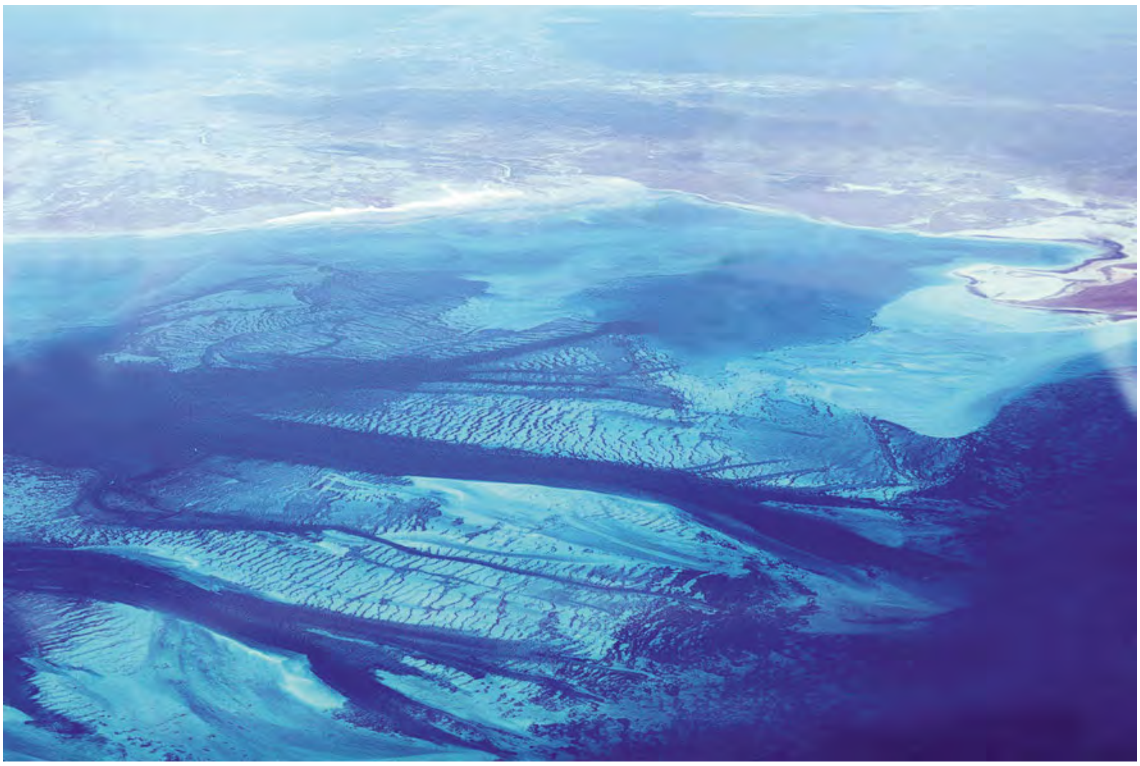

Figure 63. Aerial view of part of Faure Sill looking east towards Kopke Point and Gladstone Embayment (centre right), showing tidal-exchange channels and dark 'stripes' of seagrass at right angles to those channels.

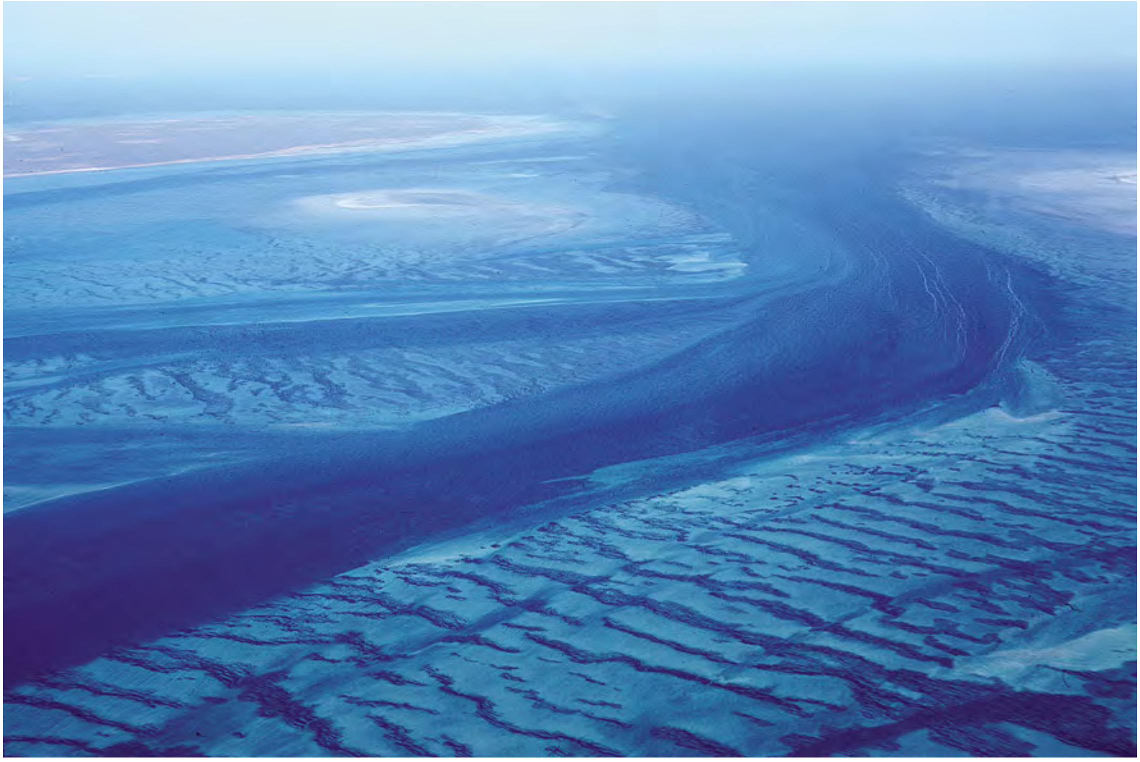

Figure 64. Aerial view of part of Faure Sill looking west towards Faure Island, showing tidal-exchange channels and dark 'stripes' of seagrass, separated by sand. The largest channel, about 1.5 km wide, in the middle of the photo, is the Will Succeed Channel.

Figure 65. Aerial view of distinctive fine networks of seagrass on Faure Sill, south of Pelican Island, beside widely spaced seagrass stripes.

Figure 66. Aerial view of L'Haridon Sill looking southwest, showing tidal-exchange channels passing through the sill into L'Haridon Bight on the left. A small part of Nanga Peninsula is visible in the left foreground, and the southern part of Peron Peninsula, with many birridas, can be seen in the middle. Hoult Channel, the largest tidal-exchange channel in this sill, is near Peron Peninsula.

Figure 67. Aerial view looking west over a birrida, filled with gypsum, on the west side of Peron Peninsula, near the old Peron Homestead. This typical subcircular birrida has a diameter of about 0.4 km. Note the dark circle in the inner part of the birrida, formed by dense samphire shrubs growing beside a 'moat', which fills with water after heavy rain. The 'moat' is below the edge of the more-elevated central 'plateau' with sparse samphire shrubs. The rest of the birrida supports little vegetation.

Figure 68. View on the ground looking northwest over the birrida shown in Figure 67. Note the elevated 'plateau', covered with sparse samphire shrubs, in the centre, surrounded by a dense dark band of samphire and a shallow 'moat'.

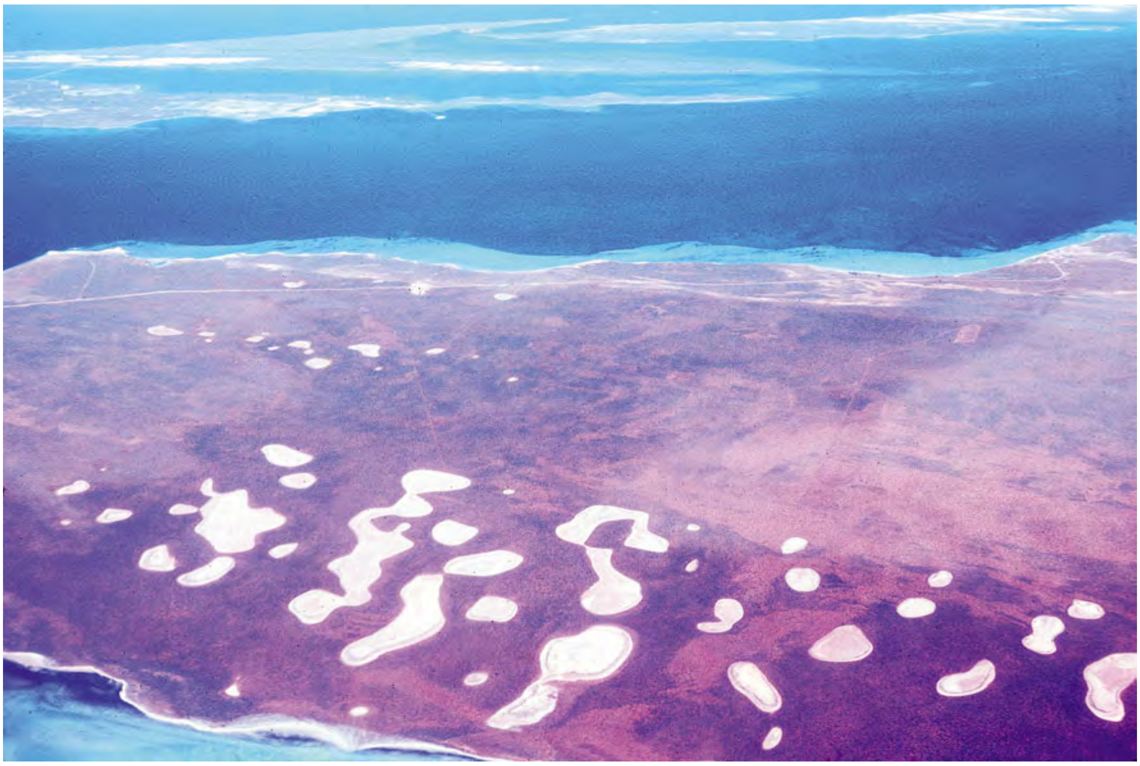

Figure 69. Aerial view looking west over part of Peron Peninsula with numerous birridas, towards Edel Land Peninsula and Dirk Hartog island in the distance.

Figure 70. Aerial view looking southwest over parts of Hamelin Pool (foreground), Nanga Peninsula (with birridas), L'Haridon Bight, and Tailifer Isthmus.

Figure 71. Aerial view looking south over the southern part of Nanga Peninsula, showing elongate parallel birridas that have formed in interdune areas between transverse sand dunes.

Figure 72. Aerial view looking east over Little Lagoon near Denham. This marks a birrida that has been drowned by the ingress of the sea. It is connected to Denham Sound along a narrow winding channel.

Figure 73. Aerial view looking northwest over Little Lagoon, with Denham township in the left background.

Figure 74. Aerial view looking south over Big Lagoon, a chain of drowned birridas on the northwest side of Peron Peninsula.

Figure 75. Aerial view looking east over a drowned birrida connected with Big Lagoon. Peron Sandstone outcrops in low cliffs on the left.

Blue holes

Intriguing features of the east side of Hamelin Pool are 12 circular holes, up to 2.5 m deep and 2 to 30 m across, in a wide tidal flat, up to 650 m wide, at around 794540E 7092070N. For some time after rain, the water in these holes becomes dark blue, and accordingly these features are referred to as 'blue holes' (Figs 76–85).

The periodic flow of rainwater into and around the holes results in a surface water layer (up to 0.5 m thick) that is lower in salinity, density, and temperature than the underlying hypersaline water, forming what is known as a solar pond. This stratification in the water column is responsible for both the blue colour and the high temperature of the lower water layer. The temperature difference between these two layers can be up to 20ºC. The contact between the layers is abrupt, and closed shells of the bivalve *Fragum erugatum* (washed in from Hamelin Pool) can sometimes be seen 'floating' on the contact between the two layers due to the higher density of the lower, more-saline, water. Dead samphire bushes that have blown into some of the deeper blue holes have become covered with gypsum (Fig. 85).

The origin of these blue holes has not been proved, but they have probably formed as a result of groundwater dissolution of gypsum in a birrida that has been covered by sediment of the tidal flat. Gypsum was probably dissolved in lower salinity groundwater below the tidal flat, resulting in the collapse of overlying sediment. Such a collapse is seen to have resulted in the formation of one of the most recent blue holes (Figs 81, 82).

Stratification in the water column eventually breaks down as a result of inundation during very high tides, or through wind action. Once the water in the holes loses its density and temperature layering, it also loses its blue colour, becoming greenish and more translucent (Figs 83, 84).

Dune systems

Six types of dunes are recognized in the area: massive, seif, parabolic, transverse, barchan, and undulating dunes (Figs 30–32, 38–41, 86–94). Some bare, flat, wind-blown sand sheets also occur, with only minor dune developments.

The red colour of dune sands at and near the land surface over many parts of the Shark Bay area is a striking feature of this area. Similar red sands occur throughout much of the arid northern parts of Western Australia, extending south to about 28ºS. Further south, in wetter climates (as in the Perth area), residual and wind-blown sands are typically white, yellow, or black. Thin coatings of iron oxide on the sand grains are responsible for the red and yellow colours (anhydrous iron oxide for red sands, hydrous iron oxide for yellow sands). The black colour of some sands is due to their high content of organic carbon.

Test pits for mineral sands south of Hamelin Pool show that the sands below near-surface calcrete are yellow, whereas those above the calcrete are red (Environmental Protection Authority, 2005).

Massive dunes

Massive dunes are the largest and oldest dunes in the area. They consist of limestone and calcareous sand, in massive bodies up to 5 km across, that rise as much as 90 m above the adjoining interdune valleys. These dunes are elongated north–south and have formed in response to the prevailing very strong southerly winds (Fig. 38). Most are composed of mid-Pleistocene Tamala Limestone, usually with an overlying layer of sand.

Seif dunes

Seif dunes in the Shark Bay area are long, narrow dunes up to 40 km long (Figs 38–41, 45, 86–88). Most have formed parallel, or nearly parallel, to the prevailing southerly winds, and are best developed along Edel Land Peninsula. Some coalesce at their northern ends, forming parabolic dunes. The seif dunes are typically about 10 m high, and the distance between their crests ranges from about 250 to 500 m.

Most seif dunes are composed of medium-grained limesands, with variable amounts of quartz sand. Nearly all of those dunes are now fixed by vegetation and many are partly cemented below the surface, although a few have been reactivated in recent years, possibly as a consequence of intense grazing, especially by feral goats.

A horizontal core sample taken from a weakly cemented seif dune in a road-cut south of Brown Inlet (756707E 7053917N) has been optically stimulated luminescence (OSL) dated as mid-Holocene, 4900 ± 700 years BP (Matt Cupper, 2010, written comm.), but many of those seif dunes must be older than this, as they are truncated at the present shoreline, and are thought to have been deposited during the early Holocene when sea level was significantly lower than it is today (Figs 39–41).

Bellefin Prong, Heirisson Prong, Boorabuggatta Prong, and Carrarang Peninsula probably formed along massive Pleistocene dunes that are now partly overlain by weakly lithified Holocene to upper Pleistocene seif dunes.

Parabolic dunes

Parabolic dunes are long, scoop-shaped dunes that are best developed on Peron Peninsula (Figs 31, 32, 89) and Dirk Hartog Island and also occur in parts of Edel Land Peninsula and south of Hamelin Pool (Fig. 89). On Peron Peninsula the parabolic dunes are truncated by the sea along the northeast and southwest coasts of the peninsula, showing that they were formed when sea level was lower than it is now (Fig. 32).

The longest parabolic dune on Peron Peninsula is about 28 km long and as much as 30 m high. It consists of two 'arms', up to about 5 km apart, joining in a smooth curve at the leading (northern) end of the dune (Fig. 32). Such dunes are usually composed of medium-grained quartz sand, covered by thin films of anhydrous iron oxide. Some are calcareous, especially where they interfinger with Tamala Limestone along the southwest coast of the peninsula. They generally have only low relief and are oriented north to northeast, essentially parallel to the prevailing southerly winds. The dunes have not been dated, but are interpreted as late Pleistocene and/or early Holocene in age.

Transverse dunes

Transverse dunes are low parallel dunes of quartz sand that have formed between the arms of parabolic dunes on Peron Peninsula. They generally trend approximately east–west, and are typically 1–2 km long, 2 km apart, and 10 m high. Birridas commonly occupy depressions between transverse dunes (Fig. 32).

Barchan dunes

Barchan dunes are distinctive crescent-shaped mobile dunes of pale-red limesand, best developed in two north–south belts about 10–18 km south of Tamala Homestead (Figs 86, 90–94). They also occur, to a lesser extent, elsewhere on Edel Land Peninsula and Dirk Hartog Island. The two belts on Tamala Station, almost bare of vegetation, are 500–800 m wide, and 7.5 and 8.5 km long. Each dune has its convex side directed upwind and has steep concave slopes between its 'wings', oriented downwind. The 'wings' are about 50–200 m apart and 50–150 m long.

Undulating dunes

Small, gently undulating, irregularly shaped sand dunes, up to about 10 m high, cover large areas south of Hamelin Pool (Figs 86, 89). Most are composed of quartz sand, and generally lack any clear orientation in relation to the prevailing wind direction.

Figure 76. Vertical airphoto (north to the top) showing circular blue holes located in a broad microbial tidal flat, rimmed on the east side by a narrow dark-coloured stromatolite reef, with adjoining subtidal stromatolites below water level. The supratidal shoreline, west of the blue holes, is marked by a narrow white band of *Fragum erugatum* shells. The adjoining sparsely vegetated Hamelin Coquina was deposited over a small birrida, part of which is seen in the left centre. Red sands of the Denham Sand occur west, north, and south of that birrida. The width of the field of view is about 1.9 km. Airphoto courtesy of Landgate, Western Australia.

Figure 77. **Airphoto looking southeast over the blue holes. This photo was taken at a time when the water levels were high in the holes, which were dark blue as a result of density, salinity, and temperature stratification in the water.**

Figure 78. **Closer aerial view looking south over the blue holes at a time when water levels were high and water in the blue holes was strongly stratified.**

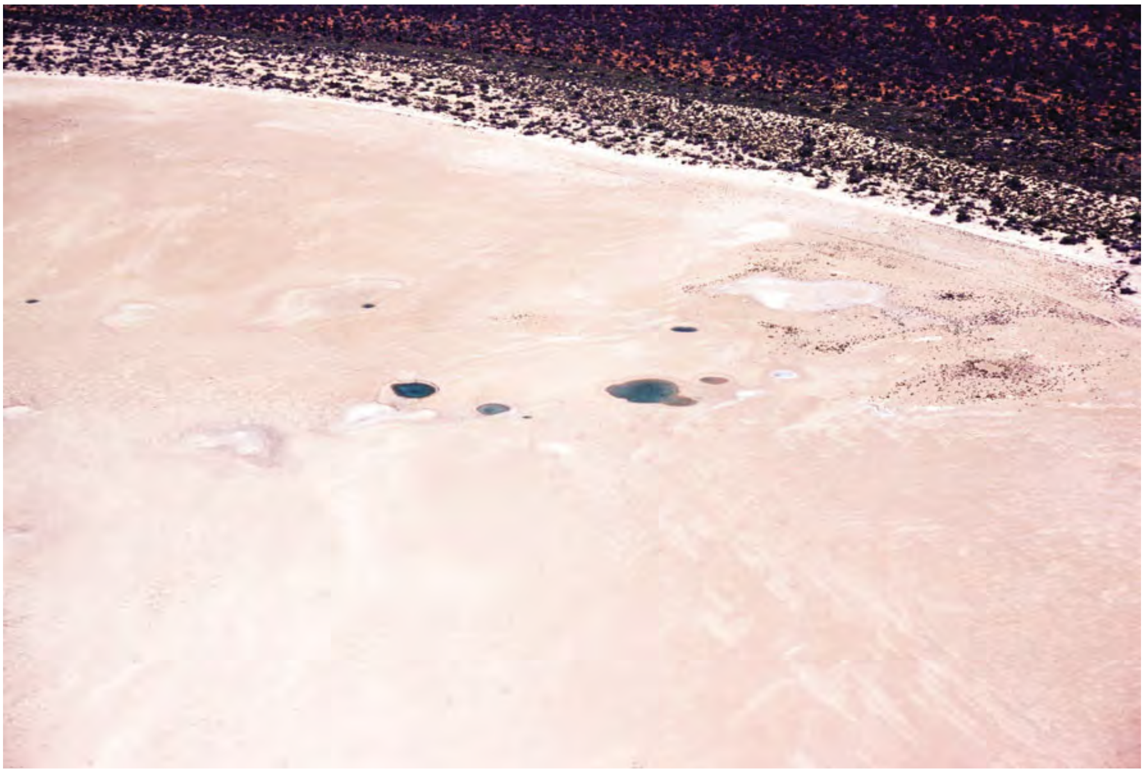

Figure 79. Aerial view looking west over the holes after most had dried out. The remaining holes contained greenish water, no long stratified.

Figure 80. View looking east over the largest blue hole, at a time when there was strong temperature and salinity stratification in the water column, with cooler and lower salinity in the shallower water and hotter and higher salinity in the deeper water. As a result of this stratification the holes were coloured dark blue.

Figure 81. Small hole, about 2 m across, thought to have resulted from collapse, during 1997, due to dissolution in groundwater of gypsum in an underlying birrida.

Figure 82. Photo taken in 2010 of the same hole shown in Figure 81, after further collapse had occurred, enlarging the hole to be about 3 m across. The dark layer in deeper water at the base of the hole was anoxic and had a higher temperature and salinity than the overlying water.

Figure 83. View looking west over one of the holes, which at that time was pale green, because there was no salinity or temperature stratification in the water column.

Figure 84. Another of the holes, where part of the floor had collapsed. That part is darker green, perhaps because of minor stratification, whereas the unstratified part above is very pale green.

Figure 85. Crystalline gypsum coating a dead samphire bush, from the base of the blue hole shown in Figure 80.

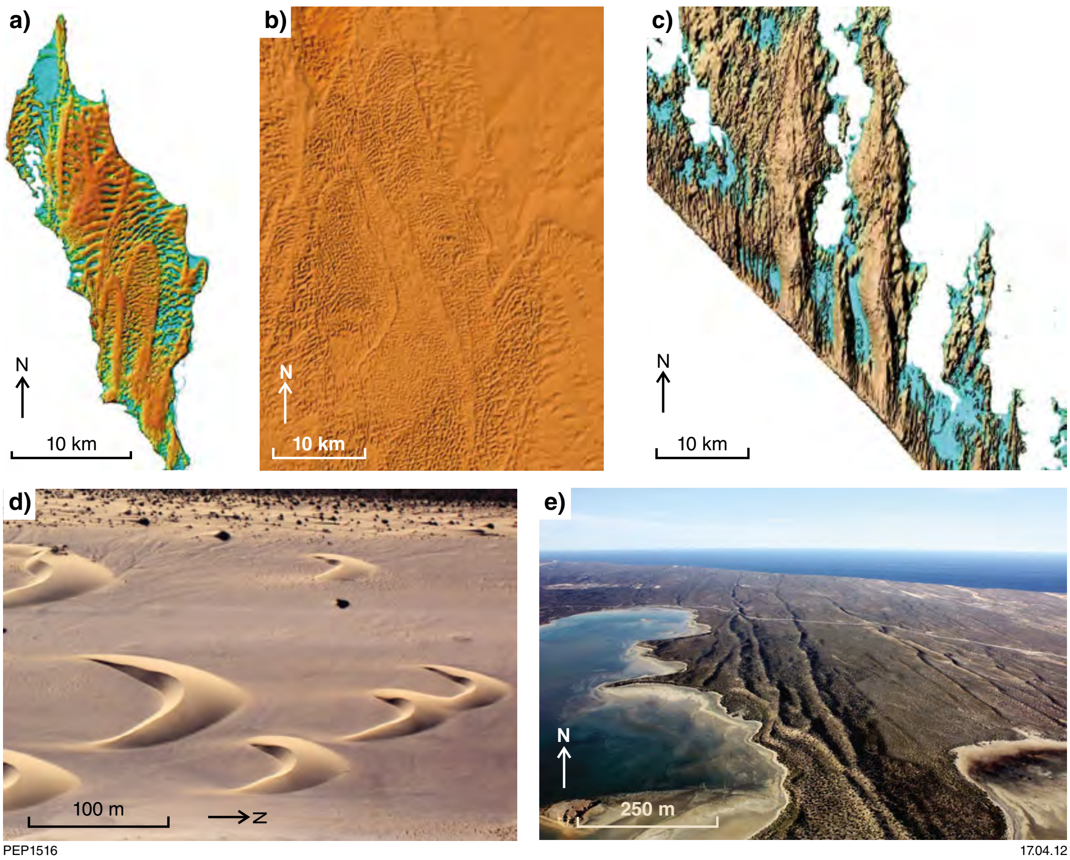

Figure 86. Images illustrating the various types of dunes developed in the Shark Bay area — (a) parabolic and transverse dunes in Denham Sand on Peron Peninsula, (b) undulating and parabolic dunes in Nilemah Sand south of Hamelin Pool, (c) massive and seif dunes in Tamala Limestone and Carrarang Sand on Edel Land Peninsula, (d) barchan dunes in Carrarang Sand on Tamala Station, and (e) seif dunes in Carrarang Sand at Boorabuggatta Prong and Edel Land Peninsula.

Figure 87. Aerial view looking northeast over part of the Zuytdorp Cliffs and Edel Land Peninsula, showing well-developed north–south seif dunes, fixed by vegetation.

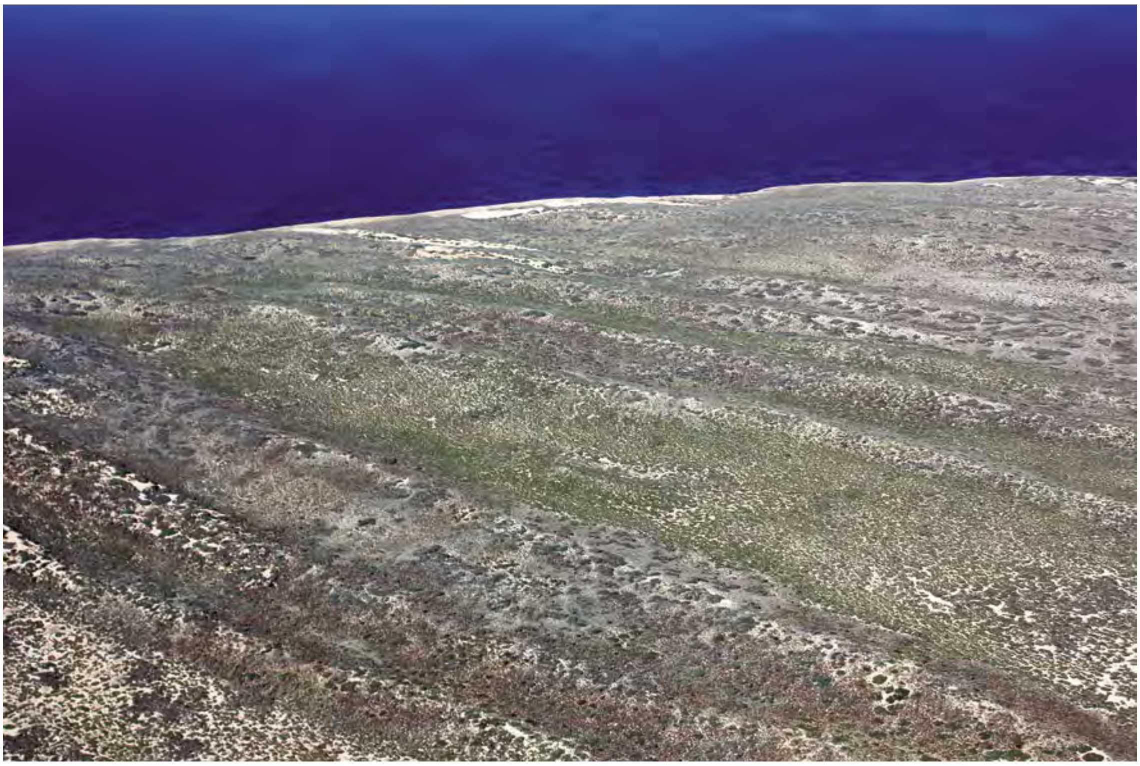

Figure 88. Aerial view of vegetated north–south seif dunes on Edel Land Peninsula, behind the Zuytdorp Cliffs. The dunes are about 10 m high and 250 to 500 m apart.

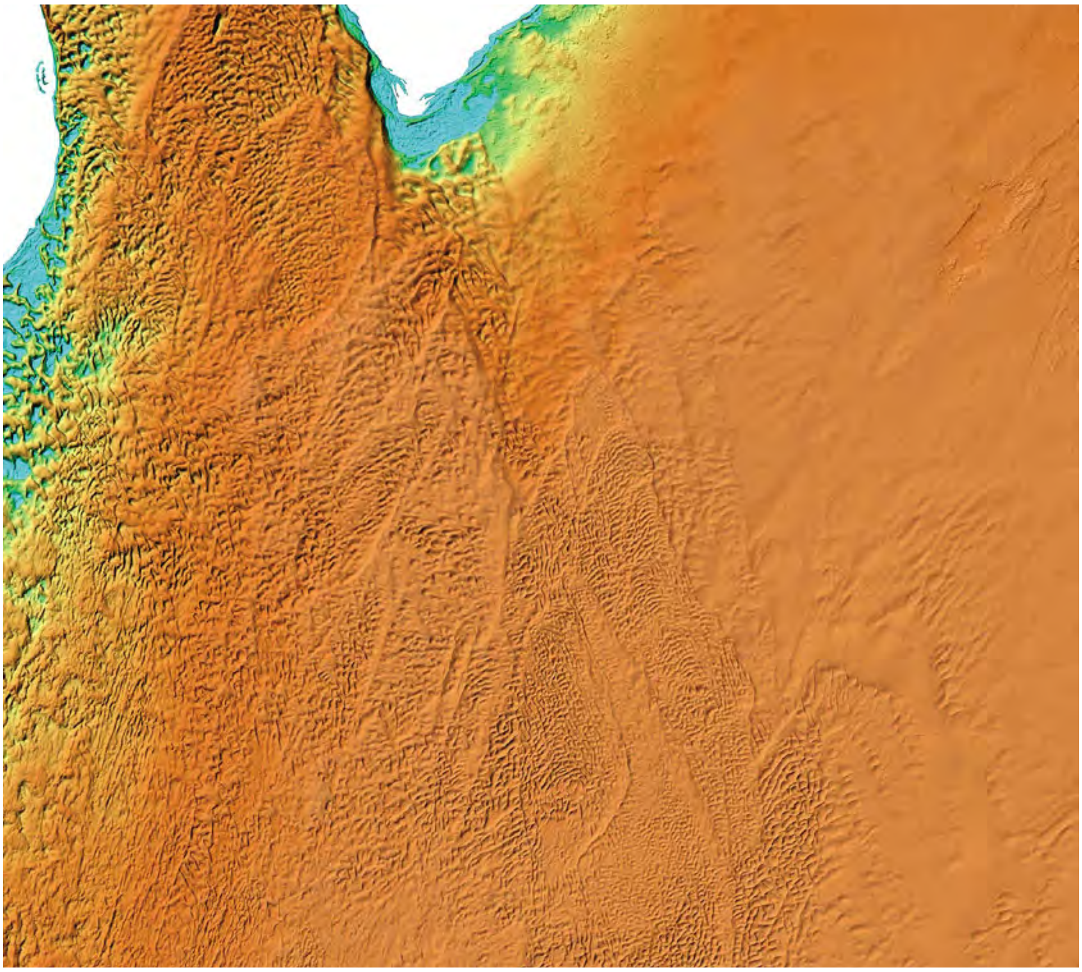

Figure 89. **DEM image of the area south of Hamelin Pool, showing undulating and parabolic dunes developed in Nilemah Sand.**

Figure 90. **Aerial view, looking east, of barchan dunes in a belt of mobile Carrarang Sand south of Tamala Homestead. The prevailing southerly wind blows from right to left.**

Figure 91. Aerial view, looking east, of barchan dunes in two belts of mobile Carrarang Sand south of Tamala Homestead. The prevailing southerly wind blows from right to left.

Figure 92. Aerial view looking southwest over a belt of mobile barchan dunes in the Carrarang Sand south of Tamala Homestead. The belt of dunes begins a short distance behind the the Zuytdorp Cliffs (upper right) and the width of the belt in the lower part of the photo is about 600 m.

Figure 93. Aerial view of the same two belts of mobile barchan dunes in the Carrarang Sand, south of Tamala Homestead, looking northeast. The width of the belt of dunes in the lower-right part of the photo is about 500 m. Vegetated seif dunes are seen in the left foreground.

Figure 94. Ground view of a barchan dune in Carrarang Sand, about 9.5 km south of Tamala Homestead. The dune is crescent shaped, about 70 m wide and up to 10 m high. The highest part of the dune is on the south (upwind) side and its two 'wings' point north (downwind).

Islands

There are scores of islands in the Shark Bay area, ranging from tiny islets covering less than a hectare to Dirk Hartog Island, the largest island in Western Australia, covering more than 600 km^2.

Dirk Hartog Island

This long narrow island, in the central west part of Shark Bay, trends north-northwest to south-southeast. It is nearly 80 km long and averages about 8 km wide (Fig. 95). At its southern end the island is separated from Edel Land Peninsula by a narrow channel known as South Passage (in its western part) and Blind Strait (in its northeast part).

Much of the island is covered by dune sands and low scrub (Fig. 96). Eolianite of the Tamala Limestone outcrops along most of the west coast and on headlands along the east coast.

Dirk Hartog Island was operated as a sheep station from about 1868 until 2004 (Fig. 97), after which it was purchased by the Western Australian Government to become a national park. It is intended that all exotic animals (cats, goats, and sheep) will be eliminated over the next few years, so that the island can become a conservation area through the re-introduction of marsupials and other native fauna. There are no foxes on the island, and the biggest challenge will be to eliminate cats, which are thought to have been mainly responsible for extinction of the island's native-marsupial fauna.

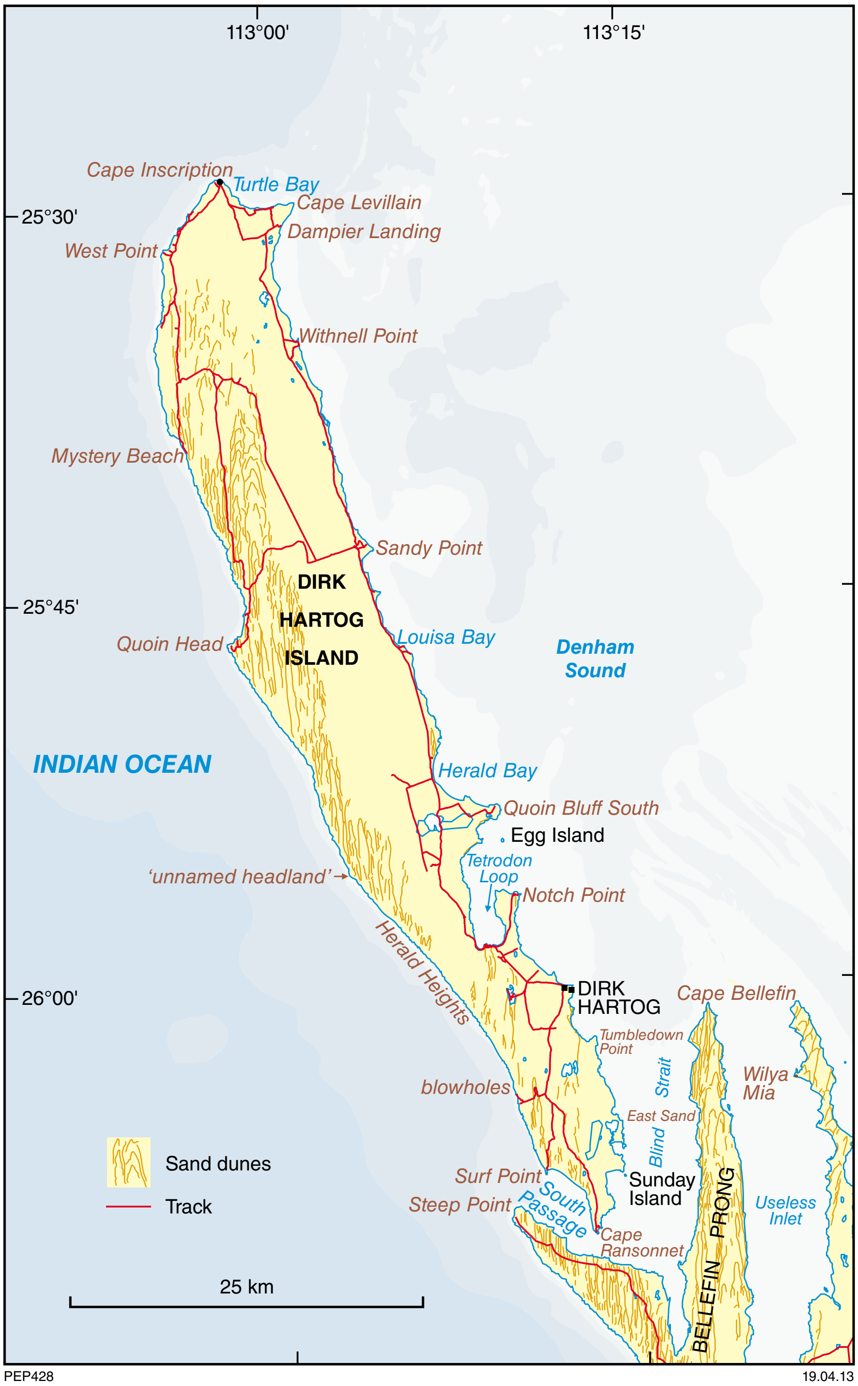

Figure 95. Map of Dirk Hartog Island, showing places mentioned in the text and other localities.

The west coast of Dirk Hartog Island is marked by cliffs with a few intervening beaches. An eroded scarp, known as Herald Heights, extends for 25 km along the western coast, from Surf Point to an unnamed headland 8 km west of Tetrodon Loop. This scarp, up to 160 m high, may be a fault-line scarp. Lower cliffs, up to 110 m high, extend north of this unnamed headland (Fig. 98) to Quoin Head, Mystery Beach, West Point, and Cape Inscription (Figs 99, 100). The most prominent of the beaches, Mystery Beach, has a remarkable concentration of driftwood on and behind the beach.

The geology of Dirk Hartog Island was first described by Playford and Chase (1955). They showed that the sedimentary succession exposed there consists of Holocene sand dunes overlying Pleistocene eolian limestone (Tamala Limestone) and shelly limestone. The Tamala Limestone forms precipitous cliffs, up to 150 m high on the west coast, and on discontinuous cliffs and headlands, up to 30 m high, on the east coast. The vegetation consists of low heath, with very few trees more than 3 m high (Burbidge and George, 1978).

Playford and Chase (1955) concluded that the island is probably localized by an anticline or fault block, and recommended that WAPET undertake a program of drilling to define the subsurface structure. A drilling program proved that the Quaternary deposits on the surface of the island overlie an anticlinal structure in Paleogene and Neogene strata (Butcher et al., 1984; Fig. 49). This anticline was tested for petroleum by Dirk Hartog 17b, which proved to be a dry hole.

Faure Island

Faure Island is the second largest island in the Shark Bay area, covering some 52 km^2 and extending about 11 km north–south and 6.5 km east–west (Figs 101–111). From the late 19th century until 1999 the island was utilized as a pastoral lease, stocking sheep and goats, after which it was purchased by the Australian Wildlife Conservancy, with the intention that it become a conservation area for preservation of the native fauna and flora of the Shark Bay area (Playford and Berry, 2002, Richards and Wilson, 2008).

Foxes never reached the island, and feral cats have now been eliminated through a successful eradication program carried out by the Australian Wildlife Conservancy. Goats have also been eliminated, and a small number of sheep have remained in order to meet the minimum requirement for a pastoral lease. Several species of endangered mammals, once native to the island, have now been successfully re-introduced. This is an outstanding example of an effective wildlife-conservation project.

Faure Island is situated between the western end of Faure Sill and the eastern end of L'Haridon Sill (Figs 66, 101). The island is separated from the mainland at Petit Point by a stretch of water some 6 km wide. However, when sea level is at its lowest, during summer, about 4 km of the sea floor is exposed between Faure Island and Petit Point, leaving only the Hoult Channel, about 2 km wide, and a much smaller channel remaining submerged. Emus have been seen to swim from the mainland to Faure Island during a period of very low tide (D Hoult, 2011, pers. comm.).

Faure Island has a maximum elevation of 33 m near the central west coast. Much of its surface is occupied by red sand dunes of the Denham Sand, although the irregular morphology of those dunes is somewhat different from that of dunes on Peron Peninsula (Fig. 101). The red Holocene sand dunes overlie late Pleistocene sandstones of the Peron Sandstone (Fig. 102). White beaches and beach ridges are present around much of the island, and the sand has been blown into a narrow belt of seif dunes beside the south coast.

Birridas are present in the central and western parts of the island. One of the largest, known as The Tadpole, in the northwestern part, is 'drowned'. It is connected to the sea by a narrow channel, 'the tail' of The Tadpole (Figs 103, 104).

Mangrove thickets (mangals), of the white mangrove, *Avicennia marina*, thrive at several places along the coast, largely behind sand bars and spits (Fig. 102). The largest of these thickets occurs behind a long sand spit on the southwest side of the island and around The Tadpole and its 'tail' (Figs 103, 104).

Very large numbers of the pied cormorant (*Phalacrocorax varius*) build rookeries in mangroves at various places around the island (Mather, 2011; Figs 105, 106). Excrement from these birds soon kills the mangroves and accumulates in a layer of cyanobacterial black mud below the dead trees. This layer, up to about 10 cm thick, commonly contains white hydroxylapatite and cormorant skeletal material. Fish bones, bivalve shells, and rounded gastroliths also occur there, having been swallowed and regurgitated by cormorants when nesting and roosting in the mangroves. The gastroliths are mainly composed of red calcareous sandstone of the Pleistocene Peron Sandstone (Fig. 107), together with some igneous rocks and indurated Pleistocene siliceous sandstone. Shells of the mangrove mud whelk, *Terebralia sulcata*, and the periwinkle, *Littorina scabra*, also occur in the mangal deposits (Figs 108, 109). The mangroves have vertical pneumatophores that grow vertically above subhorizontal roots (Figs 108, 110, 111).

The modern mangal (guano) deposits are geologically important because of the closely similar older deposits that occur at elevations of up to 14.5 m above sea level at various localities on the island, pointing to Holocene uplift, as discussed later in this Bulletin.

Dorre, Bernier, and Koks Islands

Dorre and Bernier Islands are two long narrow islands trending north-northeast along the west side of Shark Bay, separated from each other by a channel, 430 m wide (Fig. 1). Bernier Island is 31.5 km long and up to 3.7 km wide, and Dorre Island is 26 km long and up to 2.4 km wide. Koks Island is much smaller, only about 290 m long and up to 150 m wide, situated 400 m north of Dorre Island. These islands are included in the Shark Bay World

Heritage Area and are also covered by an A-class nature reserve. None of these islands were visited on the ground during the present investigation, other than a brief visit to Bernier Island.

Pleistocene eolian limestone of the Tamala Limestone outcrops in cliffs along the west and east sides of Dorre and Bernier Islands and around Koks Island. The cliffs are continuous on the west coasts of Dorre and Bernier Islands, where they are generally 10–50 m high. They are discontinuous on the east coasts, separated by narrow beaches, and reach a maximum height of 50 m at Quoin Bluff North, on the east side of Dorre Island.

The linear trend of these two long narrow islands is thought to be controlled by an underlying Cenozoic structure, either an anticlinal fold or a fault block, or a combination of both.

A pastoral lease was held briefly on Bernier Island during the late 19th century, and lock hospitals for Aboriginal people were maintained on Bernier and Dorre Islands from 1908 to 1918. These infamous hospitals were for people infected with leprosy or venereal diseases, although many supposed venereal cases are likely to have involved yaws, an endemic non-venereal disease caused by a spirochete similar to that which causes venereal syphilis. The hospital for men was on Bernier Island (Fig. 112), and that for women was on Dorre Island.

Those hospitals resulted in the introduction of domestic goats to both islands. Their feral descendants were eventually eliminated through an eradication program over 20 years, from the 1950s to the 1970s.

The Bernier and Dorre Islands Nature Reserve is extremely important for the conservation of four species of marsupials that still live there but disappeared from the mainland long ago because of predation by cats and foxes (Ride et al., 1962). Foxes have never reached the islands; and although some cats seem likely to have been kept at the hospitals, they never became feral.

Figure 96. The east side of Dirk Hartog Island, looking north along the track near Quoin Bluff South, illustrating the typical low vegetation that covers the island. Richard Chase is standing beside a battered Landrover, on loan from the station, in 1955.

Figure 97. Dirk Hartog Homestead (right), shearers' quarters, shearing shed, and the *Dirk Hartog* lying at anchor, in 1955.

Figure 98. Aerial view looking north along cliffs, about 100 m high, north of Herald Heights, Dirk Hartog Island.

Figure 99. **Aerial view looking south over Cape Inscription, showing the lighthouse and lighthouse keepers' quarters, beside the site of Dirk Hartog's post and inscribed plate, after the quarters had been partly restored.**

Figure 100. **Aerial view looking west over Cape Inscription. Note the concentration of large limestone blocks on and at the base of the cliffs at the north end, thought to have resulted from a mega-tsunami that struck the island long ago.**

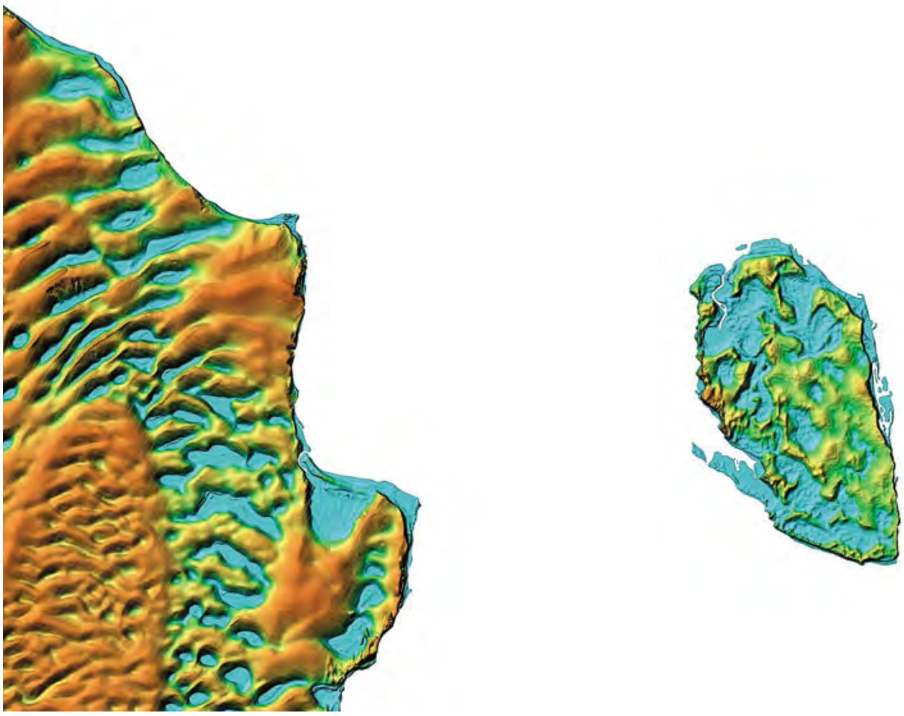

Figure 101. DEM image of Faure Island and the adjoining part of Nanga Peninsula, showing the patterns of sand dunes.

Figure 102. Red dune sand and sandstone of the Peron Sandstone, and mangroves growing behind a sand bar, beside the east coast of Faure Island.

Figure 103. The northwest coast of Faure Island showing a large 'drowned' birrida, known as The Tadpole. A narrow channel connected to the sea forms the 'Tadpole's Tail'. Many mangroves grow in the 'drowned' birrida and along its 'tail'.

Figure 104. Mangroves beside part of the 'tail' of The Tadpole in the northwest part of Faure Island. Most of the mangroves (light grey and white) are dead, having been killed by the excrement of pied cormorants nesting in the trees.The living mangroves are green.

Figure 105. Pied cormorants in mangroves beside the 'tail' of The Tadpole on Faure Island. Excrement from the birds has killed many of the mangroves. Photo by Wayne Lawler, courtesy of Australian Wildlife Conservancy.

Figure 106. Abandoned cormorant nests in dead mangroves beside the north coast of Faure Island.

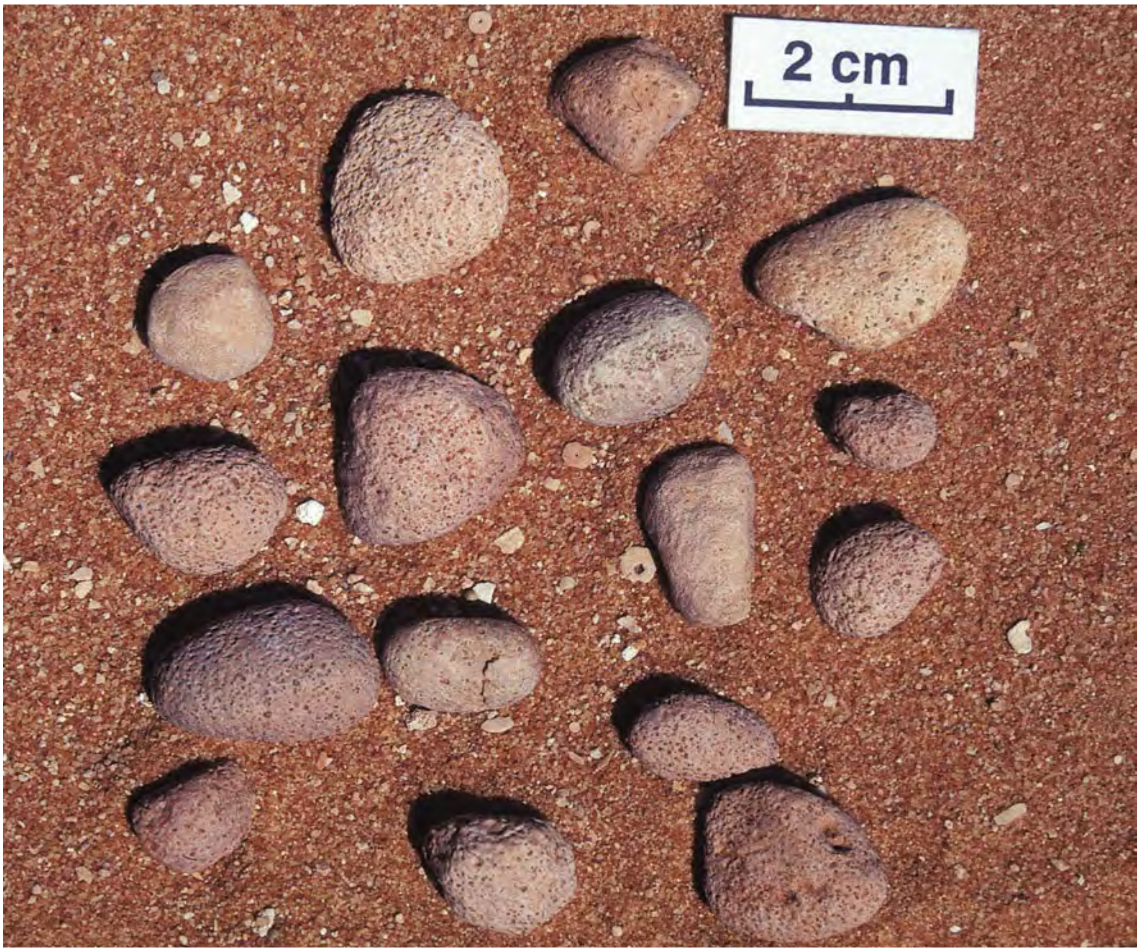

Figure 107. Gastroliths of rounded, indurated, Peron Sandstone, collected from below cormorant nests near the north coast of Faure Island.

Figure 108. Shells of the mud welk, *Terebralia sulcata*, lying between vertical mangrove pneumatophores, beside the north coast of Faure Island.

Figure 109. Shells of the mangrove periwinkle *Littorina scabra*, attached to the base of a mangrove tree near the north shore of Faure Island.

Figure 110. Mangroves with vertical pneumatophores that have grown upward from subhorizontal roots, beside the north coast of Faure Island.

Figure 111. Horizontal mangrove roots exposed by erosion, beside the south coast of Faure Island.

Figure 112. Remains of the lock hospital for Aboriginal men in the northern part of Bernier Island. Note the island's low shrubs and low relief.

Zuytdorp Cliffs

The Zuytdorp Cliffs are a line of precipitous cliffs, formed of Pleistocene Tamala Limestone, which extend for nearly 200 km, from just north of the mouth of the Murchison River to Steep Point (Figs 113–130). These cliffs are interpreted to be a fault-line scarp resulting from movement along a normal fault, the Zuytdorp Fault. The fault itself is not seen at the surface, as it must be below water, several metres west of the scarp base. The fault's presence is deduced from the sharply linear nature of the scarp, which abruptly truncates dune limestones of the Pleistocene Tamala Limestone and overlying Holocene dunes. The scarp is only mildly eroded, and is considered to have been formed by repeated movements along the fault during the Pleistocene and perhaps early Holocene (Playford, 2003).

The Zuytdorp Cliffs can be subdivided into five main sections (Figs 113–129). Along Section 1 (the southernmost section), the scarp is relatively low, about 100 m high in the north and falling progressively to the south, disappearing just before the mouth of the Murchison River. South of the same river, an irregular offset scarp extends south-southwest for 18 km to join another straight section of coast about 30 km long, interpreted to be a fault, named the Wagoe Fault (Figs 130–132). Unlike the Zuytdorp Fault, that fault is not expressed as a scarp. It forms a very straight line, along which contemporary seismic activity has been recorded (Fig. 131). There is also fracturing of beach rock beside the straight coastline, interpreted to be a consequence of that faulting (Fig. 132).

The coast along Section 1 of the Zuytdorp fault-line scarp is backed by hundreds of small regularly spaced creeks incised into the narrow belt of Middle Pleistocene Tamala Limestone that extends behind the scarp (Figs 114–119). Those creeks, which only flow after heavy rain, are up to 30 m deep, average 300 m wide, and extend inland for up to 2 km. Based on the presence of these creeks, the Zuytdorp Fault along this section of the scarp appears likely to have experienced no major movement since about the late Pleistocene. Section 2 of the scarp is a short offset connecting Sections 1 and 3 (Figs 120, 121).

A subsidiary fault which developed behind the main scarp is seen to die out about 3 km north of the junction between Sections 1 and 2 (Figs 120, 121). An alternative explanation for this feature is that it represents a major landslide caused by slope failure along that part of the cliffs (RM Hocking, 2013, pers. comm.).

The most recent movement on the Zuytdorp Fault is thought to have occurred along Section 3, where the fault-line scarp shows relatively little erosion (Figs 113, 122–126). It seems likely that the fault in this section was last active in early Holocene or latest Pleistocene times.

The scarp at the type section of the Tamala Limestone in front of Womerangee Hill is 250 m high. That section extends down a spur in the cliff face, where a rabbit-proof fence once extended almost to the base of the cliff. Near the base there are spectacular exposures of cross-bedding and a very narrow shoreline platform that is estimated to extend to about 1 m above mean sea level (Figs 127–129).

The coast along Sections 4 and 5 of the scarp is interpreted to mark a series of en-echelon faults that are less sharply defined and are unlikely to have moved as recently as the fault along Section 3. The last movement along Sections 4 and 5 may have been during the late Pleistocene. The coastline between Bluff Point and Kalbarri appears to form a relay ramp between the Zuytdorp and Wagoe Faults (Figs. 130–132).

Shoreline platforms

Flat shoreline platforms, some with 'paddy-field' terraces, are developed in outcrops of the Tamala Limestone at the base of the Zuytdorp Cliffs (Figs 129, 133–137), also around various islands, and along the coast near Point Quobba (Fig. 138). Comparable platforms and terraces have been described at Rottnest Island by Playford (1988; Figs 139, 140), but whereas most of those platforms on that island are a few centimetres below low-water mark, the platforms below the Zuytdorp Cliffs are generally up to about 2 m above sea level. Some paddy-field terraces reach as much as 3 m above sea level (Fig. 134). At Rottnest Island the highest platforms with paddy-field terraces are along those parts of the coast that are subject to the strongest wave action (Playford, 1988; Fig. 139). The reason why the shoreline platforms at the foot of the Zuytdorp Cliffs are higher than those at Rottnest Island is probably because the deeper water in front of the Zuytdorp Cliffs allows powerful waves to impact directly on the coast, whereas shallower water, with weaker waves, adjoins the coast at Rottnest Island.

The steps between individual paddy-field terraces in front of the Zuytdorp Cliffs commonly have amplitudes of 10–50 cm, and each terrace has a raised rim standing about 1–2 cm above the level of the platform. Water cascades from one terrace to another as the water flows away after each wave impact.

The rim around each platform is usually composed of the same limestone as that forming the surface of the platform (Fig. 137). The raised rim is commonly partly coated with red-algal limestone. A similar raised rim is evident around platforms on Rottnest Island (Fig. 140). The limestone below the surface of the platforms is strongly indurated, apparently as a result of the precipitation of calcium carbonate in voids in the limestone at times when the platforms are exposed during low tides.

Extensive karstification, including cave systems, occurs below some platforms, formed during the recent past, with the development of cavernous systems and blowholes. The blowholes penetrate shoreline platforms and a few cliff tops that are as much as 20 m above sea level, for example beside Pepper Point (Fig. 141), west of Karkura (on Tamala Station), near the south end of Dirk Hartog Island, and at the *Zuytdorp* wreck site (Figs 142–144).

Another prominent feature is a remarkable network of circular holes, 0.1–1 m in diameter, on the shoreline platform below Cape Inscription on Dirk Hartog Island (Figs 145, 146). Small oyster mounds growing on the platform are younger than those holes (Fig. 146), indicating that they developed in the platforms prior to growth of the oyster mounds, probably by rainwater solution associated with periods of lowered sea level during the recent past.

Similar circular holes, although much larger, occur at Thunder Bay (727247E, 7089981N), in a shoreline platform below the northern part of the Zuytdorp Cliffs. There they are associated with algal polygons similar to those on shoreline platforms at Rottnest Island, where they mark the territories of a kyphosid fish, the Western Buffalo Bream (Berry and Playford, 1992).

The origin of the shoreline platforms and their paddy-field terraces has yet to be determined. The platforms may have formed through a combination of bio-erosion by marine organisms (especially gastropods) and mechanical erosion by waves, combined with some form of chemical corrosion (Playford, 1988). Further research is warranted to clarify the origin of these enigmatic features.

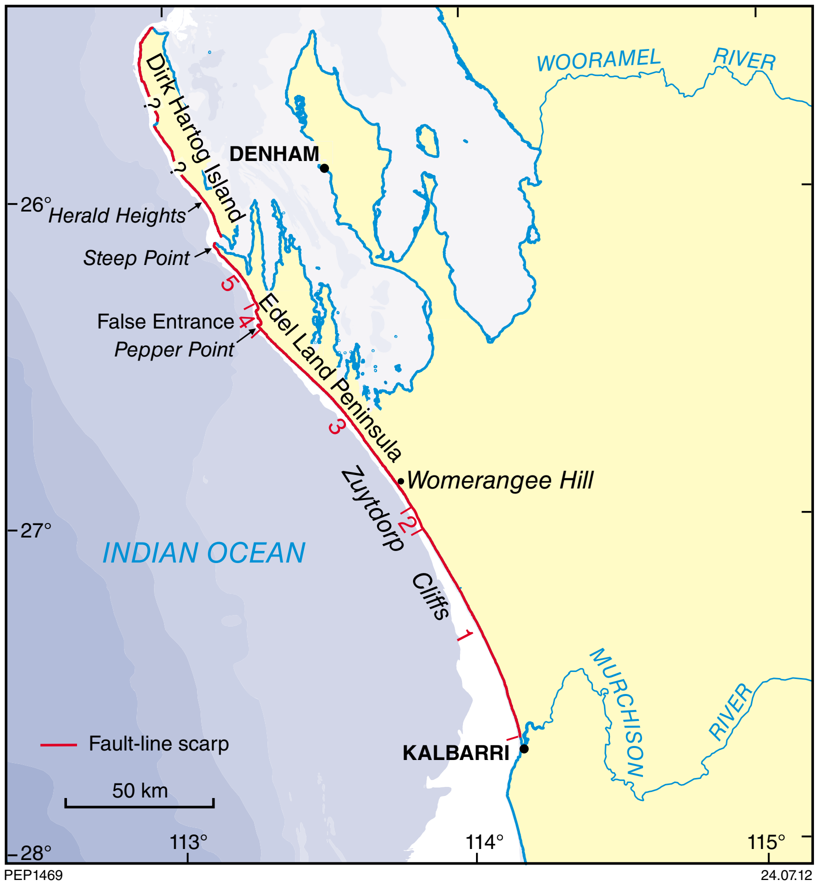

Figure 113. Map showing the five sections of the Zuytdorp Cliffs fault-line scarp and other possible fault-line scarps on Dirk Hartog Island. The Zuytdorp Fault is interpreted to have operated as a normal fault during the late Pleistocene, and perhaps most recently, along Section 3, during the early Holocene.

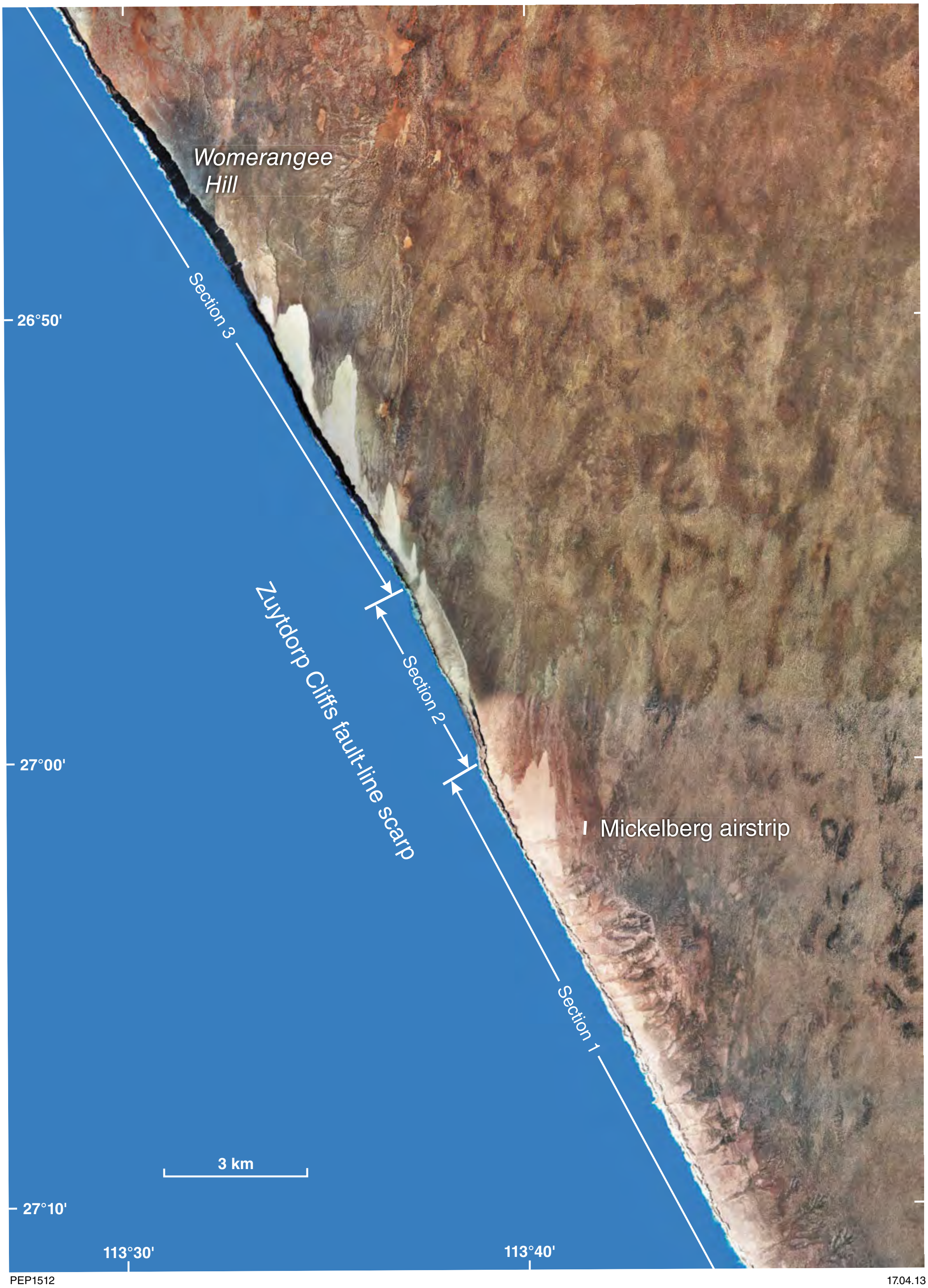

Figure 114. Composite vertical airphoto and DEM image of Sections 1 and 2, and part of Section 3, of the Zuytdorp Cliffs fault-line scarp. Section 1 shows many closely spaced creeks cut into the scarp, Section 2 is the offset between Sections 1 and 3, and Section 3 has resulted from the most recent movement along the fault. Note the bare patches of white sand extending north behind parts of the scarp. Airphoto image courtesy of Landgate, Western Australia.

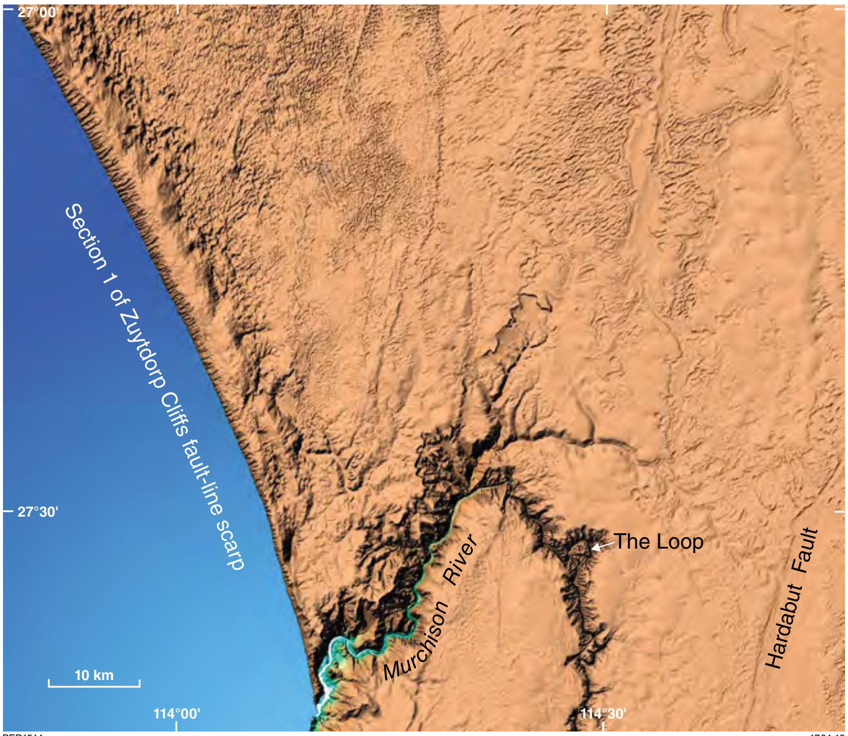

Figure 115. DEM image of part of Section 1 of the Zuytdorp Cliffs fault-line scarp, north of the Murchison River, showing a narrow belt of Tamala Limestone behind the scarp, cut by many closely spaced short creeks. Note the Hardabut Fault, a reverse fault, in the bottom right.

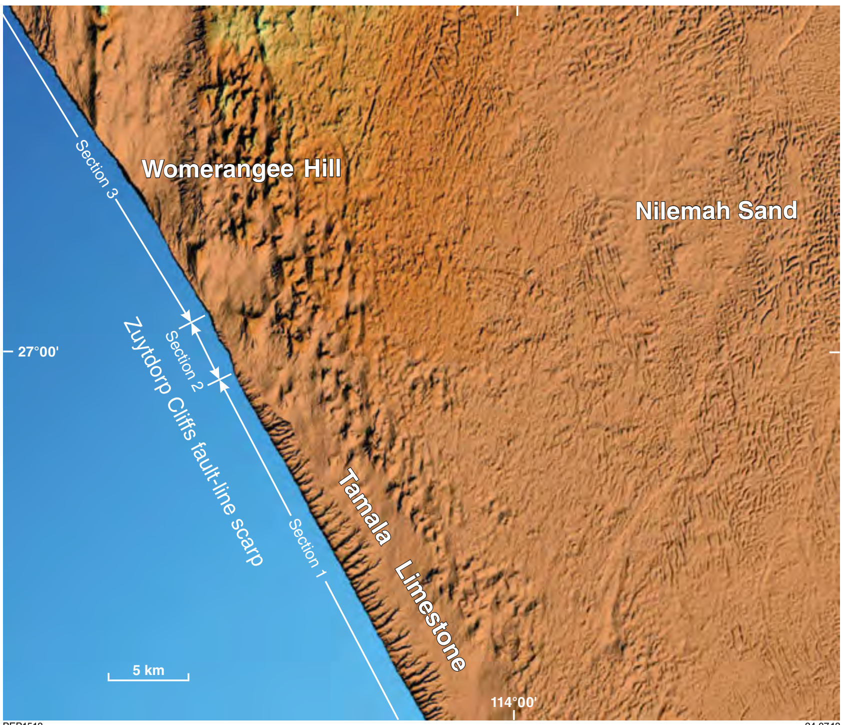

Figure 116. DEM image of Section 2 and parts of Sections 1 and 3 of the Zuytdorp Cliffs fault-line scarp. Many small, youthful, creeks are incised into the ridge of Tamala Limestone along Section 1. Behind that ridge are undulating and parabolic dunes of the Nilemah Sand. Section 2 marks the small offset between Sections 1 and 3, and Section 3 is the youngest part of the fault-line scarp, which may have formed during the early part of the Holocene.

Figure 117. Aerial view looking north from just north of the *Zuytdorp* wreck site along Section 1 of the Zuytdorp Cliffs fault-line scarp, showing many small creeks deeply incised into the Tamala Limestone behind the scarp. The offset between Sections 1 and 3 of the scarp can just be seen in the far distance.

Figure 118. Aerial view looking east-southeast over part of Section 1 of the Zuytdorp Cliffs fault-line scarp, showing many small creeks deeply incised into the Tamala Limestone behind the scarp. The *Zuytdorp* wreck site is situated just right of centre of the photo.

Figure 119. Low-level aerial view of the *Zuytdorp* wreck site, where the cliff of Tamala Limestone is about 35 m high, showing masses of boulders on the cliff slope, some of which may have resulted from the impact of a mega-tsunami. The ship was wrecked in June 1712, and its remains lie below the white water left of centre in the photo.

Figure 120. Aerial view looking south along the Zuytdorp Cliffs fault-line scarp, from about 9 km north of Mickelberg airstrip, showing Section 3 in the foreground and Sections 2 and 1 in the background.

Figure 121. Aerial view looking east over Section 2 of the Zuytdorp Cliffs fault-line scarp. The line behind the cliff marks an extension of the offset fault.

Figure 122. Aerial view of the Zuytdorp Cliffs fault-line scarp at Womerangee Hill. The cliffs, composed of mid-Pleistocene Tamala Limestone, are up to 260 m high. The type section of the formation, 250 m thick, is situated left-of-centre in the photo, running down the spur in the cliff face below the old fenceline.

Figure 123. Aerial view of the Zuytdorp Cliffs fault-line scarp at Womerangee Hill. The cliffs, composed of Tamala Limestone, are up to 260 m high. A layer of calcrete, up to 5 m thick, caps the cliff. Note the youthful v-shaped incision in the scarp, right of centre.

Figure 124. Closer aerial view of the fault-line scarp at Womerangee Hill. The type section of the Tamala Limestone, 250 m thick, runs down the spur in the cliff face, from where the old fenceline meets the top of the cliff on the left side of the photo.

Figure 125. Aerial view looking northeast over Womerangee Hill and the fault-line scarp of the Zuytdorp Fault. The top of the cliff at its crest and further north is marked by a layer of calcrete up to 5 m thick, whereas on the south side (right) the calcrete is overlain by residual sand. Some of the pale-pink quartz sand has been blown into sand sheets behind the cliff top by the prevailing southerly winds.

Figure 126. View on the ground looking north along the Zuytdorp Cliffs at Womerangee Hill, showing the thick layer of calcrete at the cliff top. The tracks on the cliff face are made by feral goats. Tony Cockbain is standing beside the youthful incision in the scarp that is seen in Figure 123.

Figure 127. Large-scale cross-bedding near the base of the Tamala Limestone type section at Womerangee Hill.

Figure 128. Eolian foreset above a red soil horizon near the base of the Tamala Limestone below Womerangee Hill, adjoining Figure 127.

Figure 129. Narrow shoreline platform at the base of the Zuytdorp Cliffs below Womerangee Hill, with water cascading down after a wave impact.

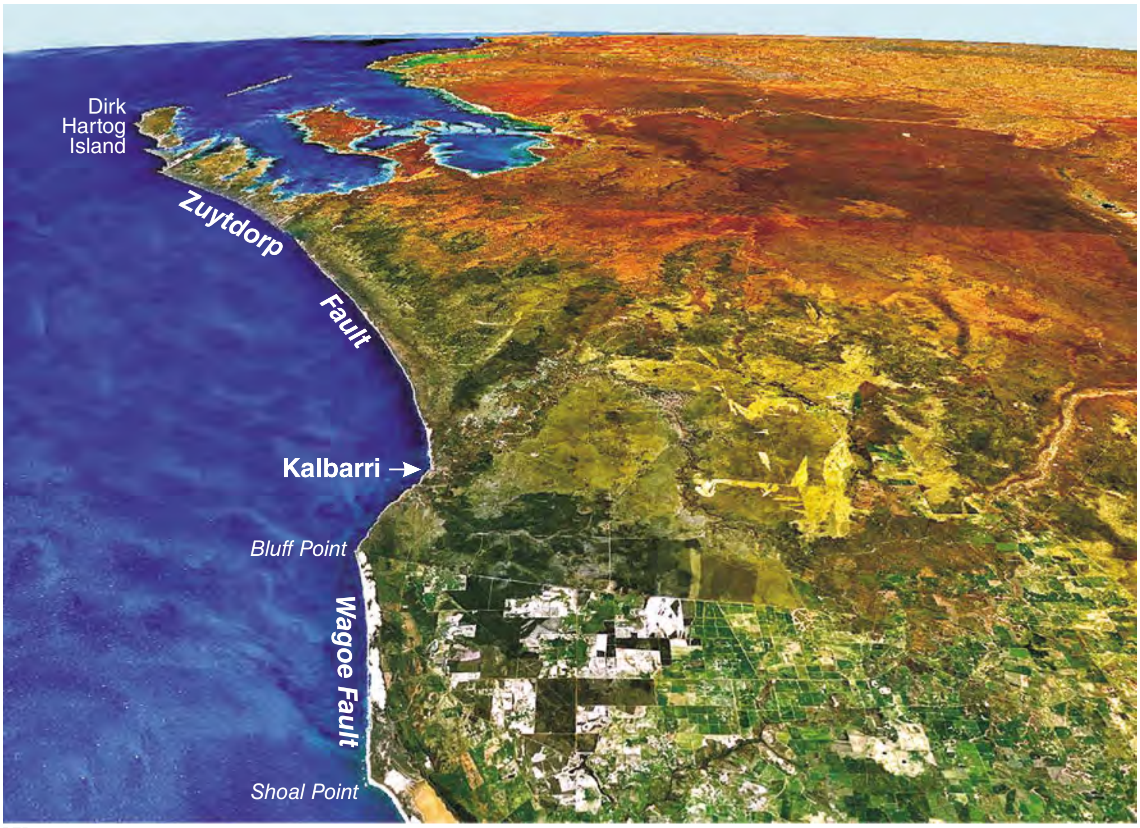

Figure 130. National Aeronautics and Space Administration (NASA) World Wind Image looking north over the Wagoe and Zuytdorp Faults towards Shark Bay.

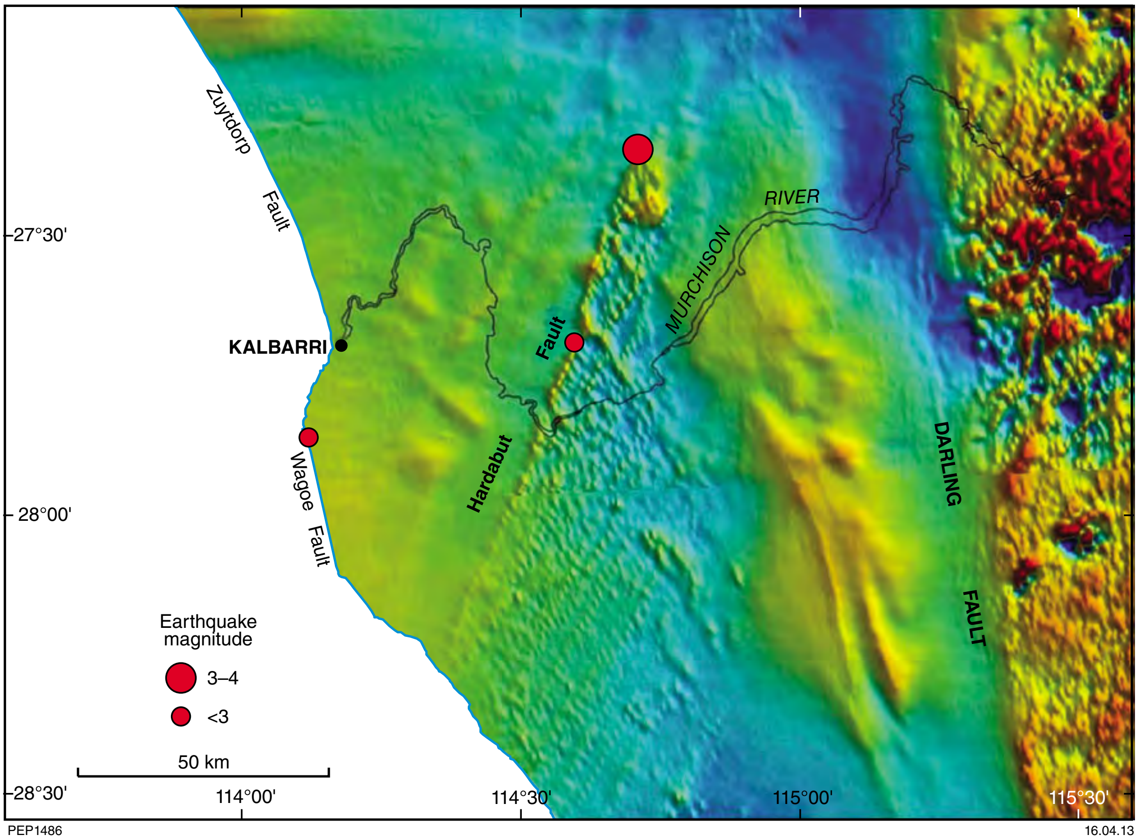

Figure 131. Total magnetic intensity map of the Kalbarri area showing the Hardabut, Zuytdorp, Wagoe, and Darling Faults, and epicentres of recent earthquakes associated with the Hardabut and Wagoe Faults.

Figure 132. Fractured beach rock beside the Wagoe Fault. This fracturing may have resulted from recent movement along that fault.

Figure 133. View looking south from the *Zuytdorp* wreck site along Section 1 of the Zuytdorp Cliffs fault-line scarp, showing elevated shoreline platforms, about 1 to 2 m above mean sea level, at the base of the cliffs.

Figure 134. Series of paddy-field terraces in indurated Tamala Limestone below Womerangee Hill, extending over a vertical height of about 3 m. Water from wave impacts cascades down the terraces.

Figure 135. Shoreline platform and paddy-field terraces near the *Zuytdorp* wreck site, showing a wave impacting on the shoreline platform and water cascading down over the terraces.

Figure 136. Shoreline platform with rimmed paddy-field terraces, just south of the *Zuytdorp* wreck site. The raised rims are composed of indurated Tamala Limestone, partly coated with red algal limestone.

Figure 137. Detail of rimmed paddy-field terraces on the shoreline platform just south of the *Zuytdorp* wreck site. The raised rims are composed of Tamala Limestone, partly coated with red algal limestone. A geological hammer shows the scale.

Figure 138. Shoreline platform below a low cliff of Tamala Limestone at 'the blowholes' near Point Quobba. The platform is about 1 m above mean sea level.

Figure 139. Paddy-field terraces on a shoreline platform at Wilson Bay, Rottnest Island, extending over a vertical range of about 0.7 m.

Figure 140. Shoreline platform at The Basin, Rottnest Island, during very low tide, showing the raised rim of the platform.

Figure 141. Blowholes in Tamala Limestone at the cliff top just south of Pepper Point, beside False Entrance, on the Zuytdorp Cliffs. The person is Evert Van de Graaff.

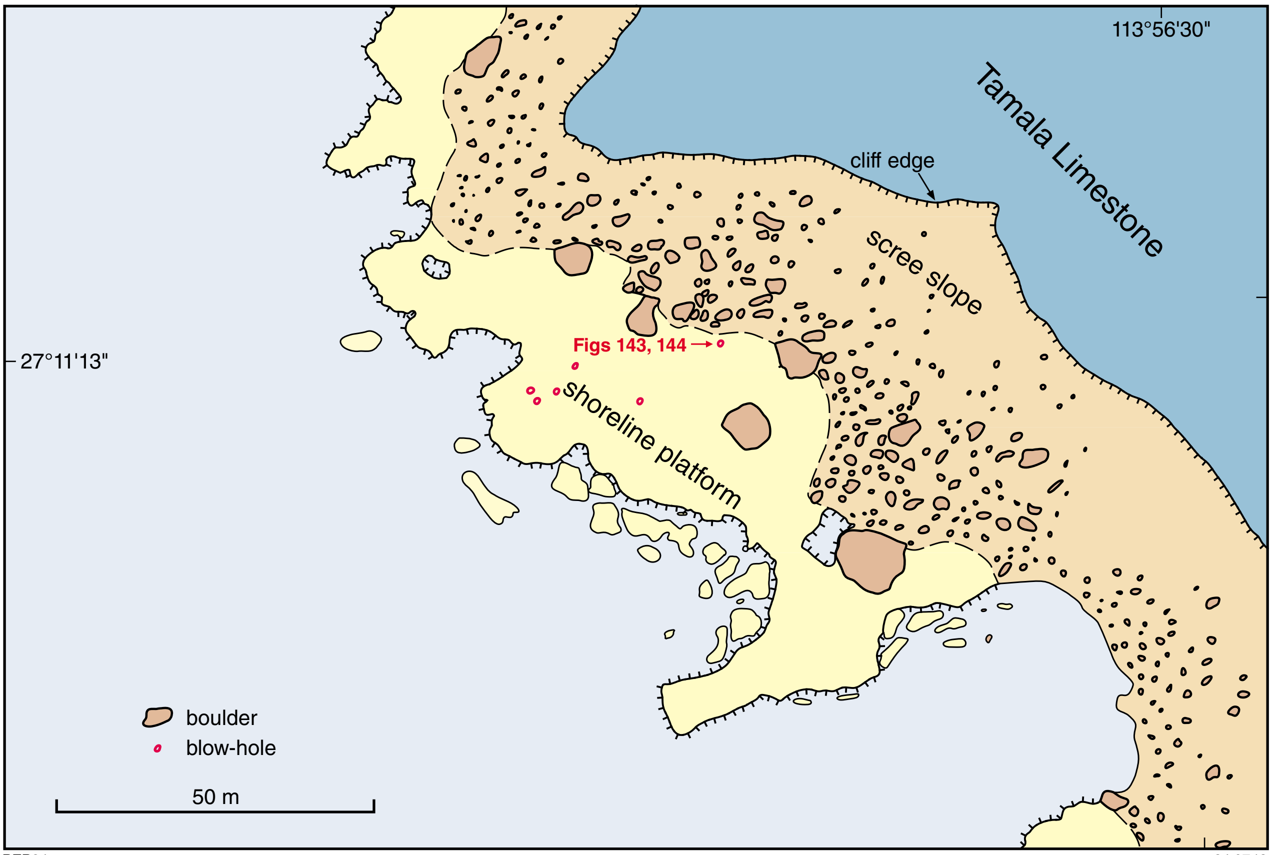

Figure 142. Map of the *Zuytdorp* wreck site area, showing the locations of blowholes (including the one shown in Figures 143 and 144). Boulders of Tamala Limestone are on the scree slope and the wide shoreline platform. Some of the larger boulders may have been dislodged from the cliff by a mega-tsunami. The cliff here is 30 to 35 m high.

Figure 143. Cavern below a blowhole at the *Zuytdorp* wreck site. The waterlevel in the cavern rises by up to about 1 m after the impact of moderate waves on the shoreline platform, forcing air out of the blowhole. Photo (taken in 1954) by John Campbell, courtesy of West Australian Newspapers. The person is Phillip Playford.

Figure 144. The blowhole above the cavern shown in Figure 143. Photo by John Campbell, courtesy of West Australian Newspapers.

Figure 145. Circular holes in the shoreline platform below Cape Inscription, Dirk Hartog Island. These are interpreted to be karst features, formed during a period of lower sea level during the recent past.

Figure 146. Mounds of oyster limestone and circular karst holes on the shoreline platform below Cape Inscription, Dirk Hartog Island. The oyster mounds have grown since the karst holes were developed in the platform.

Geology

General

The near-surface geology of the Shark Bay area consists predominantly of Pleistocene Tamala Limestone and Peron Sandstone, covered over most of the area by superficial red sand of the Denham, Nilemah, and Carrarang Sands (Figs 30, 147). Calcretized Cretaceous chalk (Toolonga Calcilutite), and some Paleogene and Neogene sandstone and calcarenite, outcrop east of Hamelin Pool. Drilling has shown that the Cenozoic rocks in parts of the area are underlain by Silurian to Lower Devonian Sweeney Mia Sandstone and Kopke Sandstone, and Silurian Dirk Hartog Limestone and Ordovician Tumblagooda Sandstone (Hocking, 1990, 2000). The Tumblagooda Sandstone and Toolonga Calcilutite are well exposed in the valley of the Murchison River, about 100 km south of Shark Bay (Figs 148, 149).

Details of the subsurface stratigraphy and petroleum prospectivity of the Shark Bay area are described by Hocking et al. (1987), Hocking (1990), Iasky and Mory (1999), Mory et al. (2003), Iasky et al. (2003), and Lockwood and D'Ercole (2003). None of the exploration wells in the area found more than minor traces of oil (Fig. 150).

Cretaceous

Toolonga Calcilutite

The Toolonga Calcilutite, of Late Cretaceous (Santonian–Campanian) age, is the oldest rock unit exposed around Shark Bay. It outcrops discontinuously along the east side of Hamelin Pool, from Flagpole Landing and Flint Cliff (Fig. 151) to near Yaringa Homestead (Van de Graaff et al., 1983; Denman et al., 1985). The formation consists of white chalk and greenish-white calcareous mudstone, frequently containing many flint nodules. The chalk and mudstone are commonly altered to calcrete at the surface. Flint nodules were collected, broken apart and knapped by Aborigines to make knives and adzes, for use in cutting meat and fashioning wooden artefacts. Fragments of knapped chert remaining from those activities are scattered through parts of the area.

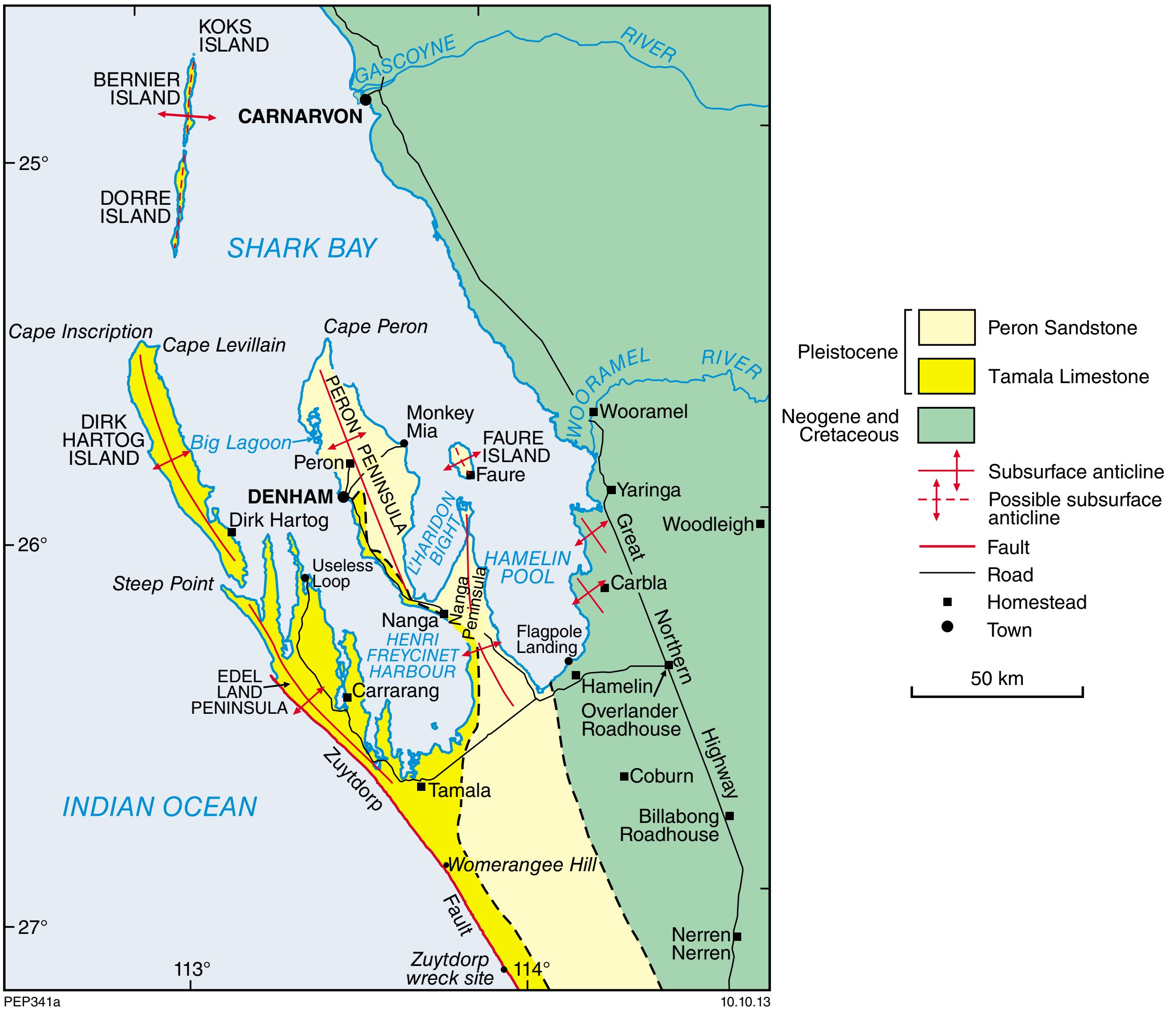

Figure 147. Generalized geological map of part of the Shark Bay area, showing rocks below the superficial dune formations shown in Figure 30.

Figure 148. Aerial view of the Toolonga Hills in the lower Murchison River area, showing outcrops of white Cretaceous Toolonga Calcilutite above older Cretaceous units and dark-red Ordovician Tumblagooda Sandstone. The coastline in the background marks the top of the Zuytdorp Cliffs fault-line scarp.

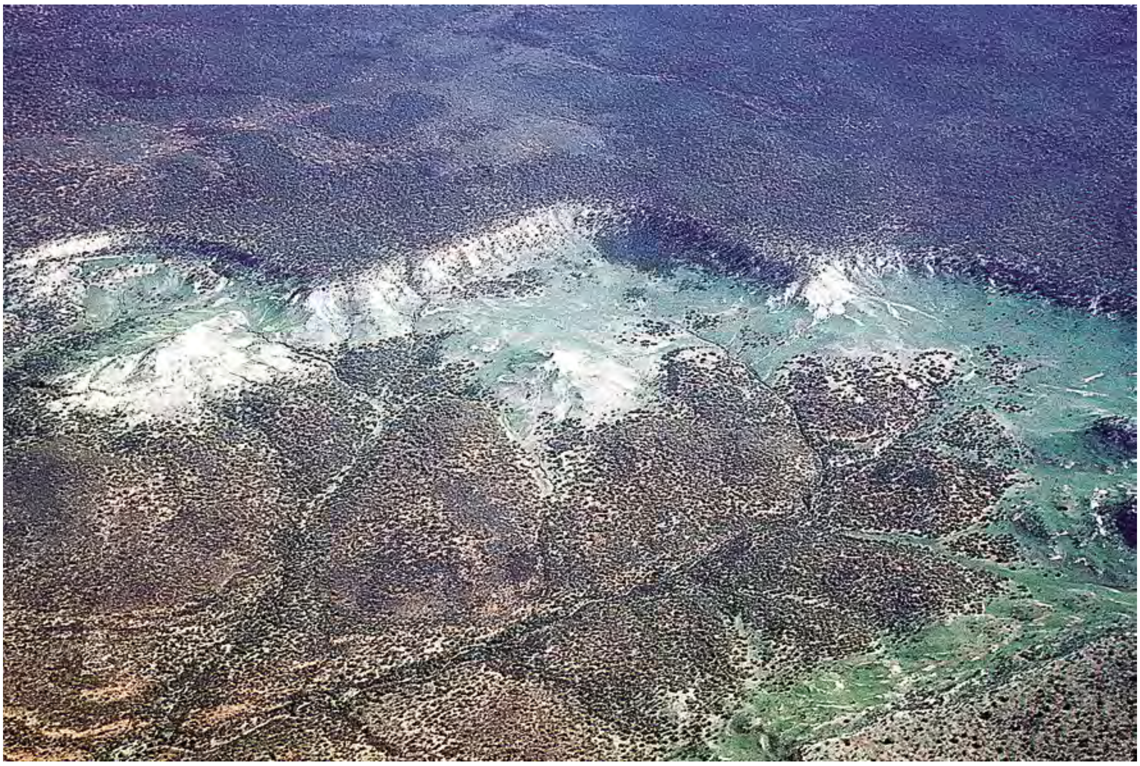

Figure 149. Closer aerial view of white chalk of the Toolonga Calcilutite at Jannawa and Pillawara Hills, where it overlies older Cretaceous units and Ordovician Tumblagooda Sandstone.

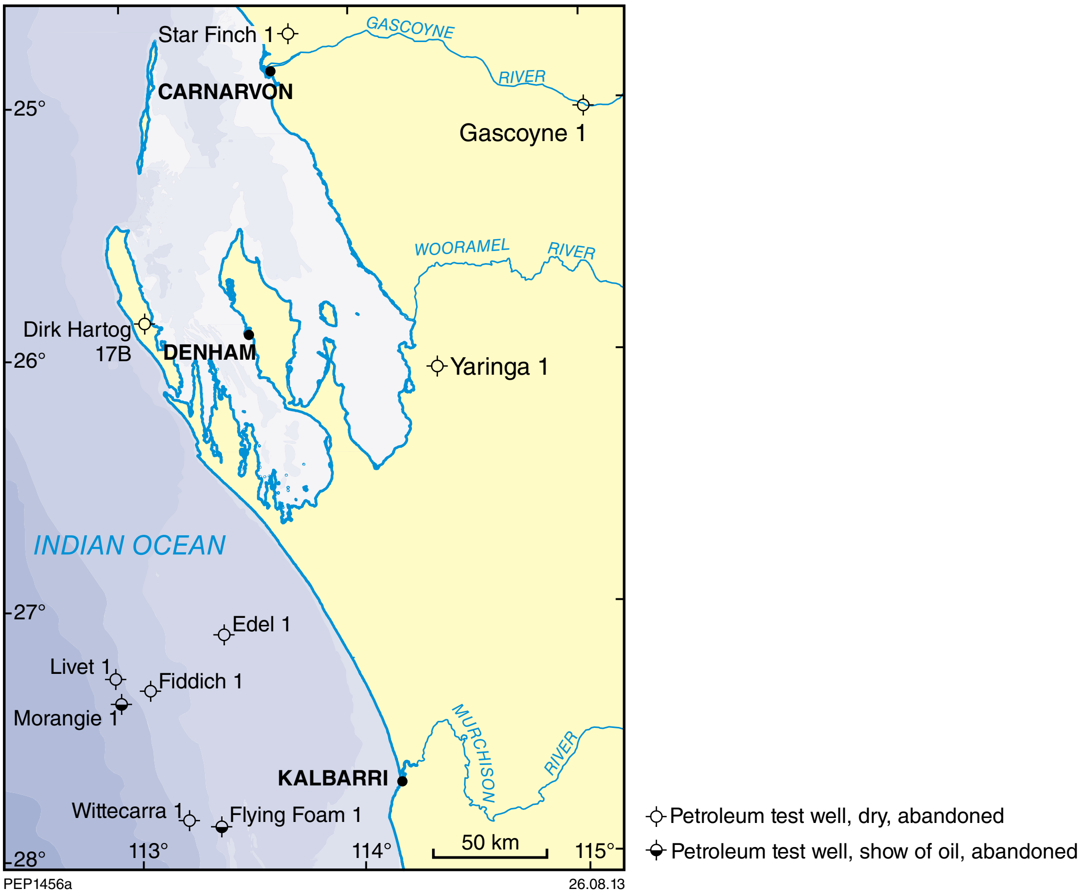

Figure 150. Map showing the locations of test wells drilled for petroleum in the Shark Bay area.

Figure 151. Outcrop of Toolonga Calcilutite, largely calcretized, at Flint Cliff, on the east side of Hamelin Pool.

Paleogene and Neogene

Paleogene and Neogene (Tertiary) units in the area are generally poorly exposed (Van de Graaff et al., 1983; Denman et al., 1985). The Eocene Giralia Calcarenite is exposed at a few localities east of Hamelin Pool, where it consists of greenish-grey calcarenite overlying Toolonga Calcilutite. The Miocene Lamont Sandstone, a unit of silicified sandstone, is exposed as rocky outcrops in some headlands on the east side of Hamelin Pool.

Pleistocene

The principal Pleistocene units in the Shark Bay area are the Tamala Limestone and the Peron Sandstone, both of which are wind-blown deposits (eolianites).

There are also a few outcrops of Pleistocene marine limestone and sandstone, placed in the Dampier Limestone, Carbla Oolite Member of the Dampier Limestone, Bibra Limestone, and Depuch Limestone. These units were originally named 'Dampier Formation', 'Carbla Oolite', Depuch Formation', and 'Bibra Formation' by Logan et al. (1970b). The Dampier Limestone, Carbla Oolite Member and Bibra Limestone were renamed as such by Van de Graaff et al. (1983). The Depuch Limestone is similarly renamed here, as limestone is its dominant lithology.

The Dampier Limestone, Depuch Limestone, Bibra Limestone, and Carbla Oolite Member of the Dampier Limestone have not been studied in detail during the present investigation, but it seems likely that the three limestone formations are at least partly equivalent to one another, having been laid down during the last interglacial period of the late Pleistocene, Marine Isotope Stage (MIS) 5e. More paleontological and field studies, and OSL datings, are needed to test that conclusion.

Dampier Limestone

Fossils in the Dampier Limestone show that it was deposited during the last interglacial period, MIS 5e (Kendrick, 1990; Kendrick et al., 1991). The formation consists of shelly and coralline limestone, laid down under water of open-ocean salinity.

GW Kendrick (1995, written comm.) identified 21 bivalve and nine gastropod species from the Dampier Limestone in a quarry 0.9 km east-southeast of the old Flint Cliff Telegraph Station (217935E, 7076562N). He stated that this fauna points to the last interglacial period (130–120 ka). An OSL dating of the limestone at this locality is 74.10 ± 11.0 ka (M Cupper, 2010, written comm.), but this seems implausible, as it would point to part of the last glacial period when sea level was as much as 50 m lower than it is now, whereas there is no evidence that recent tectonic uplift of such magnitude has occurred in the area.

Several small limestone outcrops on Dirk Hartog Island are correlated with the Dampier Limestone. A limestone containing abundant heads of colonial corals is exposed sporadically along the west side of Tetrodon Loop, where it is largely covered by dune sand. O'Leary et al. (2008) recorded the presence of the corals *Platygyra*, *Porites*, and *Galaxia* in these outcrops, samples of which returned an average age of 126.5 ± 1.5 ka, showing that they were deposited during the last interglacial period, MIS 5e. Other small exposures of shelly limestone and calcrete on the island, containing large bivalves, are here assigned to the Dampier Limestone (Figs 152–154). The best outcrops are at 715570E, 7132440N (West Well, Fig. 154); 710760E 7130360N; 711620E, 7132930N; and 711680E 7133230N.

On Dirk Hartog Island, at 711635E, 7132440N, about 10 m above sea level, a hole has been blasted through Dampier Limestone. The limestone dips to the southwest at about 2º, and overlies about 1.5 m of dark reddish-brown sandstone (Fig. 152). The upper 5–10 cm of the hard limestone is calcretized, and overlies shelly limestone about 1.5 m thick containing large bivalves and lesser numbers of gastropods. Many of the bivalves are closed shells (Fig. 153). This shelly limestone has not been dated, but it is thought to correlate with the last interglacial (late Pleistocene, MIS 5e). The observed dip of 2º southwest suggests that tectonism associated with the Dirk Hartog Anticline probably persisted into the Pleistocene and, perhaps, Holocene times.

Carbla Oolite Member

The Pleistocene Carbla Oolite Member of the Dampier Limestone is exposed at several localities beside the east coast of Hamelin Pool. It has not been examined in any detail during the present study.

Bibra Limestone

The Bibra Limestone consists largely of beach-ridge deposits, with some tidal-flat and coralline deposits, that occur at scattered localities throughout much of the Shark Bay area (Logan et al., 1970a). The formation contains an open-marine fauna of molluscs and corals that grew prior to the Holocene restriction of circulation in Hamelin Pool. It seems possible that this formation correlates with last interglacial Dampier Limestone and Depuch Limestone. However, Logan et al., (1970b) reported an unconformity between the Bibra Limestone and Dampier Limestone.

Depuch Limestone

The Depuch Limestone is a unit of calcarenite and calcirudite exposed along the east side of the Edel Land Peninsula (Logan et al., 1970b). The formation consists of strongly cemented red-brown calcarenite and calcirudite, apparently derived by the erosion and reworking of Tamala Limestone. It seems likely that the formation is late Pleistocene in age, equivalent to the Dampier Limestone and Bibra Limestone.

Tamala Limestone

The Tamala Limestone is exposed in the western coastal part of the Shark Bay area, from Koks Island in the north to Kalbarri in the south. From there it extends south into coastal areas of the Perth Basin, where it was originally known as the 'Coastal Limestone' (Saint-Smith, 1912). In the Shark Bay area it was named the 'Tamala Eolianite' by Logan (1968), after Tamala Station. It was renamed Tamala Limestone by Playford et al., (1976b), because it consists almost entirely of limestone, and 'eolianite' is a genetic, rather than lithological, term. A type section for the formation was not designated by Logan (1968) and Logan et al. (1970b), but it was defined by Playford et al., (1976b) as the cliff face below the north side of Womerangee Hill, on Tamala Station, where the thickness of the unit above sea level is 250 m. An interesting review of historical aspects of the Tamala Limestone is given by Mayer (2012).

The Tamala Limestone correlates with the Bundera Calcarenite and possibly also with the Exmouth Sandstone in the northern Carnarvon Basin (Hocking et al., 1987). The Bossut Formation of the Pilbara coastline and coastal Canning Basin also correlates with the Tamala Limestone.

The last part of the track leading to Womerangee Hill follows the line of an old rabbit-proof fence constructed during the 1920s (Figs 122–124). It was effectively the southern boundary of Tamala Station for many decades, although the pastoral lease once extended to south of the *Zuytdorp* wreck site. This fence continued down a spur in the precipitous cliff at Womerangee Hill, ending at a small cliff above the water. Some of the original fence posts remained in place on the cliff face until about 1995, but long before then most of the rabbit-proof netting along the fence had rusted away, and it has now virtually disappeared. During the shearing season at Tamala it was once an annual ritual for shearers and their rousabouts to catch fish from the base of the scarp at this locality (T Pepper, 1958, pers. comm.). It is hard to imagine how they were able to carry large catches up such a precipitous cliff. The type section, which passes down the cliff face below the fenceline at Womerangee Hill, was first measured by Playford in 1954, and it was documented and sampled for OSL analysis by Haines and Brooke in 2004 (Fig. 155). Their description of this section is shown in Table 2.

Samples collected from this section were sent for OSL dating to Tim Pietsch and Jon Olley of CSIRO Land and Water (Pietsch and Olley, 2005a), returning dates of 360 ± 30 ka at 85 m, 270 ± 30 ka at 120 m, 205 ± 18 ka at 132 m, and 230 ± 30 ka at 215 m (measured below the top of the section; Fig. 155; Table 2). Another sample, from 33 m below the top of the section, may be about 260 000 years old. Those dates are problematic, as they show age inversions; and the sample at 85 m cannot be the oldest. Pietsch and Olley have stated that these anomalies might be explained by inaccuracies in the dose-rate calculations, due to differences in rates between red horizons (linked with paleosols), and adjoining cross-bedded strata. They also concluded that the major part of this section was probably deposited about 250 000 years ago, that is within glacial period MIS 8 (Fig. 156; Pillans et al., 1998; Sidall et al., 2006; Cohen and Gibbard, 2011; Smith et al., 2011). Further sampling and OSL dating will be needed to clarify these results.

Figure 152. A hole blasted through the Dampier Limestone on Dirk Hartog Island at MGA Zone 49, 711635E, 7132440N, apparently in an attempt to obtain water. The upper part of the limestone is calcretized.

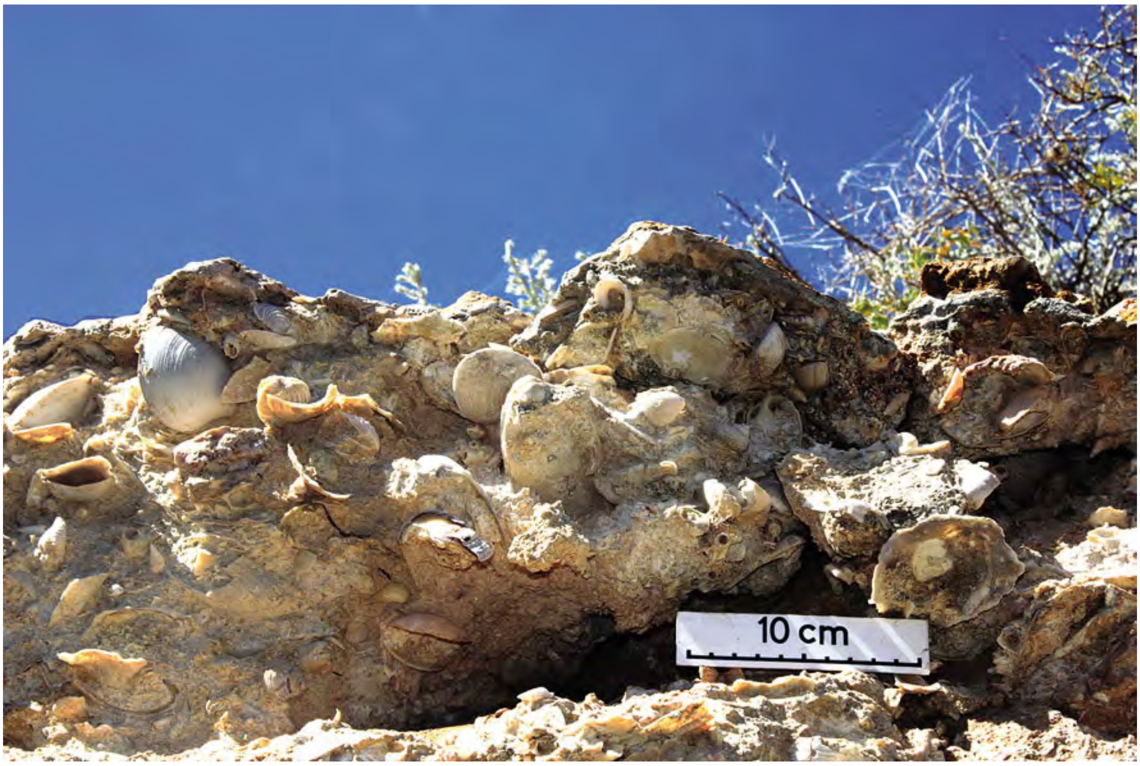

Figure 153. Calcretized Dampier Limestone containing fossil bivalves (including closed shells) at the site on Dirk Hartog Island shown in Figure 152.

Figure 154. West Well on Dirk Hartog Island, situated in a wide expanse of calcretized Dampier Limestone. This well supplies fresh water to the homestead. White mobile dune sand can be seen in the background. Photo was taken in 1955.

Table 2. Type section of the Tamala Limestone at Womerangee Hill

Top of cliff, 250 m above sea level	
2.5 m	Massive nodular calcrete
2.5 m	Reddish pisolitic calcrete, 30 cm thick, at the base, overlain by well-cemented calcarenite with gastropods and abundant rhizoliths
7.0 m	Massive brown calcarenite with abundant rhizoliths, gastropods, and calcified pupal cases
4.0 m	Red nodular calcarenite with gastropods
6.0 m	Well-cemented massive calcarenite; no visible bedding
3.0 m	Nodular paleosol with abundant rhizoliths and gastropods
4.0 m	Calcarenite with weakly developed foresets
3.0 m	Nodular paleosol with abundant rhizoliths and gastropods
5.0 m	Weakly cross-bedded calcarenite
3.0 m	Red paleosol with rhizoliths and gastropods
16.0 m	Mostly scree covered, but apparently mainly calcarenite
6.0 m	Four thin, red, sandy paleosol horizons interbedded with calcarenite
14.5 m	Mostly scree covered, but apparently mainly calcarenite
0.5 m	Irregularly exposed, red, sandy paleosol
22.0 m	Largely scree covered, but apparently mainly yellowish-brown calcarenite; large foresets in upper part; possible poorly exposed paleosol in middle
1.0 m	Reddish sandy paleosol
3.0 m	Mostly scree covered, but appears to be mainly calcarenite
4.0 m	Two nodular sandy paleosol horizons separated by a thin, irregular calcrete unit; slightly reddened below calcrete; rhizoliths, gastropods, and calcified pupal cases in paleosols
25.0 m	Yellowish-brown, quartz-rich calcarenite with very large foresets, having grain-size alternation from thin (a few millimetres) fine-grained to thicker (2–5 cm) coarse-grained sand beds; foresets dip up to 35° towards east–northeast; burrows preserved on the surface of bottomset beds
4.0 m	Pink nodular paleosol with gastropods, rhizoliths, and calcified pupal cases, capped by soft recessive red sand bed approximately 1 m thick
29.0 m	Yellowish-brown calcarenite with very large foresets; the central part of this interval is scree covered
5.0 m	Nodular paleosol overlain by red sandy paleosol
50.0 m	Yellowish-brown calcarenite with very large foresets; two lenticular units separated by red sandy paleosol
1.0 m	Red nodular paleosol
4.5 m	Massive lenticular red sandstone
1.5 m	Lenticular yellowish-brown calcarenite with foresets
1.0 m	Lenticular red nodular and conglomeratic calcrete
22.0 m	Yellowish-brown calcarenite with large foresets; becoming reddish towards the top
Base of cliff, at sea level	

The OSL conclusions conflict with those reached by Hearty and O'Leary (2008), who claimed that for the Tamala Limestone below Womerangee Hill the middle and upper beds are of early Pleistocene age, and those lower in the section may perhaps be as old as late Pliocene (interglacial stages MIS 25, 31, and 37). However, the OSL results indicate that the Tamala Limestone at its type section was deposited during the Middle Pleistocene, within glacial period MIS 8.

Playford et al., (1976b) and Playford (1988, 1990, 1997) used the term 'Tamala Limestone' for coastal occurrences of limestone eolianite in the Perth and Carnarvon Basins. Hearty and O'Leary (2008) claimed that this name has since been applied to 'all of WA', but did not quote any source to support that assertion. In fact, usage of this name has hitherto been restricted to the Perth and Carnarvon Basins, but it may now be extended to include outcrops of Pleistocene dune limestone along the south coast between Augusta and Esperance. Smith et al. (2011) claimed that this formation is the world's most extensive eolianite deposit. That may be true with respect to limestone eolianites, but some quartz-sand eolian deposits, such as those forming the major deserts of the world, are even more extensive.

Playford et al. (1976b) and Playford (1988) maintained that the Tamala Limestone was largely deposited during glacial periods of the Pleistocene, when wide areas of the continental shelf were exposed, and carbonate productivity was high. That conclusion was reached because dune limestones are known to extend well below modern sea level between Shark Bay and the south coast of Western Australia, and, moreover, many of those dunes were much higher and more extensive than those forming along the coast today. Clearly the prevailing southerly to southwesterly winds were considerably stronger, and conditions were much drier, during the glacial periods than they are now. Larger amounts of sand were mobilized during those periods, building much higher dunes.

Those conclusions are confirmed by the type section at Womerangee Hill (Fig. 155). The hillcrest at this location reaches 287 m above sea level. The top of the original dune system must have been appreciably higher than this, because the Tamala Limestone extends below sea level at this locality (and indeed all along the Zuytdorp Cliffs). Moreover, the dune limestone is capped by calcrete that must once have been covered by a layer of leached sand. Accordingly it is inferred that the dune here must have attained heights of 300 m or more above sea level. The winds responsible for such a huge dune must have been much stronger than those prevailing in the area today, which are themselves among the strongest winds now experienced along the coast of Western Australia.

Rottnest Island, off Fremantle, contains some of the best exposures of the Tamala Limestone in the Perth Basin, and dates obtained for the formation there are relevant to the study of this unit in the Shark Bay area (Figs 156 and 157). Hearty (2003), discussing the Tamala Limestone on Rottnest Island, claimed that most of the formation there was deposited during interglacial rather than glacial periods. However, that claim is not supported by the OSL dating of Pietsch and Olley (2005b), nor by the thermoluminescence (TL) dating of Price et al. (2001). At least three phases of eolianite deposition during the Pleistocene are evident in the Tamala Limestone on Rottnest Island. Two of these eolian limestone phases, deposited during the last glacial period, are well exposed on the eastern coast of the island at Bathurst Point (Fig. 157). Pietsch and Olley (2005b) have dated the older, and more strongly lithified, of these two limestones as 77 ± 12 ka, and the overlying younger and more weakly lithified unit as 27 ± 4.5 ka. The OSL dates obtained on Rottnest Island broadly agree with two earlier TL dates from the same site (Price et al., 2001), which gave last glacial dates of 67 ± 9 ka (for the older unit) and 20 ± 2 ka (for the younger unit). Other last-glacial TL dates, obtained from the Tamala Limestone on the island, were 19 ± 3 ka at South Point and 34 ± 3 ka at The Basin (Price et al., 2001).

Those dates show that the dunes forming most of the Tamala Limestone on Rottnest Island were deposited during the last glacial period, when sea level was lower than it is today — some 50 m lower for the limestone dated as about 77 ka, and 100 m lower for the limestone dated as about 27 ka. The shoreline was then far west of what is now Rottnest Island, when today's sea floor in that area was a low-lying coastal plain, across which sand dunes migrated. At the site of the present island those late Pleistocene dunes were piled against and over an exhumed last interglacial coral reef (Playford, 1988, 1997, Brooke et al., 2010).

At Fairbridge Bluff on Rottnest Island, an older, much less extensive, part of the Tamala Limestone underlies the exhumed last interglacial coral reef (Rottnest Limestone), showing that this part of the Tamala Limestone must have accumulated prior to growth of the reef, some 130 000 years ago (Playford, 1988, 1997). The reef has been uranium-series dated as 132 ± 5 ka by Szabo (1979), uranium-series thermal ionization mass spectrometry (TIMS) dated as between 121 and 128 ka by Stirling et al. (1995, 1998), and TL dated as 132 ± 18 ka by Price et al. (2001).

Hearty (2003) obtained whole-rock amino acid racemization (AAR) dates on Rottnest Island that suggested to him that the Tamala Limestone there was deposited during MIS 5e and continued during MIS 5c, peaking at the end of MIS 5a, about 70 000–80 000 years ago. This author also stated that eolianite deposition resumed in the mid-Holocene (about 6000 years ago) and continued up to the present, and concluded that the Tamala Limestone on Rottnest Island must have been deposited primarily during, or shortly after, the interglacial highstands, when the shoreline was near the present datum, rather than during glacial lowstands. That conclusion is puzzling, as MIS 5e corresponds with the last interglacial period, and MIS 5a–d belong to the last glacial period (Gibbard and Van Kolfschoten, 2005; Siddall et al., 2006; Cohen and Gibbard, 2011).

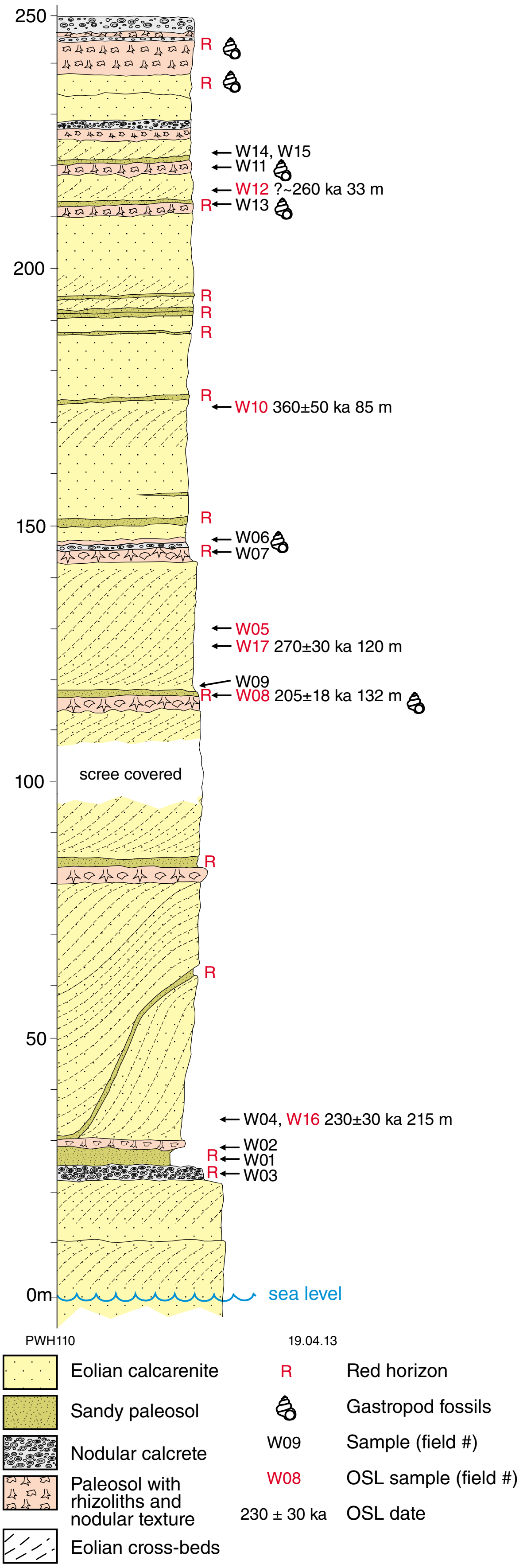

Figure 155. Stratigraphic column illustrating the type section of the Tamala Limestone below Womerangee Hill.

Hearty (2003, table 1) indicated that Playford (1988, 1997) considered that most of the Tamala Limestone was deposited during the early and middle Pleistocene, and also showed a question mark regarding Playford's views on deposition of the formation during the last glacial period. But Playford (1988, 1997) maintained that most of the Tamala Limestone on Rottnest Island was deposited during the last glacial period, a conclusion that was subsequently confirmed through TL and OSL dating.

Hearty and O'Leary (2008) stated that the type locality of the Tamala Limestone should be representative of Quaternary eolianites across Western Australia. However, they apparently did not study or sample the type section, instead examining a much thinner section (127 m thick) situated 3 km north of the type section. Although these authors used the name 'Tamala Limestone' they also refer to the informal names 'Zuytdorp Limestone' and 'Woomerangee [sic] member' in a table, apparently using them for the part of the formation that is exposed in the type section at Womerangee Hill and elsewhere along the Zuytdorp Cliffs. However, those names serve no useful purpose and are, in any case, invalid.

There can be little or no doubt that the AAR method, as used by Hearty and O'Leary (2008), is unreliable in dating the Tamala Limestone.

Peron Sandstone

The name Peron Sandstone was proposed by Logan (1968) and further discussed by Logan et al. (1970b). The type locality at Cape Peron is 120 m thick (Figs 33, 34).

The Peron Sandstone is characterized by red, poorly bedded, partly calcareous, sandstone that outcrops discontinuously along the shorelines of Peron Peninsula and Faure Island. It is a lateral equivalent of the Tamala Limestone, with which it interfingers along parts of the west coast of Peron Peninsula, notably at Eagle Bluff (Fig. 158). The Peron Sandstone is considered to be an eolianite, but unlike the limestone eolianites of the Tamala Limestone it is composed mainly of poorly bedded quartz sandstone. The cross-bedding that is so clearly evident in the Tamala Limestone is generally absent in the Peron Sandstone. The red colour of the sandstones is due to a thin coating of anhydrous iron oxide on the quartz sand grains.

Pietsch and Olley (2005a) reported an OSL date of 275 ± 30 ka for a sample from the Peron Sandstone in its type section, and 128 ± 16 ka for another at Eagle Bluff. Clearly, more datings are needed before definitive statements can be made regarding the timing of deposition of the Peron Sandstone, but it is expected to be largely of the same age as the Tamala Limestone in the Shark Bay area.

Logan et al. (1970b) suggested that the Peron Sandstone may have been derived through the leaching of calcareous eolianite dunes, in the same way that the Bassendean Sand in the Perth area formed by dissolution of part of the Tamala Limestone. That view is supported here, with much of the sand thought to have been transported far from its presumed source in the Edel Land Peninsula area, when sea level was much lower than it is today and the area between Edel Land and Peron Peninsulas was dry land.

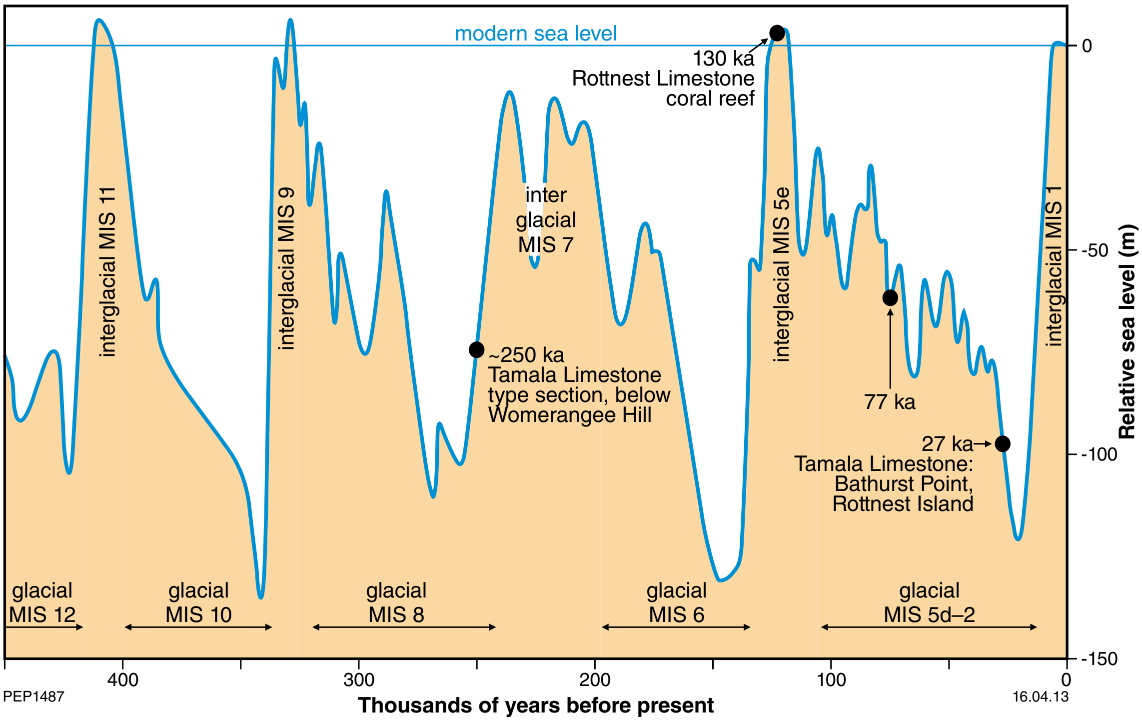

Figure 156. Simplified isostatic sea-level curve and marine-isotope stages for the late and middle Pleistocene (MIS 2-12) and Holocene (MIS 1), modified after Cohen and Gibbard (2011) and Smith et al. (2012), showing dates for the Tamala Limestone at Bathurst Point on Rottnest Island, the type section of the Tamala Limestone below Womerangee Hill, and the Rottnest Limestone coral reef.

Figure 157. Tamala Limestone exposed in the cliff face below the Bathurst Point Lighthouse on Rottnest Island. OSL dating has shown that the age of the lower indurated limestone is 77±12 thousand years, and that of the overlying softer limestone is 27 ± 4.5 thousand years, both having been deposited during the last glacial period, when sea level was about 50 and 100 m respectively, below its present level.

Figure 158. Aerial view of Eagle Bluff on Peron Peninsula, where Tamala Limestone interfingers with Peron Sandstone.

Red or yellow sand overlies calcrete at the top of the Tamala Limestone on Edel Land Peninsula and further south (Fig. 159). This sand is regarded as a residual deposit, formed by deep weathering and dissolution of sandy Tamala Limestone, leaving an insoluble residue of quartz sand over the calcrete layer. The calcrete may have formed in the zone of fluctuation of a former water table, and at least part of this layer is thought to have been precipitated by microbes in the soil profile, forming stromatolitic and oncolitic structures (Figs 160, 161). The interpretation of an organic origin for this type of calcrete has been subject to some debate (Read, 1974, 1976; Arakel, 1982; Wright and Tucker, 1991), and more research on this topic seems warranted.

Some of the residual sand formed over the Tamala Limestone must have been blown northward, during glacial periods of lowered sea level, when the present Shark Bay area was occupied by dry land (Fig. 162). That interpretation is supported by an aeromagnetic survey discussed in a later part of this Bulletin. Such residual sand is thought to have been the source for sediments forming the Peron Sandstone and the Denham and Nilemah Sands.

In the Perth Basin, the importance of residual sand resulting from weathering of the Tamala Limestone has been shown by Bastian (1994, 1996), Newsome (2000), and Tapsell et al. (2003). They discussed the origin of bands of quartz sand in the Perth area, and as this work is considered to be relevant in explaining the source of sand in the Peron Sandstone, it is discussed in some detail here. These authors pointed to the characteristic heavy-mineral assemblages in individual bands of sand in the Perth area, concluding that those sands resulted from leaching, over long periods of time, of calcium carbonate from sandy limestones of the Tamala Limestone, leaving behind residues of quartz sand and heavy minerals. Individual bands of the sands contain specific heavy-mineral assemblages, and the minerals most susceptible to weathering have been progressively leached out, from the oldest to the youngest bands (east to west).

On the other hand, Hearty and O'Leary (2008) claimed that the sands are wind-blown deposits derived from the east over the Archean Yilgarn Craton. Bastian (2010) contradicted Hearty and O'Leary's conclusions, reiterating the evidence that the bands of sand were formed by dissolution of Tamala Limestone, and could not have been derived from the Yilgarn Craton by eolian transport. In turn Hearty and O'Leary (2010) responded, rejecting Bastian's arguments, but without addressing his key observations. In our opinion there is no doubt that the interpretations of Bastian (1994, 1996, 2010), Newsome (2000), and Tapsell et al. (2003) are soundly based. If the sand on the Swan Coastal Plain had been blown from many kilometres to the east, as asserted by Hearty and O'Leary, that could not have resulted in the observed north-south bands of sand, each containing a characteristic heavy-mineral assemblage, consistent with the more soluble minerals having been progressively leached out from east to west.

Hearty and O'Leary (2010) pointed out that the process of dissolving calcium carbonate to produce quartz sand should have produced karst features at the top of each limestone body, and they claimed that such karst is absent in the area of the Perth Basin. Furthermore, they claimed that neither extensive karst nor cavernous weathering associated with the dissolution needed to account for the abundance of pure quartz that can be seen in the basin. That statement is clearly incorrect: karst developed below yellow or white quartz sand has been well exposed at several localities around Perth and Fremantle (Figs 163–165). Moreover, cavernous karst in Tamala Limestone is widespread in the southwest of Western Australia, extending for some 500 km from Augusta in the south to Jurien in the north. Hearty and O'Leary (2010) claimed to have conducted a comprehensive and unbiased survey of outcrops of Tamala Limestone in the Perth Basin. However, they evidently failed to observe a conspicuous exposure of karst, with yellow sand between and overlying karst columns, on the south side of Mt Eliza, near Perth (Figs 163, 164). Moreover, comparable features have been observed from other localities in the Perth–Fremantle area (e.g. Fig. 165). Indeed there can be no doubt that the widespread yellow and white sands in the Perth area have resulted from dissolution of sandy Tamala Limestone.

Among the most striking karst features in the Perth Basin are 'The Pinnacles' in Nambung National Park (Fig. 166). Playford et al. (1976b) interpreted these features as having formed around 'solution pipes', and McNamara (2009) interpreted them as having developed around the roots of large trees, whereas Hearty and O'Leary (2008) claimed that they represent casts and moulds of large trees in ancient forests. Lipar (2009) suggested a polygenetic origin, with roots playing a major role. We basically agree with McNamara that most of the pinnacles formed around tree roots (perhaps the tap roots of large eucalypts) during a pluvial period of the Pleistocene.

Studies of the weathering products of Tamala Limestone in the Perth Basin are in accord with the interpretation accepted here, that sands in the Peron Sandstone are derived from leaching of Tamala Limestone. It is desirable that studies of the heavy minerals in the Peron Sandstone, comparable with those carried out in the Perth Basin, should be conducted in the Shark Bay area.

Hoult Sandstone Member

The name Hoult Sandstone Member is proposed for a Last-Interglacial unit within the Peron Sandstone that is exposed along the south margin of Faure Island (Figs 167–169). The member name is taken from Hoult Landing on Faure Island, which is itself named after the Hoult family, who owned the Faure Island pastoral lease for many years. Playford and Berry (2002), in an unpublished report, used the name 'Faure Sandstone Member' for this unit, but that name is inappropriate because Iasky and Mory (1999) had used the name Faure Formation for a Lower Devonian unit in the subsurface of this area.

The type section (788606E 7133716N) of this member consists of 3.2 m of fossiliferous, reddish-yellow, calcareous sandstone, which is both underlain and overlain by typical red sandstone of the Peron Sandstone. The member dips at 2º east (Fig. 167).

A rich bivalve and gastropod fauna (Table 3; Fig. 169) has been collected from the Hoult Sandstone Member, and identified by GW Kendrick of the Western Australian Museum (in Playford and Berry, 2002). Thirty-two species were described from the member, of which 12 are known only in the lower part, 15 only in the upper part, and five are common to both parts. This fauna is considered by Kendrick to be indicative of the last interglacial period of the late Pleistocene.

Figure 159. White calcrete overlain by red sand northeast of Womerangee Hill. The sand is residual, resulting from the leaching of sandy limestone of the Tamala Limestone.

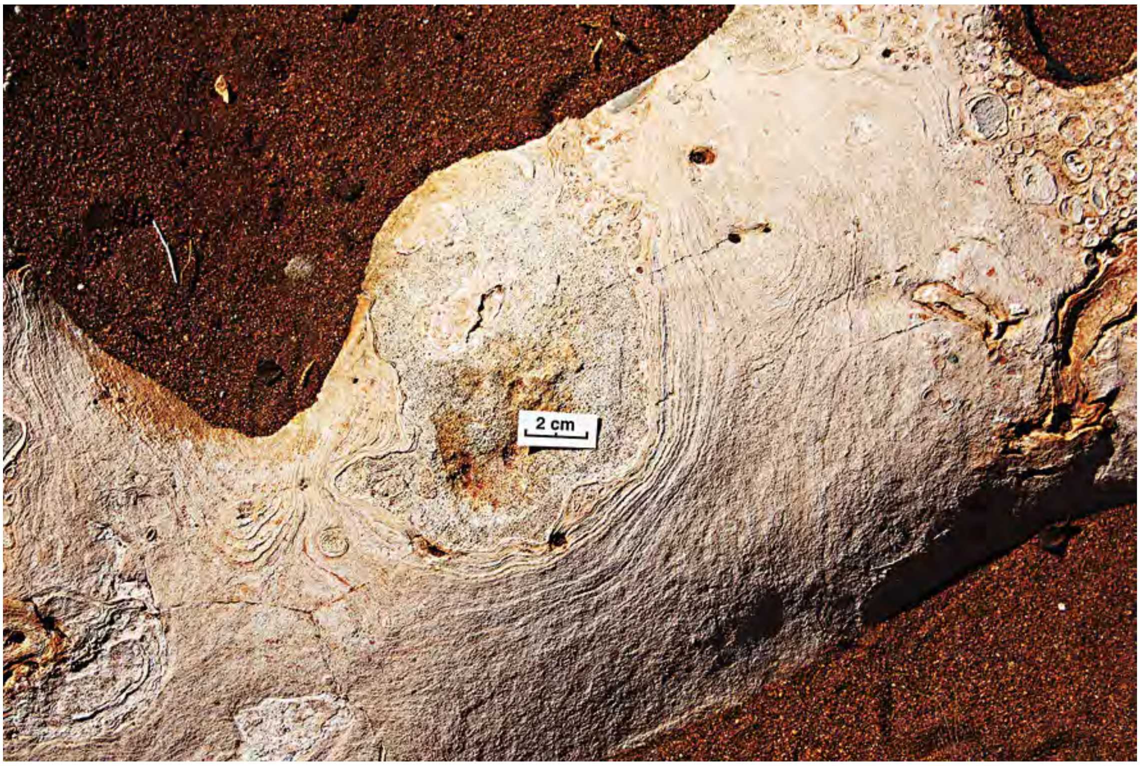

Figure 160. The top of the calcrete layer near the site shown in Figure 159, with stromatolitic and oncolitic layering attributed to soil microbes. This is thought to have formed at or near the water table during a wetter period of the late Pleistocene or early Holocene.

Figure 161. Closer view of oncolites in calcrete near the site shown in Figure 160.

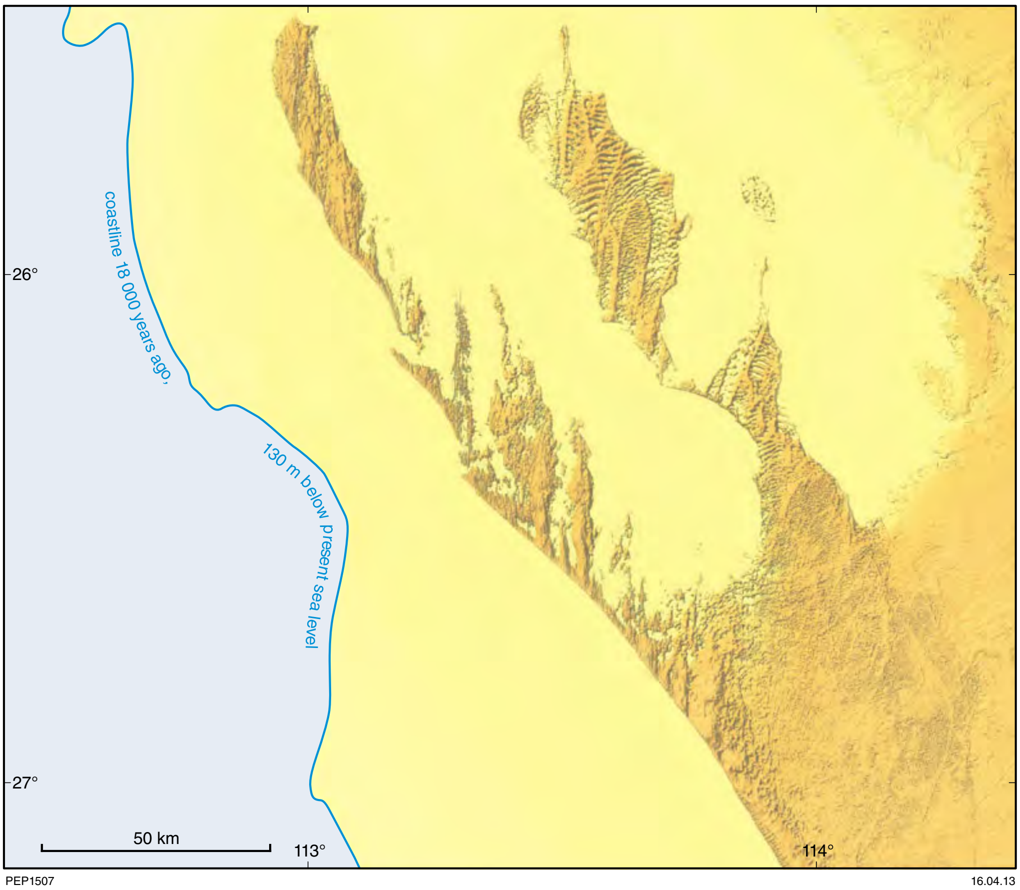

Figure 162. Diagrammatic map, superimposed on a DEM image of the Shark Bay area, illustrating the shoreline at the peak of the last glacial period, about 18 000 years ago, when sea level was around 130 m lower than it is now.

Figure 163. Cliff face on the south side of Mount Eliza, near Perth. This cliff shows white and yellow sand above Tamala Limestone, the contact between them being a dissolution surface, with vertical pipes now filled with yellow sand. The pipes are thought to have formed through the decay of large tree roots.

Figure 164. Closer view of the pipes filled with yellow sand that are shown in Figure 163.

Figure 165. Photo of a quarry near Fremantle, taken in 1955, showing yellow sand filling karst pipes in Tamala Limestone, overlain by thin black soil and a large heap of white sand spoil. This quarry and several others in the area are no longer extant, having been filled with garbage and sand.

Figure 166. Columns of calcretized limestone, thought to have developed around the tap roots of large trees, in Tamala Limestone at 'The Pinnacles', near Cervantes. The columns were once surrounded by residual yellow sand that has since been largely blown away. Tony Cockbain is the person in the photo.

Figure 167. Hoult Sandstone Member of the Peron Sandstone, dipping east at about 2°, in the lower half of a cliff of Peron Sandstone along the south coast of Faure Island. Paddy Berry is the person in the photo.

Figure 168. **Closer view of the Hoult Sandstone Member of the Peron Sandstone in the lower half of the cliff beside the south coast of Faure Island. The hammer is at the top of the member.**

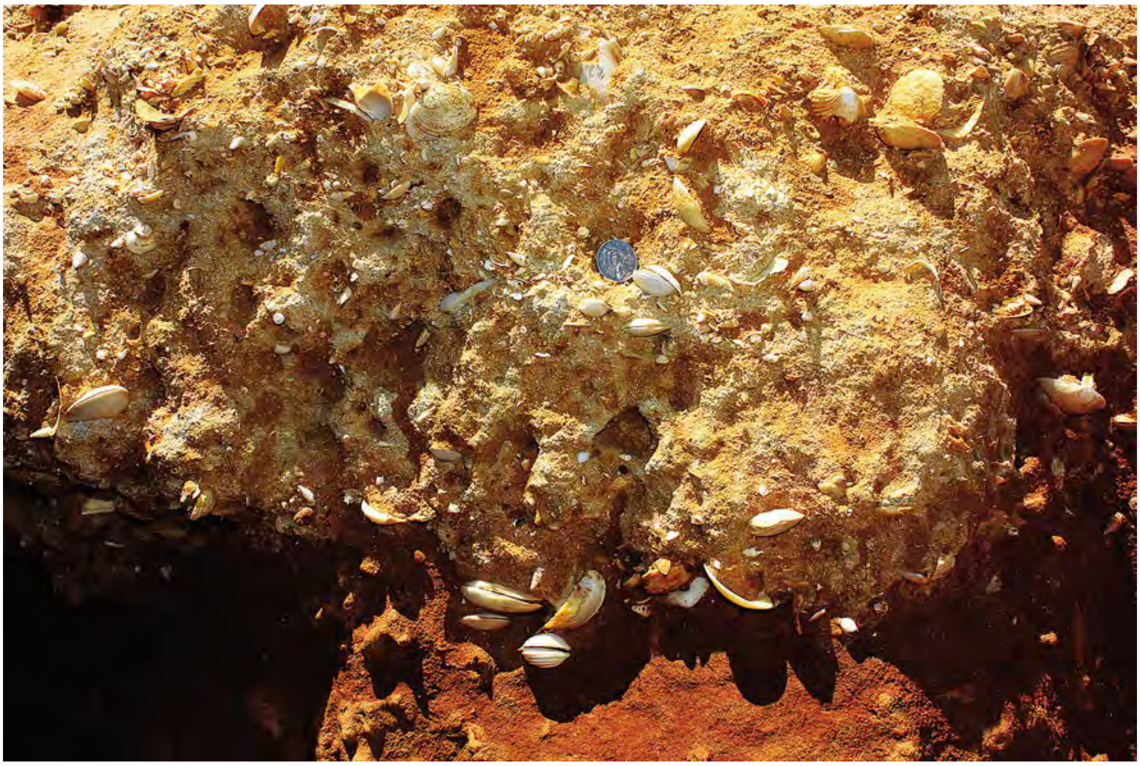

Figure 169. **The basal bed of the Hoult Sandstone Member, overlying red quartz sandstone of the Peron Sandstone, beside the south coast of Faure Island. Note many closed bivalve shells, indicating subtidal deposition. The 10-cent coin is 2.3 cm in diameter.**

Table 3. Fossils recorded from the Hoult Sandstone Member of the Peron Sandstone

Taxa	*Lower part of unit*	*Upper part of unit*	*Remarks*
Bivalves			
Ostrea sp.	+	+	
Dendostrea folium		+	
Pinna sp.		+	Specimen poorly preserved
Anodontia (A.) pila		+	
Wallucina assimilis	+		
Divalinga bardwelli		+	
Megacardita turgida		+	
Acrosterigma dupuchense		+	Not known living south of Warroora
Fragum carinatum	+		Not known from the Holocene of WA
Fragum unedo	+		
Tellina (Tellinella) virgata	+		
Tellina (Tellinella) staurella		+	
Anomalocardia squamosa	+	+	
Gafrarium intermedium	+	+	
Tapes dorsatus		+	
Tapes literatus	+		
Circe lenticularis		+	
Pitar citrina	+		
Placamen gravescens		+	
Placamen berrii	+		
Gastropods			
Calliostoma sp.		+	
Turbo (Euninella) gruneri		+	
Clypeomorus bifasciata	+		
Cerithium tenellum	+	+	
Bittium icarus	+		
Polinices conicus		+	
Cantharus (Pollia) undosus		+	
Nassarius (Niotha) albinus	+		
Pyrene scripta		+	
Vexillum vulpeculum	+	+	
Acteocina sp.	+		
Bullaampulla sp.	+		

Quaternary

Much of the Shark Bay area is covered by sand-dune systems that probably range in age from late Pleistocene to early Holocene. These dunes are included in three sand formations, here named the Carrarang Sand, Denham Sand, and Nilemah Sand.

Carrarang Sand

The name Carrarang Sand is proposed for limesands forming dunes over Pleistocene limestones on Edel Land Peninsula, and extending south almost to the Murchison River. The type locality is Bellefin Prong (730000E, 7117800N) and the formation is named after the former Carrarang Station. The Carrarang Sand also covers much of the surface of Dirk Hartog, Dorre, and Bernier Islands. In most of those areas the dunes are fixed by vegetation, but in some places they have recently been reactivated, forming 'blowouts' where the vegetation has been removed, probably as a result of intense grazing by feral goats.

The Carrarang Sand (Fig. 30) typically consists of pale-red and yellow to white medium-grained, weakly lithified, calcareous sands, made up of fragments of molluscs and foraminifers, and containing varying amounts of quartz sand. It forms seif, parabolic, barchan, massive, and undulating dunes. These types of dunes are described and illustrated earlier in this Bulletin (Figs 30–32, 38–41, 86–94). The seif dunes, up to 40 km long, are truncated along the present shorelines (Figs 39–41), indicating that they were once significantly longer when sea level was lower than it is now.

The Carrarang Sand was deposited on the Edel Land Peninsula, probably during the late Pleistocene to the Holocene. Sand forming the Carrarang Sand must have originally been blown up and over the scarp of the Zuytdorp Cliffs, by dust storms driven by very strong southerly winds during the last glacial period, when sea level was much lower than it is now. During those times, large areas of the continental shelf were exposed in front of the Zuytdorp fault-line scarp (Fig. 162). Barchan dunes and some bare areas of sand are still active in the area today, but most other dunes are now stabilized with vegetation.

As noted earlier, a core sample taken from a weakly cemented seif dune in the Carrarang Sand (at 756707E 7053917N) has been dated by OSL as mid-Holocene, 4900 ± 700 years BP (M Cupper, 2010, written comm.). However, it seems likely that much of the formation is older than this, and many more OSL (and/or TL) and radiocarbon datings will be needed to more adequately determine the depositional history of these dunes.

Denham Sand

The name Denham Sand is proposed for a unit of red sand that forms parabolic and transverse dunes on the Peron Peninsula, Nanga Peninsula, and Faure Island (Figs 30, 32, 71). The unit consists of quartz sand and limesand grains, which are mainly medium grained, and coloured red by a thin coating of anhydrous iron oxide. Peron Peninsula is designated as the type locality (759000E 7145000N), and the formation is named after the township of Denham.

The Denham Sand overlies the Pleistocene Peron Sandstone, and may be largely a weathering product of that formation. The Denham Sand has not been dated, but seems likely to be late Pleistocene to mid-Holocene in age. The parabolic and associated transverse dunes that characterize the formation are stabilized by vegetation and truncated along the present shoreline; hence, they must have formed when sea level was lower than it is today. The parabolic and transverse dunes are well displayed in DEM images (Figs 31, 32), but are obscure on the ground and on airphotos.

Nilemah Sand

The name Nilemah Sand was introduced (as 'Nilemah Sands') by Logan et al. (1970b) for the dune deposits in their 'Peron Province'. The name was taken from the abandoned Nilemah Homestead (Fig. 50; derived by spelling 'Hamelin' backwards). The Nilemah Sand consists of sand dunes and sand plain extending south over a wide area from just north of Nilemah Homestead to the Murchison River, east of the coastal belt of Tamala Limestone. The type locality is along the west side of Hamelin Pool, from just north of the abandoned Nilemah Homestead to the Nilemah Embayment (202000E 7072000N). The dunes are classed as parabolic and undulating dunes (Figs 86, 89).

The Nilemah Sand consists of red sand, grading from sandy calcarenite adjoining the coast, to quartz sand further inland. It was probably largely derived by leaching of the Tamala Limestone and Peron Sandstone. The quartz fragments are medium to fine grained, and have thin coatings of anhydrous iron oxide.

Some of the Nilemah Sand south of Hamelin Pool contains concentrations of the heavy minerals ilmenite, zircon, rutile, and leucoxene, forming an orebody 33 km long, known as the Coburn heavy mineral sands or the 'Amy Zone' (Fig. 170; Environmental Protection Authority, 2005; Gunson Resources Limited, 2012; Harley, 2004, 2008).

Accumulations of heavy minerals, mainly garnet, can commonly be seen from the air at low tide below parts of Section 1 of the Zuytdorp Cliffs, in places where narrow beaches have developed below those cliffs. These minerals, and those in the Coburn heavy-mineral sands, have been derived by weathering of Precambrian rocks of the Northampton Complex. They were carried to the sea by the Murchison River, and swept north, in front of the Zuytdorp Cliffs, by the prevailing longshore drift.

Birrida gypsum deposits

As discussed earlier, birridas are flat-floored gypsum-filled depressions in low-lying interdune areas along Peron, Nanga, and Edel Land Peninsulas, and on Dirk Hartog and Faure Islands (Figs 32, 66–71). They are especially well developed between transverse dunes on Peron and Nanga Peninsulas, and range in size from less than 100 m^2 up to 18 km^2. The thickness of gypsum in birridas ranges from less than 1 m to a maximum of at least 9 m (Butler, 1985). The gypsum must have been derived from seawater aerosol, carried inland by winds, and concentrated by rainwater leaching.

One birrida west of the old Peron Station Homestead (750952E 7140584N; Figs 67, 68), was drilled using a hand auger, and found to contain a layer of gypsum 1.87 m thick. The elevation of the flat upper surface of this birrida is about 5 m above sea level.

Two adjoining birridas near Booldah Well (at 792936E 7096143N; Figs 171, 172) are overlapped by Hamelin Coquina, and are therefore older than the oldest beds of that formation, that are radiocarbon-dated as 5316 ± 42 years BP. Those birridas, and others in the Shark Bay area, must be older than this, and it is likely that they were formed during the late Pleistocene or early Holocene.

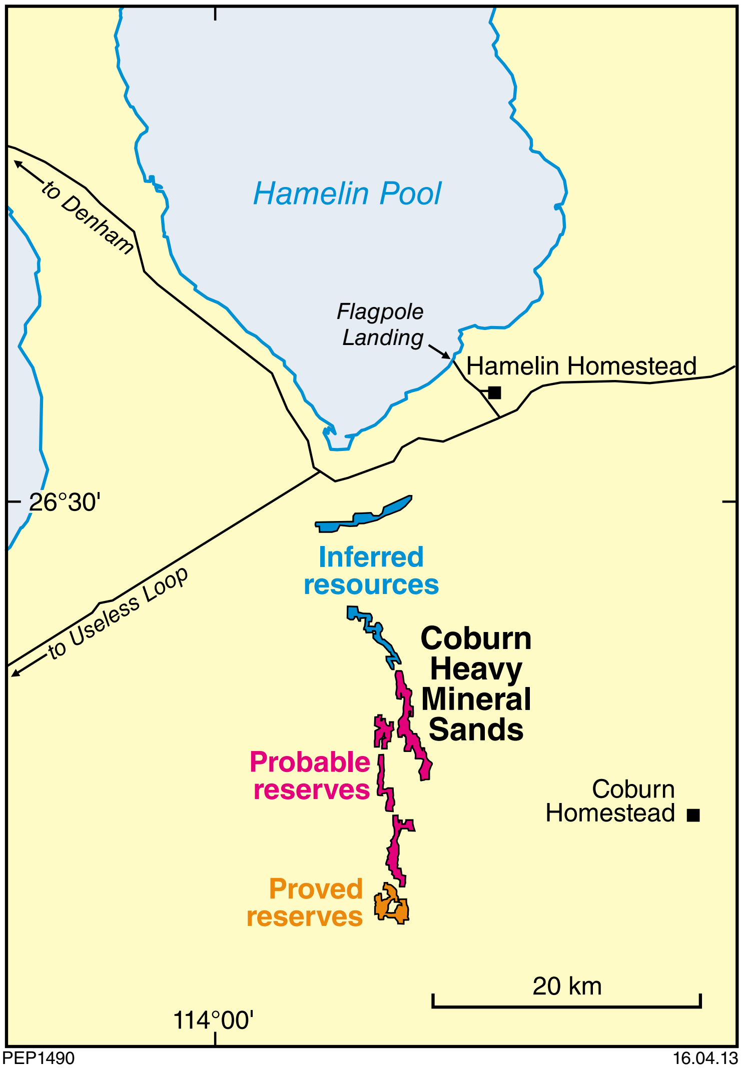

Figure 170. Map showing the extent of known heavy-mineral-sand deposits south of Hamelin Pool. From Harley (2008).

Figure 171. Aerial view looking north over the east side of Nanga Peninsula, showing two birridas onlapped on their eastern sides by the oldest beds of the Hamelin Coquina, radiocarbon dated as 5316 ± 42 years BP.

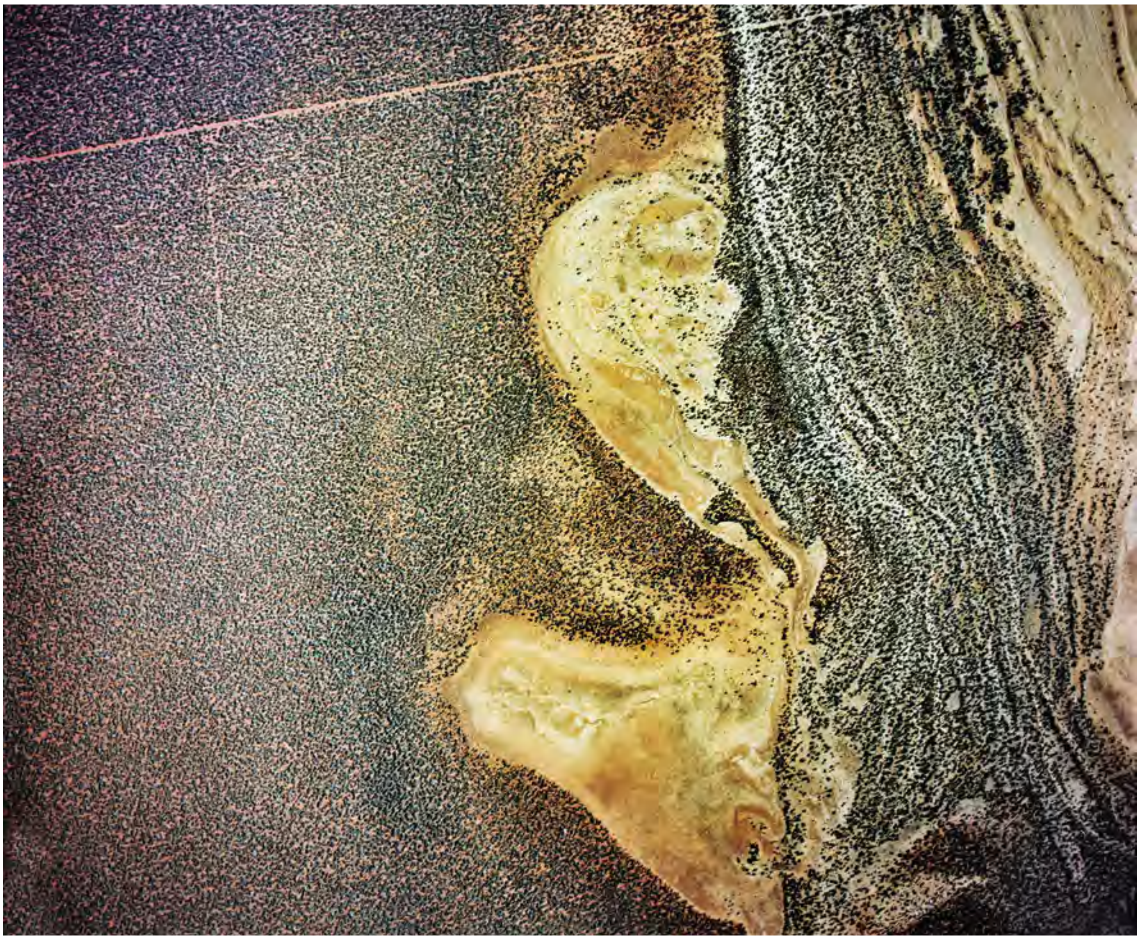

Figure 172. Vertical aerial view of the two birridas shown in Figure 171, both onlapped on their eastern sides (right) by the Hamelin Coquina and surrounded to the west, north and south by red sand of the Denham Sand. The distance from the top to the bottom of the photo is 1.9 km. Airphoto courtesy of Landgate, Western Australia.

Holocene

Three aspects of the Holocene geology of Shark Bay area are discussed in some detail in this section — tsunami deposits, Hamelin Coquina, and stromatolites.

Tsunami deposits

Prominent features of the Shark Bay area, along the west coasts of Dirk Hartog, Dorre, Bernier, and Koks Islands, and Point Quobba, are huge blocks of calcrete (weighing up to 700 t or more), lying on flat karstified surfaces behind coastal cliffs. The measured specific gravity of the calcrete in these blocks ranges from 2.44 to 2.55, and taking account of open space in the calcrete due to karstification, 2.4 has been taken as a conservative measure of the specific gravity in calculating the approximate weights of the blocks. These boulder deposits in the Shark Bay area are comparable with those on Legendre and Barrow Islands off the Pilbara coast (Fig. 173), and all are thought to have been emplaced by tsunamis (Fig. 174).

The boulders were torn from coastal cliffs and carried up to 400 m inland and 15 m above sea level. They rest on subhorizontal karstified calcrete over eolian limestone, some blocks being isolated, while others are more extensive. Most are angular and right-way-up or on their sides. The largest boulder deposits are thought to have been emplaced by mega-tsunamis, some of which are estimated to have been more than 20 m high, with runups of at least 35 m above sea level.

Tsunami is the Japanese name for such large waves (Fig. 175; Bryant, 2001, 2008). They are catastrophic events, mostly caused by large earthquakes, but can also result from submarine landslides, underwater volcanism, and asteroid impacts. Tsunamis are generally less than a metre high, moving at speeds of up to 700–900 km/hour where they pass over deep oceans. However, as a tsunami traverses shallower water while approaching the coast, it slows down and rises into a high wave, up to several tens of metres high. In some cases there may be two or more tsunami waves up to two hours apart, and the arrival of the first is commonly preceded by a fall in sea level. Tsunamis

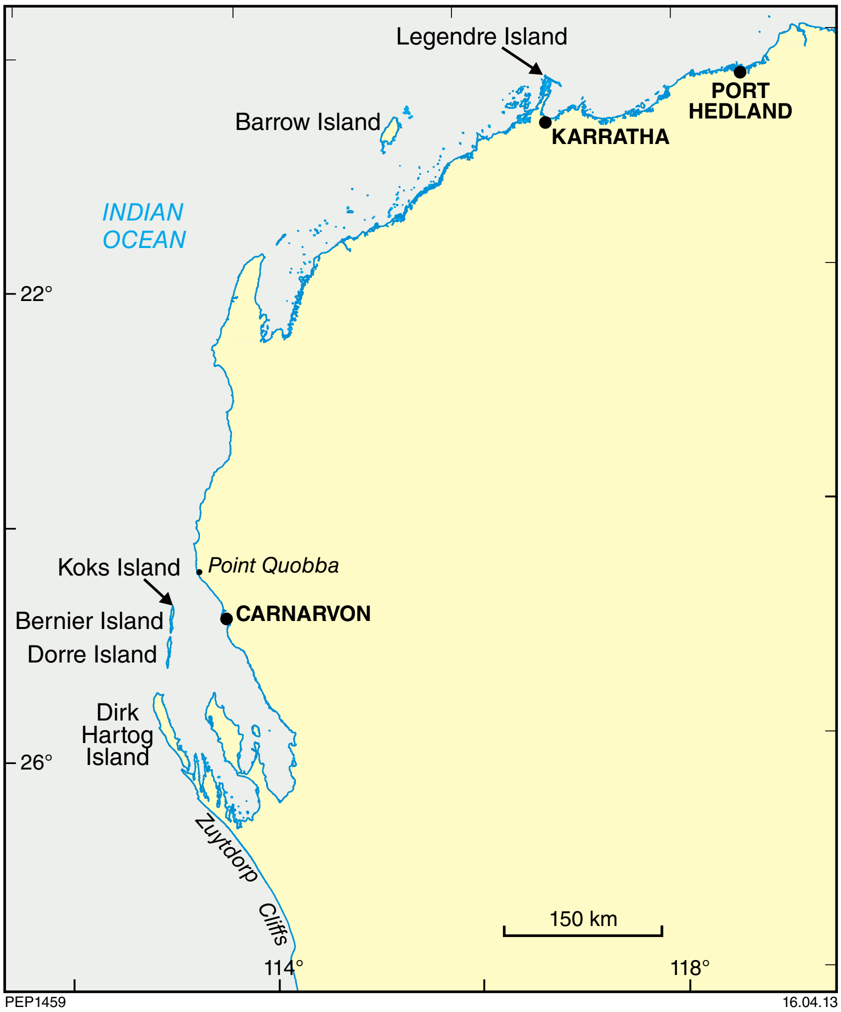

Figure 173. Map showing localities between the Zuytdorp Cliffs and Legendre Island where boulder deposits were emplaced by mega-tsunamis during the past few thousand years.

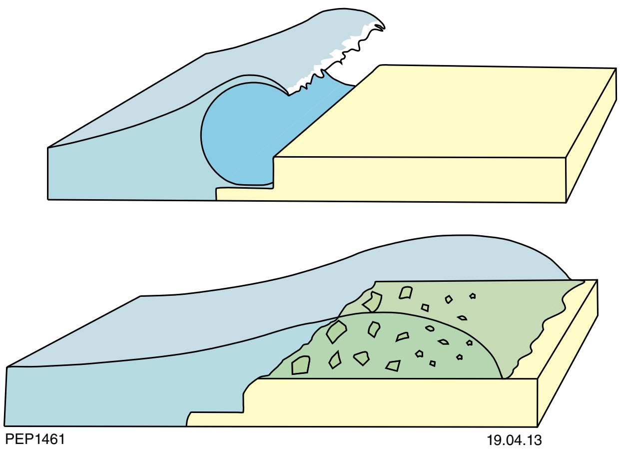

Figure 174. Diagram illustrating a tsunami crashing onto a limestone cliff, tearing off parts of the upper cliff face and depositing large boulders on the land surface behind the cliff.

may cause catastrophic damage and loss of life where they impact on a coast.

Burbidge and Cummins, (2007) and Burbidge et al. (2008) consider that a large earthquake originating off Java has the potential to have a significant impact on the Western Australian coast, especially between Carnarvon and Dampier. That is virtually the same stretch of coast (between Shark Bay and Legendre Island) where the largest boulder deposits described here occur. However, the magnitudes of the boulders in those deposits are surely much too large to have resulted from tsunamis originating so far away in the Sunda Arc off Indonesia, some 1700 km north of Dirk Hartog Island. Moreover, if the Sunda Arc were to be the source, then the boulders would be expected to be larger in the north (Legendre Island) than the south (Dirk Hartog Island). But that is not the case — the maximum size of calcrete blocks at both of these localities is similar. These tsunamis seem most likely to have been generated by local tectonic activity, large submarine landslides on the continental slope (possibly initiated by earthquakes, or large asteroid impacts in the Indian Ocean. Underwater volcanic activity is less likely to have been the source.

The largest recent tsunami affecting the Indian Ocean was the Boxing Day Tsunami of 2004. It was generated by a magnitude 9+ earthquake caused by movement on a mega-thrust along the northwest part of the Sunda Arc, beside the Andaman Islands and the northern end of Sumatra (Fig. 176). This catastrophic tsunami, felt all the way around the Indian Ocean, is estimated to have caused the deaths of more than 270 000 people and the destruction of more than 170 000 houses in countries around the Indian Ocean. Burbidge et al. (2008) recorded that people bathing off some Western Australian beaches were dragged out to sea as a result of that tsunami, but all survived.

Another recent tsunami, resulting from a magnitude 7.8 earthquake off Java in 2006, had a significant impact on Western Australia. That impact would have been much greater if the earthquake had been as large as that for the Boxing Day tsunami. Campers at Steep Point (at the north end of Edel Land Peninsula) were lucky to escape after that tsunami, which had a maximum recorded runup (height reached above sea level) along the coast of Western Australia of 9 m. Prendegast and Brown (2012) reported it was the largest of five significant tsunamis known to have hit that coast in historic times (Burbidge and Cummins, 2007; Burbidge et al., 2008). The tsunami hazard on this coast was further analysed by Jones et al. (2005).

There has been considerable discussion in the literature on issues involved in distinguishing between tsunami and storm deposits (Chen et al., 2011; Courtney et al., 2012; Dominey-Howes, 2007; Fichaut and Suanez 2011; Goto et al., 2011; Hall; 2011; Imamura et al., 2008; Knight and Burningham, 2011; Lorang, 2011; McKenna et al., 2011; Nandasena et al., 2011; Nott, 2003a, b, 2004; Paris et al., 2007, 2011; Richmond et al., 2011; Scheffers et al., 2008; Scheffers et al, 2010; Stephenson and Naylor, 2011).

Goto et al. (2011) reported field evidence from Okinawa that recent storm waves there have lifted 100 t boulders over a reef and onto cliff tops up to 15 m high. They also reported that such waves may be capable of moving 200 t boulders on a reef, and drew attention to accounts elsewhere of storm waves moving boulders weighing up to 235 t. They point out that boulders lifted by storm waves remain concentrated close to the edges of cliffs, whereas those transported by tsunamis may be deposited much further inland.

Nott and Bryant (2003) discussed various boulder deposits along the Western Australian coast, and concluded that they have resulted from tsunamis rather than storm waves. Scheffers et al. (2008) discussed in some detail why the boulder deposits that they described at Point Quobba and elsewhere along the Western Australian coast must have resulted from tsunamis rather than storm waves. They concluded that storm waves could barely move boulders weighing up to 20 t, and heavier boulders could only be lifted and transported by tsunamis.

The boulder deposits described in this Bulletin, on Dirk Hartog and Legendre Islands, and other islands in the Shark Bay area, contain blocks that are much larger (up to at least 700 t) than those described in the publications listed above. There can be no reasonable doubt that the deposits described here from Shark Bay and Legendre Island are the products of tsunamis, and are perhaps the largest such deposits known in the world. On the other hand the boulder deposits at Barrow Island and most of those in the Kimberley are made up of smaller boulders (weighing less than 100 t) and some of these could conceivably be storm rather than tsunami deposits.

The mega-tsunamis evidenced here, dating from several thousand years ago, are of such magnitudes that they must have extended up to several kilometres inland along low-lying areas of the coast, with the potential to cause the deaths of thousands of Aborigines then living in the coastal areas. Those mega-tsunamis were probably the largest catastrophic events to be experienced in Western Australia during the past few thousand years. If a similar tsunami were to occur today, it would have devastating consequences for populated coastal towns and industries in the area concerned.

Figure 175. 'The Great Wave off Kanagawa' by Japanese artist Hokusai (1832), interpreted as depicting a tsunami ('harbour wave'), with Mount Fuji in the background.

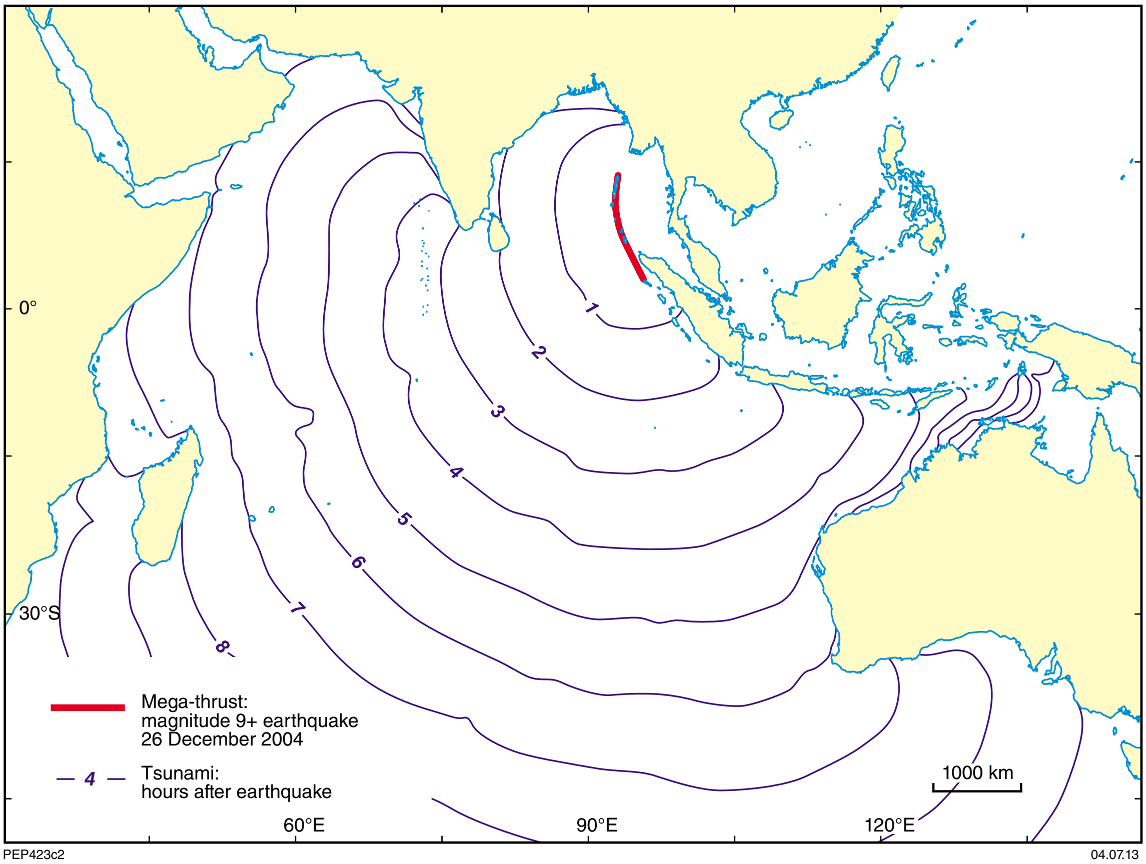

Figure 176. Diagram illustrating the hourly path of the 'Boxing Day Tsunami', generated on 26 December 2004 along the northern end of the Sunda Arc by a magnitude 9+ earthquake. The approximate path of the tsunami is shown for hours after the earthquake.

Zuytdorp Cliffs

No tsunami-induced boulder deposits have been positively identified on top of the Zuytdorp Cliffs. Presumably these cliffs are too high (from about 30 m to 260 m) for a tsunami to have been able to lift boulders above them. However, there are many large boulders on the cliff slopes and at the base of the cliffs, some of which may have been dislodged by a large tsunami, although others have presumably fallen through ordinary processes of erosion. Good examples of such large boulders can be seen at the *Zuytdorp* wreck site (Figs 119, 142).

Deposits of shells on the tops of cliffs about 30 m high in this area have been identified as Aboriginal kitchen middens, some 4000 years old (Morse, 1988; Playford, 1996). Those deposits should now be re-examined and dated in order to determine whether they can be reinterpreted as tsunami deposits. Even though the cliffs in that area are too high for boulders to have been lifted over them, shells and sand could conceivably have been carried there by a tsunami.

Dirk Hartog Island

Many deposits composed of large boulders occur along the west coast of Dirk Hartog Island, and most are interpreted to have resulted from mega-tsunamis (Figs 177–184).

The largest of these blocks is a conspicuous limestone (calcrete) block, 6.5 km southwest of Cape Inscription (693995E 7176456N), that is known locally as 'The Block' (Figs 177, 178). Its visible extent measures 10.5 x 7.1 x 4 m, and it is estimated to weigh at least 700 t. However, the base of this block is buried in sand, so that its full height must be more than 4 m and its weight correspondingly greater. The limestone in the block was karstified before being dislodged from the coastal cliff and thrown or pushed to nearly 15 m above sea level. It came to rest, apparently right-way-up, 120 m from the edge of the cliff.

Calcrete blocks of comparable dimensions, some isolated and others in groups, are known at various places above the coastal cliffs on the west side of Dirk Hartog Island. A notable example is a series of closely spaced imbricate blocks 5 km north-northwest of Mystery Beach (Figs 179–182; 693232E, 7166855N). The largest imbricate block, nearly as large as 'The Block', measures 13 x 7.5 x 3 m, and is estimated to weigh about 700 t (Fig. 181). These huge blocks have been wrenched from the cliff top and propelled more than 60 m behind the cliff, eventually coming to rest about 15 m above sea level, on a flat strongly karstified limestone surface. The blocks are wedge shaped and imbricate, sloping east, away from the sea. Their wedge shapes and imbricate orientations evidently resulted from being pushed across the rough limestone surface by the extremely strong backwash of water after the tsunami had achieved its highest runup on dune sands behind the coast. Where land inland from the coast rises to more than about 35 m above sea level there must have been a powerful backwash, rushing back to the sea after the tsunami had reached its maximum runup. This resulted in imbrication of large calcrete blocks, dipping away from the coast (Figs 179–182). Most of the smaller blocks that had been carried inland by the tsunami are expected to have been taken back into the sea by this powerful backwash.

It seems that the tsunami responsible for transporting these blocks reached more than 1 km inland (based on airphoto patterns). Elevation data suggest that the wave was more than 20 m high and had a runup of at least 35 m. It resulted in some of the largest tsunami blocks known anywhere in the world.

Other deposits, of smaller and more weathered boulders (maximum about 2.5 m across), extend as far as 200 m from the cliff face and up to about 25 m above sea level, for example at 694865E 7176456N (Fig. 183). They are thought to have resulted from an earlier mega-tsunami that may have been even larger than the one discussed above.

Another deposit of smaller boulders occurs closer to the coast southwest of Cape Inscription, around 695150E 7176900N. These are regarded as being younger than the other deposits described above. The boulders measure up to 2.3 x 1.5 x 0.5 m, weigh up to about 3.5 t, and are very angular and unweathered (Fig. 184). Some with smooth upper surfaces are imbricate, but, unlike the much larger imbricate boulders described earlier, they slope towards the sea. This boulder deposit may have resulted from a more recent tsunami, much smaller than the other two. However, because of the relatively small size of its boulders, a storm origin is possible.

Photographic evidence shows that large calcrete boulders at the foot of Cape Inscription, that may have been dislodged from the cliff top by a mega-tsunami, have not moved during the past 100 years, despite the passage of at least seven tropical cyclones over or near Cape Inscription during that period (Figs 185–188).

Some sandy deposits, near the northwest coast of the island, some 20–30 m above sea level, may have been transported by a tsunami. They contain mollusc shells (including the giant clam *Tridacna*) and coral fragments up to 16 cm across, overlying red sand. One deposit, about 30 m above sea level, at 694160E 7166895N, contains scattered gastropods and small boulders of indurated limestone. A clump of coral from another similar deposit, at 697952E 7180228N, south-southwest of the Cape Inscription Lighthouse and 30 m above sea level, has been radiocarbon dated as 4004 ± 41 years BP. Another radiocarbon dating, from a giant clam in a similar sandy deposit at 695968E 7177900N, returned an age of 38 522 ± 605 years BP (A Hogg, 2010, written comm., 17 October; Table 4). This indicates that the *Tridacna* bivalve must have died long before being swept up by a tsunami.

Bob Sheppard (2010, written comm., 14 April) has observed bivalve shells lying on limestone ridges in inland parts of Dirk Hartog Island, some 4 km south-southeast of Cape Inscription. That locality is about 30 m above sea level. If the shells were carried there by a tsunami they indicate that much of the island must have been inundated by a wave having a runup of more than 30 m.

Figure 177. 'The Block', situated 6.5 km southwest of Cape Inscription, beside the west coast of Dirk Hartog Island. This calcretized limestone block measures 10.5 x 8 x 4 m, and is calculated to weigh more than 700 t. It is derived from the top of the shoreline cliff and was thrown about 15 m above sea level and 120 m behind the cliff by a mega-tsunami.

Figure 178. Aerial view of 'The Block' shown in Figure 177, with some associated smaller blocks of limestone. The block is 120 m from the cliff front and about 15 m above sea level.

Figure 179. Aerial view of a group of closely spaced imbricate blocks beside the west coast of Dirk Hartog Island, 15 km south-southwest of Cape Inscription. The blocks rest on a strongly karstified surface of calcrete, the same lithology as that of the blocks. These imbricate blocks slope inland, and were oriented by the powerful backwash after the tsunami had reached its highest runup and water was rushing back to the sea. The cliff here is about 5 m high.

Figure 180. View of several of the limestone blocks shown in Figure 179, showing their strong imbrication, sloping east, away from the coast, as a result of the backwash after the tsunami. Note the wedge shape of the nearest block, that resulted from abrasion as the block was dragged across the karstified land surface by the backwash that followed the tsunami. Photo by Shaun Coldicutt.

Figure 181. The largest of the imbricate blocks shown in Figure 179, sloping eastward, away from the coast. It measures 13 x 7.5 x 3 m, and has a calculated weight about 700 t. Photo by Shaun Coldicutt.

Figure 182. Another of the imbricate blocks shown in Figure 179, sloping eastward, away from the coast. The wedge shape of the block resulted from abrasion as it was pushed across the rough karstified land surface by the backwash that followed the tsunami. Photo by Shaun Coldicutt.

Figure 183. Deposit of smaller more-weathered boulders on Dirk Hartog Island, about 25 m above sea level and 200 m from the cliff face. The largest blocks are about 2.5 m across. This deposit may have resulted from a tsunami older than that responsible for the blocks in Figures 177–182.

Figure 184. Deposit of unweathered boulders, up to 2.3 m across, immediately beside the west coast of Dirk Hartog Island. This is considered to be younger than the other boulder deposits illustrated in Figures 177–183, and it might have resulted from a smaller tsunami.

Figure 185. Aerial view looking south over Cape Inscription on Dirk Hartog Island, showing many angular slabs of calcretized eolianite lying on the cliff slope and at its base. The cliff here is 30 m high. These boulders are interpreted to have been dislodged by mega-tsunami. Note that the numbers of blocks at the base of the cliffs decreases moving south from the headland.

Figure 186. Photo taken in 1910 of part of the scarp on the northeast side of Cape Inscription, looking north. It shows blocks of limestone (calcrete), several metres across, at the foot of the cliff, and a thick layer of calcrete at the cliff top. The SS Minilya, a steamship last used on the Western Australian coast in 1910, can be seen in the background. Photo by Adjee Cross.

Figure 187. Photo taken from the same position as Figure 186, in 2010. Note that the large blocks of limestone at the foot of the cliff have not moved during the past 100 years, despite seven tropical cyclones having passed over or near Cape Inscription since 1948 (Figure 188).

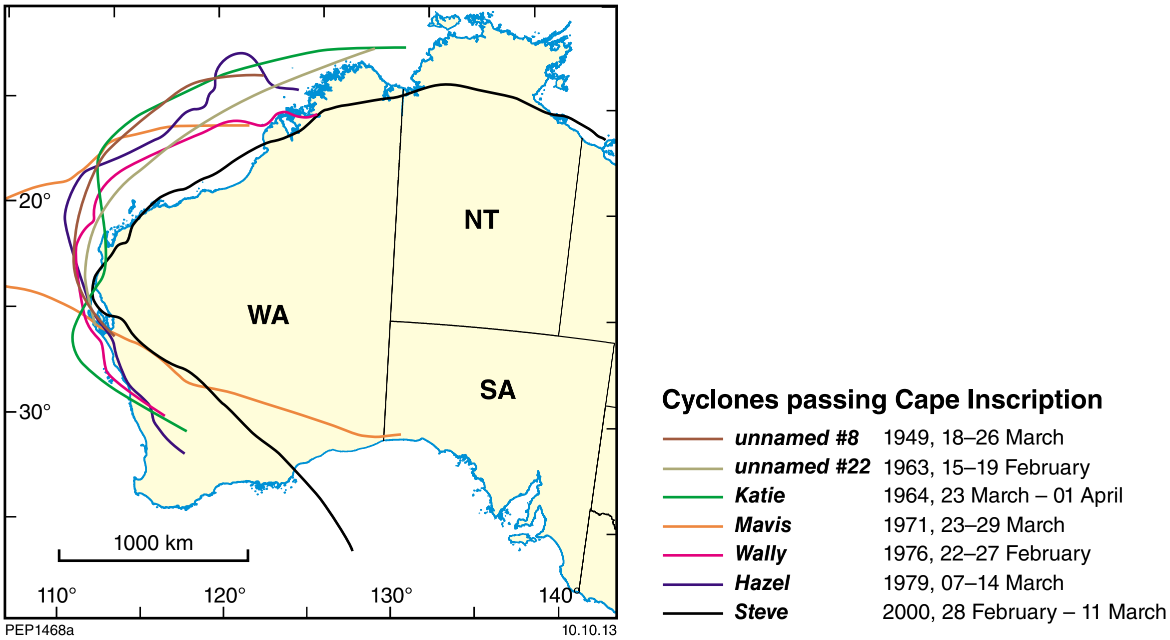

Figure 188. Map showing the paths of seven tropical cyclones that passed within 50 km of Cape Inscription since 1948. Data provided by the Australian Government Bureau of Meteorology.

Table 4. Results of radiocarbon dating of tsunami deposits on Dirk Hartog, Legendre, and Barrow Islands

Analyst: The University of Waikato Radiocarbon Dating Laboratory

Sample no.	*Locality*	*Description*	*Elevation (approximate)*	*Age (years BP)*
135221	Dirk Hartog Island 697952E 7180228N	Clump of coral	30 m	4004 ± 41 BP
135219	Dirk Hartog Island 695968E 7177900N	*Tridacna* shell	27 m	38 522 ± 605 BP
135239	Legendre Island 482630E, 7749047N	Small block of oyster shells	4 m	2895 ± 35 BP
135240	Legendre Island 482630E, 7749047N	Larger block of oyster shells	4 m	3777 ± 40 BP
135270 (3A)	Barrow Island 325470E, 7697835N	Oyster shells encrusted on block of calcrete	5 m	5444 ± 37 BP
135271 (3B)	Barrow Island 325470E 7697835N	Oyster shells encrusted on block of calcrete	5 m	4586 ± 37 BP
135272 (6A)	Barrow Island 336760E 7713650N	Oyster shells encrusted on block of calcrete	3 m	5245 ± 38 BP
135273 (6B)	Barrow Island 336760E 7713650N	Block of oyster shells	3 m	3498 ± 36 BP
135279 (6C)	Barrow Island 336760E 7713650N	Block of oyster shells	3 m	7123 ± 49 7080 ± 25 (AMS)*
135274 (8A)	Barrow Island 325530E 7697960N	Oyster shells encrusted on block of calcrete	8 m	4091 ± 39 BP
135275 (8B)	Barrow Island 325530E 7697960N	Oyster shells encrusted on block of calcrete	8 m	4652 ± 28 BP
135277 (8D)	Barrow Island 325530E 7697960N	Oyster shells encrusted on block of calcrete	8 m	4571 ± 41 BP

* Accelerator Mass Spectometry

It appears that boulder deposits are not known above cliffs that are more than 15 m high. Large boulders, several metres across, are commonly clustered together at the base of those higher cliffs or are plastered on the cliff slopes. Most were probably dislodged by tsunamis that hit the coast thousands of years ago.

Dorre and Bernier Islands

The narrow north–south-trending Dorre and Bernier Islands are situated north of Dirk Hartog Island along the western margin of Shark Bay. Blocks of limestone lie on subhorizontal calcrete surfaces behind coastal cliffs along the west coasts of both Dorre and Bernier Islands (Figs 189–193). These blocks have been observed from the air, but have not been examined on the ground. They appear closely similar to the calcrete blocks on Dirk Hartog Island, and are thought to have resulted from the same mega-tsunami.

Masses of boulders derived from the calcrete layer at the tops of cliffs are common on Dorre and Bernier Islands (Figs 190–194). Recent undermining of the indurated calcrete layer at the cliff tops can be seen clearly from the air, and a similar undermined layer must have collapsed when impacted by a mega-tsunami. Where the coastal cliffs are lower than about 15 m, blocks of the dislodged calcrete have been carried above the cliff to as far as 300 m inland, reaching maximum elevations of about 25 m. Where a cliff is higher than 15 m, blocks are seen to be lying on or at the base of the slope (Figs 189, 194).

The mega-tsunamis are expected to have killed many indigenous animals on Dorre and Bernier Islands, but no Aborigines had lived there since about 6000 years ago. Large parts of those islands are higher than 35 m above sea level, the expected runup height reached by the tsunami. Consequently four species of marsupials were able to survive on these islands. Those species have become extinct on the mainland because of predation there by foxes and cats, feral animals that were never introduced on these islands.

Figure 189. Aerial view looking east near the southern end of Dorre Island, over cliffs of Tamala Limestone about 35 m high. The cliffs here are too high to have allowed blocks to be lifted over them by the mega-tsunami, but many of the large blocks on and at the base of the cliffs seem likely to have been dislodged by that mega-tsunami.

Figure 190. Aerial view of the west side of Dorre Island looking east, showing a boulder deposit, thought to be due to a mega-tsunami, that extended inland for up to 300 m, behind cliffs of Tamala Limestone about 15 m high. The large angular boulders on and below the cliff face were probably also dislodged by the mega-tsunami and plastered on and below the cliff face.

Figure 191. Aerial view looking northwest behind coastal cliffs on the west side of Dorre Island, showing a tsunami deposit composed of limestone blocks up to about 10 m across. Note that some of the blocks are imbricate, sloping inland, apparently resulting from the strong backwash that followed the tsunami.

Figure 192. View looking east over part of Bernier Island, showing boulder deposits behind coastal cliffs of Tamala Limestone, up to about 12 m high. These deposits extend inland nearly as far as a belt of sand dunes that are more than 40 m high.

Figure 193. Aerial view looking east over part of the central east coast of Bernier Island, showing undermining of the calcrete layer, and a hole in the calcrete surface that formed by collapse or alternatively by an upward explosion resulting from impact by the mega-tsunami. Note blocks on the right and left sides of the photo, and very large blocks on and at the foot of the cliff, which is up to about 15 m high.

Figure 194. Aerial view looking east over the northern end of Bernier Island, showing undermining of the calcrete layer on the top of the cliff and many blocks on the cliff face, thought to have been dislodged by the mega-tsunami. The cliffs are up to about 20 m high.

Koks Island

On tiny (2.86 ha) Koks Island, nine limestone blocks, the largest measuring about 8 x 6 x 4 m and weighing about 500 t, lie on a flat calcrete surface, about 10 m above sea level (Figs 195–197). One isolated block at the southern end of the island is perched, seemingly precariously, at the top of the cliff (Fig. 196).

These boulders are conspicuous when viewed from a ship, and as a result the island is labelled as 'Koks Island (boulders)' on Admiralty charts. The explorer George Grey recorded that in February 1839 he had passed Koks Island in a boat, noting that it was 'very remarkable' being 'nearly a table land', on which there are 'several large rocks' (Grey, 1841). It is surprising no one since then seems to have documented this striking feature. Playford sailed past the island on the STS *Leeuwin* in 1998, tentatively interpreting these boulders as tsunami deposits similar to those he had observed previously on Legendre Island.

The blocks on Koks Island evidently resulted from the impact of a mega-tsunami on an undermined calcrete layer on the north and northwest sides of the island. The sculpted rectilinear inlets there are apparently the source of those blocks (Figs 195–197).

Point Quobba

Large blocks of calcrete and calcretized eolianite rest on bare karstified calcrete surfaces behind coastal cliffs about 4 m high, on the mainland coast and a small island at Point Quobba, near the north end of the Shark Bay area (Figs 198–200). The blocks extend inland for up to 300 m and reach heights of at least 15 m above sea level.

These boulders were first described as tsunami deposits by Scheffers et al. (2008). They recorded the presence of blocks weighing up to 100 t that were torn from coastal cliffs, 3–4 m high, and the adjacent sea floor. Some of the blocks derived from the sea floor are extensively bored by bivalves (Fig. 200), which shows that those blocks were in subtidal positions before being thrown up by a tsunami.

The boring bivalves have been radiocarbon dated as 610–1060 years BP by Scheffers et al. (2008) and they did not seek to explain that range in dates. Scheffers et al. (2008) also recognized that at least one older tsunami event occurred in the Point Quobba area, depositing sandy deposits further inland than the blocks, about 5740 years BP, based on the dating of marine shells (limpets) that they contain. However, our dating of coral and a *Tridacna* shell in similar deposits on Dirk Hartog Island shows that reliance cannot be placed on the dating of shells in tsunami deposits because they could have remained on or below the sea floor for thousands of years before being swept up by a tsunami.

A small island at Point Quobba is also capped by many blocks of calcrete, one of which was recorded by Scheffers et al. (2008) as weighing more than 100 t. The blocks near the blowholes (Figs 198, 199) measure up to 4.6 x 2.6 x 2.5 m, and weigh up to about 70 t.

Scheffers et al. (2008) claimed that at least two tsunami events are evident at Point Quobba, ranging in age from 550 to 5780 years BP. The largest block at Point Quobba (100 t) is much smaller than the largest on Dirk Hartog Island (at least 700 t). However, the presence of large blocks lying on flat calcrete pavements at Point Quobba is so similar to the occurrences at other localities around Shark Bay that they probably resulted from the impact of the same mega-tsunami. The smaller size of the blocks at Point Quobba is presumably because the tsunami wave in reaching there had passed over shallower water than at the other localities, causing it to diminish in size and intensity as it moved towards the coast.

Barrow Island

Barrow Island, the second-largest island in Western Australia, is the site of a producing oilfield. A liquefied-natural-gas (LNG) facility is now being built there to process gas from Chevron's offshore gasfields (Fig. 201). A two-day visit was made to the island in May 2013, accompanied by Russell Lagdon, Environment Manager of Chevron Australia, for a reconnaissance of possible tsunami deposits along the west coast of the island.

Boulder deposits occur at various localities above and below coastal cliffs along the west coast of the island (Figs 201, 202). The indented cliff margins are thought to have been sculpted by successive tsunami impacts (Fig. 202). The boulders consist of calcrete blocks up to 5.2 x 2.5 x 2.0 m in size and weighing up to about 60 t (Figs 203–205). Many of the blocks are encrusted with closely packed oyster shells, which were collected at three localities for radiocarbon analysis (Fig. 201, Table 4). Others consist entirely of oyster limestone. The boulders are smaller, generally more eroded, and probably older than the large blocks in the Shark Bay area and on Legendre Island. Radiocarbon dating of attached oysters in eight boulders returned ages of 3498 ± 36, 4091 ± 39, 4571 ± 41, 4586 ± 37, 4652 ± 28, 5245 ± 38, 5444 ± 37, and 7080 ± 25 years BP (F Petchey, 2013, written comm.). These dates are believed to be reliable and may suggest that oyster layers of differing age are present on the sea floor near the coast, representing changing sea levels in the recent past. More fieldwork, below water and on land, together with many more radiocarbon datings, will be needed to solve this issue. It seems likely that more than one tsunami was involved, and the most recent of these may have been about 3500 years ago.

The boulders observed on top of Barrow Island are much smaller than the largest on Dirk Hartog and Legendre Islands, and could possibly have resulted from intense tropical cyclones, rather than tsunamis. However, it is significant that on 10 April 1996 an intense tropical cyclone, Cyclone Olivia, passed over Barrow Island. The strongest gust of wind ever recorded on Earth (408 km/hr) was registered on the island during the passage of that cyclone (Courtney et al., 2012). However, despite its strength and the extensive damage it caused to infrastructure on the island, Cyclone Olivier had no discernible effects on existing boulder deposits, nor did it seem to have resulted in any new boulder deposits (R Lagdon, 2013, written comm.). In view of this it is likely that the boulder deposits on Barrow Island are tsunami rather than storm deposits.

Figure 195. Aerial view looking south over Koks Island and the northern end of Bernier Island, showing large blocks of limestone on top of the island, thought to have been carried there by a mega-tsunami. The north–south length of the island is 280 m.

Figure 196. Aerial view looking southwest over Koks Island, showing scattered boulders lying on the karstified surface, mainly in the northern part of the island. A large block lies perched on top of the cliff at the southern end. These blocks are expected to have been derived from the area of the two U-shaped re-entrants sculpted by the tsunami on the north side of the island.

Figure 197. Aerial view looking northwest over the northern part of Koks Island, showing boulders lying on the karstified surface, with finer-grained deposits in the centre foreground and a large U-shaped re-entrant, thought to have been sculpted on the north coast by the tsunami.

Figure 198. Blocks of karstified limestone, attributed to a mega-tsunami, at 'the blowholes' near Point Quobba

Figure 199. Blocks of karstified limestone, attributed to a mega-tsunami, at 'the blowholes' near Point Quobba. The larger block, in the centre of the photo, weighs about 70 t.

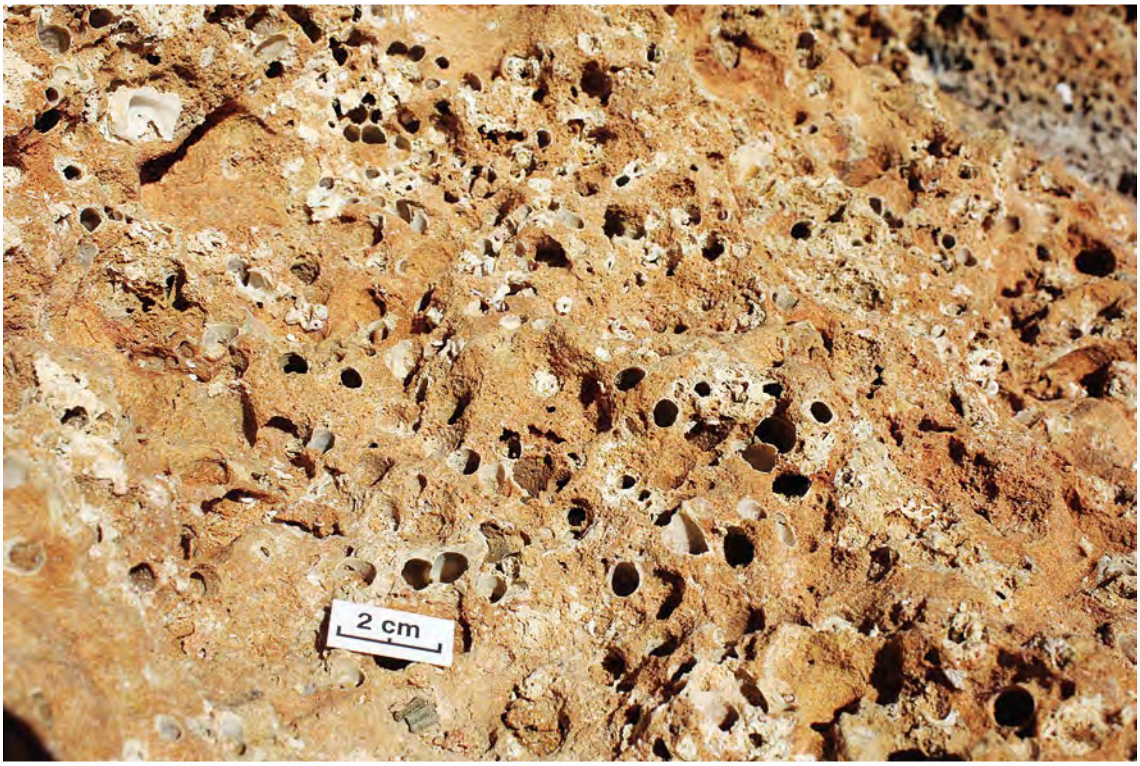

Figure 200. North side of the larger block in Figure 199 showing many borings, thought to have formed below sea level by boring bivalves.

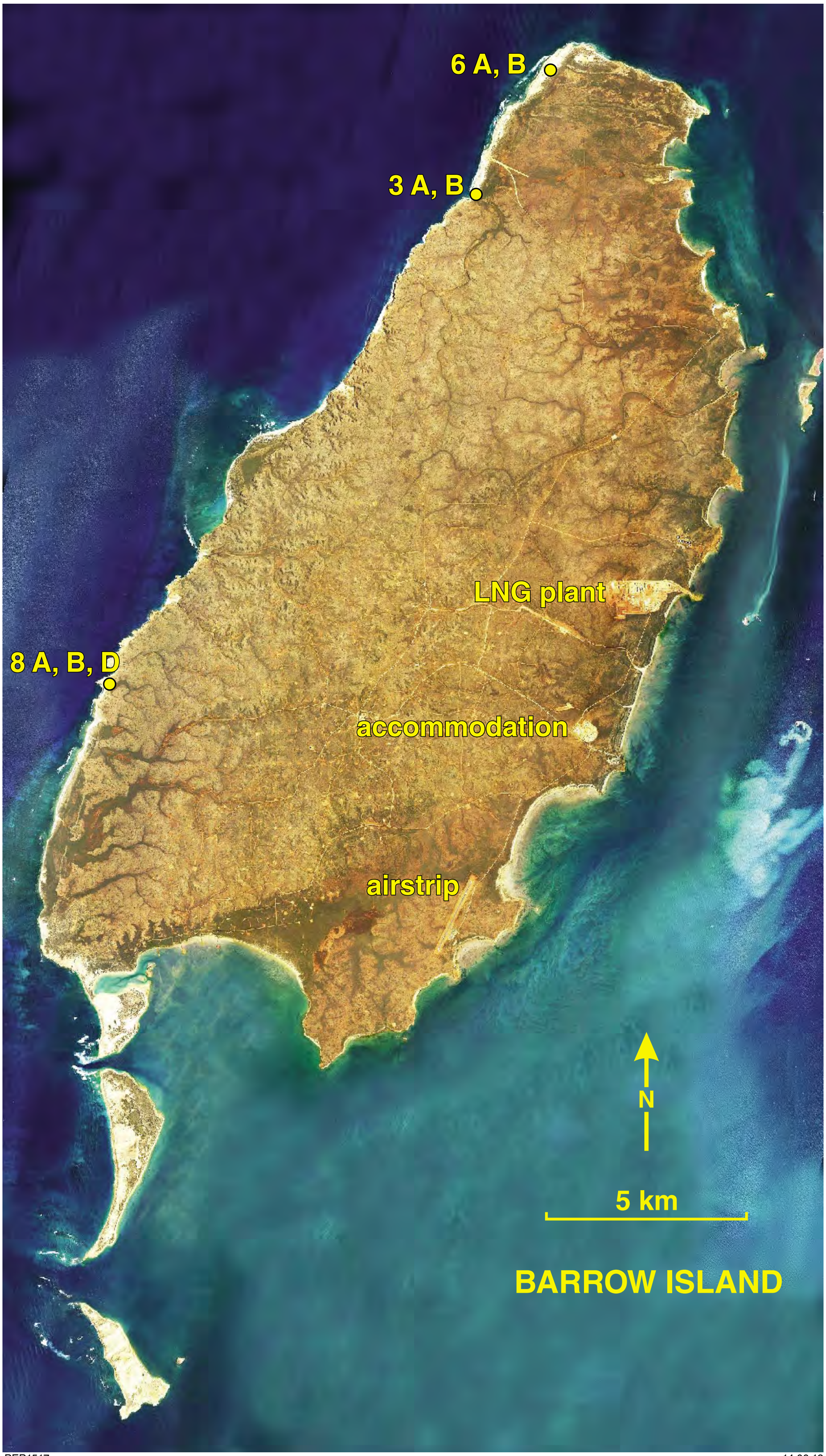

Figure 201. **Composite airphoto of Barrow Island showing Localities 3, 6 and 8 sampled for radiocarbon dating of tsunamis, from orthophotos supplied by Landgate, Western Australia.**

Figure 202. Airphoto of part of the west coast of Barrow Island showing the intricately indented coast, thought to have been sculpted by successive mega-tsunamis.

Figure 203. Boulder deposit at Locality 8 on Barrow Island, showing eroded boulders of calcrete, about 8 m above sea level. Photo by Russell Lagdon.

Figure 204. Weathered boulder of calcrete lying on a calcrete surface at Locality 8 on Barrow Island. Photo by Russell Lagdon.

Figure 205. Boulder of calcrete encrusted by oysters near Locality 8 on Barrow Island. Karst holes on the boulder pre-date growth of the oysters.

Figure 206. Limestone cliffs, about 25 m high, some 6 km south-southwest of the north end of Barrow Island, showing large boulders lying on the slope near the base of the cliffs. These boulders must have been carried there by a tsunami or very large storm.

Some oyster accumulations are encrusted on pre-existing boulders of karstified calcrete, and the oysters extend into karst holes on those boulders (Fig. 205). These karstified boulders may have been carried offshore in the backwash of an earlier tsunami or storm and were then encrusted by oysters before being thrown up on top of the coastal cliffs by a mega-tsunami. Large boulders, likely to include calcrete encrusted by oysters, can also be seen at the base of cliffs about 25 m high, in the northwest part of the island, but those boulder occurrences have yet to be examined (Fig. 206).

Legendre Island

Legendre Island is a long, narrow, northwest-trending, limestone island off the Pilbara coast, north of the Burrup Peninsula and some 700 km north-northwest of Shark Bay (Figs 173, 207–220). It is 15 km long, up to 1.5 km wide, and is underlain by cross-bedded Pleistocene limestone similar to the Pleistocene Tamala Limestone of Shark Bay (Fig. 220). This limestone is capped by a layer of calcrete, up to about 4 m thick, which is commonly exposed in coastal cliffs along the north and northeast sides of the island. The calcrete forms a rough karstified pavement for up to 250 m behind the cliffs. Much of the calcrete surface around the island lacks soil and vegetation, because it is subject to repeated seawater inundations, and spray from large storms.

Limestone cliffs along the north and northeast sides of the island are up to 25 m high, and consist of calcrete overlying eolian limestone (Fig. 220). The calcrete layer is commonly undermined by erosion, and in several places it has been broken into groups of blocks that have been carried as far as 400 m behind the cliff, with the blocks furthest from the coast lying in vegetated areas. The larger blocks at the northern end of the island consist of calcrete and calcretized eolianite, with some smaller blocks (up to 2 m across) having been constructed entirely by oysters (Fig. 215). One of the largest calcrete blocks (at 482547E 7749173N), measures 12.5 m x 5 m x 4 m, is 8 m above sea level, and weighs about 600 t. Most of the blocks show evidence of having been karstified before being dislodged. Many were rotated during transport, some having come to rest on their sides or upside down (Figs 213, 214).

These blocks were first tentatively recognized as tsunami deposits by Playford during a boat trip past the island in 1977. However, the first published report on the geology of the island, by Biggs and Denman (1978), stated that storm action had moved blocks of limestone weighing ‘several tens of tonnes’. However, in fact many of the blocks weigh hundreds of tonnes, and even the strongest cyclonic storm would have been inadequate to carry such blocks over the cliffs — a tsunami must have been responsible, as discussed earlier.

The blocks of oyster limestone in the deposit were derived from oyster buildups that grew around the rims of shoreline platforms below coastal cliffs at the north end of the island (Figs 209, 216). Oysters were sampled from two of these blocks, at 482606E 7749129N and 482630E 7749047N, approximately 8 m above sea level. The larger of these oyster blocks measures 2 m x 1 m x 0.7 m. The samples yielded radiocarbon dates of 2895 ± 35 years BP and 3777 ± 40 years BP (A Hogg, 2010, written comm.). It is possible that the age difference between them can be attributed to the relatively slow rates of accumulation of oysters forming these limestones, and the younger of the two dates may be the age of the tsunami, rounded to 2900 years BP. However, that remains to be tested through further geochronological study of the deposits.

The tsunami that lifted the huge blocks onto Legendre Island seems to have swept right over the island, impacting on Dolphin Island and Burrup Peninsula, before flowing onto the mainland around the sites of the present towns of Dampier and Karratha and the liquified natural gas plant on the Burrup Peninsula (Fig. 207).

Near the north end of Dolphin Island, separated from Burrup Peninsula by Searipple Passage, there are masses of rounded gabbro boulders (Fig. 221), some of which could have been rotated by the tsunami. It will be interesting to find whether any such boulders are inscribed with Aboriginal petroglyphs of the type that is so common in this area (Donaldson, 2010). There are no definitive datings of those petroglyphs, and if they are present on blocks that have clearly been moved by a tsunami, it might show that those petroglyphs are more than 2900 years old.

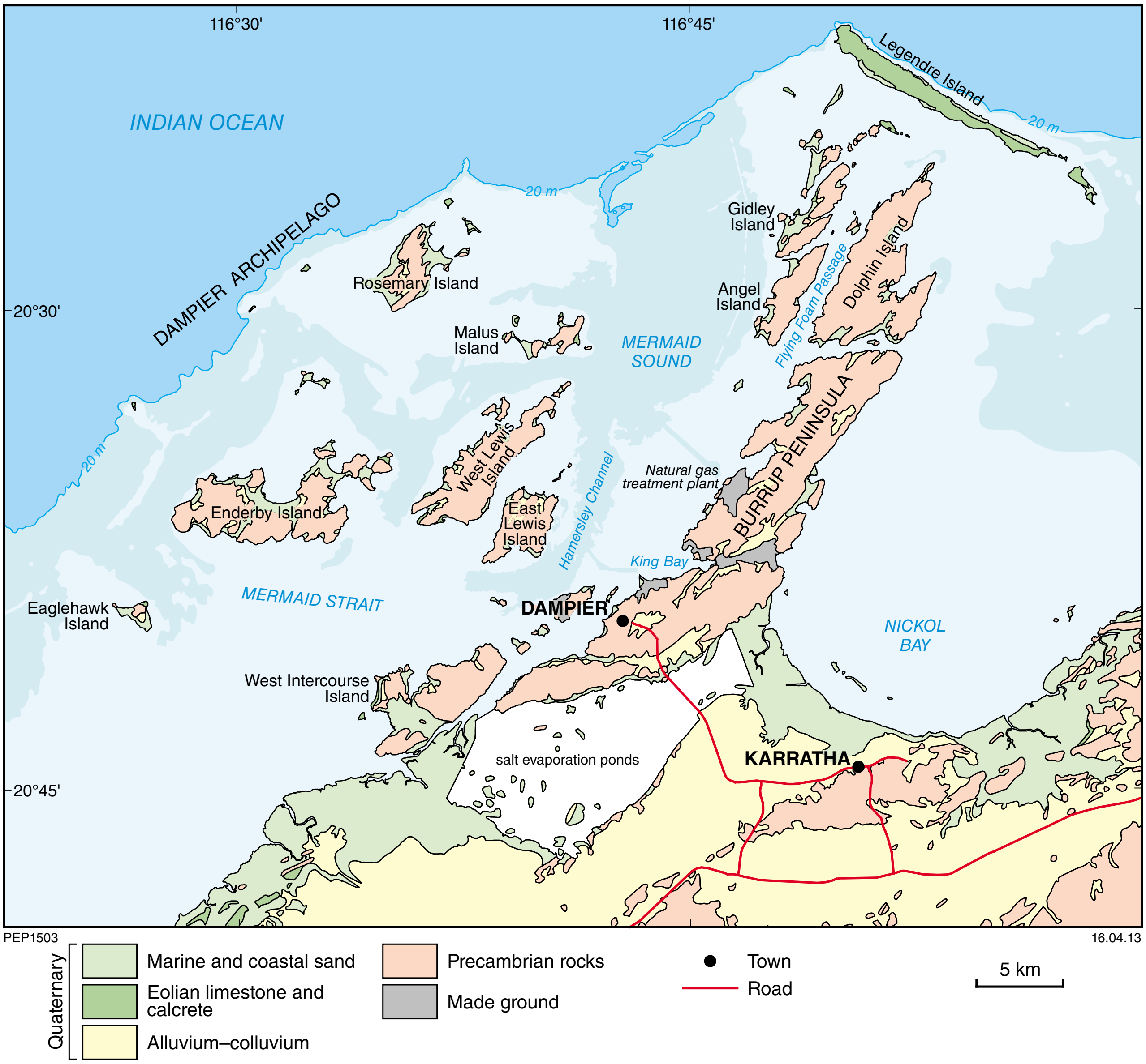

Figure 207. Geological map of the Legendre Island — Burrup Peninsula area.

Figure 208. Aerial view looking southeast along Legendre Island. Note the jagged coastal cliffs in the foreground, thought to have been sculpted by mega-tsunami impacts.

Figure 209. Aerial view looking southeast along Legendre Island, showing the jagged shape of the coastal cliffs. Behind the cliffs is a wide surface of bare calcrete, with scattered large blocks of calcrete extending into vegetated areas up to 400 m behind the coast. Note the light-coloured rims of shoreline platforms, constructed by oysters.

Figure 210. Aerial view looking north over the northwest end of Legendre Island, showing large calcrete blocks, thought to have been deposited by a mega-tsunami, resting on a strongly karstified calcrete surface.

Figure 211. View on the ground of the large blocks shown in Figure 210, lying on a karstified calcrete surface. The largest of these blocks, on the skyline, is 12.5 m long.

Figure 212. Blocks of calcrete and calcretized limestone at the northwest end of Legendre Island. These blocks, thought to have been deposited by a mega-tsunami, rest on a strongly karstified surface of calcrete. The largest block, in front of the person (Shaun Coldicutt), is estimated to weigh more than 600 t.

Figure 213. Block of calcrete with abundant karst holes, lying on its side, at the northwest end of Legendre Island, thought to have been thrown up by a mega-tsunami. The scale is 16 cm long.

Figure 214. Upside-down block of calcretized eolianite, at the northwest end of Legendre Island, about 8 m above sea level and 250 m inland, thought to have been thrown up by a mega-tsunami.

Figure 215. Block of oyster-encrusted limestone, thought to have been thrown up by a mega-tsunami, at the northwest end of Legendre Island, about 250 m inland. The oysters must have originally fringed the intertidal shoreline platform at the base of the cliffs. One of these blocks has been radiocarbon dated as 2895 ± 35 years BP.

Figure 216. Aerial view looking south over part of the northwest coast of Legendre Island, showing some tsunami blocks at the top left. The narrow yellowish-grey ridges at the edge of the shoreline platform below the cliff are built by oyster limestone in the intertidal zone.

Figure 217. Aerial view of part of the northwest coast of Legendre Island, showing large calcrete blocks above and behind the cliff and many larger angular blocks, displaced by a mega-tsunami, lying on the terrace below the cliff.

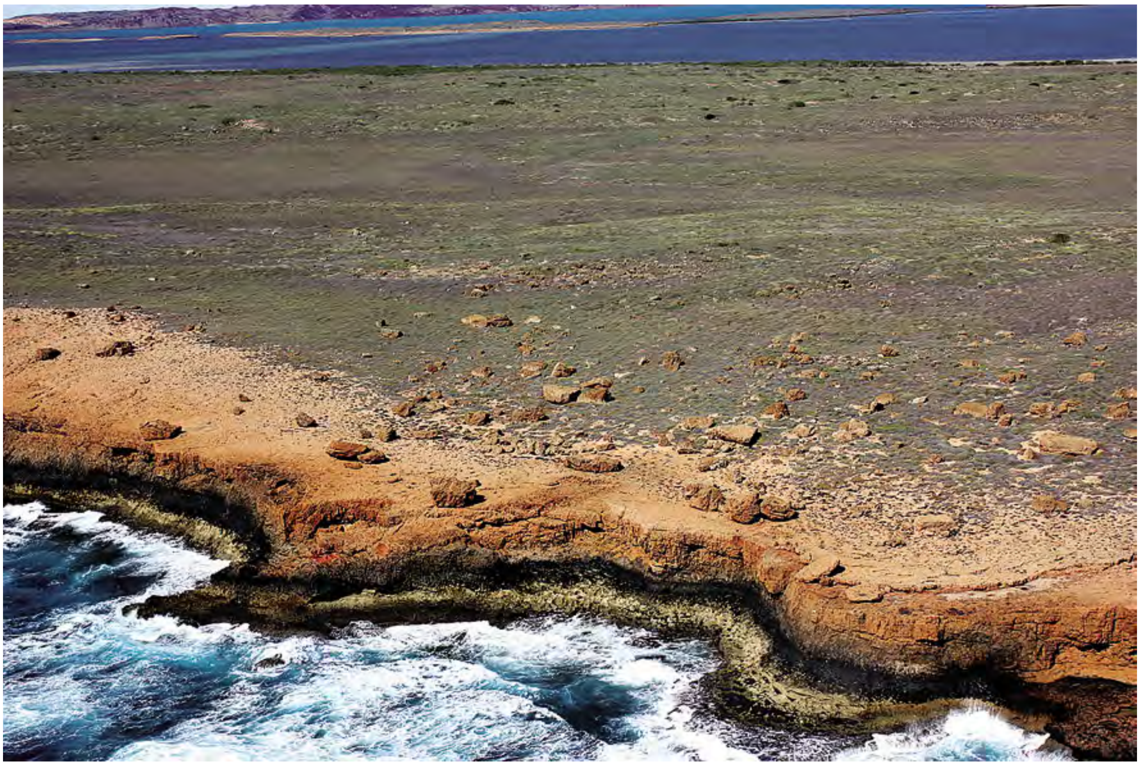

Figure 218. Aerial view of part of the northwest coast of Legendre Island, showing erosion of the cliff face attributed to a mega-tsunami, with many resulting blocks of limestone scattered over the land surface behind the cliff and extending up to 300 m inland.

Figure 219. Aerial view of part of the northwest coast of Legendre Island, showing 'scoop' erosion attributed to a mega-tsunami, with blocks behind the 'scoop' scattered over the land surface, and extending inland for more than 250 m.

Figure 220. Aerial view of part of the northwest coast of Legendre Island, looking south, showing cross-bedded eolianite capped by a calcrete layer about 4 m thick. Many angular blocks, probably displaced by a mega-tsunami, lie at the base of the cliff. The highest part of the cliff here is about 25 m above sea level.

Figure 221. Aerial view, looking east, of the northern part of Dolphin Island, showing large boulders of Archean gabbro, some of which may have been rotated by a mega-tsunami.

Kimberley coast

Many deposits consisting of large boulders of siliceous sandstone and volcanic rocks are present along the Kimberley coast, and are interpreted to be the products of tsunamis, although some may have resulted from major storms (Figs 222–229). It seems likely that at least part of the intricate sculpting of that coast is linked with the impacts of mega-tsunamis over millions of years. The presence of such deposits is to be expected in this area, in view of its close proximity to a very active seismic zone along the Sunda Trench in the eastern part of the Sunda Arc, and a less-active seismic zone along the Banda Arc in the Timor Trough.

At its closest, the Sunda Arc is less than 1000 km from the Kimberley, and large earthquakes originating there would have generated tsunamis that could have had a significant role in sculpting the Kimberley coast. A tsunami caused by an earthquake along relevant parts of the Sunda and Banda Arcs could be expected to reach the Kimberley in less than 80 minutes. The same tsunami, with progressively decreasing strength, would take more than two hours to reach the Pilbara and three hours to reach Shark Bay.

Detailed study of low-lying coastal areas of the Kimberley (such as behind King Sound, Fig. 230) should show evidence of the extent of the runup achieved by mega-tsunamis, especially in the form of marine shells carried inland. However, no such studies have been undertaken to date.

It has not been possible to link any major tsunami events along the coast from Shark Bay to the Pilbara with any particular tsunami that struck the Kimberley. The Sunda Arc off Indonesia is too far away for earthquakes along that arc to have been responsible for the major-tsunami deposits known between the Pilbara and Shark Bay, especially as blocks in those deposits do not diminish in size moving south between those places. As discussed earlier, it seems more likely that local fault activity, or major submarine slumping on the continental slope, or asteroid impacts on the Indian Ocean, were responsible for the major tsunami deposits at Legendre Island and Shark Bay. Submarine volcanic eruptions are other possible, if less likely, causes.

Human and faunal impacts

The evidence of major tsunamis during the last few thousand years leads to consideration of the possible impacts on Aboriginal people who had occupied coastal areas of Australia for thousands of years, and also on animals then living in those areas. In some low-lying areas tsunamis must have extended several kilometres inland, and may have caused the deaths of thousands of people and animals.

Tsunamis are likely to have been the largest catastrophic events experienced in Western Australia during the last few thousand years. If a major tsunami were to occur today along that coast it could have devastating consequences for coastal towns and industries.

Tsunamis are likely to have eliminated, or partly eliminated, the native faunas that lived on certain islands, or fortuitously allowed one, or a few, species to survive. Because large parts of Dorre and Bernier islands were high enough to escape inundation by the tsunamis described here, four species of marsupials were able to survive there.

Bryant et al. (2007) have recorded that the stories of some Aboriginal people in the Kimberley tell of the inundation of coastal areas by large waves. Those authors have observed evidence of a single mega-tsunami that struck as recently as the 17th century along at least 1500 km of the Kimberley coastline.

One recorded account tells of the near-extinction of a coastal tribe in the Kimberley as a result of a big wave that struck about a century ago. Aubrey Tigan, an Aboriginal elder of the Lombadina (Djarindjin) community on the Dampier Peninsula, recounted that his grandfather had told him that many years ago a huge wave swept over the Montgomery Islands (140 km east northeast of Lombadina), killing all but two of the estimated 300 people who had lived there while gaining their food from the bountiful Montgomery Reef. Patrick Sampji, another elder from the same community, recounted how his grandfather had told him that long ago a big wave had struck the coast near Lombadina Mission, during the night and without warning. No one was killed, but the wave threw up a line of small boulders on the beach, about 200 m from the shore in Thomas Bay. Sampji thought that this event had occurred during the early part of the 20th century. These two accounts are recorded in video interviews with the two men by Moya Newman of the Fire and Emergency Services Authority of WA (FESA). Gordon Hall of that organization provided DVDs of those two interviews.

Hamelin Coquina

The Hamelin Coquina forms a series of Holocene beach ridges and linear and isolated mounds around the shores of Hamelin Pool, L'Haridon Bight, and parts of Henri Freycinet Harbour. The formation was named and first described by Hagan and Logan (1974a).

Nott (2011) described the Hamelin Coquina in the Nilemah Embayment, at the southern end of Hamelin Pool, as a series of up to 26 Holocene beach ridges, interpreted as having been linked to successive tropical cyclones passing through the area every 190–270 years.

Jahnert et al. (2012) described the formation as being a series of beach-ridge deposits comprising 'tabular layers complex', 'convex-up ridges', and 'washover deposits'. We are unable to agree with many of their conclusions.

Little is known about details of mean sea-level changes at Hamelin Pool during deposition of the Hamelin Coquina, although evidence from stromatolites (discussed later in this Bulletin) indicates that sea level about 1000 years ago was up to 1 m higher than it is now.

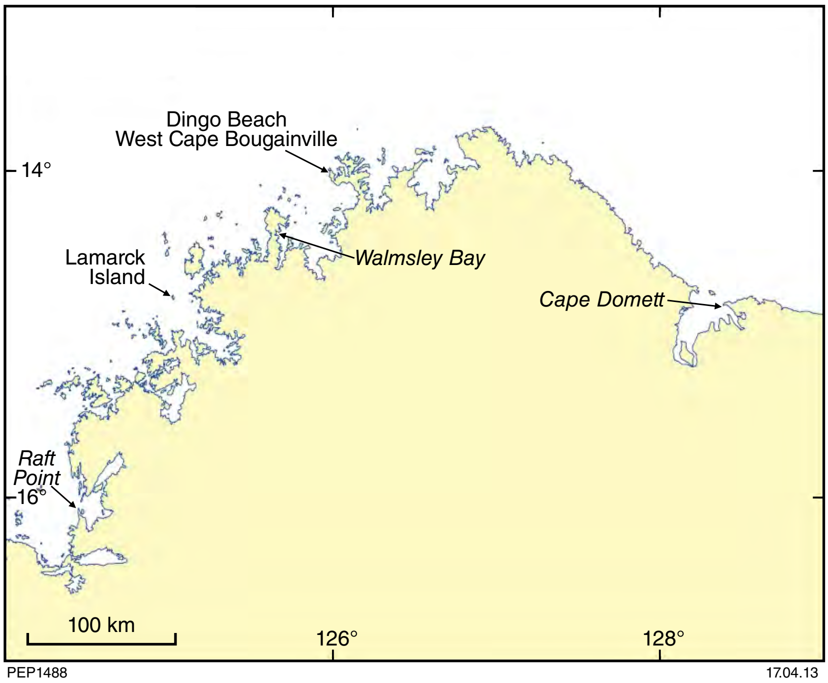

Figure 222. Map of the Kimberley showing the intricately sculpted nature of the coast and the locations of photos included in the text. This intricate sculpting is thought to have resulted partly from the impacts of mega-tsunamis over millions of years.

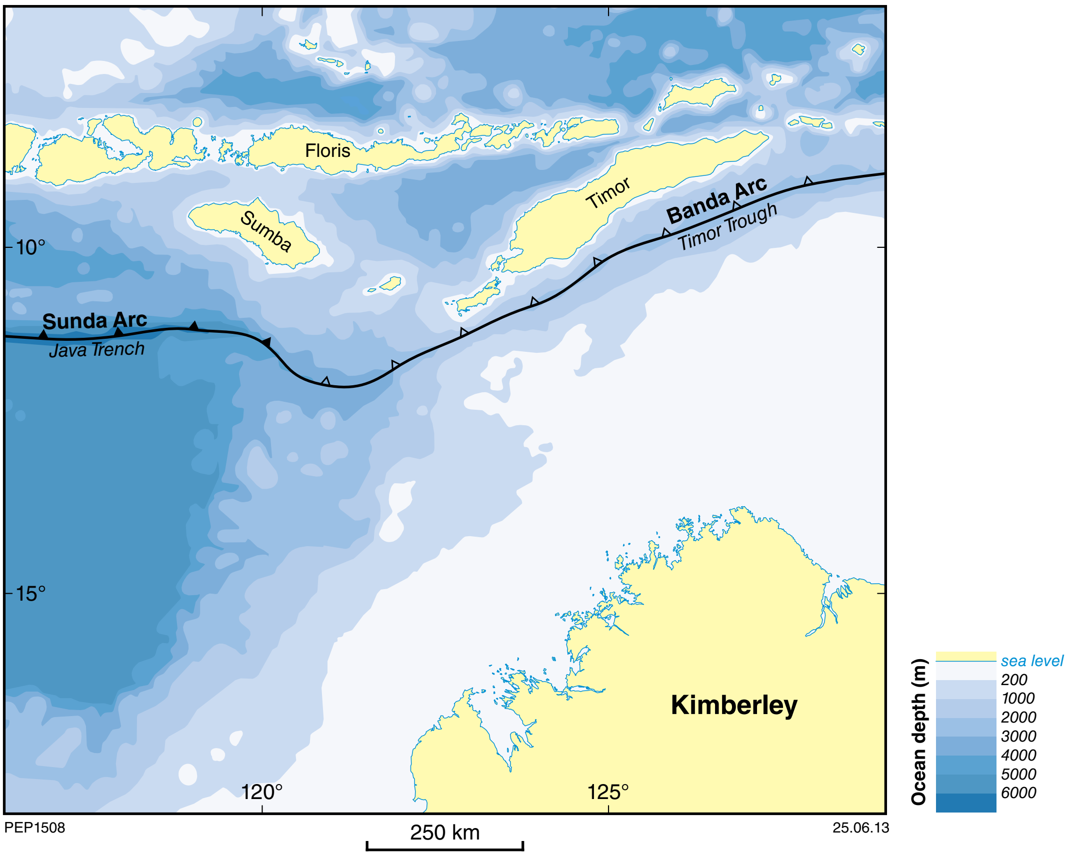

Figure 223. Map of the Kimberley coastline in relation to the eastern part of the Indonesian Archipelago and parts of the Banda and Sunda Arcs. Faulting along these arcs is thought to have resulted in many mega-tsunamis striking and sculpting the Kimberley coast.

Figure 224. Boulder deposit on the lee (east) side of Lamarck Island in the Kimberley. The boulders in this deposit are interpreted to have been torn from the west side of the island and carried to this site by one or more mega-tsunamis.

Figure 225. Boulder deposit lying on top of siliceous sandstone on the south side of Walmsley Bay, near the mouth of the Mitchell River, Kimberley District. These boulders are thought to have been deposited there by a mega-tsunami.

Figure 226. Huge boulders of basalt beside Dingo Beach, West Cape Bougainville, in the Kimberley. These boulders (up to about 15 m across) are thought to have been transported there by a mega-tsunami.

Figure 227. Column of siliceous sandstone, about 6 m high, near Raft Point, showing angular boulders at its base, probably due to successive mega-tsunami impacts.

Figure 228. Column of sandstone in a silicified fault zone near Cape Domett, with two reddish-orange boulders of siliceous sandstone perched near the top, about 9 m above ground level, thought to have been carried there by a mega-tsunami.

Figure 229. The upper part of the column of sandstone near Cape Domett, showing two boulders of silicified sandstone near the top of the column, thought to have been carried there by a mega-tsunami.

Figure 230. Aerial view of the coast of King Sound near Derby, looking northeast, showing last-glacial vegetated seif dunes extending below supratidal to intertidal mud flats. This part of the coast would be a suitable place to determine the extent of the runup associated with mega-tsunamis that seem likely to have extended several kilometres inland.

The Hamelin Coquina can be regarded as a model for some ancient coquinas that are known to be reservoirs for petroleum (Davies and Sherwin, 1997). Jahnert et al. (2012) claimed that the progradational model of beach ridge construction at Hamelin Pool is 'a useful analog for ancient coquina reservoirs deposited in lacustrine systems, since the hydrodynamic setting and semi-closed environment affected by storms is similar to some ancient examples such as the coquina reservoirs in the Campos Basin, Brazil'. However, the Hamelin Coquina has been laid down in marine, not lacustrine, conditions, and a key to its origin is the hypersaline marine conditions that prevail in Hamelin Pool.

Composition

The Hamelin Coquina forms Holocene beach ridges and mounds adjoining the shores of Hamelin Pool, L'Haridon Bight, and parts of Henri Freycinet Harbour (Figs 231, 232, 234–246, 248–272). The oldest part has been radiocarbon-dated as 5316 ± 42 years BP, at a place where it overlies the eastern part of a birrida on the east side of the Nanga Peninsula (Figs 171, 172; 792936E 7096143N).

The beach ridges are composed almost entirely of single shells, uniform in size, of the bivalve *Fragum erugatum* (Fig. 231, 232). This species was originally recorded from Hamelin Pool by Logan (1961) as '*Fragum hamelini*', but is now regarded as belonging to the species *Fragum erugatum*. The beach ridges along the shorelines consist of loose coquina, which, moving away from the coast, is progressively cemented to form coquinite. Wide areas of the Hamelin Coquina near the shoreline form a subhorizontal surface, with little or no vegetation (Fig. 233).

As the formation is composed predominantly of cemented coquinite, rather than loose coquina, it may have been more appropriate to name the unit the 'Hamelin Coquinite'. However, for continuity of nomenclature the long-standing name Hamelin Coquina has been retained. No type locality has been designated, but is here taken to be the area immediately north of Flagpole Landing (217200E, 7077100N; Figs 234–239).

The modern shells in coquinas are composed of aragonite, and the shells become progressively altered to calcite and cemented to form coquinite by percolating rainwater. Some wells excavated in coquinite have encountered only saline groundwater, and in those wells it is evident that uncemented aragonite coquina is present for up to 1.5 m above the water table, whereas higher indurated parts consist entirely of calcite (Fig. 240). Saltwater at the base of such wells rises through capillary action and inhibits the transformation of aragonite to calcite (M Wallace, 2009, 2011, pers. comm.). In other beach wells, where a layer of freshwater is present above the saltwater, the coquinite is composed entirely of calcite. Beach-rock cementation by aragonite is known in the formation at a few localities (Fig. 241).

The belt of beach ridges and mounds forming the Hamelin Coquina is up to 1 km wide and 7 m thick. The outcrop width is variable, and the formation is absent or narrow in various localities around the shores of Hamelin Pool, L'Haridon Bight, and Henri Freycinet Harbour. In some places it is subject to active shoreline erosion (Fig. 242). It is clear from field observations and radiometric datings that few, if any, of the sections through the Hamelin Coquina around Hamelin Pool record continuous deposition. When deposition occurred at one locality, erosion prevailed at another.

Some radiocarbon dates of shells in the Hamelin Coquina apparently do not represent valid ages of the deposits in which they occur. Anomalous results can result from: (a) mixing of contemporary and older shells when they are transported by waves, storms, cyclones, and tsunamis; (b) shells of *Fragum erugatum*, originally composed of aragonite, are wholly or partly replaced by calcite when subjected to percolating rainwater, so that radiocarbon dating of those shells will give dates that are younger than the beach ridge in which they occur; (c) Pleistocene contaminants in samples will yield anomalously old dates for those samples; and (d) *Fragum* shells can remain on the sea floor for many decades before being incorporated into beach ridges, thereby returning anomalously old dates for such ridges.

A series of eight auger holes was drilled across the belt of Hamelin Coquina northwest of the old Flint Cliff Telegraph Station, to determine the thickness of the formation in that area (Figs 235, 239; Table 5). The thickness of the formation ranges from 6.65 m in the first of these holes, which penetrated the thickest and oldest linear mound and underlying coquinite, to 3.2 m in the seventh hole, which penetrated only beach-ridge coquinite. Other holes penetrated 3.3 – 4.3 m of coquinite (Table 5).

Fragum erugatum

Berry and Playford (1997) studied living *Fragum erugatum* in Hamelin Pool, L'Haridon Bight, and Henri Freycinet Harbour, and the following account of this species is based largely on their work. The species at Shark Bay has also been described by Morton (2000). Living *Fragum erugatum* was found by Berry and Playford to be widely distributed over the deep-subtidal pavements in Hamelin Pool and L'Haridon Bight, in water depths of 1.2 – 6.0 m. They were observed and collected in two successive years at specific locations in Hamelin Pool and L'Haridon Bight, and at one location, near Nanga, in Henri Freycinet Harbour.

The brown flesh of *Fragum erugatum* can be seen through its translucent shells. The colour is due to the presence of dense aggregations of zooxanthellae — symbiotic photosynthetic organisms that provide the host bivalve with energy through the products of photosynthesis. The maximum depth limitation of living *Fragum erugatum*, about 6 m, is apparently limited by the light penetration required for photosynthesis by the zooxanthellae.

Figure 231. Shells of *Fragum erugatum* in coquina of the Hamelin Coquina near Flagpole Landing, showing 'nesting' of shells, one upon another, in parts of the deposit. This convex-down 'nesting' is characteristic of coquinas that were carried and deposited en masse, probably as a result of intense tropical cyclones.

Figure 232. Shells of *Fragum erugatum* in weakly cemented coquinite of the Hamelin Coquina near Flagpole Landing. Note the convex-down 'nesting' of shells in parts of the coquinite, thought to be indicative of transport and deposition en masse.

Figure 233. Overnight campsite on Hamelin Coquina, 2 km south of Flagpole Landing, soon after Cyclone Hazel had passed west of Hamelin Pool on 27 March 1979. Note the subhorizontal surface of the coquinite, swept clean and lacking in vegetation. Photo by Cynthia Playford.

Figure 234. Aerial view looking north over the type locality of the Hamelin Coquina, near Flagpole Landing. Note the succession of linear mounds overlying planed-off beach ridges. The oldest and highest mound (on the right) may have been deposited by a mega-tsunami. The other linear mounds, with periodicities of about 400 years, may have been formed by a succession of very intense tropical cyclones. Quarries can be seen for cemented coquinite in the central middle distance and for loose shells near the shoreline. The main buildings are those of the old Flint Cliff Telegraph Station and Post Office.

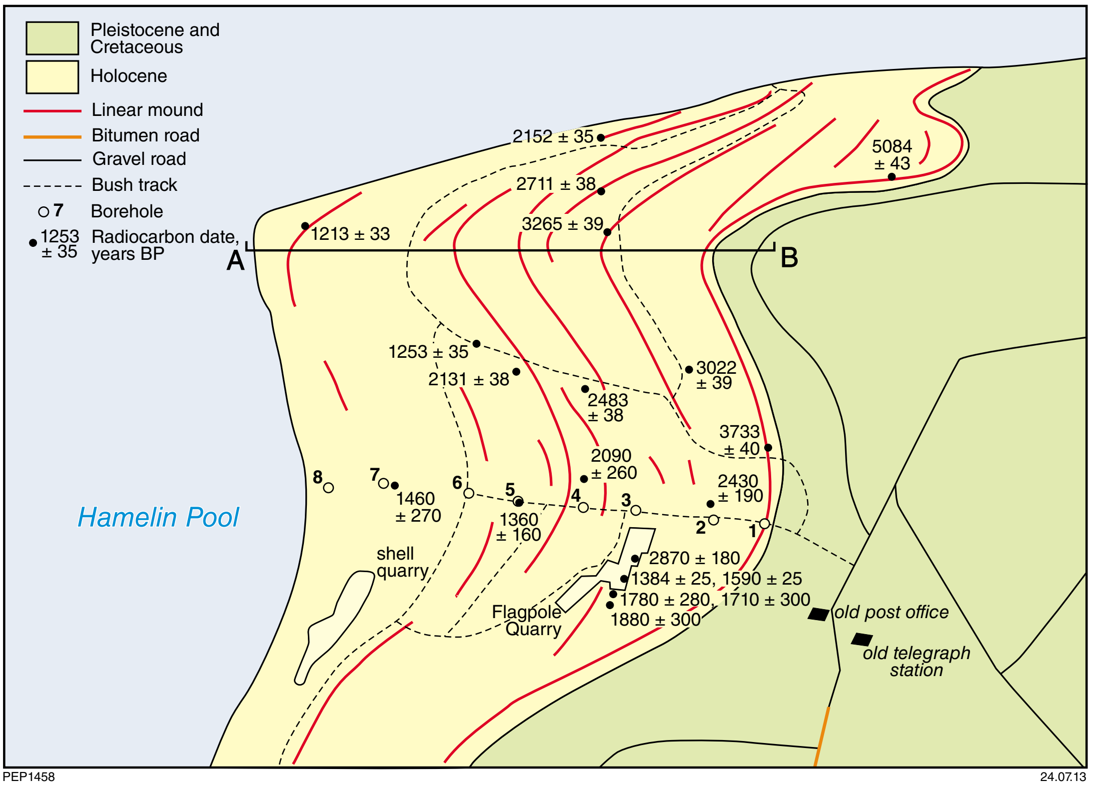

Figure 235. Oblique diagram, looking north, covering the area shown in Figure 234, illustrating the geology and geomorphology of the area, the line of drillholes listed in Table 5, and the section A–B, 680 m long, shown in Figure 239. Note also the locations of the shell quarry and the Flagpole Quarry (coquinite).

Figure 236. Higher aerial view looking north over the Flagpole Landing area, showing the succession of linear mounds in the Hamelin Coquina, the oldest and highest of which (on the right) may have resulted from a mega-tsunami. Note the lines of subtidal and intertidal stromatolite reefs, and the narrow white bands of ooid sand in front of those reefs.

Figure 237. Aerial view looking south over the Flagpole Landing area, the type locality of the Hamelin Coquina, showing lines of vegetated linear mounds over a succession of bare truncated beach ridges (the finely laminated areas). Note the largest, highest, and oldest linear mound on the left, which may have been thrown up by a mega-tsunami probably less than 3000 years ago.

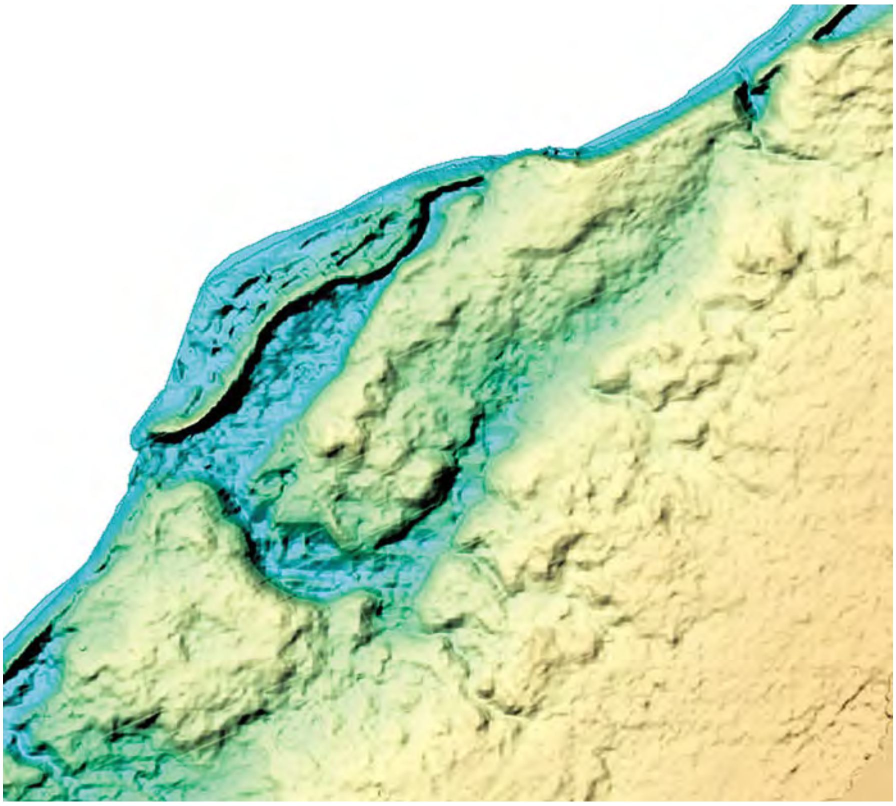

Figure 238. **DEM image of the Flagpole Landing area to illustrate the largest, highest, and oldest linear mound, shown as the undulating black line in the greenish-blue area in the centre-left part of the image. The width of the image is 5 km. This high linear mound may have resulted from a mega-tsunami thought to have impacted on the coast probably less than 3000 years ago.**

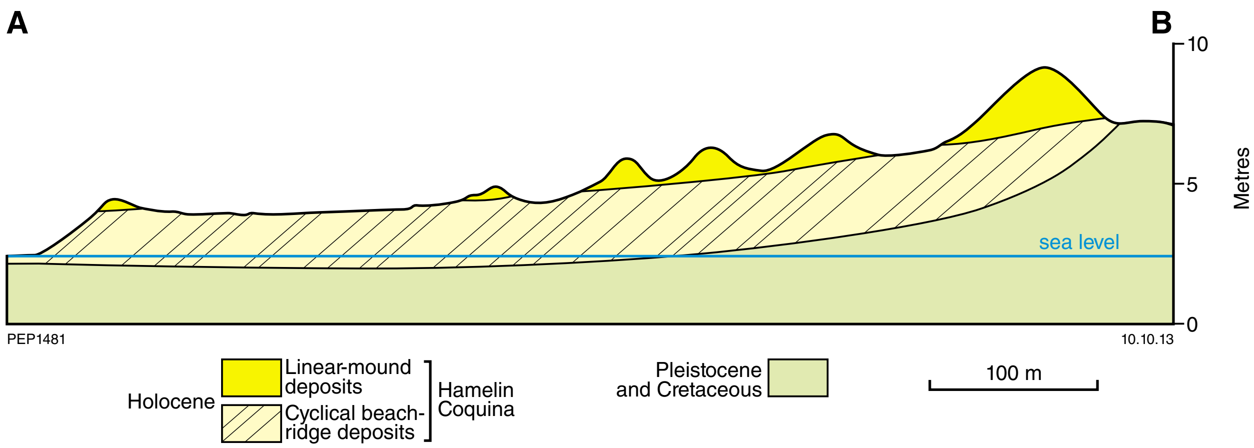

Figure 239. Cross-section along the line of section A–B in Figure 235, showing linear mounds overlying cyclical coquinite.

Shells of living *Fragum erugatum* are smaller and less abundant in Hamelin Pool than in L'Haridon Bight. The estimated mean annual shell production for the whole of L'Haridon Bight is 127 g per square metre, compared with 10 g per square metre for Hamelin Pool (Berry and Playford, 1997). The seawater is more saline in Hamelin Pool than in L'Haridon Bight, and this may explain the differences in productivity of *Fragum erugatum* between those two places.

In Henri Freycinet Harbour *Fragum erugatum* is much less common than in either L'Haridon Bight or Hamelin Pool. Moreover, the presence or absence of this bivalve at a monitored locality (beside Nanga) in Henri Freycinet Harbour changes from year to year, and the factors controlling those populations are not adequately understood. More observations, over a longer timeframe, are needed to clarify these issues.

The life span for *Fragum erugatum* individuals in Hamelin Pool seems to be two years or rarely three years. More individuals live into a third year in L'Haridon Bight (Berry and Playford, 1997). The shells remain closed when the molluscs die and dead shells can remain on the sea floor for considerable periods of time, during which many pairs become weakly cemented in a closed position by the precipitation of small amounts of aragonite. They remain closed when carried ashore by storms (Figs 243–245).

Figure 240. Cylindrical well, 3.15 m in diameter and 3.8 m deep, excavated in Hamelin Coquina north of Flagpole Landing. The well has saltwater at its base, in chert of the Toolonga Calcilutite. The lower 1.5 m of the coquinite above the water table is weakly cemented, composed of aragonite, because saltwater rises through that section by capillary action, inhibiting the transformation of aragonite to calcite. The overlying section, 2.3 m thick, is well cemented, and has been transformed to calcite because it is subject to percolating rainwater.

Figure 241. Yellow-brown beach rock in the Hamelin Coquina, in the intertidal zone near the southeast end of Hamelin Pool.

Figure 242. Eroded blocks of Hamelin Coquina, rising to about 2 m above sea level, along the shoreline near Booldah Well.

Table 5. Boreholes drilled through the Hamelin Coquina, from northwest of the old Flint Cliff Telegraph Station to the coast of Hamelin Pool (see Fig. 235 for borehole locations)

Bore no.	*Elevation (m ASL)*	*Hamelin Coquina thickness (m)*
1	10.725	6.65
2	5.470	4.3
3	4.098	4.2
4	4.040	3.9
5	3.238	3.8
6	3.228	3.5
7	2.838	3.2
8	3.263	3.3

However, the shells soon separate after being heaped into beach ridges. Examination of the present shorelines along Hamelin Pool show that closed shells of *Fragum erugatum* are often accompanied by fragments of microbial mats and other organic debris, but the adjoining high beach ridge, probably resulting from an intense tropical cyclone, and most smaller ridges in front of that high ridge, contain only disarticulated shells. The organic fragments associated with the most recent shells are soon lost by decay. Some of the closed shells of *Fragum erugatum* may have floated ashore, buoyed up by gas generated through the decay of soft parts of the organism (Fig. 243).

Shells of the bivalves *Circe nummulina* and *Irus carditoides* occur sporadically in the Hamelin Coquina and can occasionally be found as closed shells in small beach ridges along the present shorelines (Fig. 246). The gastropod *Clypeomorus batillariaeformis* occurs rarely in the Hamelin Coquina, but is abundant in some metahaline shoreline deposits around Henri Freycinet Harbour (Fig. 247).

The maximum observed thickness of dead shells remaining on the sea floor in deep-subtidal parts of Hamelin Pool was 30 cm (Berry and Playford, 1997). Clearly, most of those dead shells will eventually be swept ashore by storms and cyclones, some as closed shells. Samples of closed shells from two localities along the modern shoreline on the west side of Hamelin Pool have been radiocarbon dated as 138 ± 34 years BP and 109 ± 0.5% pMC (percent modern carbon) respectively (F Petchey, 2011, written comm.). The *Fragum erugatum* bivalves in the second of those samples must have lived as recently as 1965–70 AD.

Berry and Playford (1997) estimated that the mean annual deposition of shell per metre of shoreline is 64 kg in Hamelin Pool and 451 kg in L'Haridon Bight. That gives an estimated average rate of deposition of coquina of about 11 800 t/year around Hamelin Pool and 39 700 t/year around L'Haridon Bight. Those amounts testify to the extraordinarily high productivity of *Fragum erugatum*, especially in L'Haridon Bight.

Ridges of *Fragum erugatum* coquina are now prograding seaward along the shores of Hamelin Pool and L'Haridon Bight, and in parts of Henri Freycinet Harbour (Figs 248–254). Some larger and higher beach ridges may have resulted from large tropical cyclones passing directly over Hamelin Pool, while smaller beach ridges have resulted from smaller storms. Offshore barriers and spits are well developed in some areas (Figs 248, 253, 254).

Izuno (2012) measured the height/length ratio of shells of *Fragum erugatum* from 13 localities around Hamelin Pool, in an attempt to reconstruct paleosalinities there over the past 4000 years. He concluded that the salinity of Hamelin Pool rose rapidly about 1250 years BP, when he concluded that stromatolites first appeared there. This is an important conclusion that warrants further research.

Figure 243. Closed shells of *Fragum erugatum* and rounded fragments of microbial mat in very shallow water (about 20 cm deep), near Booldah Well. The shells have remained closed because of the minor precipitation of aragonite cement at the junction between the shells. Note that the shells have similar orientations, some almost floating, as a result of contained gas, perhaps derived by decomposition of the dead shellfish.

Figure 244. Closed shells of *Fragum erugatum* and fragments of microbial mat in the most recent of the small beach ridges near Booldah Well. Small amounts of aragonite cement can be seen on most of the shells, which are kept closed by that cement.

Figure 245. Closed shells of *Fragum erugatum*, associated with algal and other organic debris in a modern minor beach ridge north of Booldah Well.

Figure 246. Closed shells of the bivalves *Circe (Circe) nummulina* (10 shells) and *Irus (Irus) carditoides* (the single shell on the left). These shells are uncommon constituents of the most recent minor beach ridge at Flagpole Landing and some other parts of the Hamelin Coquina.

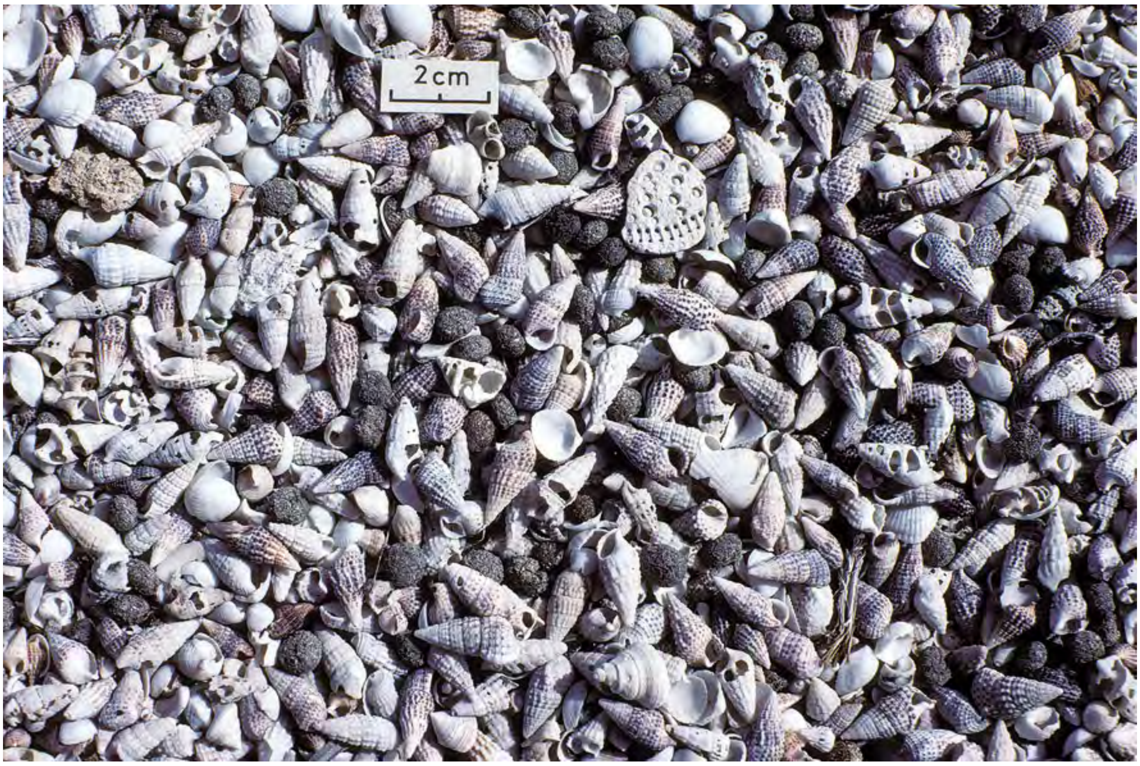

Figure 247. Abundant shells of the gastropod *Clypeomorus batillariaeformis*, a few shells of *Fragum erugatum*, a solitary other species of gastropod, and a fragment of an echinoid, from a beach ridge on the west side of Henri Freycinet Harbour.

Figure 248. Aerial view looking south over the western shoreline of Nanga Peninsula and the adjoining L'Haridon Bight, showing white deposits of Hamelin Coquina along the shoreline and forming offshore bars. *Fragum erugatum* thrives on the adjoining sea floor, extending to water depths of up to 6 m.

Figure 249. Beach ridges on the east side of Hamelin Pool, south of Sweenymia Point. The most recent ridges have resulted from storms, the higher and older ridge is thought to have resulted from an intense tropical cyclone.

Figure 250. Aerial view looking north along the west side of Hamelin Pool towards Spaven Point, showing the cuspate nature of the shoreline. Note submerged seif stromatolites in the centre foreground, and laminar cyclic bedding in the unvegetated part of the Hamelin Coquina. Red sand of the Denham Sand is behind the vegetated part of that formation.

Figure 251. Prominent beach ridges on the west side of Hamelin Pool, north of Spaven Point. They are considered to have resulted from successive large storms.

Figure 252. Beach ridges near Booldah Well on the west side of Hamelin Pool. Minor storms formed the small ridges along the shoreline (right), larger storms formed the intermediate ridges (middle left), and an intense tropical cyclone is thought to have formed the highest ridge (upper left). Note the abundant microbial debris associated with the lower ridges. The lowest ridge includes many closed shells of *Fragum erugatum*.

Figure 253. Aerial view of Taillefer Isthmus looking north, showing two spits built by *Fragum erugatum*, extending into Freycinet Harbour at Goulet Bluff (right), and an unnamed headland (centre). A large birrida, partly inundated by seawater and connected to L'Haridon Bight, is shown in the middle right.

Figure 254. Beach ridges and a spit built of shells of *Fragum erugatum*, at Goulet Bluff on the east side of Henri Freycinet Harbour. Calcrete outcrops in the foreground.

Cyclicity

The horizons of coquinite beach ridges commonly show well-developed cyclicity, expressed as major cycles about 0.3 – 1.5 m thick, and intervening smaller cycles, about 0.1 – 0.3 m thick (Figs 255–258). The beds of cyclical coquinite dip seaward, towards Hamelin Pool (Figs 255, 261–264). Those dips are entirely depositional.

The lower part of each cycle consists of a dense 'mass-transport' coquina of *Fragum erugatum* shells that were jostled together; developing prominent 'nesting' in some places (Figs 231, 232, 257). The upper part of each cycle normally consists of a layer of medium-grained sandy or shelly calcarenite containing disoriented single valves of *Fragum erugatum* in a calcarenite matrix. The top of each cycle is commonly more indurated, and may be marked by a layer of convex-up shells, apparently resulting from wind action at the close of each cycle (Fig. 259).

The major beach ridges are thought to have resulted from intense tropical cyclones passing directly over Hamelin Pool, raising the sea level by several metres, associated with strong wind and wave action.

It is estimated that about 50 major cycles in the Hamelin Coquina in the Flagpole Landing area can be attributed to such intense tropical cyclones, with an average frequency of about once every 100 years. This compares with the conclusion by Nott (2011) that up to 26 tropical cyclones were responsible for the Holocene beach ridges exposed in the Nilemah Embayment area. In that area Nott found evidence of a 1700-year period when terrigenous sand was deposited, without any beach ridges. He ascribed that period to a very dry climate. However, no evidence to support that interpretation has been found in the Flagpole Landing area. The series of beach-ridge cycles has been extensively levelled by wind erosion, and the cycles characteristically dip towards Hamelin Pool (Figs 239, 255, 261–264).

Based on records of historic tropical cyclones from the Australian Government Bureau of Meteorology <www.bom.gov.au/cyclone/history/>, seven tropical cyclones have passed within 50 km of Hamelin Pool between 1916 and 2011 (averaging about once every 13.6 years; Fig. 260). One of these, Cyclone Hazel, a Category 2 System, passed 40 km west of Hamelin Pool on 12 March 1979, causing the water level in the southern part of Hamelin Pool to rise to about 2.8 m, and waves to about 4 m, above mean sea level (observations made by Playford at Hamelin Pool on 27 March 1979). That moderate cyclone made no obvious changes to the shoreline at Hamelin Pool. It did not result in deposition of a new major beach ridge, but presumably added shells to the existing ridge. The shoreline around Flagpole Landing shown in successive airphotos of the area taken since 1952 demonstrates that no significant change has occurred in that shoreline during the past 60 years. Indeed it seems likely that the seven tropical cyclones that passed over or beside Hamelin Pool since 1916 were not sufficiently intense to result in the deposition of any large new beach ridges.

The main part of each major coquina cycle must have resulted from masses of jostled shells being pushed up, en masse, by huge waves associated with intense tropical cyclones, perhaps Category 5 systems (wind speeds of more than 250 km/hour) passing over Hamelin Pool. The resulting 'mass-transport' coquina characteristically includes chains of convex-down, 'nested' shells of *Fragum erugatum* (Figs 231, 232, 257). Such 'nesting' can be replicated by shaking loose shells (without any sand) in cupped hands. The upper sandy part of each cycle (Figs 255, 257) may have been deposited at the peak of the cyclone in this area. Thin layers of convex-up shells, commonly present on the top of each cycle, may have resulted from strong winds after the water level had fallen (Fig. 259).

Smaller cycles, generally about 0.1 – 0.3 m thick, are considered to have resulted from storms or less-intense cyclones (Figs 252, 258). Each of these smaller cycles shows masses of close-packed shells in the lower part of the cycle, and limesand with scattered shells in the upper part.

Mounds

Linear and isolated mounds, up to several metres high, overlie the cyclic beach-ridge coquinites in many areas. They have been swept over the coquinites, truncating older beach ridges (Figs 234–237, 264). These mounds have sandy matrices and contain fragmentary or entire single shells of *Fragum erugatum*, some having convex-up orientations.

The mounds rise a few metres above the underlying planed-off beach-ridge coquinites. Unlike those beach ridges they support some small trees and shrubs. In the area north of Flagpole Landing there are eight such linear ridges, terminated to the south against a headland localized by calcretized Toolonga Calcilutite. Some of the ridges closest to the coast, some 2 km north-northwest of the landing, have been truncated, probably by cyclonic action that exposed the bare surface of the underlying coquinite beach ridges. The periodicity of the linear mounds near Flagpole Landing is estimated to be about once in 400 years.

Isolated mounds also occur in many places, especially beside the west coast of Hamelin Pool (Fig. 264). In contrast to the linear mounds they are irregular to subcircular in shape.

The oldest of the succession of linear mounds west and west-northwest of the former Flint Cliff Telegraph Station is also by far the highest, standing nearly 11 m above mean sea level (Figs 234–238). *Fragum* shells from that mound at different localities have been radiocarbon dated as 3770 ± 270, 3910 ± 340, 4120 ± 320, and 4340 ± 260 years BP (Table 6; A Hogg, 2010, written comm., 17 October). It seems possible that this mound, so much higher than the rest, is a product of a major tsunami that struck the west coasts of Dirk Hartog, Dorre, Bernier, and Koks Islands, probably less than 3000 years ago. The older radiocarbon dates of *Fragum* shells in this mound may be a result of the mixing of shells derived from older coquinas with contemporary shells.

The contact between a mound and underlying cyclone and storm deposits is well displayed beside the southern end of the coquinite quarry near Flagpole Landing (Figs 265–268) and beside a small creek 2.5 km southwest of Flagpole Landing (Figs 269–272). The lower part of the mound beside the quarry consists of up to 11 cm of weakly lithified to unlithified sandy coquinite with convex-up shells of *Fragum erugatum*, overlain by limesand containing abundant fragmentary *Fragum* shells (Figs 266–268). The contact between the mound and the coquinite is horizontal. It is deduced, based on radiocarbon analyses (Table 6), that the age of this mound is about 1900 years, and that of the underlying coquinite is about 2800 years.

The origin of the linear mounds may be debateable, but the presence in them of broken-up and convex-up shells, combined with their linear configuration, parallel to the present shoreline, suggests that these are dune deposits — products of extremely strong cyclonic winds (or a large tsunami in the case of the oldest and highest mound). The presence of a bed of convex-up shells at the base and in the upper part of the linear mound adjoining the Flagpole Quarry (Figs 266–268), and of convex-up shells in the flat-lying bed beside the creek southwest of Flagpole Landing (Figs 269–272), points to very strong wind action when those mounds were deposited.

At least some of the mounds have been localized by clusters of small trees and shrubs. Once a mound is initiated in this way it can be progressively enlarged by strong wind action, probably associated with intense tropical cyclones.

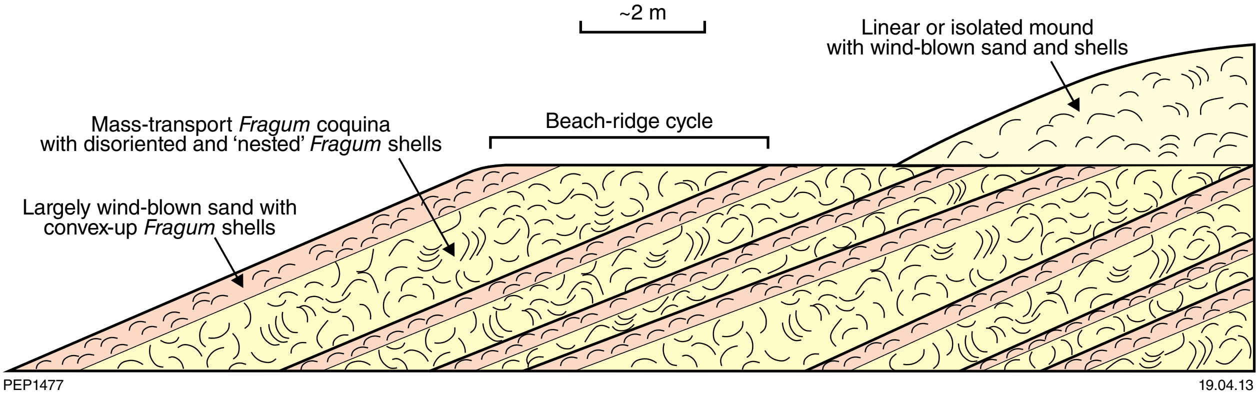

Figure 255. Diagrammatic cross-section illustrating some characteristics of cycles and mounds in the Hamelin Coquina

Figure 256. Two complete cycles, and the base and top of two other cycles, in the Hamelin Coquina in a quarry near Carbla Point. Each cycle begins with 'mass-transport' coquinite and is overlain by shelly calcarenite. Thin indurated layers of limesand, near the top and base of the photo, mark the tops of two of the cycles.

Figure 257. Parts of two cycles in the Hamelin Coquina in a quarry near Carbla Point. 'Mass-transport' jostled coquinite is at the base of each cycle, and shelly sandy limestone with scattered shells is at the top of the lower cycle. Some 'nested' shells can be seen in the 'mass-transport' coquinite of the upper cycle. The contact between the two cycles is a sharp indurated bedding plane. Note the large reworked Pleistocene bivalve shell in the older cycle.

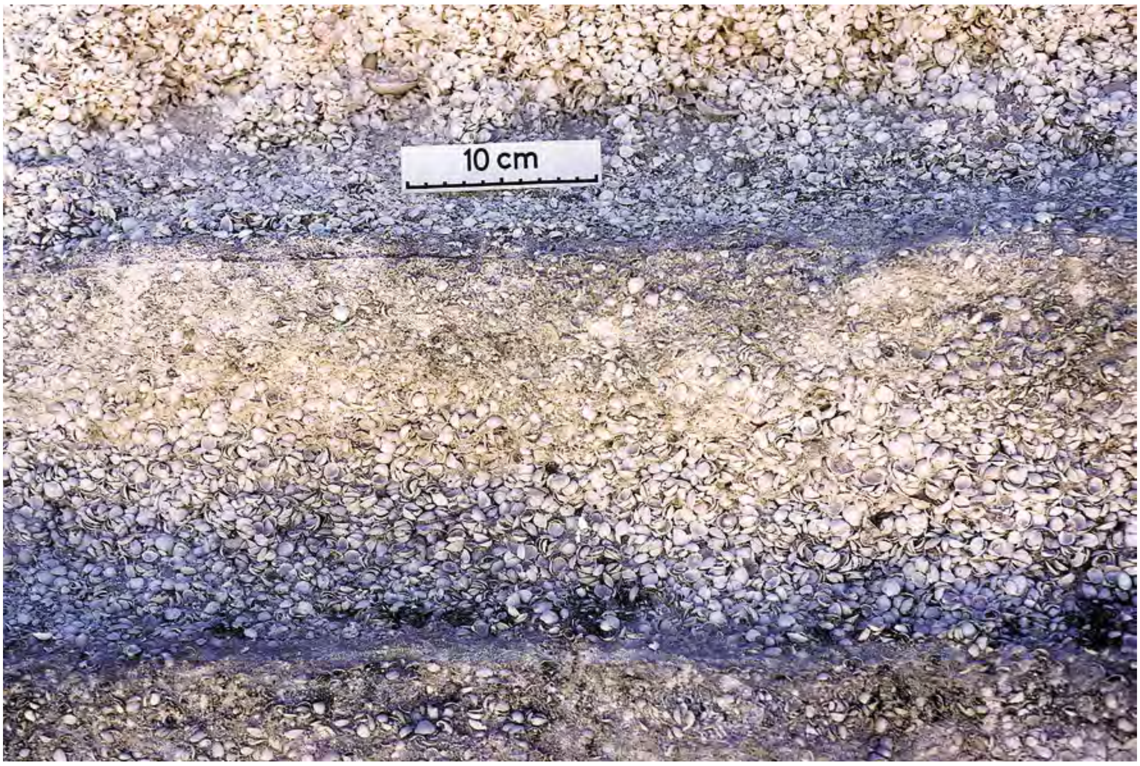

Figure 258. A small cycle and the upper and lower parts of two other cycles in the Hamelin Coquina near Carbla Point. The cycles begin with 'mass-transport' coquinite, overlain by shelly calcarenite. These small cycles are evidently products of winter storms.

Figure 259. Convex-up shells of *Fragum erugatum* in a thin layer at the top of a large cycle in the Hamelin Coquina near Booldah Well. These shells are thought to have been oriented by strong wind action.

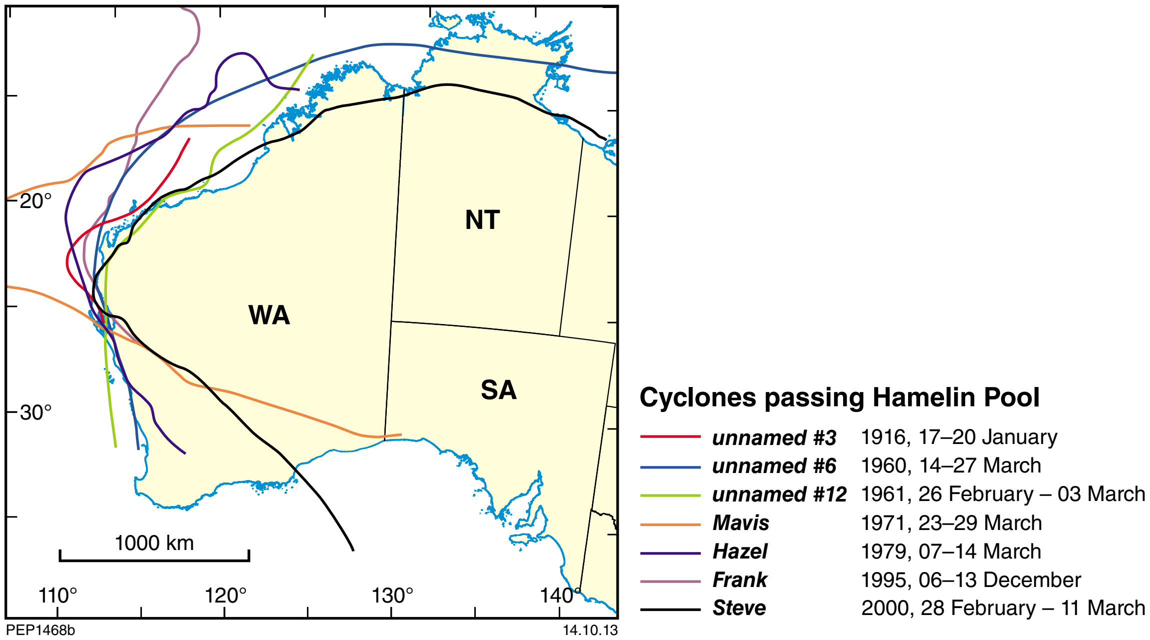

Figure 260. The paths of tropical cyclones that have passed within 50 km of Hamelin Pool between 1916 and 2000. From the Australian Government Bureau of Meteorology.

Figure 261. Succession of planed-off large cycles in Hamelin Coquina, dipping east (towards the coast), beside Booldah Well.

Figure 262. Succession of large cycles in Hamelin Coquina, dipping west (towards the coast) near Flagpole Landing.

Figure 263. Succession of planed-off large cycles in Hamelin Coquina, dipping west (towards the coast) near Flagpole Landing.

Figure 264. Isolated mound of eolian coquina overlying beach ridges of east-dipping cyclic coquinite, in Hamelin Coquina beside the west coast of Hamelin Pool, north of Booldah Well.

Figure 265. The south wall of the main Flagpole Landing quarry, showing a weakly indurated linear-mound deposit underlain by indurated 'mass-transport' coquinite, with a horizontal, planed-off contact between them. The base of the scale is at the top of a bed, 10 cm thick, with convex-up single shells of *Fragum erugatum* in a sandy matrix. This bed is underlain by indurated coquinite (with saw marks), and is overlain by 2 m of limesand containing scattered shells and irregular layers of convex-up *Fragum* shells.

Table 6. Results of radiocarbon dating conducted on samples of Hamelin Coquina

Analyst organisations: ANU — Australian National University; GSWA — Geological Survey of Western Australia; Waikato — University of Waikato. Other abbreviation used: pMC — percent modern carbon.

Sample no.	*Locality*	*Analyst*	*Age (years BP)*
LE 1	SE side of L'Haridon Bight	ANU	2060 ± 60
LW 2	SW side of L'Haridon Bight	ANU	1890 ± 60
46697	At back of oldest and highest beach ridge, 200 m southwest of Hamelin post office	GSWA	3910 ± 340
46698	Oldest *Fragum* immediately west of old post office, at water tank	GSWA	3770 ± 270
46699	Oldest beach ridge of the Hamelin Coquina, north of the Flagpole Landing area	GSWA	4340 ± 260
46700	Oldest *Fragum* ridge	GSWA	4120 ± 320
46705	25 m along-strike from drillsite 2	GSWA	2430 ± 190
46706	25 m along-strike from drillsite 4	GSWA	2090 ± 260
46707	10 m along-strike from drillsite 5, by edge of soak well	GSWA	1360 ± 160
46709	15 m inland from drillsite 7	GSWA	1460 ± 270
46710	Booldah Well area, 10 m along-strike from Booldah 1 drillsite	GSWA	4610 ± 270
46711	Halfway between Booldah 3 and 4 drillsites	GSWA	1370 ± 320
46717	Oldest *Fragum* beach ridge, 7 km north-northwest of Coola Coolaraga Well	GSWA	4660 ± 320
46718	Oldest *Fragum* ridge, on track to Nanga no. 1 bore	GSWA	4170 ± 280
46722	Drillhole Booldah 1 near Booldah Well, depth 3 m	GSWA	5100 ± 350
46724	Shell mound over coquinite quarry near Flagpole Landing	GSWA	1880 ± 300
46725	Coquinite quarry near Flagpole Landing	GSWA	2870 ± 180
46726	Shell mound over coquinite quarry near Flagpole Landing	GSWA	1710 ± 300
46727	Coquina mound over coquinite quarry near Flagpole Landing	GSWA	1780 ± 280
102401	Oldest beach ridge south end of L'Haridon Bight (contains Pleistocene contamination; two samples)	GSWA	6220 ± 330, 8420 ± 350
102402	Oldest beach ridge south of track, near Booldah Well	GSWA	3750 ± 330
102403	Booldah quarry	GSWA	1580 ± 340
102406	Oldest beach ridge, near Booldah Well	GSWA	4660 ± 280
113698	L'Haridon Bight, beach ridge 50 m shorewards from 113697	ANU	1490 ± 60
113699	L'Haridon Bight, weakly cemented coquina, close to shore	ANU	1430 ± 40
113700	Carbla Point quarry	ANU	1820 ± 50
113701	Carbla Point, another quarry	ANU	1990 ± 70
113702	Near Carbla Point, very weakly lithified coquina	ANU	1240 ± 40
113703	Carbla Point, another quarry	ANU	1790 ± 40
113704	Base of dry well near Carbla Point	ANU	2660 ± 50
113716	Cylindrical well at Boolagoorda, 3.0 – 3.1 m below top	ANU	2970 ± 60
113719	Cylindrical well at Boolagoorda, 1.5 – 1.6 m below top	ANU	2620 ± 70
113720	About 40 cm stratigraphically above top of Sweeney Mia circular well	ANU	2570 ± 70
113721	Well near old post office, 2 m depth	ANU	2830 ± 60
113725	West side of L'Haridon Bight, 1 m below top of elongate beach well	ANU	1700 ± 70
135206	Near Booldah Well, closed shells of *Fragum* from modern shoreline	Waikato	138 ± 34
135209	West of Hamelin Pool, coquina over southern half-covered birrida	Waikato	5316 ± 42
135212	Small excavation near base of the oldest mega-dune, Hamelin Pool	Waikato	3661 ± 36
135216	West side of Hamelin Pool closed shells of *Fragum*	Waikato	109 ± 0.5% pMC
135237	Flagpole Landing area, shells from burrow	Waikato	2712 ± 35
135239	Legendre Island, oyster shells from small block	Waikato	2895 ± 35
135240	Legendre Island, oyster shells from larger block	Waikato	3777 ± 40
135252	Ridge near present coast, Flagpole Landing area	Waikato	1213 ± 33
135253	Ridge further inland from 135252	Waikato	2152 ± 35
135254	Ridge of broken shells, Flagpole Landing area	Waikato	1253 ± 35
135255	Shell ridge inland from 135254	Waikato	2131 ± 38
135256	Shell ridge inland from 135255	Waikato	2483 ± 38
135257	Sandy shell ridge inland from 135256	Waikato	5074 ± 43
135258	Shell ridge inland from 135257	Waikato	3022 ± 39
135259	Very high shell ridge, furthest inland, Flagpole Landing area	Waikato	3733 ± 40
135260	Broken shell and sand	Waikato	3265 ± 39
135261	Broken shell and sand	Waikato	2711 ± 38
135262	Broken shell on the highest beach ridge	Waikato	5062 ± 43
135264	Shell in shelly sand above the Flagpole quarry	Waikato	2199 ± 37
135265	Coquinite in Carbla quarry	Waikato	1384 ± 25
135265a	Coquinite in Carbla quarry	Waikato	1590 ± 25
135266	Sandy coquinite ridge on fenceline north of Hamelin Landing	Waikato	5084 ± 43
135268	Top of an isolated mound, east side of Hamelin Pool	Waikato	1618 ± 37
135269	Below an isolated mound, east side of Hamelin Pool	Waikato	1849 ± 35

Figure 266. Contact (immediately below the scale) between 'convex-up' coquinite above, and 'mass-transport' coquinite below, in the southern wall of the Flagpole quarry.

Figure 267. Closely packed convex-up shells of *Fragum erugatum*, thought to have been laid down by strong winds, above the base of the linear-mound deposit shown in Figure 265, at the south end of the main Flagpole quarry.

Figure 268. Shells of *Fragum erugatum*, many convex-up and others fragmentary, in a sandy matrix, near the top of the linear-mound deposit shown in Figure 265. Note the channel filling in the lower part of the photo.

Figure 269. View looking east beside the track 2.4 km southwest of Flagpole Landing, showing cross-bedding. The dipping beds are below a near-horizontal bed at the base of a linear mound, which is partly vegetated with small shrubs. The bare white sandy material immediately above the horizontal bed consists of spoil derived through excavating the track.

Figure 270. Cross-bedding in Hamelin Coquina at the locality shown in Figure 269. The beds dipping to the right (towards Hamelin Pool), consist of a series of storm-induced cycles. The near-horizontal upper bed is at the base of an eolian linear mound. It contains convex-up shells of *Fragum erugatum* in a sandy matrix.

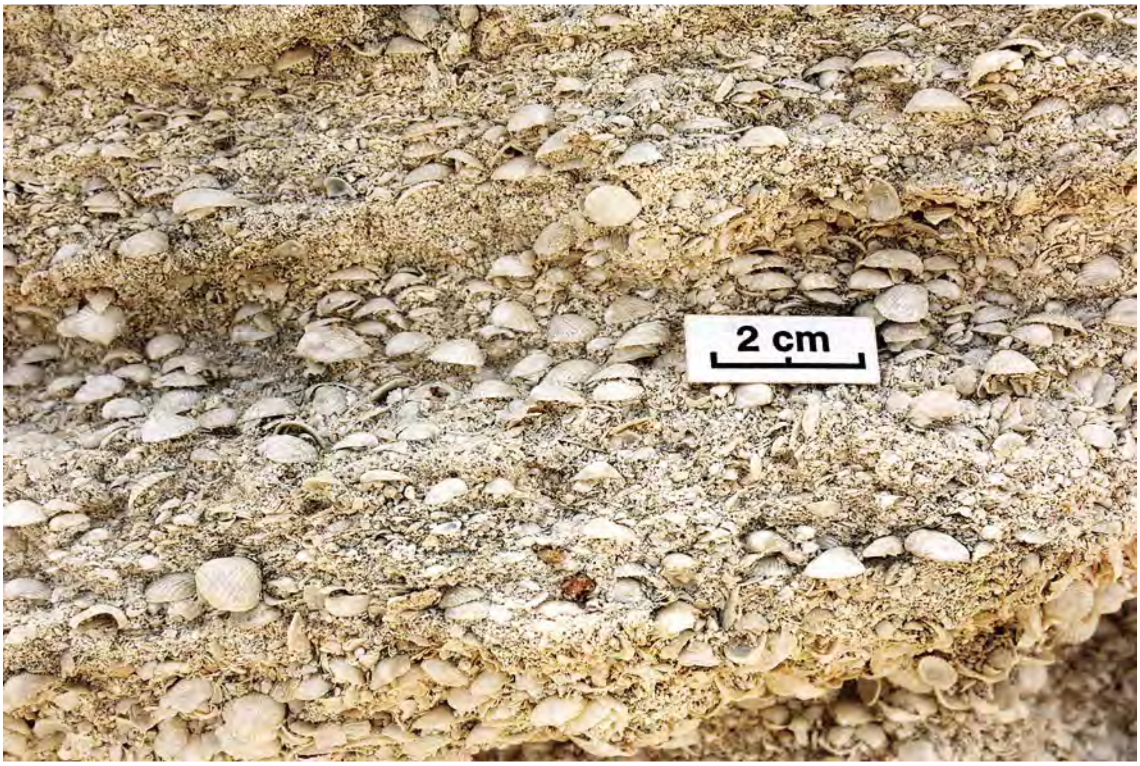

Figure 271. Eolian shelly calcarenite with convex-up shells of *Fragum erugatum*, at the base of the linear mound shown in Figures 269 and 270.

Figure 272. Closer view of the cross-bedding shown in Figures 269 and 270. Note the convex-up shells in the near-horizontal eolian bed at the base of the linear mound.

Stromatolites

Definition

In accordance with the definitions adopted by Playford (1990), McNamara (1992), and Reid et al. (2003), we apply the term stromatolite to organosedimentary structures that have relief above the substrate, produced by sediment trapping and micrite precipitation through the growth of microbial communities, especially cyanobacteria. Unlaminated or poorly laminated structures at Hamelin Pool would be termed 'thrombolites' by those who require stromatolites to be laminated (e.g. Riding, 1999). If that usage were to be adopted here, then the Hamelin Pool forms, or parts of those forms that lack lamination would be termed thrombolites (Kennard and James, 1986). It would then be necessary to differentiate between stromatolites and thrombolites by sectioning individual heads to determine whether or not they are laminated. Moreover, many heads are partly laminated and partly unlaminated. Consequently, in accord with long-standing usage, it is deemed best for the term stromatolite to be used here to embrace all microbial structures in Hamelin Pool that have grown with positive relief above the sea floor.

Flat microbial mats, which occur extensively in intertidal to subtidal environments in Hamelin Pool and L'Haridon Bight, are not classed as stromatolites, because they lack relief. Burne and Moore (1987) introduced the term 'microbialite' to cover both stromatolites, laminated or unlaminated, and flat microbial mats.

History of investigations

The following account of the discovery of the Hamelin Pool stromatolites stems from email exchanges, during January 2010, between Robert Ginsburg, Phillip Playford, and Richard Chase, and a verbal discussion at that time between Playford and Daryl Johnstone. This resulted from Ginsburg's request for clarification of how the stromatolites came to be discovered, and it was agreed by those concerned that the following account would be included in this Bulletin in order to clarify the matter.

The Hamelin Pool stromatolites were discovered by Playford in July 1954, when he and Daryl Johnstone were working in the Shark Bay area for WAPET. They were mapping the area and assessing its petroleum potential, camping in an old woolshed beside Flagpole Landing. At that time Playford was intrigued to find many prominent 'algal mounds' (as he termed them) that formed limestone reefs beside the shoreline at Flagpole Landing and elsewhere around Hamelin Pool. He drew them to the attention of Johnstone who agreed that they must be built by 'blue-green algae' (now known as cyanobacteria).

In December 1954, Playford returned to this area with Richard Chase, who had just completed a BSc in geology at UWA. They were locating water bores in the Shark Bay area, determining their elevations by barometric means, and obtaining relevant records of the bores from station managers. They camped in the old woolshed beside Flagpole Landing, the place where Playford had identified the algal mounds five months before. Playford showed them to Chase, at the same time taking the first known photos of these features (Figs 273, 274).

In 1955, Richard Chase and Brian Logan jointly undertook a research project on the Proterozoic Moora Group, for their BSc Honours degrees at UWA. Those Proterozoic rocks contain stromatolites (originally identified as such by Rhodes Fairbridge), and in mid-1955 Chase suggested to Playford that the algal mounds and algal reefs he had seen at Hamelin Pool might be modern analogues of the Proterozoic stromatolites in the Moora Group and asked if he could collect a sample for biological examination. The specimen that Playford collected was examined by David Churchill of the UWA Botany Department, and he confirmed the presence of blue-green algae (now termed cyanobacteria) on the specimen.

In 1956 Logan consulted Playford, seeking his suggestions about possible research projects for a PhD degree at UWA, indicating his preference to work on modern rather than ancient sedimentary rocks. Playford suggested that Shark Bay would be an excellent place for a study of Holocene sedimentation, pointing especially to the living stromatolites there as an example of important features in the area. Logan accepted that suggestion and was the first person to publish a description of the Hamelin Pool stromatolites, but without acknowledging their prior discovery (Logan, 1961). It was published in the same year that Logan and Chase (1961) described the Proterozoic stromatolites in the Moora Group, but, surprisingly, they did not compare them with the stromatolites in Hamelin Pool, instead pointing to modern stromatolite analogues known elsewhere in the world.

Logan (1961) concluded that the living stromatolites at Hamelin Pool are confined to the intertidal zone, with eroded forms occurring in the supratidal zone (Fig. 275). That conclusion was reiterated by Logan et al. (1964), and it became widely accepted that the presence of stromatolites in ancient sedimentary rocks was definitive evidence of an intertidal origin. However, that conclusion was disputed by some, including Fischer (1965) and Monty (1965). Playford (1972) recorded that living stromatolites at Hamelin Pool are not restricted to the intertidal zone, but extend into the subtidal environment. Moreover, Playford and Cockbain (1969), Playford (1972), Playford et al. (1976a), and Playford et al. (2009) showed that many Devonian stromatolites in the Canning Basin grew in water depths of at least 45 m, and probably more than 100 m.

The Department of Conservation and Land Management (CALM, now Department of Parks and Wildlife), in accord with a recommendation by Playford (1993), constructed a walkway at Flagpole Landing, at the very place where the stromatolites had first been discovered in 1954, in order to allow members of the public to conveniently view the stromatolites without damaging them (Fig. 276). Moss (1996) prepared a management plan for the area, on behalf of the Shire of Shark Bay.

Flagpole Landing had been the place where camel-drawn drays transported bales of wool out from the shore, in order to load them onto a dinghy. That system was used until the mid-1930s, when road transport by motor vehicles became feasible in this area.

The path cut through stromatolites at Flagpole Landing for the camel dray is shown in Figure 277, and other photos show the bales being put into a dinghy (Fig. 278), and the loaded dinghy about to be taken out to a lighter anchored in deeper water (Fig. 279). The lighter (commonly the *Will Succeed*; Fig. 20) in turn took the bales to a ship anchored in Denham Sound.

Playford and Cockbain began studying the modern stromatolites at Hamelin Pool in 1968, primarily to compare and contrast them with deepwater Devonian stromatolites that they had been studying in the Devonian reef complexes of the Canning Basin (Playford and Cockbain, 1969). It was soon evident that the stromatolites in Hamelin Pool extend below the intertidal zone rather than being solely intertidal as claimed by Logan (1961). The presence of these subtidal stromatolites was first recorded by Playford (1972). He stated that well-developed living columnar forms in this area extend to depths of at least 2 m, where they are undergoing contemporary lithification.

Logan et al. (1974a) re-affirmed most of the conclusions reached by Logan (1961) and Logan et al. (1964), but indicated that although the living Hamelin Pool stromatolites characterize the intertidal zone, some ‘cryptalgal structures’ also occur in water depths of up to 2 m at Carbla Point and a few other localities. They concluded that these subtidal forms are likely to be relics of stromatolites that grew originally in the intertidal zone and were subsequently submerged. However, Hoffman, a co-author of that paper, recorded that living subtidal forms, built by colloform mat, have grown in water depths of up to 2 m at Carbla Point (Hoffman, 1976).

Playford and Cockbain (1976) concluded that living algal stromatolites in Hamelin Pool ‘are forming today over wide areas’ of the sublittoral pavement as well as the adjacent intertidal zone, and that they extend to water depths of about 3.5 m. The results of subsequent work were described by Playford (1979; 1980a,b; 1990). Playford (1979) concluded that subtidal stromatolites and algal mats at Hamelin Pool are more widespread than intertidal forms. The maximum depth reached by living stromatolites was recorded as 4 m, by Playford (1990).

Other significant contributions dealing with various aspects of the Hamelin Pool stromatolites have been published by Bauld et al. (1979), Bauld (1984), Skyring and Bauld, (1990), Golubic (1976, 1982, 1983, 1985), Chivas et al. (1990), Reid et al. (2003), and Jahnert and Collins (2011, 2012).

Figure 273. The first known photo of Hamelin Pool stromatolites taken in December 1954. It shows stromatolites exposed at low tide beside Flagpole Landing. The grey- and orange-coloured tops of most stromatolites are dead, but pustular mat is still alive on their sides. Many have coalesced to form a stromatolite reef. Black knobbly-mat stromatolites are seen in the middle left, and shallow-subtidal stromatolites are seen to the right, behind the person (Richard Chase).

Figure 274. View looking towards the shore from the same place and at the same time as Figure 273, showing dead and partly living intertidal to supratidal stromatolites in the foreground, and dead supratidal forms closer to the shore. A prominent beach ridge of Hamelin Coquina rises behind the shoreline. Part of the old woolshed can be seen on the left and a red WAPET Landrover is on the right.

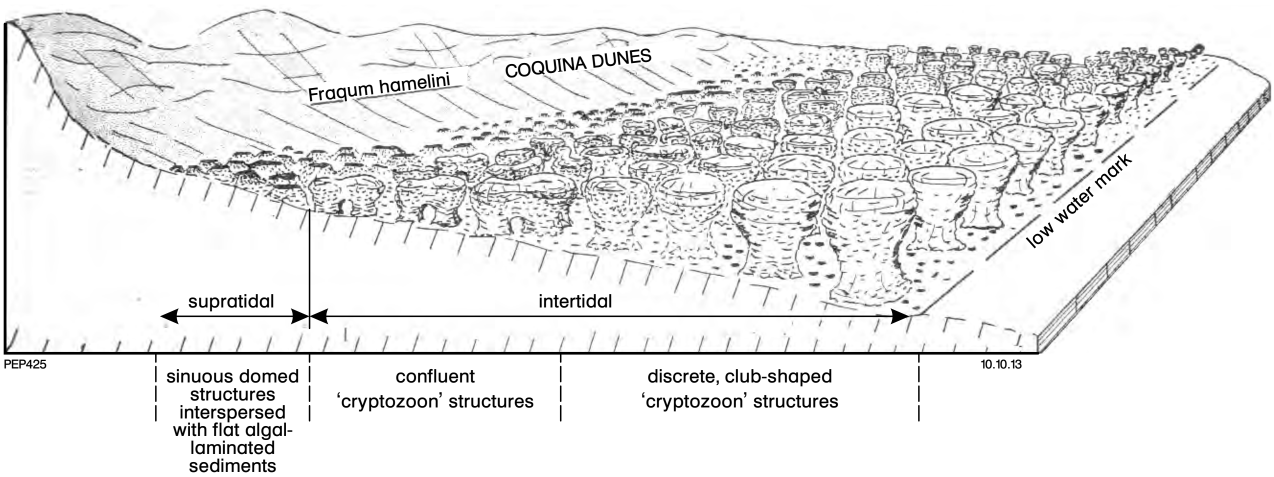

Figure 275. Diagram by Logan (1961) showing the supposed distribution of stromatolites in Hamelin Pool.

Figure 276. Walkway constructed by the Department of Conservation and Land Management (CALM, now the Department of Parks and Wildlife) beside Flagpole Landing, reaching very close to the place where the photos shown as Figures 273 and 274 were taken.

Figure 277. Path cut more than 80 years ago through stromatolites at Flagpole Landing to allow camel-drawn drays to carry bales of wool out to dinghies, which then took them to a lighter anchored in deeper water.

Figure 278. Dray, drawn by camels and loaded with bales of wool, about to be transferred to a dinghy beside Flagpole Landing. Photo courtesy of Mary Wake.

Figure 279. Dinghy laden with wool bales, about to be taken to a lighter anchored in Hamelin Pool, which in turn took them to a ship anchored off Denham. Photo courtesy of Mary Wake.

Reid et al. (2003) showed that microbial precipitation of micrite, forming muddy micritic structures, is the primary cause of stromatolite growth in the subtidal zone, and is also responsible for cementation of intertidal and supratidal stromatolites. Jahnert and Collins (2011, 2012) confirmed the widespread occurrence of subtidal stromatolites in Hamelin Pool, and produced maps of the distribution of stromatolites and associated sediments.

A significant recent paper relating to photosynthesis in stromatolites at Hamelin Pool is by Chen et al. (2010). They showed that a new variety of chlorophyll, termed 'chlorophyll f', is important in photosynthesis occurring deeply within Hamelin Pool stromatolites. This chlorophyll utilizes lower levels of light energy than any other known varieties of chlorophyll. It is the first new form of chlorophyll to have been discovered in more than 60 years.

Diagrammatic cross-sections showing stromatolite depth distributions in Hamelin Pool were published by Playford (1990), Reid et al. (2003), and Jahnert and Collins (2011, 2012). Figure 280 shows a simplified representation of the living stromatolite distributions that are discussed here.

The Hamelin Pool stromatolites are recognized as being among the most important natural features of the Shark Bay area. Indeed, their presence was largely responsible for the creation of the Shark Bay World Heritage Area. Many television programs featuring the stromatolites have been produced, notably David Attenborough's BBC series 'Life on Earth' (with a printed version by Attenborough, 1979), and the Japanese NHK series 'Miracle Planet' (NHK 1987; Figs 281 and 282).

The most dramatic of the TV presentations was a direct telecast by NHK on the evening of Saturday 9 July 1994, when Japan's first female astronaut, Dr Chiaki Mukai, was orbiting the earth in a space shuttle. This live program, lasting one hour, began at 7 pm Perth time (8 pm Tokyo time), and had as its themes the evolution of life on Earth and the development of the Earth's atmosphere. Two localities were selected to illustrate those themes, one at Carbla Point in Hamelin Pool (to mimic life on Earth as it was during the Precambrian) and the other at the Amazon in Brazil (to illustrate the diversity of life on Earth today). The presentation at Carbla Point required major transmission equipment (brought in from the Eastern States), together with searchlights and underwater lights to illuminate the scene. Playford was the presenter at Hamelin Pool. His contribution included discussion of an experiment conducted by placing a transparent plexiglass dome, with a capacity of about 10 L, over a shallow-subtidal stromatolite, for a period of 11 days. The objective was to illustrate the amount of oxygen (about 2 L) given off by the stromatolite through photosynthesis during that period.

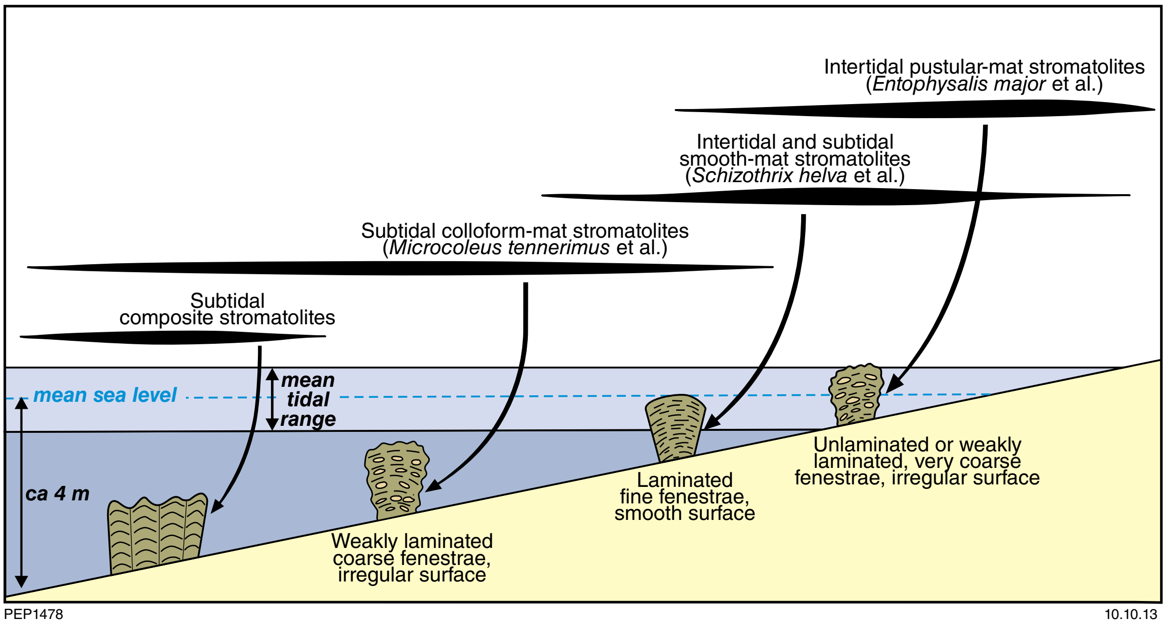

Figure 280. Simplified diagram to illustrate the distribution of the various types of stromatolites in Hamelin Pool, modified after Playford (1990).

Figure 281. Cover of an NHK manga book (NHK, 1987) describing the Hamelin Pool stromatolites. Courtesy of NHK, supervisor Takashi Hamada, author Shinji Hikino.

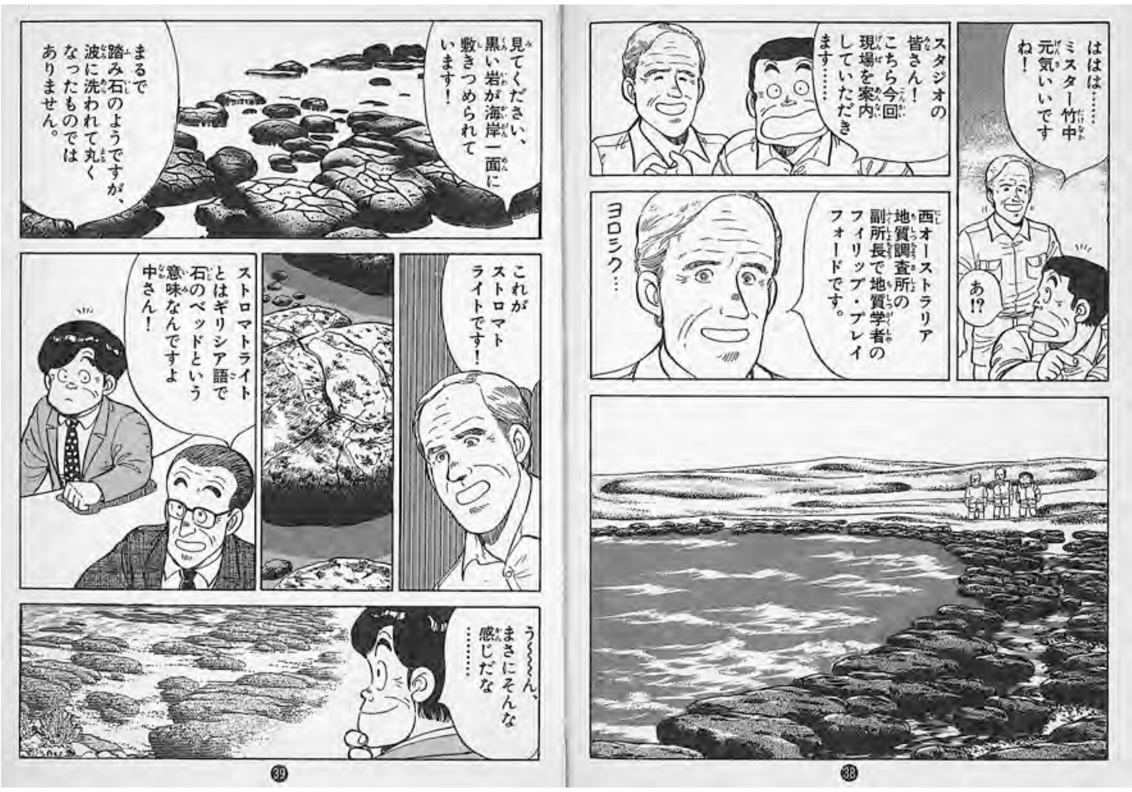

Figure 282. Pages from the NHK manga book showing Playford discussing the Hamelin Pool stromatolites with an NHK TV presenter. Courtesy of NHK, supervisor Takashi Hamada, author Shinji Hikino.

Stromatolite distribution

Stromatolites and associated flat microbial mats occur for some 100 km around the coast of Hamelin Pool. Their morphologies, distribution, and factors controlling the morphologies, are illustrated in Figures 283–297 and 299–382. The stromatolites and associated flat microbial mats, collectively known as microbialites, cover wide areas of the intertidal, supratidal, and shallow subtidal zones, extending to maximum water depths of about 4 m. Subtidal stromatolites are more extensive than intertidal and supratidal forms. The intertidal stromatolites commonly form rigid wave-resistant reefs. Supratidal stromatolites are dead and eroded, having grown when relative sea level was as much as 1 m higher than it is today.

Many individual stromatolites along the Hamelin Pool shoreline are partly intertidal and partly supratidal. They are still growing in their intertidal lower parts, while the supratidal parts are dead, with cracked upper surfaces, commonly black or dark red (Figs 283–288, 294–296). In some cases, parts of the cracked upper layer of a stromatolite head has been displaced upwards, forming a tepee structure (Figs 287, 288). Stromatolites along the shorelines are commonly being covered progressively by the advancing Hamelin Coquina (Fig. 289).

Stromatolites in some areas form a series of terraces, a good example being 4.5 km south of Booldah Well (796450E, 7083590N; Figs 294–297). Those stromatolites, from the top down, consist of: (a) lustrous pale-orange to grey dead stromatolites, forming the highest terrace, with their tops about 0.7 m above mean sea level, that are currently being eroded in the supratidal zone and overlie fossiliferous limestone of the late Pleistocene Dampier Limestone (Fig. 298); (b) bright-orange stromatolites in the supratidal zone, now dead and being actively eroded, with their tops about 0.35 m above mean sea level, (c) dark-grey supratidal to intertidal stromatolites, partly dead, with their tops about 0.19 m above mean sea level, being eroded in their upper (supratidal) parts and fringed by living *Entophysalis* in their lower (intertidal) parts; and (d) dark-brown, columnar, living stromatolites, built by *Entophysalis*, in the intertidal zone. Chivas et al. (1990) dated the oldest of the stromatolites at this locality as being 1000–1250 years old.

These terraces have resulted from either eustatic falls in sea level or pulses of tectonic uplift. The uplift hypothesis may be most likely, as folding of the peninsulas and islands in Shark Bay is thought to have continued during the Holocene, and the locality described above is situated over the east flank of an anticline below Nanga Peninsula.

It is clear that not all stromatolites in the intertidal and subtidal zones in Hamelin Pool are alive and actively growing — some are being eroded and are dead (or dormant). Some stromatolites have been overwhelmed by moving waves of ooid or pelloid sand (Figs 299, 300), and others have been uncovered when those waves moved on. In some cases the uncovered stromatolites have apparently resumed growth after being recolonized by stromatolite-building microbial mats, but in others they have remained hard and seemingly dead after being uncovered. However, thin films of cyanobacteria coat the surfaces of such hardened stromatolites and may still be precipitating calcium carbonate, albeit extremely slowly. Similarly, around the margins of emerged stromatolite reefs in the intertidal zone there can be a band of black 'knobbly-mat' stromatolite formed by a type of film mat (Figs 290–293).

Meischner (1994) stated that most stromatolites at Hamelin Pool date back to the last interglacial period of the Pleistocene, as he claimed to have found Pleistocene limestone overlying and interfingering with the stromatolites. However, in the localities where Pleistocene Dampier Limestone occurs alongside stromatolites, the limestone always underlies the stromatolites. In some of those places the contact between them is irregular, with abrupt relief of up to 40 cm, and that may have given the false impression that stromatolites underlie or interfinger with Pleistocene limestone.

Burne and James (1986) concluded that stromatolites now living in the intertidal zone were initiated as subtidal stromatolites and have since emerged because of falling relative sea level. Indeed it seems clear that some subtidal stromatolites must have moved into the intertidal zone as a result of relative falls in sea level during about the past 1000 years. However, other intertidal stromatolites are expected to have grown entirely in that zone.

Stromatolites are abundant in Hamelin Pool but are rare elsewhere in the oceans of the world. There are two probable reasons, linked with the hypersalinity of Hamelin Pool, why stromatolites are able to thrive there but not in most areas of the open ocean. Firstly, it is clear that grazing animals, such as gastropods, that could otherwise consume stromatolite-building microbes, are absent or rare in Hamelin Pool, and secondly, very few species of thallophytic algae, that might occupy niches now occupied by stromatolites, grow in Hamelin Pool, apparently because of its high salinity.

The Hamelin Pool stromatolites have been widely regarded as modern analogues for fossil stromatolites, which are especially common in Precambrian rocks (Fig. 301; Hoffman, 1974). Stromatolites flourished during the Precambrian because animal life and thallophytic algae did not exist for all but the latest part of that time. The situation in Hamelin Pool mimics that of the Precambrian, as most marine animals and plants cannot survive the hypersaline conditions in Hamelin Pool.

Perhaps surprisingly, Hamelin Pool supports many fish (Figs 321, 323), although there are fewer species than in the open marine part of Shark Bay. The jellyfish *Phyllorhiza pacifica* (Figs 324, 325; Marsh and Slack-Smith, 2010) is common, as are sea snakes (Figs 326, 327).

Figure 283. Emerged stromatolite reef in the lower part of the supratidal zone near the southeast end of Hamelin Pool. The grey and orange tops of the pustular-mat stromatolites that built the reef are now dead and being eroded. Living shallow-subtidal stromatolites are present below the water in front of the reef.

Figure 284. Club-shaped intertidal to supratidal pustular-mat stromatolites, partly coalesced to form a reef, near the southeast end of Hamelin Pool. The grey cracked tops of the stromatolites are dead, and have living *Entophysalis* on their sides.

Figure 285. Club-shaped and coalesced pustular-mat stromatolites near the southeast end of Hamelin Pool. These are supratidal stromatolites, now dead, with cracked, grey and orange tops.

Figure 286. A pustular-mat stromatolite at Carbla Point, with a dead, cracked, grey top, surrounded by dark-grey living *Entophysalis*.

Figure 287. The dead, orange and grey, cracked top of a pustular-mat stromatolite at Flagpole Landing, with a developing tepee structure above the scale.

Figure 288. The cracked dead top of a pustular-mat stromatolite at Flagpole Landing, with a tepee structure on its crest being forced upwards by growth of *Entophysalis*.

Figure 289. Pustular- and smooth-mat stromatolites near the southeast end of Hamelin Pool. The tops of the pustular-mat stromatolites are dead, and they have living *Entophysalis* on their sides. The stromatolites are being progressively covered by Hamelin Coquina.

Figure 290. **Club-shaped pustular-mat stromatolites at Flagpole Landing, with dead tops and a band of black knobbly-mat stromatolites where the person (Tony Cockbain) is standing. Shallow-subtidal smooth-mat living stromatolites can be seen below the water.**

Figure 291. **A band of black knobbly-mat stromatolites at Flagpole Landing, fringing cracked, dead, grey, club-shaped, pustular-mat stromatolites (above the water) and smooth-mat stromatolites (below the water).**

Figure 292. A stromatolite at Flagpole Landing, with a strongly indurated knobbly-mat core surrounded by living pustular mat.

Figure 293. Dark-coloured, strongly indurated, knobbly-mat stromatolite at Flagpole Landing.

Figure 294. Terraced stromatolites on the east side of Nanga Peninsula, south of Booldah Well, showing: lustrous pale-orange to light-grey dead supratidal stromatolites in the highest level, about 0.7 m above mean sea level; bright-orange supratidal dead stromatolites in the next level, about 0.35 m above mean sea level; dark-grey supratidal to intertidal stromatolites, fringed by living *Entophysalis*, in the next level, about 0.19 m above mean sea level; and dark-brown living intertidal stromatolites in the lowest level, built by *Entophysalis major.*

Figure 295. Terraced stromatolites on the east side of Nanga Peninsula, south of Booldah Well, at the locality shown in Figure 294, with red sand dunes of the Nilemah Sand in the background.

Figure 296. Closer view of the terraced stromatolites shown in Figures 294 and 295. Tony Cockbain is shown with his hand on fossiliferous Pleistocene Dampier Limestone, on which the stromatolites grew.

Figure 297. View looking east (towards Hamelin Pool) at high tide at the same place as Figures 294–296, showing terraced stromatolites over Dampier Limestone, and seif stromatolites below water in the middle distance.

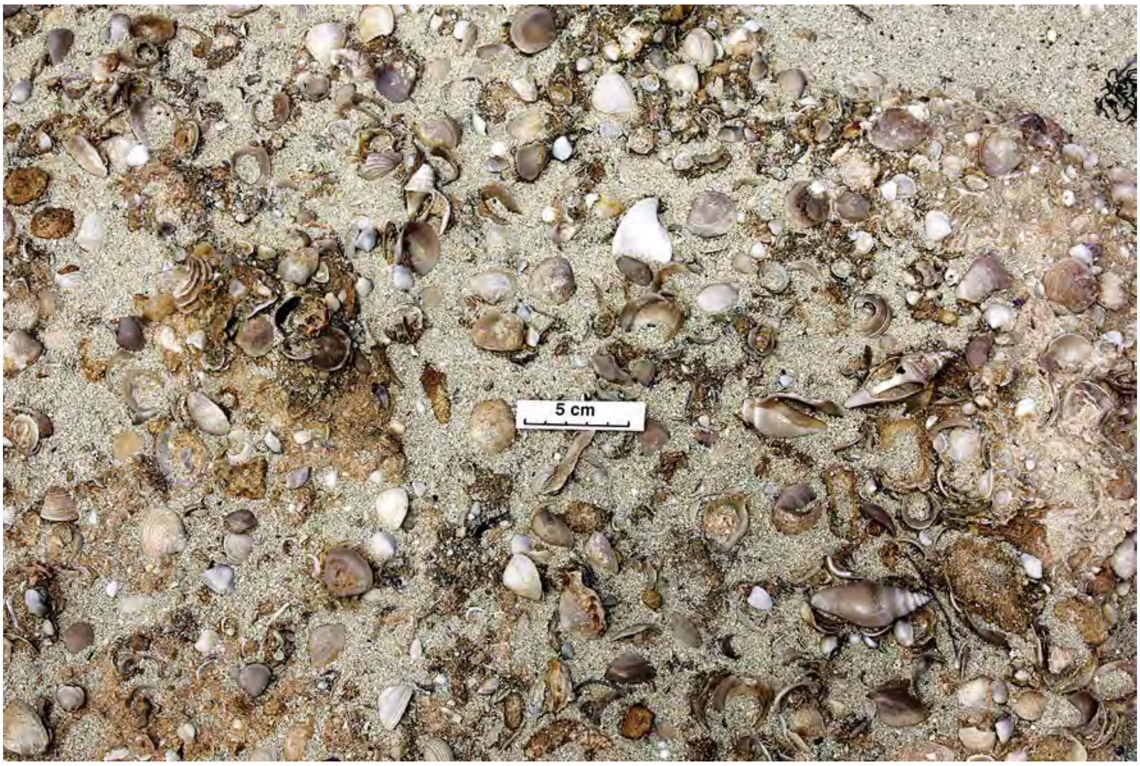

Figure 298. Fossiliferous Late Pleistocene Dampier Limestone underlying the stromatolites shown in Figures 294–297. This is an open-marine fauna of bivalves and gastropods.

Figure 299. Airphoto looking south near the southwest end of Hamelin Pool, showing active mega-ripples of white ooid sand partly covering stromatolites.

Figure 300. Airphoto looking north-northwest near the southwest end of Hamelin Pool, showing active mega-ripples of ooid sand partly covering stromatolites, with 'fingers' of sand extending into deeper water.

Figure 301. Proterozoic longitudinal stromatolites on the shore of Great Slave Lake, North West Territories, Canada, with a hammer for scale. These forms are analogous to the longitudinal stromatolites at Hamelin Pool. Photo courtesy of Paul Hoffman.

Figure 302. Club-shaped intertidal to supratidal stromatolites at Carbla Point, built by pustular mat. Those in the foreground are largely dead, but have some living *Entophysalis* growing on their lower sides.

Figure 303. Stromatolites at Carbla Point, passing from grey forms with dead tops and living pustular mat on their sides (foreground), to dark-brown living forms built by pustular mat in the middle distance, and shallow-subtidal forms built by pustular and smooth mats in the background.

Figure 304. Living pustular mat built by *Entophysalis major* on top of a stromatolite at Carbla Point.

Figure 305. Wide expanse of flat microbial mat built by *Entophysalis major*, north of Booldah Well.

Figure 306. Living smooth-mat intertidal stromatolites in the southeast part of Hamelin Pool, showing desiccation cracking.

Figure 307. Smooth- and pustular-mat stromatolites beside the southeast coast of Hamelin Pool south of Flagpole Landing.

Figure 308. Smooth-mat stromatolites from the southeast coast of Hamelin Pool, south of Flagpole Landing.

Figure 309. Columnar colloform-mat stromatolites, about 40 cm tall, in water about 1 m deep, beside the southeast coast of Hamelin Pool. Note the coating of the green alga *Acetabularia* over the lower, indurated, parts of the stromatolites.

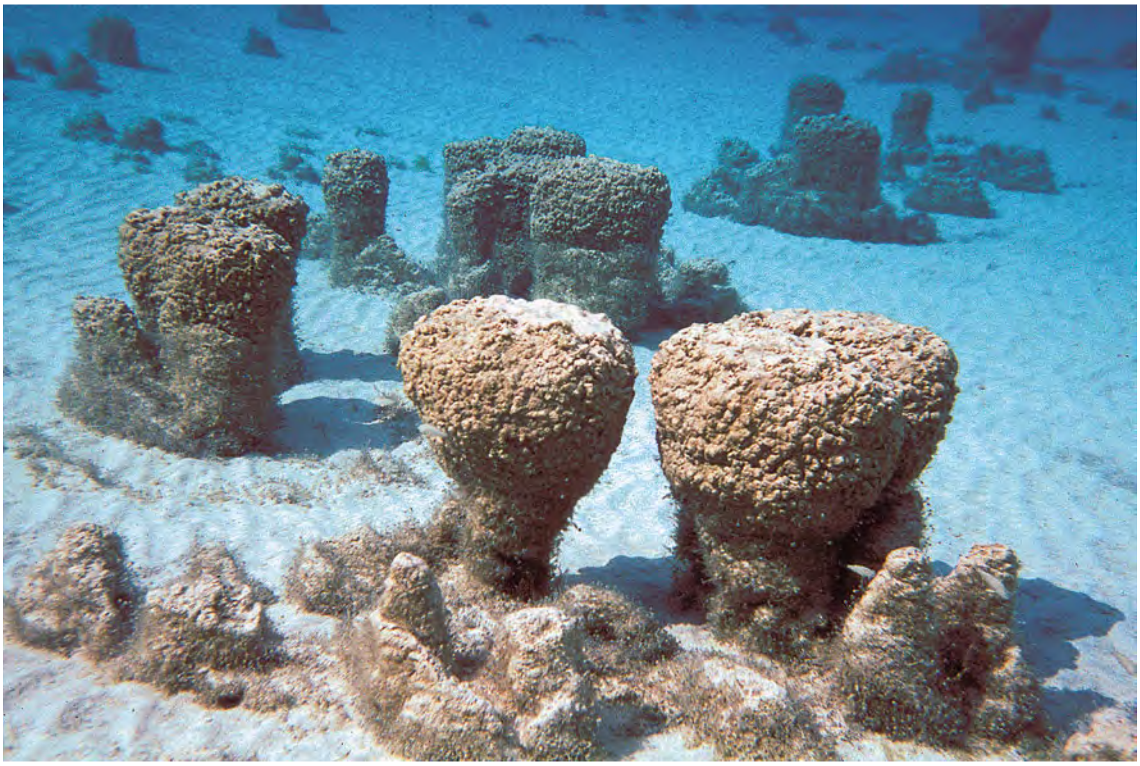

Figure 310. Club-shaped and columnar colloform-mat stromatolites, about 40 cm tall, in water about 1 m deep, beside the southeast coast of Hamelin Pool. Note the coating of the green alga *Acetabularia* over the lower, indurated, parts of the stromatolites.

Figure 311. Colloform-mat stromatolites near the southeast coast of Hamelin Pool. Note that one column has been knocked over (centre left), and another has been damaged, probably by a partly submerged animal carcass.

Figure 312. View from above the water of mound-shaped composite stromatolites, in water about 2 m deep off Carbla Point. These stromatolites are about 1 m across and 40 cm tall.

Figure 313. Mound-shaped composite stromatolites, about 40 cm tall, in water about 2.5 m deep, off Carbla Point. Green algae can be seen coating the sides of the stromatolites, and ripple-marked ooid sand lies between them.

Figure 314. Conical stromatolites and composite stromatolites, up to about 40 cm tall, in water about 2.5 m deep, off Carbla Point. Green algae cover most of these stromatolites.

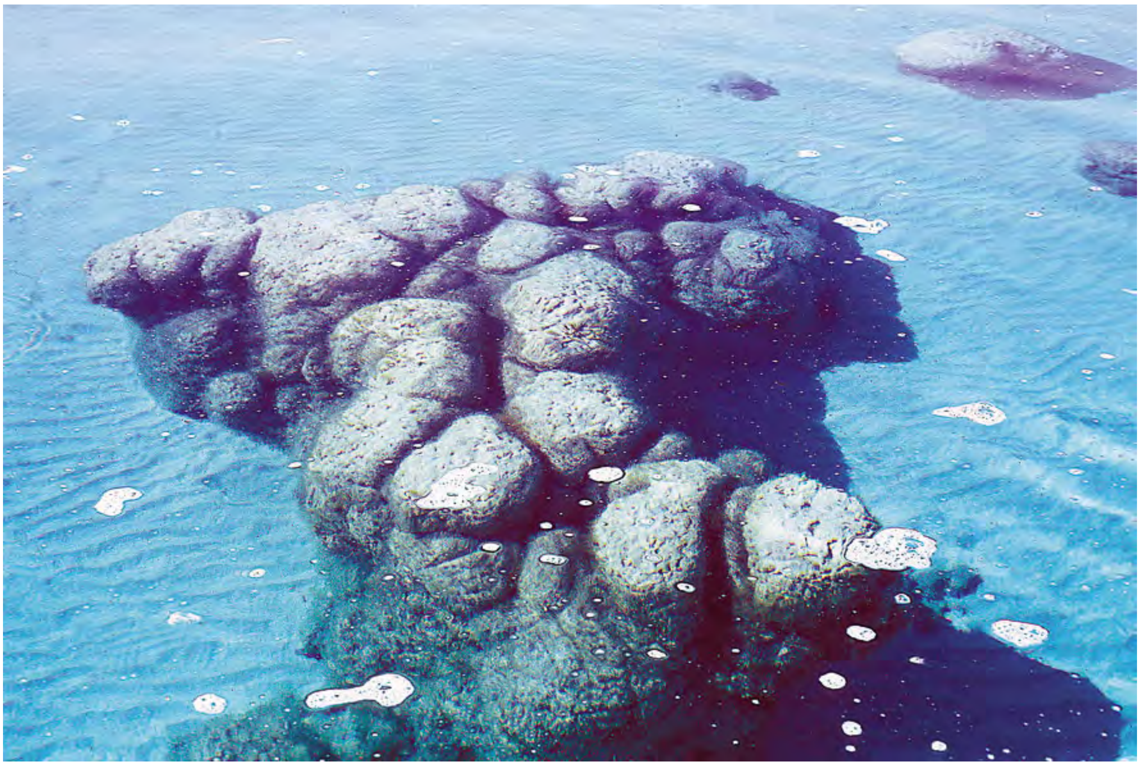

Figure 315. View from above the water of a composite stromatolite off Carbla Point, in water up to about 2 m deep. This stromatolite, about 1 m long, consists of conjoined columnar stromatolites. Green algae are attached to the lower parts of the structure, which is surrounded by ripple-marked ooid sand.

Figure 316. **U-shaped composite stromatolite, about 1.5 m long, in water about 2 m deep, off Carbla Point. Note that green algae are attached to parts of the structure.**

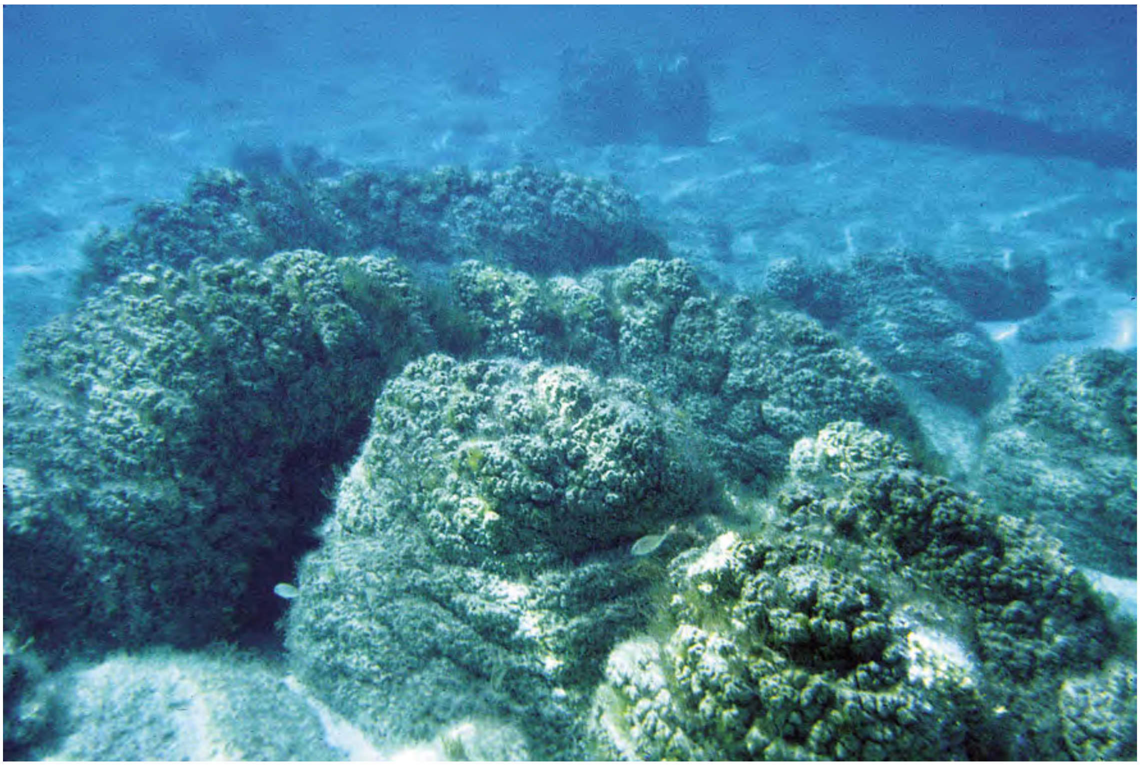

Figure 317. **Composite stromatolites, about 30 cm high, with distinctive 'knobbly' surfaces and attached green algae, in water about 2.5 m deep off Carbla Point.**

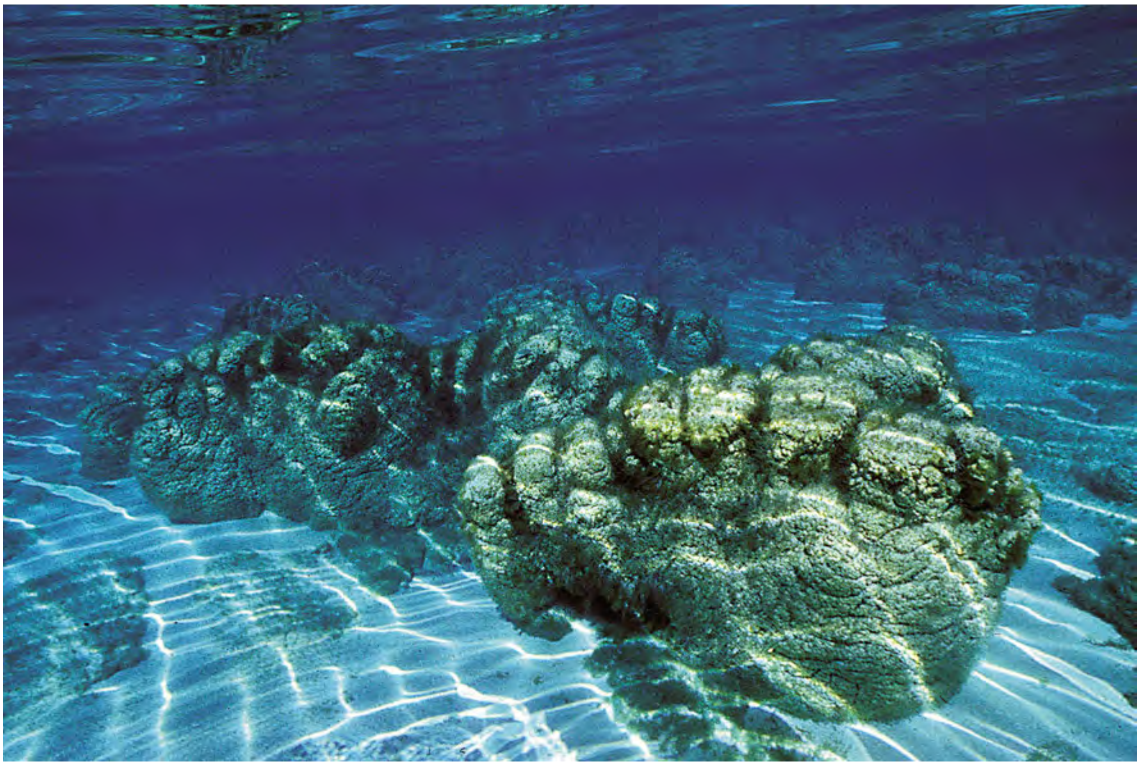

Figure 318. Composite stromatolites, up to about 40 cm high, in water about 2 m deep, off Carbla Point. They are partly encrusted by green algae, and may be dead or dormant.

Figure 319. Composite stromatolites, up to about 40 cm high, in water about 2.5 m deep, off Carbla Point. Note the knobbly surfaces of the stromatolites, a small shoal of fish, and green algae growing on the hard stromatolite surfaces.

Figure 320. Composite stromatolites, about 20 cm high, in water about 2.5 m deep, off Carbla Point. Their hard 'knobbly' surfaces are largely overgrown by green algae.

Figure 321. A shoal of small fish swimming beside composite stromatolites, about 40 cm high, in water about 2.5 m deep, off Carbla Point. The stromatolites are dead or dormant and firm to the touch.

Figure 322. Ripple-marked ooid sand off Carbla Point, with a few patches of colloform-mat stromatolites, in water about 1.5 m deep. The ripples have wavelengths of about 20 cm.

Figure 323. Juvenile fish, each about 5 cm long, between pustular-mat stromatolites at Carbla Point.

Figure 324. A medusa, *Phyllorhiza pacifica*, about 12 cm across, swimming above longitudinal stromatolites, in water about 3 m deep, off Carbla Point. Note the 'knobbly' surfaces of the stromatolites, formed by colloform mat.

Figure 325. A medusa swimming above composite stromatolites off Carbla Point, in water about 2 m deep. The medusa, *Phyllorhiza pacifica*, has a diameter of about 10 cm.

Figure 326. A sea snake, about 1 m long, swimming above composite stromatolites, about 50 cm high, off Carbla Point.

Figure 327. A sea snake, about 1 m long, between pustular- and smooth-mat stromatolites, in the intertidal zone at Carbla Point.

Classification

Several nomenclature and classification systems have been used in describing the Shark Bay stromatolites. Early work (Logan 1961) applied the formal names *Collenia* and *Cryptozoon* to them, although the details of those Precambrian taxa were not well known and do not cover the variety of forms in Shark Bay. Later, Logan et al. (1964) adopted a descriptive classification for stromatolites, based on cross-sections, that could also be applied to some Precambrian and more recent forms. Starting with the basic hemispheroid shapes of some stromatolites they developed a classification of laterally linked hemispheroids (LLH) and vertically stacked hemispheroids (SH), together with a third variety, spheroidal structures (SS), to cover oncolites. This classification allowed for compound stromatolites combining LLH and SH forms, using arrows to show the transition from one growth form to another (e.g. SH→LLH), and could differentiate between microstructure and macrostructure by means of a fraction, with microstructure the denominator and macrostructure the numerator (e.g. LLH/LLH). This classification has not been generally adopted, although fractal geometry has been used by some to describe the cross-sectional form of stromatolites (Grotzinger and Rothman, 1996; Batchelor et al. 2005).

Most recent work has classified the Shark Bay stromatolites on the basis of the microbial-mat types. Nine varieties of microbial mat were identified around Hamelin Pool by Logan et al. (1974a), termed colloform, gelatinous, smooth, pincushion, tufted, pustular, film, reticulate, and blister mats. Seven of these were recognized by Hoffman (1976) — he did not recognize reticulate and pincushion mats.

The following account of stromatolites built by some of these mats is largely based on the work of Playford and Cockbain (1976), Playford (1980a, 1990), Bauld (1984), Golubic (1985), Skyring and Bauld (1990), Reid et al. (2003), and Jahnert and Collins (2011, 2012). Each type of mat has a characteristic assemblage of one or more species of cyanobacteria, accompanied by diatoms in subtidal mats. The different mats occupy zones parallel to the shoreline, controlled mainly by their positions within the tidal range.

Three major types of mat (pustular, smooth, and colloform) build columnar and mound-shaped stromatolites at Hamelin Pool (Fig. 280; Bauld, 1984; Golubic, 1985; Skyring and Bauld, 1990; Playford, 1990; and Reid et al., 2003). Each type of stromatolite has a characteristic assemblage of one or more species of cyanobacteria, accompanied in colloform mats by diatoms. Little is known about the biology of what are here termed composite stromatolites, typified by examples at Carbla Point, but it seems clear that microbial precipitation was primarily responsible for their construction.

Jahnert and Collins (2011, 2012) recognized a fourth, deeper-water, type of subtidal stromatolite, for which they coined the term 'cerebroid' stromatolite. Here we refer to most of those forms as composite stromatolites. Some may be described as partly 'cerebroid' in appearance (resembling a brain), but others are not, and we deduce that most 'cerebroid' stromatolites have been formed by colloform mat.

Pustular mat (mamillate mat of Golubic, 1985) has formed stromatolite columns in the intertidal zone (Figs 273, 302–304), where they are commonly club shaped and as much as 1 m wide and 40 cm high. The mat is formed by the coccoid cyanobacterium *Entophysalis major*. This species may be a descendent of the Archean stromatolite-building microbe *Eoentophysalis*, which grew more than 3 billion years ago. That must represent one of the longest biological lineages known in the geological record (Golubic, 1983). Goh et al. (2006) and Burns et al. (2009) have emphasized the importance of studying modern analogues of Precambrian stromatolites, such as those at Hamelin Pool, in seeking to understand the early history of life on Earth. More recently, Flannery and Walter (2011) have described tufted mats, comparable with those now growing at Hamelin Pool, in Archean rocks up to 2.9 billion years old.

In places that are subject to active wave action, pustular-mat stromatolites are commonly wholly or partly surfaced by what seems to be a different type of mat, here referred to as 'knobbly mat' (Figs 290–292). It is described by Reid et al. (2003) as forming massive micrite in the lower parts of the supratidal zone. The upper surfaces of stromatolites built by pustular mat are often covered by film mat (Reid et al. 2003).

Smooth mats build stromatolite columns and mounds, commonly relatively small, in the lower intertidal and shallow-subtidal environments (Figs 306–308). Smooth mats may also colonize the tops of colloform-mat stromatolites, where they grow upward from the subtidal into the intertidal zone. Many stromatolites are built by a consortium of smooth and pustular mats (Fig. 307).

The principal agent of stromatolite growth in smooth mats is the filamentous cyanobacterium *Microcoleous chthonoplastes*, although *Schizothryx* sp. and various flexibacteria form minor parts of the assemblage (Bauld, 1984; Golubic, 1985).

Colloform mats form stromatolite mounds and columns up to about 0.7 m high, growing in shallow- to deep-subtidal environments, as much as 4 m deep (Figs 309–311; Playford 1980a; Walter and Bauld, 1986). The microbial assemblage consists of several types of cyanobacteria together with a diverse diatom flora. The siliceous diatoms include some stalked forms, whose role in colloform-mat construction may be significant. The stromatolites are cemented by microbial precipitation of micrite, which is also interpreted to have played a major role in growth of the stromatolites.

Composite stromatolites are large structures, up to about 1 m high and 3 m across, that have grown in water up to about 3.5 m deep. They are formed by the aggregation of adjoining columnar stromatolite heads, and are seen best beside Carbla Point (Figs 312–321), a locality where intertidal pustular-mat stromatolites, shallow-subtidal to intertidal smooth-mat stromatolites, and subtidal colloform-mat stromatolites, are also well represented.

Macroalgae, especially the green alga *Acetabularia* (Figs 309, 310, 313–321), together with worm tubes and various other fauna, are commonly attached to lithified surfaces of colloform-mat and composite stromatolites. The margins of those stromatolites have also commonly been drilled by bivalves. Ripple-marked ooid or pelloidal sand commonly occurs around stromatolites (Fig. 322).

Hamelin Pool supports large numbers of some fish (Figs 321, 323), but there are fewer species than in the open marine part of Shark Bay. The medusa *Phyllorhiza pacifica* (Figs 324, 325) is common, as are sea snakes (Figs 326, 327).

The heliotropism claimed by Awramik and Vanyo (1986) to be developed in columnar stromatolites at Carbla Point has not been verified through our observations.

Among the Hamelin Pool stromatolites, subtidal colloform-mat forms contain the most diverse microbial floras and associated biota, presumably because they remain permanently, or almost permanently, submerged, under relatively constant salinities. The least diverse biotas are in intertidal pustular-mat stromatolites, which are frequently exposed and subject to partial desiccation for prolonged periods, sometimes many days.

The Hamelin Pool stromatolites have grown by a process of accretion. This is accomplished in intertidal to shallow-subtidal pustular-mat forms by the trapping and binding of limesand and mud by a network of filamentous microbes, followed by the microbial precipitation of calcium-carbonate cement, forming what are termed ‘calcarenite stromatolites’ by Reid et al. (2003). The shallow-subtidal to intertidal smooth-mat stromatolites have formed by a combination of precipitation and sediment trapping and binding by microbes. Colloform-mat stromatolites in subtidal environments have lithified largely by the microbial precipitation of calcium carbonate, with lesser trapping and binding of sediments. In deep-subtidal composite stromatolites it seems that lime precipitation by microbes is the dominant growth mechanism, resulting in micritic stromatolites.

Despite recent advances in knowledge of the Hamelin Pool stromatolites, especially through the work of Reid et al. (2003) and Jahnert and Collins (2011, 2012), there remains a need for more research to focus on the stromatolite-building organisms and processes. Much remains to be learned about the growth mechanisms, depth ranges, and organisms responsible for these stromatolites. Many of these issues are expected to be clarified through a joint project of the University of Miami and GSWA, led by Professor Pamela Reid, that is currently in progress.

Morphology

Logan (1961) considered that the morphologies of Hamelin Pool stromatolites are governed by environmental factors, and later work has shown that organic factors are also involved. The type of microbial mat that builds a stromatolite partly controls its morphology (Playford, 1980a, 1990; Reid et al., 2003; Jahnert and Collins, 2011, 2012).

Megascopic examples of internal features of Hamelin Pool stromatolites are well displayed in slabbed specimens. Intertidal stromatolites built by *Entophysalis major* are generally unlaminated or weakly laminated (Figs 328, 329), whereas smooth- and colloform-mat stromatolites have better-defined lamination (Figs 330–336). The best-developed lamination is found in lithified smooth-mat stromatolites, which also have smaller fenestrae and smoother external characteristics. For some reason, not yet understood, the lamination in some smooth-mat stromatolites has been partly destroyed (Fig. 334). Colloform-mat stromatolites are commonly laminated, with coarse fenestrae and smooth to irregular external surfaces (Fig. 336). Many stromatolites have been built by more than one type of mat.

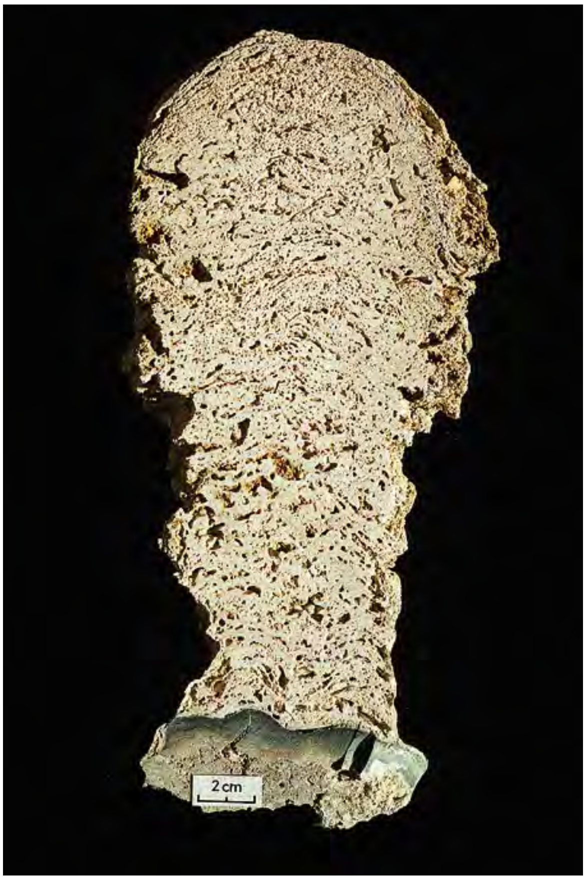

Figure 328. Section through a club-shaped pustular-mat stromatolite (intertidal) that grew on a chert hardground beside Flagpole Landing.

Figure 329. Section through a columnar stromatolite, formed in its upper part, by pustular mat, and probably by smooth mat in its lower part, from the intertidal zone at Flagpole Landing. It is unlaminated in the upper part and coarsely laminated, with large fenestrae, in the lower part.

Figure 331. Section through a club-shaped subtidal stromatolite from Flagpole Landing, laminated in the lower half (formed by smooth mat), and unlaminated in the upper half (formed by pustular mat). Note the deep indentations on the sides of the specimen, perhaps made by boring bivalves.

Figure 330. Section through a club-shaped stromatolite formed by smooth mat in the subtidal zone beside Flagpole Landing. Note the lamination and small fenestrae.

Figure 332. Section through a small columnar stromatolite formed by smooth mat, from 2.8 km southwest of Flagpole Landing, showing lamination and small to medium-sized fenestrae.

Figure 333. Section obtained by breaking open an unlithified smooth-mat stromatolite, from 2.8 km southwest of Flagpole Landing. Note the uncemented, dark-coloured, laminated, lime mud in the core, and light-coloured, unlaminated, lime mud on the exterior.

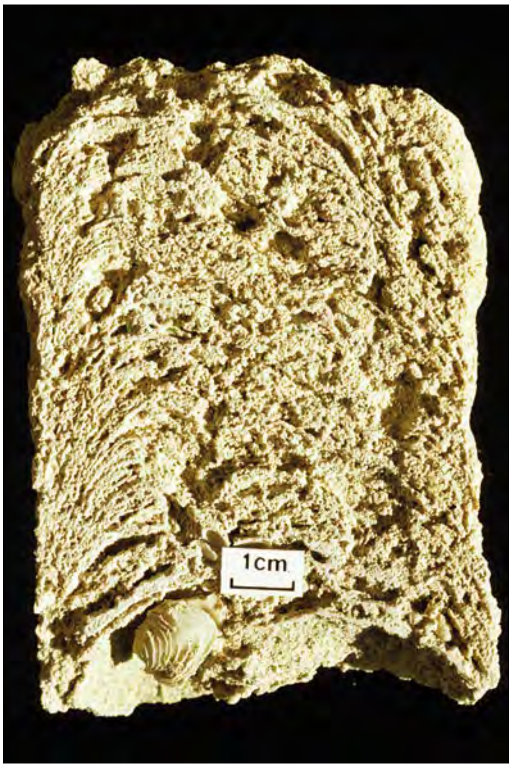

Figure 334. Section cut through a weakly lithified intertidal smooth-mat stromatolite, finely laminated on its sides, and unlaminated in the middle, from 2.8 km southwest of Flagpole Landing. A boring bivalve is embedded within the lower part of the stromatolite.

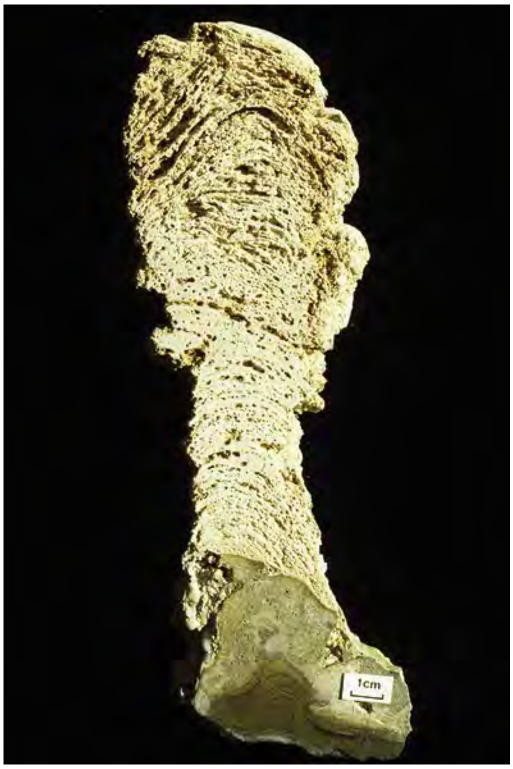

Figure 335. Section through a subtidal, well-lithified, smooth-mat stromatolite, from water about 1 m deep at Flagpole Landing, showing well-developed lamination and fenestrae, and the pebble of calcrete on which it grew.

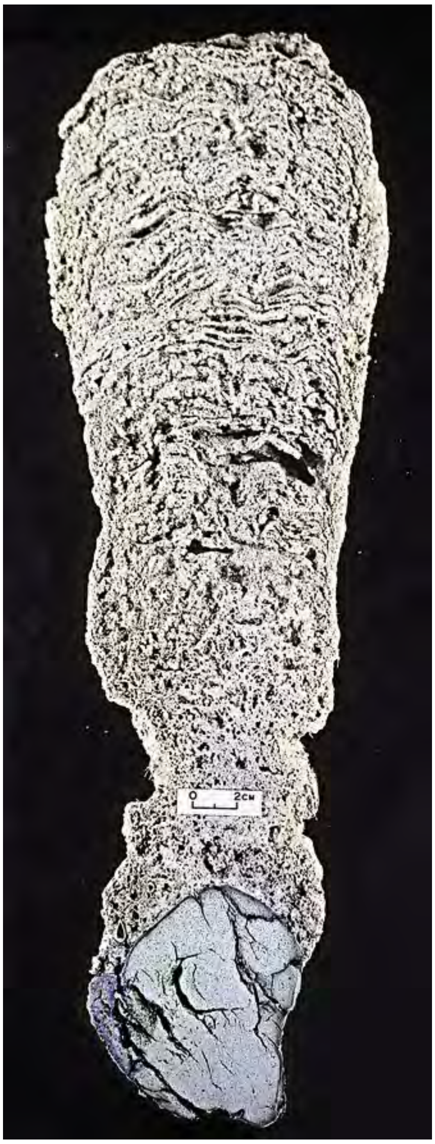

Figure 336. Section through a club-shaped columnar stromatolite built by colloform mat, 2.8 km southwest of Flagpole Landing, 190 m offshore, in water about 1 m deep. It shows well-developed lamination and small- to medium-sized fenestrae, and has grown on a pebble of calcretized Cretaceous chalk (Toolonga Calcilutite).

The intertidal stromatolites and some subtidal forms have grown partly by microbial trapping and binding of calcareous sediment. Lamination has resulted from the precipitation of calcium carbonate by cyanobacteria, forming thin laminae. Fenestrae are thought to have formed by the decay of organic matter. Figure 333 shows that some smooth-mat stromatolites, or parts of those stromatolites, are unlithified and have laminae of anoxic black mud in their centres. The processes involved in growth and lithification of such stromatolites have yet to be determined.

The largest composite subtidal stromatolites are in deeper-water environments at Carbla Point, forming mounds up to about 1 m high and 3 m across (Figs 312–321). These composite stromatolites have formed by the aggregation of adjoining columnar forms (well shown in Figs 315, 316). The sides of colloform stromatolites and many composite stromatolites are coated with fronds of the green alga *Acetabularia* (Figs 309, 310, 313–320).

The principal environmental controls on stromatolite morphology are (a) the direction of wave translation, (b) the prevailing wind direction, and (c) the nature of the substrate (Figs 337, 338; Playford, 1980a).

Stromatolites at Hamelin Pool are commonly elongate in the direction of wave translation (Figs 339, 340), apparently mainly as a result of the scouring action of waves impacting on the living mats. The resulting elongate forms are termed longitudinal stromatolites.

Inclined stromatolites some 1.1 km south of Carbla Point form rows oriented in the direction of wave translation, but with individual stromatolites inclined to the south in response to the prevailing southerly winds (Figs 341–344; Playford, 1980a). This inclination has resulted from the accretion of limesand particles on the south sides of the inclined stromatolites, blown there by the prevailing southerly winds. The stromatolites show fine lamination on their tops and north (downwind) sides and are unlaminated on their south (upwind) sides (Fig. 344).

The prevailing wind direction over most of the Shark Bay area is from the south and south-southwest, as shown by records at Carnarvon and Hamelin Pool (Fig. 28) and personal observations at Denham, Tamala, and Dirk Hartog Island. The winds are particularly strong and persistent during summer. However, the records from the Hamelin Pool weather station (which is no longer operating) showed that winds there are not as strong and are more variable than in other parts of the Shark Bay area, and the prevailing wind direction there is southeast to south (Fig. 28). This is probably because the weather station was situated near the southeast end of Hamelin Pool, where it was subject to more land-influenced atmospheric circulation than other parts of the Shark Bay area.

Playford (1980a) invoked wind-induced paired helical vortices (Langmuir circulation) to explain what he termed seif stromatolites (Figs 337, 338). These are built by pustular mat and occur along the west side of Hamelin Pool, especially near Booldah Well (Figs 345–354). They form elongate flat-topped ridges 1–3 m wide and about 0.3 m high, separated by bare sandy areas, about 3–8 m wide. These stromatolites extend up to 800 m offshore, in intertidal to shallow-subtidal areas. The seif-stromatolite ridges are subparallel, and their elongation is nearly north–south, parallel to the prevailing wind. They show some 'tuning-fork' junctions, opening to the south (i.e. upwind; Figs 345–348).

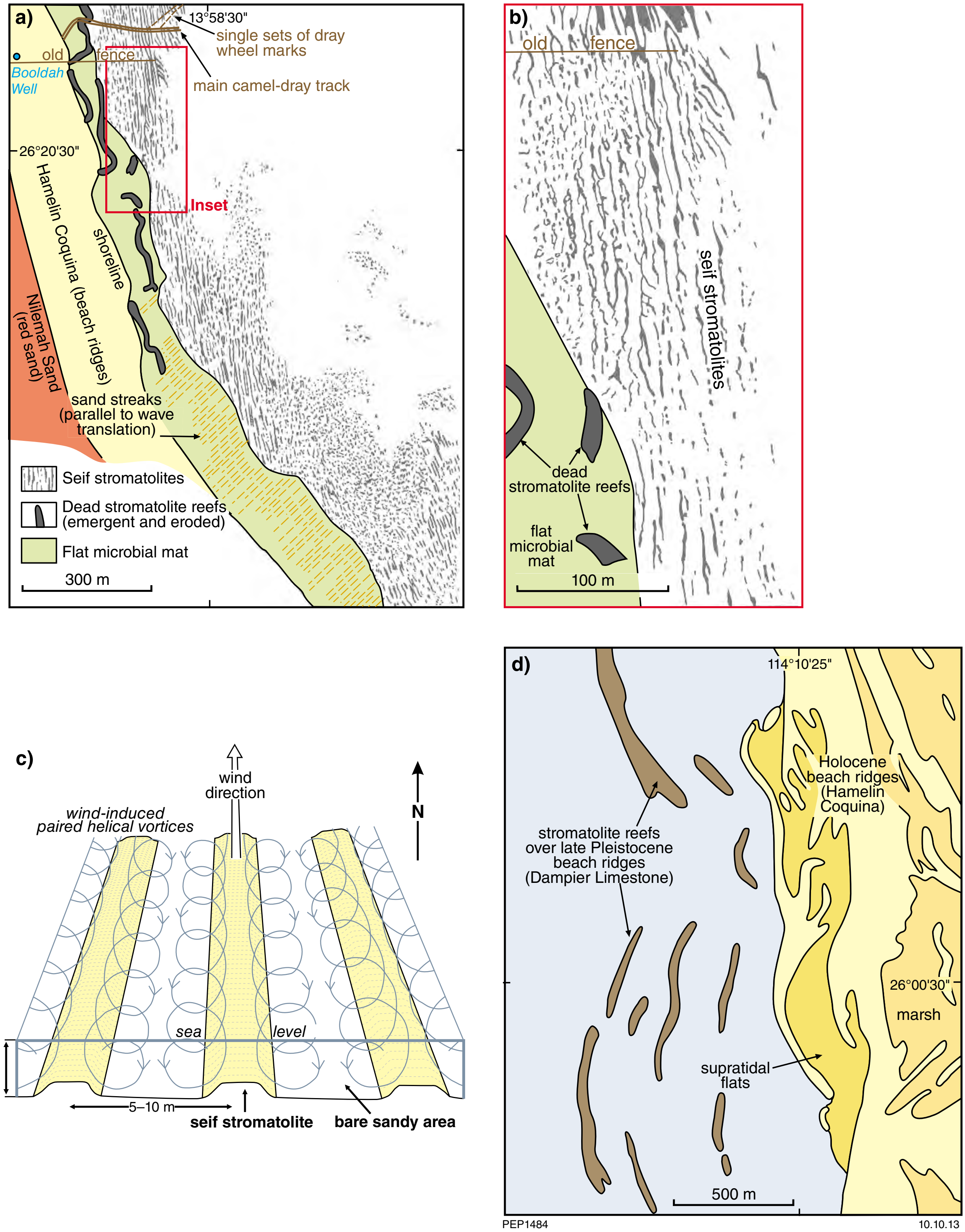

Figure 337. **Some environmental controls on the growth of stromatolites in Hamelin Pool, with (a), (b), and (c) illustrating seif stromatolites, the growth of which are controlled by strong prevailing southerly winds inducing paired helical vortices (Langmuir circulation) in the shallow water over the stromatolites, and (d) showing a map of the area 10 km north-northeast of Yaringa Point where stromatolite reefs are localized by late Pleistocene (Bibra Limestone) beach ridges (after Playford, 1980a).**

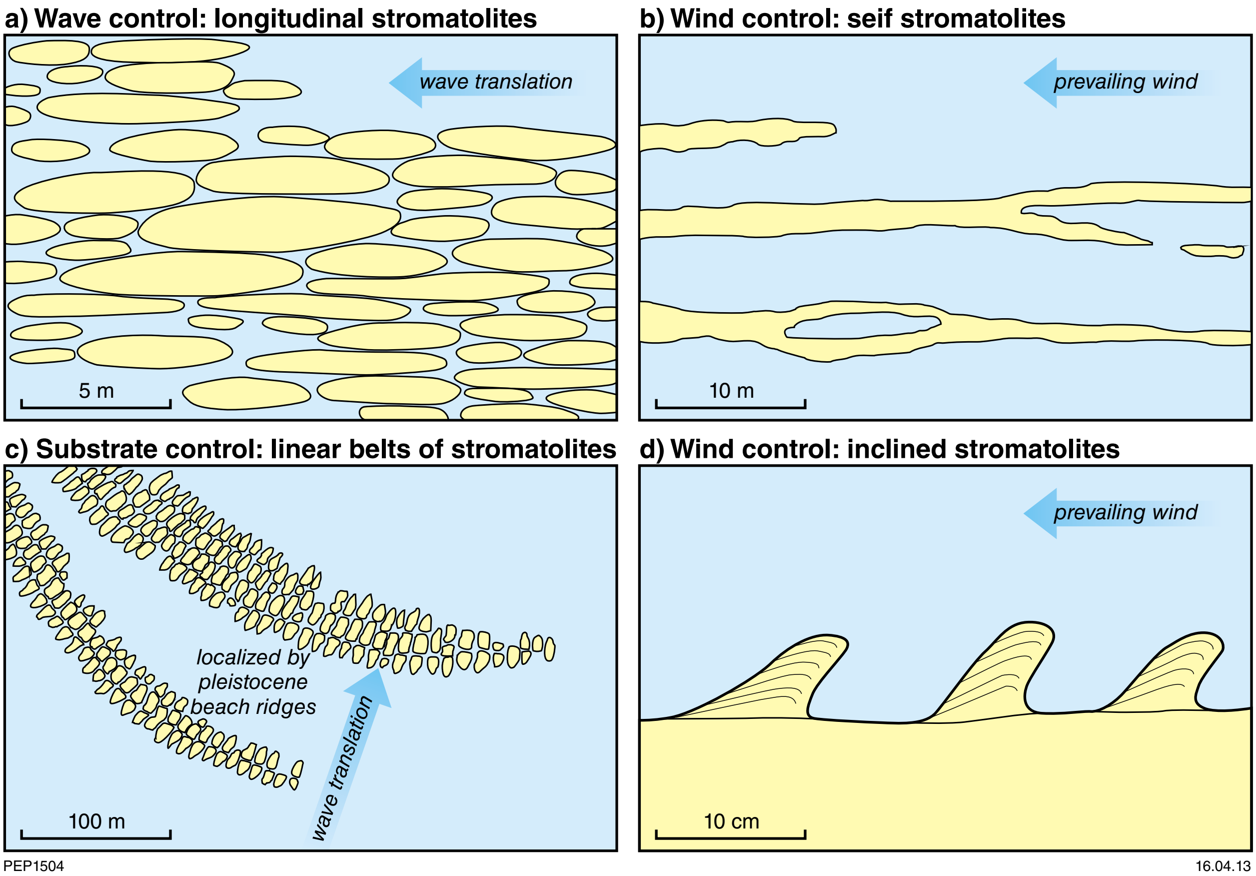

Figure 338. Some environmental controls on the growth of stromatolites in Hamelin Pool: (a) the wave-translation direction (longitudinal stromatolites), (b) the prevailing wind direction (seif stromatolites), (c) the nature of the substrate (Pleistocene beach ridges) combined with the wave-translation direction, and (d) the prevailing wind direction (inclined stromatolites).

Figure 339. Longitudinal stromatolites, up to about 3 m long, built by pustular mat in the intertidal zone near Carbla Point. The stromatolites are elongate in the direction of wave translation. Compare this with the Proterozoic forms shown in Figure 301.

Figure 340. Longitudinal stromatolites, built by pustular mat in the intertidal zone south of Carbla Point. The stromatolites are elongate in the direction of wave translation. These longitudinal stromatolites are each about 15–20 cm wide and up to several metres long.

Figure 341. Lines of inclined stromatolites south of Carbla Point, looking north. The stromatolites form rows of small columns parallel to the direction of wave translation, with the columns themselves inclined to the south, towards the prevailing southerly winds.

Figure 342. Inclined stromatolites south of Carbla Point, looking east, showing small stromatolite columns, inclined to the south, towards the prevailing southerly winds.

Figure 343. Closer view of inclined stromatolites south of Carbla Point, built by intertidal pustular and smooth mats, inclined towards the south, and surrounded by ripple-marked ooid sand.

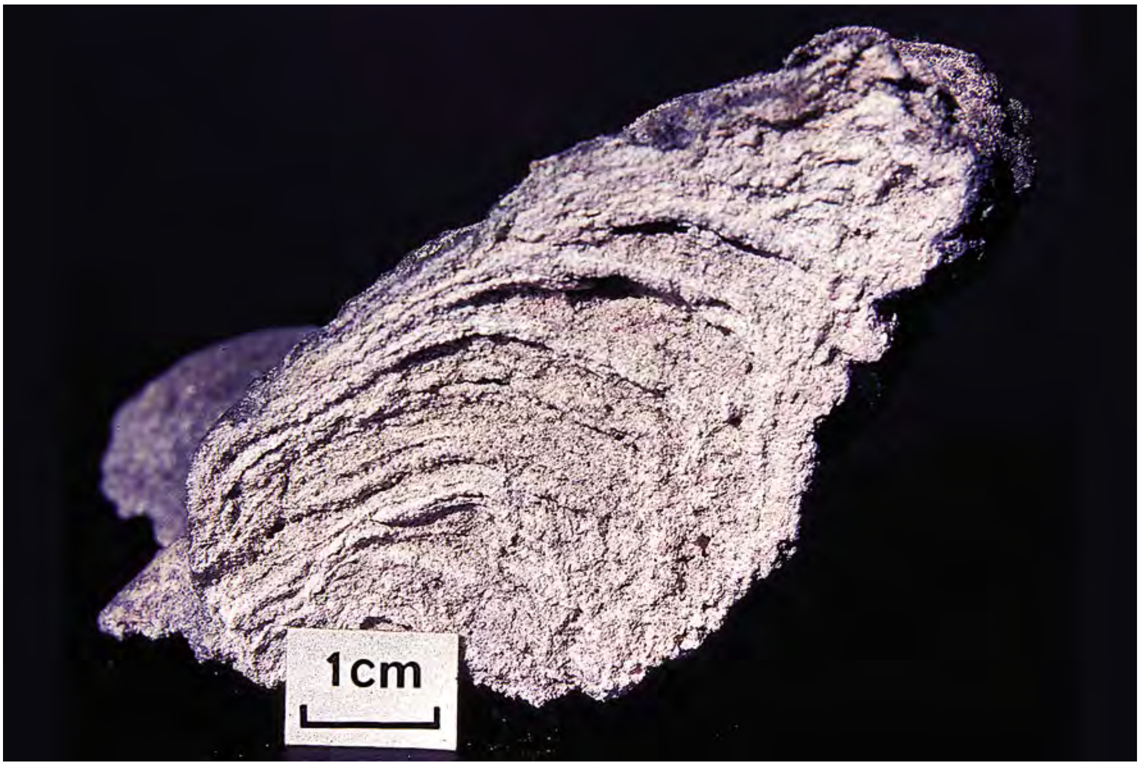

Figure 344. Section through an inclined stromatolite south of Carbla Point, unlaminated on the right (south, upwind) side and with well-developed lamination on the top and the left (north, downwind) side.

Figure 345. Aerial view looking south near Booldah Well showing seif stromatolites oriented parallel to the prevailing southerly wind, with older stromatolite reefs (now dead) forming ridges adjoining the beach. Note the path cut through the seif stromatolites by camel-drawn drays, and places on the north side of that path where single sets of wheel tracks cut through the seif stromatolites. Note also the line of ooid sand east of the main part of the dray path, and the extension of that path into deeper water east of the ooid sand.

Figure 346. Aerial view looking south near Booldah Well, showing a broader view than in Figure 345. A mild southerly wind was blowing, developing weak wind rows in the deeper water.

Figure 347. Aerial view looking east near Booldah Well, showing seif stromatolites, with Y-junctions opening to the south, towards the prevailing wind. The main camel-drawn-dray track has several single sets of tracks branching to the left of the main track. Older, indurated, dark-coloured stromatolite reefs adjoin the beach.

Figure 348. Aerial view looking east near Booldah Well (in the right foreground, to the right of a small quarry in Hamelin Coquina). The photo shows seif stromatolites, older indurated stromatolite reefs, broad, indurated flat microbial mat behind the reefs, the main dray path through the stromatolites, and a series of dark tracks cut by camel-drawn drays on the flat, indurated, microbial-mat deposits.

Figure 349. Photo taken from the main camel-dray path, showing the wheel marks left when a dray was once pulled through the adjoining seif stromatolites about 80 years ago.

Figure 350. Vertical aerial view of seif stromatolites, oblique to the shoreline, about 1 km south of Booldah Well. Older dark-coloured stromatolite reefs are near the beach. The modern vehicle track in the left foreground is about 2 m wide. Airphoto courtesy of Landgate, Western Australia.

Figure 351. Seif stromatolite ridges at low tide near Booldah Well.

Figure 352. Seif stromatolite ridges at low tide near Booldah Well, behind an older, indurated and eroded stromatolite reef (foreground), which grew on light-coloured Pleistocene limestone.

Figure 353. Seif stromatolites near Booldah Well, partly exposed, behind columnar pustular-mat stromatolites, and with some flat microbial mat beside the beach.

Figure 354. Aerial view of living seif stromatolites (left foreground) near Booldah Well, in front of linear dark-coloured stromatolite reefs (largely dead), and dead seif stromatolites forming narrow bands behind the reef, surrounded by indurated flat microbial mat. White and light-coloured Hamelin Coquina forms a wide belt behind the shoreline, with red dune sand in the upper right.

A track, some 450 m long, was cut through the seif stromatolites beside Booldah Well, about 100 years ago, on the west side of Hamelin Pool, for the use of camel-drawn drays (Figs 345–349). These were used until the mid-1930s to load wool and sandalwood from Nanga and Nilemah Stations onto dinghies, and from there onto lighters, the largest of which was the *Will Succeed* (M Hoult, 1956, pers. comm.). Another track cut through stromatolites for camel-drawn drays carrying wool bales from Hamelin Station can be seen at Flagpole Landing (Figs 277–279).

Near Booldah Well the lighters were anchored in deeper water, beyond the belt of seif stromatolites. However, although that track has not been used by drays for about the past 80 years, there has been little or no subsequent regrowth of stromatolites over the track. Furthermore, single sets of wheel marks deviating from the main track are still clearly seen cutting through the stromatolite ridges and adjoining flat microbial mats (Figs 345–349).

Tracks left by the camel-drawn drays are also remarkably well preserved where they cross indurated flat microbial mats near Booldah Well (Fig. 355) and soft living mat on the west side of the Nilemah Embayment (Figs 356, 357). The dray tracks and camel footprints in the indurated mat near Booldah Well are commonly filled with pustular mat. These tracks appear almost as clearly defined today as when they were formed, some 80 years ago.

The endurance of these very old tracks illustrates the fragility of the stromatolites and microbial mats, and their very slow growth rates. That also raises the question of whether conditions for microbial growth were more favourable in the past than they are today.

The seif stromatolites near Booldah Well are younger than the dead emergent stromatolite reefs that extend discontinuously along the shoreline in that area (Fig. 347). The narrow stromatolite reef shown in Figure 354 may be younger than the dead seif stromatolites behind the reef at that locality, but older than the living seif stromatolites in the left foreground.

The presence of Langmuir circulation explains the development of seif sand dunes, such as those in the Great Sandy Desert (Fig. 358; Crowe, 1975) and on Edel Land Peninsula (Figs 38–41). Langmuir circulation prevails in the water of Hamelin Pool when strong southerly winds are blowing, as can be seen clearly from the air (Figs 359–362). This circulation forms regular lines of white spume (wind rows) on the water surface, where descending helical vortices of water meet, and by lines of soft sediments (probably fragments of sea grass) piled into lines on the sea floor by the ascending vortices (Figs 361, 362).

Figure 355. Tracks made by a camel-drawn dray, about 80 years ago, on flat microbial-mat limestone near Booldah Well. The imprints of the camel hooves are visible between the tracks of the wheels.

Figure 356. Track made by a camel-drawn dray about 80 years ago on living microbial mat on the west side of the Nilemah Embayment. The middle track was made by hooves of the camels pulling the dray, and the two outer tracks were made by the wheels.

Figure 357. The camel-drawn dray that made the track shown in Figure 356. Photo taken at Nilemah Homestead in the early 1930s. Photo courtesy of John and Eric Lawson.

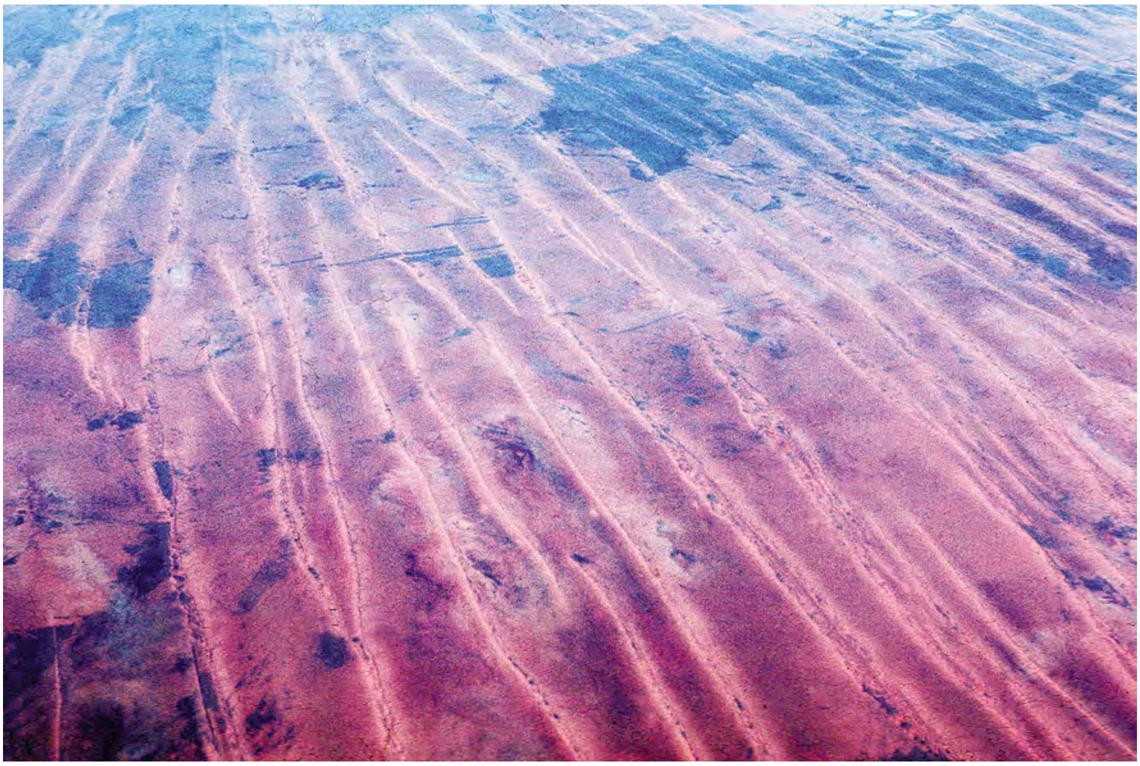

Figure 358. Red seif dunes, stabilized by spinifex, in the Great Sandy Desert, formed by strong easterly winds during the last Pleistocene ice age, when the climate was much more arid than it is today.

Figure 359. Aerial view of wind rows (lines of white spume), trending north–south, on the water surface of Hamelin Pool beside Carbla Point. The rows resulted from paired helical vortices in the water (Langmuir circulation), caused by a consistently strong southerly wind.

Figure 360. Aerial view of wind rows, trending north–south, along the east coast of Hamelin Pool, south of Kopke Point. Note the Y-junctions in the spume, opening to the south (upwind).

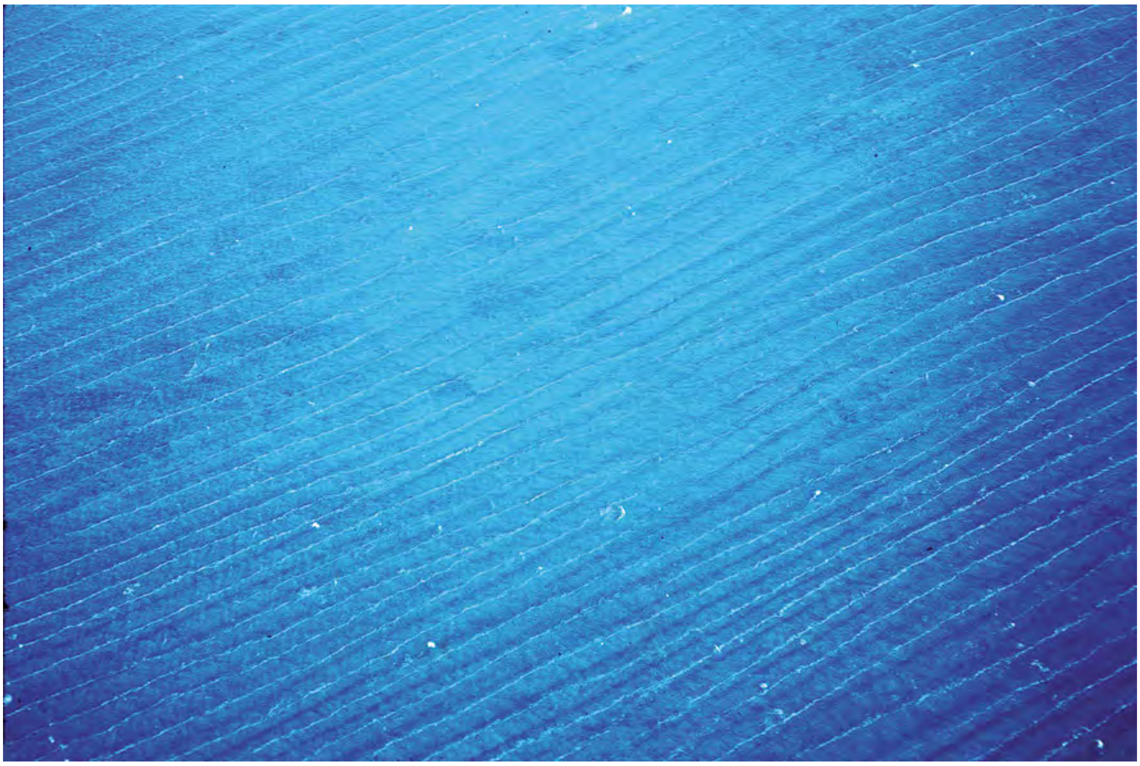

Figure 361. Near-vertical aerial view of wind rows, trending north–south, in the central part of Hamelin Pool. Note the dark lines of sediment on the sea floor (probably seagrass debris), piled up by ascending paired helical vortices in the water, induced by the strong, consistent, southerly wind.

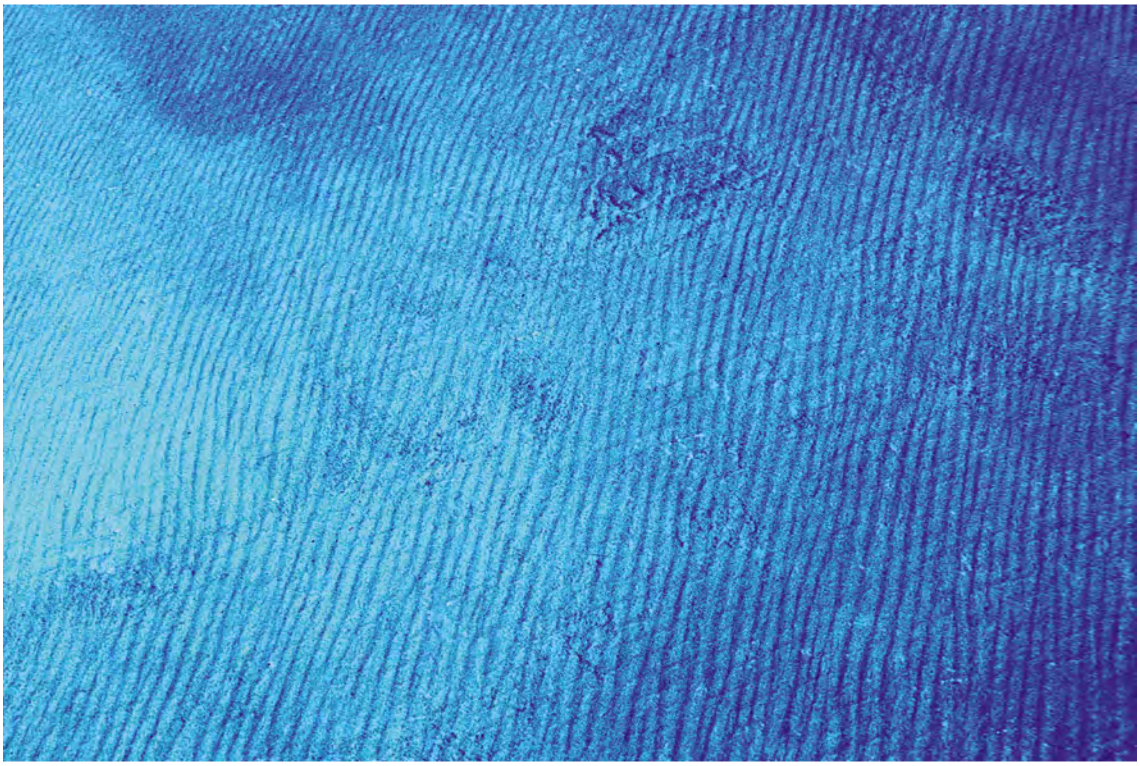

Figure 362. Near-vertical aerial view of the central part of Hamelin Pool, taken after the wind had dropped, showing north–south dark lines of sediment on the sea floor, that had been piled up there by ascending paired helical vortices in the water when the wind was blowing strongly and consistently from the south (top).

The nature of the substrate is another important factor controlling the development of stromatolites at Hamelin Pool. Stromatolites generally require a hard substrate, especially one with an irregular surface, on which to grow. This substrate variously consists of karst pipes in Cretaceous chalk (Figs 363–365), hardgrounds, pebbles, and cobbles (Figs 328, 335, 336), indurated late Pleistocene beach ridges (Figs 338c, 368–372), Dampier Limestone, Carbla Oolite Member, Miocene quartzite (Lamont Sandstone), and subtidal hardgrounds.

Stromatolites are generally better developed around headlands than bays, because the headlands are localized by rocky outcrops forming suitable substrates on which stromatolites can grow (Figs 373–386). Headlands on the east side of Hamelin Pool, with associated stromatolites, are localized by outcrops of silicified Miocene sandstone (Lamont Sandstone), oolite (Carbla Oolite Member), indurated Pleistocene beach ridges, and calcretized Cretaceous Toolonga Calcilutite. Curvilinear stromatolite reefs, often subparallel to the modern shorelines, are conspicuous features of many intertidal and subtidal areas (Figs 366–382). Some have been developed over Pleistocene beach ridges (Figs 369–372) that may consist of many parallel lines of stromatolites, in some cases meeting at angles forming major 'cross-bedding' (Figs 368–369). Pleistocene beach ridges forming linear features in the present tidal zone acted as foundations for the growth of stromatolites.

Another form of substrate control on stromatolite morphology is seen in the domal stromatolites that grew over calcrete-rimmed karst pipes in the Cretaceous Toolonga Calcilutite (Figs 363–365). Those pipes are interpreted to have developed around the tap roots of large trees that grew there during a wetter climate. They extend for several metres below the calcretized Pleistocene land surface and are now filled with cemented calcareous soil, rimmed by strongly indurated calcrete that is itself surrounded by softer, partly calcretized, chalky calcilutite. Consequently, where the Toolonga Calcilutite is truncated on tidal flats by marine erosion, the karst pipes have differentially eroded out as circular features (Fig. 365). Those features have been overgrown in some places by stromatolite-building microbial mats, forming large domal stromatolites (Fig. 363). These domal stromatolites are best displayed in the supratidal zone at Flagpole Landing, where they are now being actively eroded.

Over wide subtidal areas of Hamelin Pool, at depths of 2–6 m, there are hard pavements (hardgrounds), that are broken up in some areas. They apparently formed by a process of microbial aragonite cementation of sand on the sea floor (Figs 387–389). Stromatolites have grown on some of the broken pavements (Fig. 387).

Flat microbial mats (Fig. 305, 390–393) are best developed in bays between headlands, where there are no suitable rocky substrates to serve as foundations for stromatolite growth. The most common of these flat forms are pustular mats, built by *Entophysalis major*, and laminated forms built by smooth mat (Fig. 393). They also include additional forms listed by Logan et al. (1974a) and Hoffman (1976), including tufted mats (Figs 391, 392) that resemble forms known from Archean rocks up to 2.9 billion years old (Flannery and Walter, 2011).

Mats in the upper intertidal to supratidal zones apparently expand as they dry out, probably as a result of the precipitation of gypsum, folding the mats into low undulating ridges, which may be subparallel, polygonal, or wrinkled (Figs 394–398). Where a mat has formed an indurated crust, it may similarly expand, giving rise to miniature 'thrust faults' (Figs 396, 399). The compression that resulted in these folds was in some cases followed by contraction, resulting in tensional fracturing and sliding apart of the folded mats (Fig. 398). Experimental work is needed to obtain an understanding of the processes involved.

From the above it can be concluded that the various morphologies of stromatolites at Hamelin Pool, and their distribution in the intertidal and subtidal zones, are largely controlled by environmental factors. However, their morphologies are also partly controlled by the microbes that build them. Intertidal stromatolites, and some subtidal forms, have formed in part by the trapping and binding by microbes of sedimentary grains, and cementation by microbially precipitated micrite. However, some subtidal stromatolites have formed by microbial precipitation alone, without any significant trapping and binding of sedimentary grains (Reid et al., 2003). Living stromatolites extend from the intertidal zone to depths of about 4 m on the subtidal pavements, and their external morphologies and trends have largely been controlled by the direction of wave translation, the prevailing wind direction, and the nature of the substrate.

Growth rates

The growth rates of living stromatolites were monitored over a period of 20 years, using non-corrosive nails as markers (Playford, 1980a, 1990). This method showed that the growth rates are extremely slow, with maximum average rates of less than 0.5 mm per year. Chivas et al. (1990), using radiocarbon and uranium-series methods, have determined that the growth rate of a Hamelin Pool stromatolite was less than 0.4 mm per year. More recently Jahnert and Collins (2012) recorded growth rates of between 0.05 and 3 mm per year, most being less than 0.5 mm per year.

Bauld et al. (1979) found that the highest primary productivity is in subtidal colloform mats, and the lowest in intertidal smooth mats. Many living stromatolites seem to be almost static, with growth balanced by erosion through wave action. In intertidal and shallow-subtidal environments several years of growth can be removed in a single storm. This was shown by monitoring the heads that had been marked with non-corrosive nails — which showed that in some years the tops of a few nails protruded above the stromatolite heads, because the surrounding mat had been removed by storm erosion. The most active stromatolites are probably among those that occupy deeper water environments, although they may still experience some erosion during storms. However, Cyclone Hazel (13 March 1979) caused little visible damage to living stromatolites, probably because the sea in the area rose to 2.8 m above mean sea level, protecting most stromatolites from significant erosion.

Figure 363. Domal stromatolite in the supratidal zone at Flagpole Landing. This has grown over a karst pipe in indurated chalk of the Cretaceous Toolonga Calcilutite.

Figure 364. Exposure at Flint Cliff of indurated Toolonga Calcilutite around a karst pipe rimmed by calcrete.

Figure 365. The top of a karst pipe on the shoreline at Flint Cliff, filled with red calcareous soil and surrounded by dark yellow indurated chalk.

Figure 366. Vertical airphoto, 1.5 km north-northeast of Flagpole Landing, showing planed-off beach ridges of Hamelin Coquina in the foreground and successive lines of stromatolite reefs, built by *Entophysalis* below the water. Note a very narrow band of ooid sand in the upper left of the photo. Airphoto courtesy of Landgate, Western Australia.

Figure 367. Vertical airphoto, about 11 km south-southeast of Kopke Point, showing beach ridges, speckled linear mounds of Hamelin Coquina, yellow marsh deposits, and successive lines of stromatolite reefs (in the upper half of the photo), thought to have grown over Pleistocene beach ridges. Airphoto courtesy of Landgate, Western Australia.

Figure 368. Vertical airphoto, about 10.5 km south-southeast of Kopke Point, showing curved lines of stromatolites, controlled by Pleistocene beach ridges, that are being progressively covered by Hamelin Coquina. Airphoto courtesy of Landgate, Western Australia.

Figure 369. Oblique airphoto, about 11 km south-southeast of Kopke Point, looking northwest, showing 'cross-bedding' in lines of stromatolites, controlled by underlying Pleistocene beach ridges

Figure 370. Oblique airphoto, about 11.5 km south-southeast of Kopke Point, looking east-northeast, showing successive bands of stromatolite reefs, apparently controlled by underlying Pleistocene beach ridges.

Figure 371. Lines of longitudinal stromatolites, built by pustular mat, about 11 km south-southeast of Kopke Point, looking south. Individual stromatolites are elongate in the direction of wave translation, and the lines are thought to be controlled by underlying Pleistocene beach ridges.

Figure 372. Longitudinal stromatolites built by pustular mat, partly dead, about 11 km south-southeast of Kopke Point, looking south. The stromatolites are elongate in the direction of wave translation.

Figure 373. Aerial view looking south along the east side of Hamelin Pool, showing headlands around which stromatolites have grown, and intervening bays where flat microbial mats largely prevail. Carbla Point is in the middle left of the photo, the third major headland from the base.

Figure 374. Aerial view of Carbla Point looking northeast, showing subtidal to supratidal stromatolite reefs. Note the waves of ooid sand that have moved over the stromatolites in the lower right. The field of view at the base is about 850 m wide.

Figure 375. Aerial view of Carbla Point looking west, showing supratidal to subtidal stromatolite reefs skirting the point, and irregular belts of longitudinal subtidal stromatolites in deeper water. The field of view at the base of the photo is about 950 m wide.

Figure 376. Aerial view looking southwest over Spaven Point, on the west side of Hamelin Pool, showing submerged lines of stromatolite reefs, white beaches built of *Fragum erugatum* shells, sparsely vegetated beach ridges, spits, and linear mounds of Hamelin Coquina, and vegetated dark-red dune sand of the Denham Sand.

Figure 377. Aerial view looking south over Spaven Point, on the west side of Hamelin Pool, showing lines of stromatolite reefs and a belt of Hamelin Coquina behind the white shell beach. Note waves breaking on the outermost reef, spits of *Fragum erugatum* coquina immediately south of the point, wind rows on the water surface in the lower left, and the cuspate nature of the shoreline in the middle distance.

Figure 378. Airphoto looking southeast over Point Sweenymia, on the east side of Hamelin Pool, showing supratidal to subtidal stromatolites and subtidal white ooid or pelloid sand.

Figure 379. Vertical airphoto of the Flagpole Landing area (north at the top), showing bands of stromatolite reefs, 'fingers' and bands of white ooid sand, and the type locality of the Hamelin Coquina. The red to orange ground on the right is underlain by calcrete over Cretaceous Toolonga Calcilutite, and the grey and orange area between there and the Hamelin Coquina is underlain by Pleistocene coquinite and claystone. Buildings of the old Flint Cliff Telegraph Station and post office are in the lower centre of the photo. The width of the field of view is 5.4 km. Airphoto courtesy of Landgate, Western Australia.

Figure 380. Aerial view of the Flagpole Landing area looking northwest. A succession of dark-coloured stromatolite reefs can be seen offshore, in front of cycles and linear mounds of Hamelin Coquina. Note the bands of ooid or pelloid sand in front of the stromatolite reefs. Flagpole Landing is at the end of the narrow track in the centre-left part of the photo. Buildings are those of the old Flint Cliff telegraph station and post office.

Figure 381. Aerial view about 4 km south of Yaringa Point, looking northeast, showing bands and clumps of subtidal, intertidal, and supratidal stromatolites, developed around a small headland.

Figure 382. Aerial view about 4 km south of Yaringa Point, looking south, showing bands of subtidal, intertidal, and supratidal stromatolites, best developed around the headland.

Figure 383. Aerial view looking southeast towards the Nilemah Embayment, showing deep dark-blue water with wind rows on the surface, light-blue and greenish subtidal limestone pavement (with some stromatolites), dark intertidal mats and stromatolites, white *Fragum* coquina at the shoreline, white to grey sparsely vegetated Hamelin Coquina with spits, and red sand dunes of the Nilemah Sand.

Figure 384. Aerial view of the Nilemah Embayment, looking west towards the southern part of Nanga Peninsula and L'Haridon Bight (right background), and part of Henri Freycinet Harbour. Note beach ridges of the Hamelin Coquina, forming spits that extend into the supratidal part of the embayment.

Figure 385. Vertical airphoto of the Nilemah Embayment, at the southern end of Hamelin Pool, showing (from the top down): green subtidal limestone pavement, a very narrow subtidal band of white ooid or pelloidal sand, mottled-grey subtidal to intertidal stromatolites, black intertidal *Entophysalis* mat and stromatolites, white intertidal to supratidal *Fragum erugatum* coquina, grey, speckled, vegetated Hamelin Coquina with prominent spits, greyish-white Pleistocene coquinite (at the base of the embayment), and dark reddish-grey dune sand of the Nilemah Sand (below and on either side of the embayment). The road to Denham skirts the embayment, and the Useless Loop road is on the bottom left. The width covered by the photo is 8.5 km. Airphoto courtesy of Landgate, Western Australia.

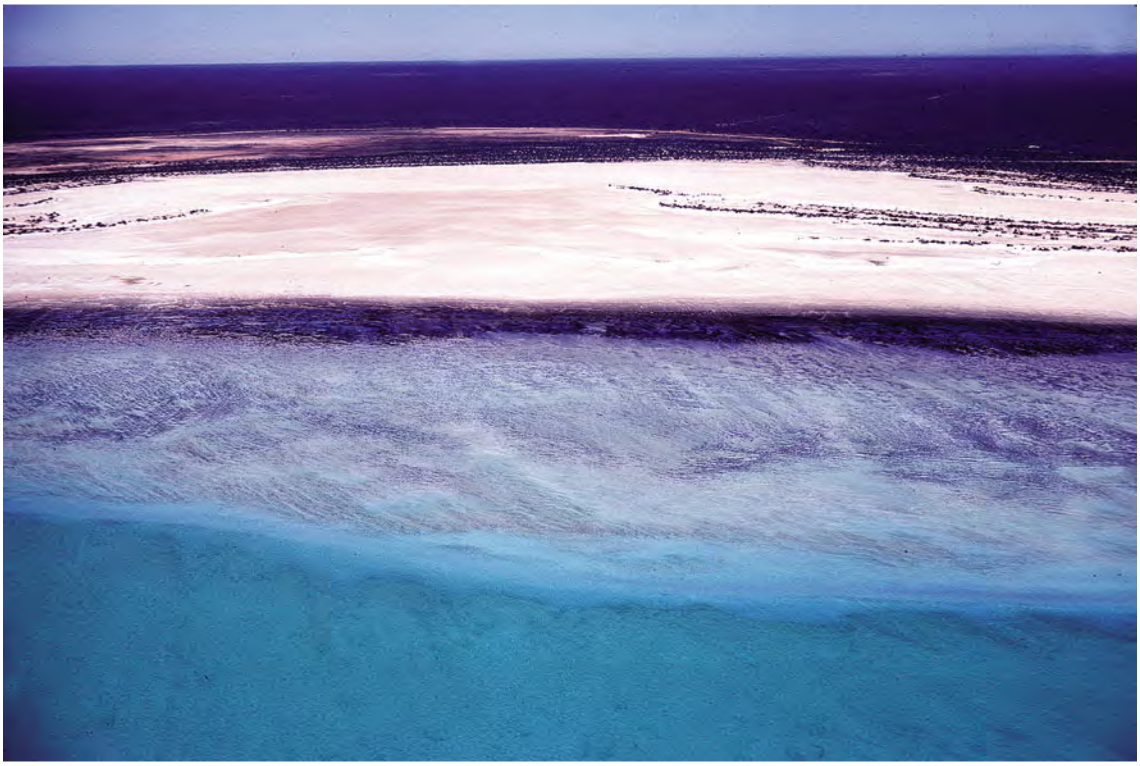

Figure 386. Oblique airphoto looking south over the Nilemah Embayment, showing greenish-blue subtidal pavement (in the foreground), a narrow belt of bluish-white ooid or pelloidal sand, mottled brownish-grey stromatolites, black intertidal *Entophysalis* mat and stromatolites, pale orange to white flat microbial mat, white curved belts of *Fragum erugatum* coquina, a belt of vegetated Hamelin Coquina (with spits), in front of pale red flats of Pleistocene coquina, and dark sand of the Nilemah Sand. The width at the base of the photo is about 2 km.

Figure 387. Microbial limestone pavement in water about 1.5 to 2 m deep, about 3 km southwest of Flagpole Landing. Some isolated stromatolite mounds have grown on top of the pavement. The width at the base of the photo is about 3 m.

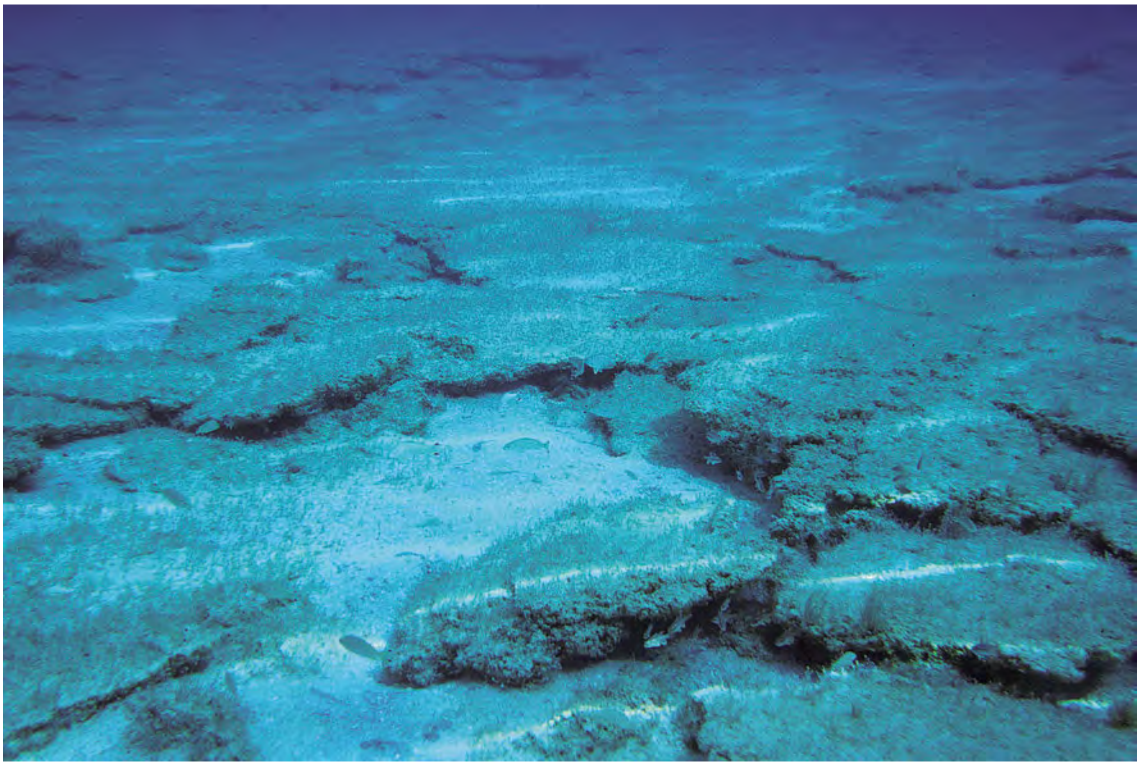

Figure 388. Microbial limestone pavement in water about 2 m deep, 3 km southwest of Flagpole Landing. Parts of the pavement have broken into slabs, and are covered by thin growths of green algae. The width of the field of view at the base of the photo is about 2 m. Note abundant small fish.

Figure 389. Microbial limestone pavement in water about 2 m deep, 3 km southwest of Flagpole Landing. The pavement is partly undermined, and has a large fish (a Chinaman Rock Cod) sheltering below the overhang. Green algae grow on the pavement surface. The width at the base of the photo is about 0.5 m.

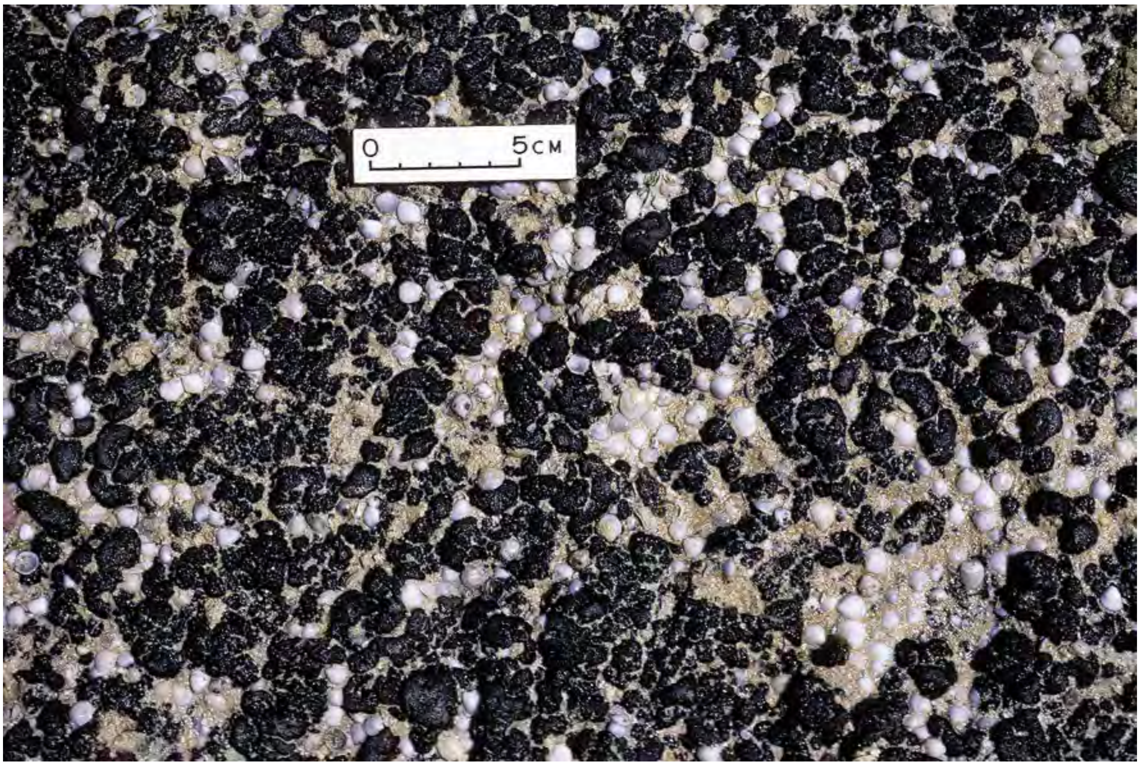

Figure 390. Flat microbial mat, built by *Entophysalis*, near Booldah Well. Scattered shells of *Fragum erugatum* and sand lie between the microbial pustules.

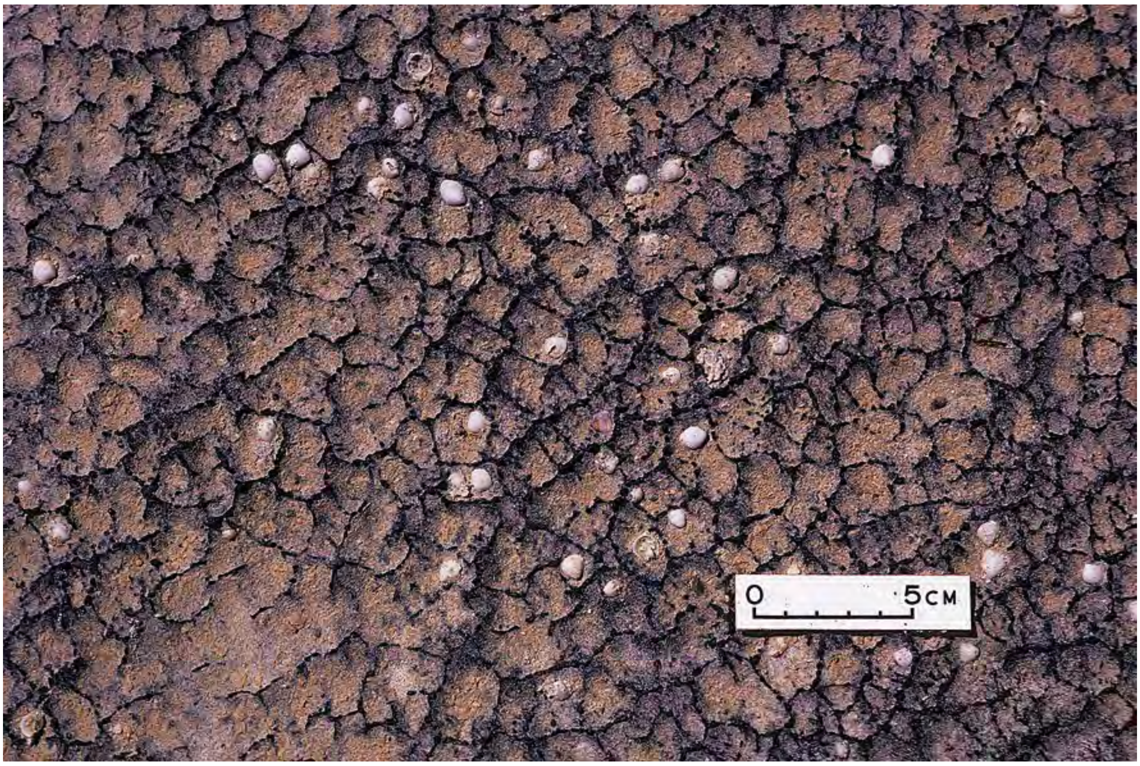

Figure 391. Tufted mat near Carbla Point forming approximately pentagonal shapes. The shells lying on the mat are of *Fragum erugatum*.

Figure 392. Tufted mat south of Carbla Point forming parallel lines. Note abundant shells of *Fragum erugatum*.The coin (lower right) is 3 cm in diameter.

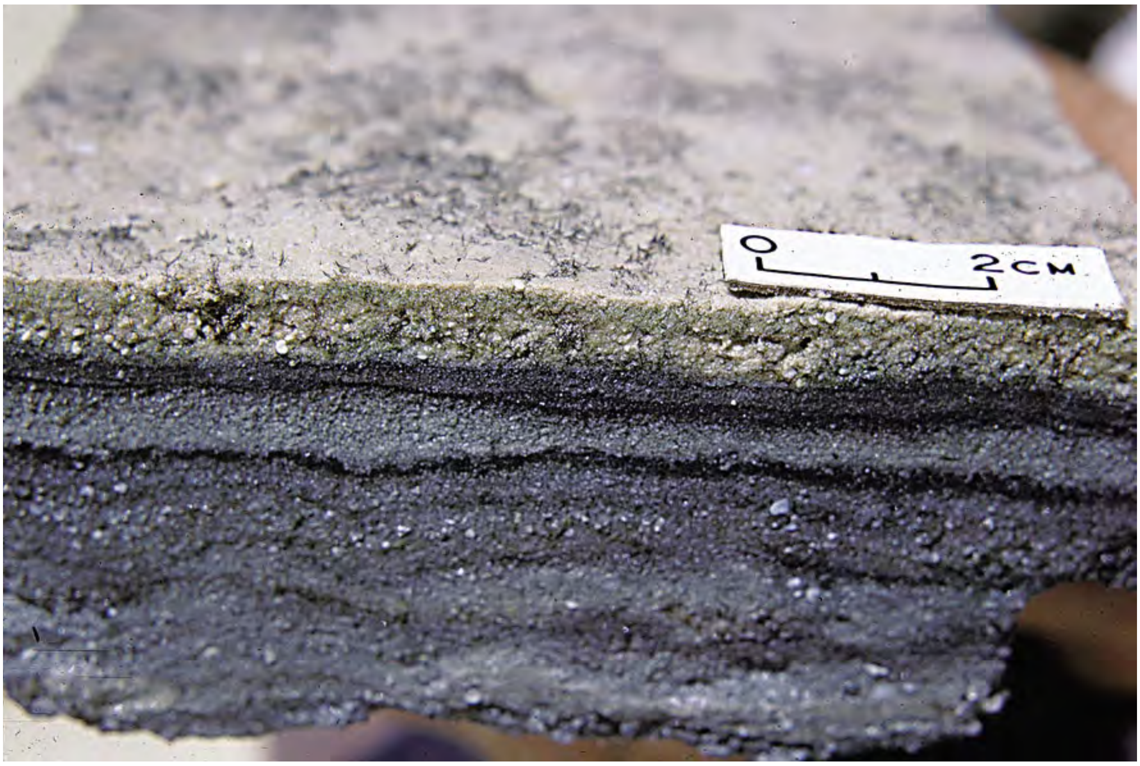

Figure 393. Section through flat, unlithified, smooth mat, about 2.5 km southwest of Flagpole Landing. The layers of black mud are anoxic. The white inclusions in the mat are shells of *Fragum erugatum.*

Figure 394. Wrinkled microbial mat on the shoreline supratidal pavement near the blue holes, on the west side of Hamelin Pool.

Figure 395. Folded microbial mat on the shoreline supratidal pavement near the blue holes, on the west side of Hamelin Pool.

Figure 396. Smooth microbial mat showing folding and over-thrusting on the supratidal pavement near the blue holes, on the west side of Hamelin Pool.

Figure 397. Strongly wrinkled microbial mat resulting from desiccation on the supratidal pavement south of Carbla Point. The coin is 3 cm in diameter.

Figure 398. Strongly wrinkled microbial mat resulting from partial desiccation followed by tearing apart of the wrinkled mat, on the supratidal pavement south of Carbla, beside Figure 397.

Figure 399. Over-thrusting in lithified microbial mat beside the shoreline near Booldah Well. The person is Tony Cockbain.

The proliferation of *Fragum erugatum* to form the Hamelin Coquina began with the onset of metahaline to hypersaline conditions in Hamelin Pool. This onset has been dated as being about 5300 years ago (5316 ± 42 years BP), by radiocarbon dating of the Hamelin Coquina on the east side of Hamelin Pool (A Hogg, 2010, written comm.). The first development of stromatolites was probably linked to the onset of strongly hypersaline conditions. Chivas et al. (1990) did not find stromatolites in Hamelin Pool older than 1000–1250 years, but Jahnert and Collins (2012) found forms that were radiocarbon dated as 1680–1915 years old. However, it seems possible that some stromatolites will prove to be even older, and further radiocarbon and uranium-series datings are needed to determine whether that is so.

Subtidal pavements

Wide areas of the subtidal zone in Hamelin Pool, extending to maximum depths of about 5–6 m, are floored by limestone pavements (hardgrounds). They are up to about 20 m thick, and have been precipitated by microbes (Figs 387–389). In many places they have been broken up, presumably by wave action during storms. Stromatolites then grew on some of the broken slabs (Fig 387). Overhangs below the slabs are sometimes used as shelters by fish, especially the Chinaman Rock Cod (Fig. 389).

Cormorant mangrove deposits

Deposits formed by cormorants, below their nests in dead or dying mangroves, are features of mangrove thickets (mangals) on Faure Island, as previous discussed (Figs 104–109). They are referred to as mangal deposits, and are laid down in mud close to sea level, consisting of the droppings of cormorants, together with their skeletal remains and scattered gastroliths and shells regurgitated by those birds, mixed with black mud. Elevated Pleistocene mangal deposits occur as thin guano layers interbedded in red sand, reaching as high as about 14.5 m above mean sea level (Figs 400–407), and testifying to recent uplift of the island.

Masses of rhizoliths forming small calcrete mounds and subhorizontal tubes (Figs 400, 401, 408, 409) are thought to have formed over mangrove stumps and roots at a large blowout, west of The Tadpole (786101E, 7140030N). About a metre above these rhizoliths is a thin horizontal layer of guano, about 20 cm thick and 10 m above sea level (Fig. 402). It contains thin lenses and pellets of hydroxylapatite, with scattered skeletal material of pied cormorants (including one almost complete skeleton; Fig. 403), together with many gastroliths and a few shells of the mangrove gastropod, *Terebralia*. This layer, with sand above and below, is a relic of a mangrove thicket that formed when sea level relative to the island was about 10 m higher than it is now. The sand above and below the hydroxylapatite bed has been OSL dated as Holocene, 2.1 ± 0.8 ka and 2.7 ± 9 ka respectively (M Cupper, 2010, written comm., 10 December). Thus it seems that this mangal layer must have been deposited about 2500 years ago.

Many other elevated mangal deposits occur around the island, up to about 14.5 m above sea level (Fig. 407; 788495E, 7133805N). Most contain cormorant skeletal material, with rounded gastroliths, bivalve shells, and the mangrove gastropod *Terebralia*. It is concluded that these beds must have been uplifted by 10 m during the past 2500 years, and up to 14.5 m during the past 3500 years. It seems likely that periodic uplift of the island is continuing today.

Figure 400. Small calcrete mounds (rhizoliths) at a large blowout west of The Tadpole on Faure Island. They are interpreted to have formed over mangrove stumps when sea level relative to the island was about 10 m higher than it is now. The person is Paddy Berry.

Figure 401. Horizontal fossil roots (rhizoliths) on Faure Island, close to the locality shown in Figure 400. They are thought to have replaced mangrove roots that formed when sea level relative to the island was about 10 m higher than it is now.

Figure 402. Horizontal layer of mangal guano bounded above and below by sand, near the localities shown in Figures 400 and 401. This is a mangal deposit, about 20 cm thick and about 10 m above sea level. It consists of pellets of hydroxylapatite, with scattered skeletal material from pied cormorants, together with many gastroliths, a few shells of the mangrove gastropod, *Terebralia*, and a few bivalve shells. The deposit formed about 2.5 thousand years ago, when sea level relative to Faure Island was about 10 m higher than it is now.

Figure 403. Pied cormorant skeleton from the mangal deposit near the localities shown in Figures 400–402. Courtesy of the Western Australian Museum.

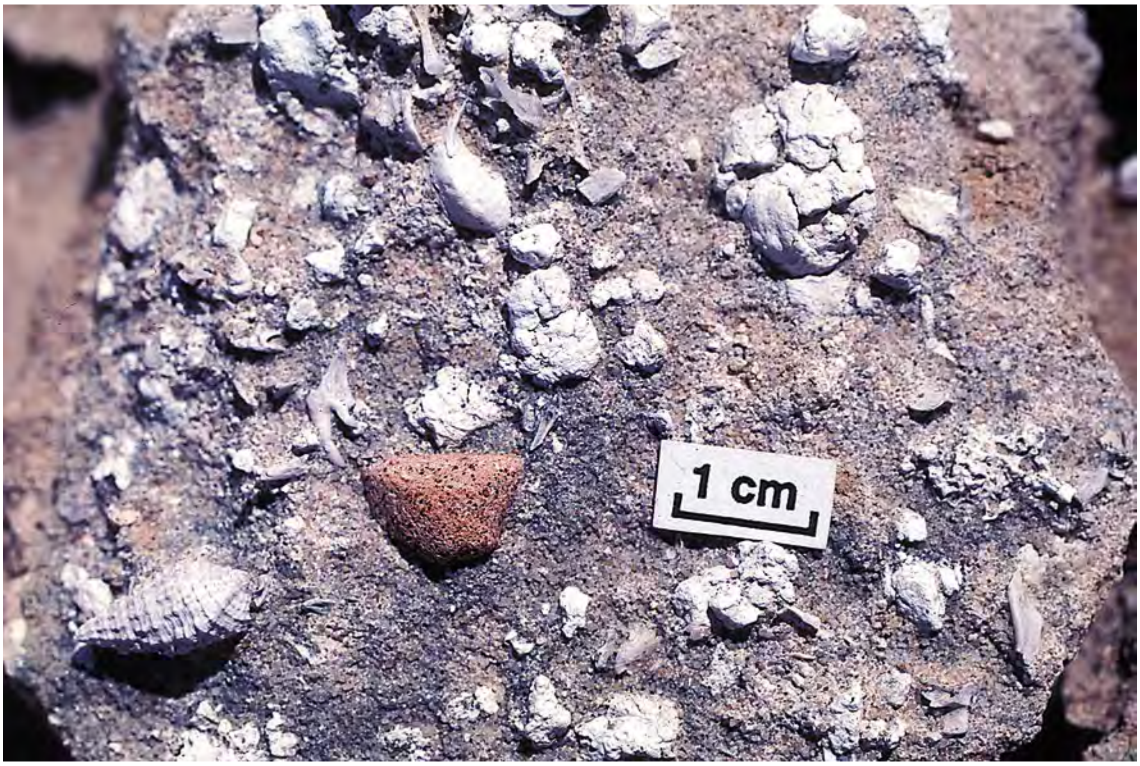

Figure 404. A piece of the mangal guano layer shown in Figure 402, showing pellets of hydroxylapatite, a rounded gastrolith of red siliceous sandstone (Peron Sandstone), small fish bones, and a *Terebralia* shell.

Figure 405. Pieces of the mangal guano layer shown in Figure 402, showing pellets of hydroxylapatite, rounded gastroliths of red siliceous Peron Sandstone, fish bones, the mangrove gastropod, *Terebralia*, and some bivalve shells.

Figure 406. Scatter of pellets of hydroxylapatite, pied cormorant skeletal material, gastroliths, and bivalves, derived by weathering of the guano layer shown in Figure 402.

Figure 407. **Thin Holocene mangal guano layer on Faure Island, about 14.5 m above sea level, with scattered debris below consisting of pellets of hydroxylapatite, pied cormorant skeletal material, rounded gastroliths, and bivalve shells. This testifies to about 14.5 m of uplift of the island during the recent past.**

Figure 408. **Fossil mangrove root, approximately horizontal, near the south coast of Faure Island a few metres above present sea level.**

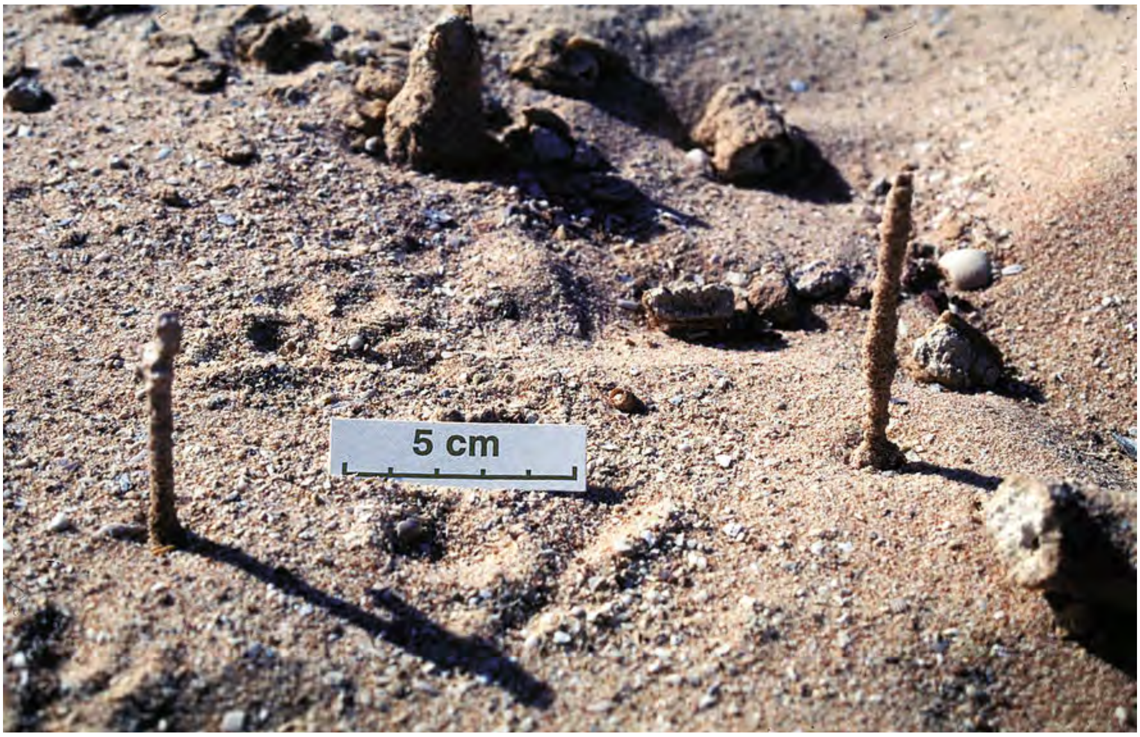

Figure 409. Fossil mangrove pneumatophores near the south coast of Faure Island, a few metres above present sea level.

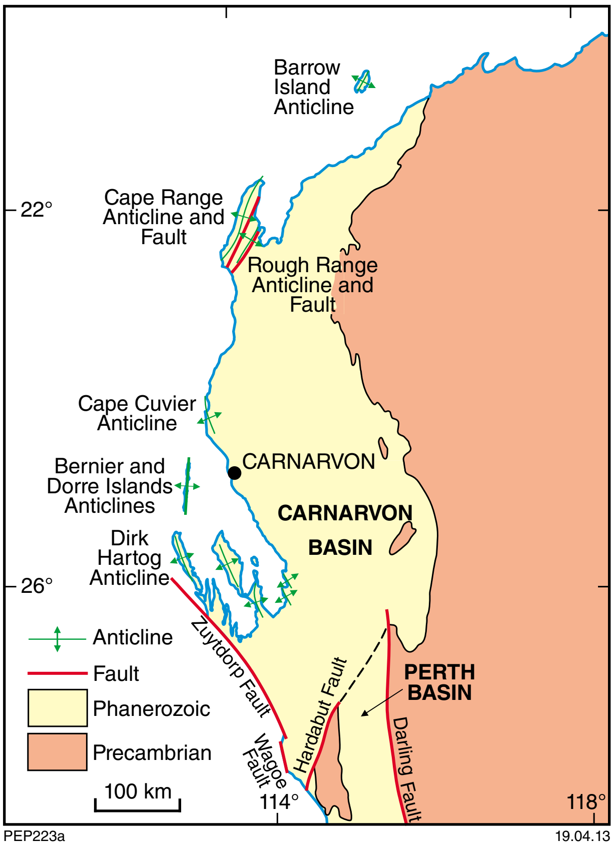

Figure 410. Folds and faults forming an arcuate belt of islands and peninsulas in the western part of the Carnarvon Basin. Also shown is the Hardabut Fault at the southern boundary of the Carnarvon Basin and the Darling Fault in the northern Perth Basin.

Structure

Folding

There is clear evidence of Cenozoic tectonism in the Carnarvon Basin, involving both folding and faulting (Van de Graaff et al., 1976, Hocking et al., 1987; Fig. 410). The prominent peninsulas and islands of the Shark Bay area are considered to have been localized by anticlinal folds in Quaternary and older rocks, with synclines marking the gulfs between them. Some of the anticlines are associated with reverse faults, localized by older normal faults.

The hypothesis that folding controlled the geography of Shark Bay was first proposed by Playford and Chase (1955) based on water-bore data, which suggested that the Kopke and Yaringa Promontories are marked by subsurface anticlines. They postulated that the Shark Bay peninsulas and Dirk Hartog Island are similarly underlain by anticlines in Paleogene and older rocks, and recommended to WAPET that this interpretation be tested through a program of scout drilling on Dirk Hartog Island. That recommendation was accepted, and drilling showed that Eocene and Paleocene limestones below the surface there are folded into an anticline, with its axis parallel to the length of the island (Butcher et al., 1984; Fig. 49). Such folding continued during the late Paleocene and Eocene, and probably on into the Quaternary. The Dirk Hartog Island anticline was subsequently tested for petroleum by a deep bore (Dirk Hartog 17b), which proved to be dry.

A small synclinal fold occurs in the Cretaceous Toolonga Calcilutite south of Yaringa Homestead (Hocking, 2000; Fig. 411). It is not clear how this feature can be related to the syncline that is interpreted to control the Gladstone Embayment.

Faulting

The Zuytdorp Cliffs are interpreted to be a fault-line scarp, formed by the Zuytdorp Fault, the most prominent Quaternary fault in the area. This fault is thought to have cut through dune limestones and overlying calcrete of the Tamala Limestone. It is considered to be a normal fault, downthrown to the west, that was active during the Pleistocene and perhaps early Holocene.

The most recent major movement along the Zuytdorp Fault post-dates dune deposition and consolidation of the limesand dunes into Tamala Limestone. Furthermore, faulting must have occurred after a thick layer of calcrete, covered with residual sand, had formed on top of the limestone. The Tamala Limestone in the cliff face below Womerangee Hill is some 250 000 years old, and the Zuytdorp Fault has been active since then.

Outcrops of Tamala Limestone between Shark Bay and Kalbarri closely follow the fault (Figs 114–116, 412), and it seems likely that an older Pleistocene fault-line scarp, lower than the present scarp, must once have once existed there, against which the dunes now comprising the Tamala Limestone were deposited. Thus it is deduced that the fault first moved before deposition of the Tamala Limestone had begun in this area, i.e. prior to the middle Pleistocene.

Five sections of the Zuytdorp Cliffs fault-line scarp, from near Kalbarri to Steep Point, have been described earlier in this Bulletin (Figs 113–126). The most recent movement of the fault must have been along Section 3, which extends for 86 km, from about 6 km north-northwest of Mickelberg airstrip to Pepper Point and False Entrance (Figs 113, 114, 116, 122–126). The highest part of the scarp in that section is beside Womerangee Hill, where it is up to 260 m high, descending precipitously into water more than 20 m deep. The last major movement along this part of the fault must have been in late Pleistocene or Holocene times. There is little evidence of seismicity along the fault today, other than a minor earthquake, magnitude 2.9, that occurred immediately south of the *Zuytdorp* wreck site on 2 November 1995. It was presumably due to minor movement along the fault. Observations at the site in 1996 showed that part of the cliff there had collapsed very recently.

Another Holocene fault in this general area is the Hardabut Fault, which is here considered to have operated as a reverse fault during the Holocene, Pleistocene, and perhaps Neogene. The fault can be observed where it crosses the Murchison River at the beginning of the gorge, at 259730E, 6914186N (Figs 413, 414). Uplift west of the fault, associated with the reverse movement, has caused the river to cut deeply into the Tumblagooda Sandstone. The reverse faulting resulted in a small anticlinal fold adjoining the fault and a deep gorge in the river downstream from there (Figs 415–417). The strong jointing in the Tumblagooda Sandstone in this area probably resulted from fissuring associated with upwarping of the area. Individual joints have opened by several centimetres (Figs 417, 418). Several faults are known in the gorge (Hocking, 1990), and some are associated with low scarps in the sandplain adjoining the gorge. Others have cemented breccias along fault lines in the gorge, thought to be due to iron-rich fluids along the fault line (RM Hocking, 2012, pers. comm.).

Geophysical evidence (gravity and magnetic), indicates that the Hardabut Fault was originally a normal fault with more than 1000 m of normal movement (RM Hocking, 2012, written comm.). Subsequent reverse faulting and uplift since the Eocene is suggested by middle or late Eocene sponge-bearing marine deposits near the gorge, 220 m above sea level, at a locality 27 km east of Kalbarri and 9 km west of the gorge (239880E 6926860N; Haig and Mory, 2003). It is estimated that the water depth during deposition of those deposits was between 10 and 30 m, suggesting that there has been more than 230 m of uplift and/or eustatic change in sea level in this area since the middle to late Eocene (about 40 million years ago).Therefore, it appears that the Zuytdorp Fault moved as a normal fault at approximately the same time that the Hardabut Fault experienced reverse movement. This apparent contradiction is still to be resolved.

Recent seismic events along the Hardabut and Wagoe Faults (Figs 130–132) show that contemporary seismic activity is continuing along both faults (Playford, 2003). Reverse faulting along older normal faults is also evident elsewhere in the Carnarvon Basin, both onshore and offshore, as shown by geophysical surveys and outcrop studies in the area (Hocking, 2000).

Reverse movement along an older normal fault was first demonstrated in the Rough Range Fault, along the east side of the Rough Range Anticline. Rough Range South 5 well penetrated a fault that had normal movement in Jurassic and Permian rocks and reverse movement in overlying Cretaceous, Paleogene, and Neogene rocks (Fig. 419; Playford, 1956; Playford and Johnstone, 1959). Similar reverse movements along older normal faults have also been recognized elsewhere in the Carnarvon Basin. Some of the anticlines developed below the peninsulas, promontories, and islands in the Shark Bay area may similarly be associated with reverse faulting, although no direct evidence has been found to support that hypothesis.

Keep et al. (2012) documented evidence for transpressional faulting in northwestern Australia (including the Shark Bay area), where 10 earthquakes have been recorded in recent times, ranging in magnitude from ML 2.2 to 5.3, on the continental shelf or slope and may also relate to the structural scene described in the present study. Alternating tension and compression that is evident in the area could well be linked with transpressional faulting (A Mory, 2013, pers. comm.).

Quaternary tectonism has undoubtedly played a major role in shaping the coastal and near-coastal geomorphology in the Carnarvon Basin between Barrow Island and Kalbarri (Fig. 410; Playford, 2003). Compressive movements in that area have resulted in broad anticlines in Cenozoic and

Cretaceous rocks, along an arcuate belt trending northeast at Barrow Island, north-northeast at Cape Range, north at Cape Cuvier, and north-northwest at Shark Bay. However, the Zuytdorp Fault is regarded as a normal fault, thought to have formed by extension during the late Pleistocene and perhaps early Holocene.

The west side of Cape Range Anticline shows a series of four Pleistocene shoreline terraces, the highest (and oldest) of which is about 60 m above sea level, while the others fall step-by-step to about 5 m in the lowest terrace, dated as about 123 000 years BP (last interglacial; Van de Graaff et al., 1976; Veeh et al., 1979; Fig. 420). The oldest and highest terrace is thought to be early Pleistocene in age. These terraces developed while the anticline was rising during successive interglacial sea-level highstands, and they show evidence of mild warping parallel to the anticlinal axis (Van de Graaff et al., 1976). In that respect it is notable that the west flank of Cape Cuvier Anticline, 250 km south of Cape Range, shows mild folding of a coral reef that grew during the last interglacial period.

Edel Land, Peron, and Nanga Peninsulas in Shark Bay consist of Pleistocene and Holocene eolianites, and are predicted to be underlain by similar anticlines in Pleistocene and older deposits. As discussed earlier, drilling at Dirk Hartog Island, along the same trend as Edel Land Peninsula, proved that the Quaternary section there overlies an anticline in Cenozoic limestones, with its axis parallel to the length of the island (Fig. 49). This anticline may also be associated with reverse faulting.

Relatively recent Cenozoic tectonism is also evident in the Perth Basin, where the Darling Scarp (Figs 421, 422) is a fault-line scarp, considered to have been produced from normal movement along part of the Darling Fault, a major suture that dates back to the Proterozoic. This fault may have last moved during the Pleistocene, although that has yet to be demonstrated. The Gingin and Whicher Scarps, which diverge from the Darling Scarp, are also interpreted to be subrecent fault-line scarps (Fig. 422). Elsewhere in the Perth Basin, near Jurien, there is evidence of recent high-angle reverse faulting in an excavation for mineral sands in the Tamala Limestone (325095E, 6641880N; Mory et al., 2005; Fig. 423). Small reverse faults at this locality cut eolian foreset beds of the Tamala Limestone, which here may be middle Pleistocene in age. These faults seem to have been localized by pre-existing jointing in the limestone.

Figure 411. A synclinal fold in the Toolonga Calcilutite, looking southeast from 3.5 km southwest of Yaringa Homestead. The Great Northern Highway is in the background. Photo by Roger Hocking.

Figure 412. DEM image of the southern part of the Zuytdorp Cliffs fault-line scarp, showing a linear ridge of Middle Pleistocene Tamala Limestone beside the coast, cut by hundreds of small parallel creeks. The Zuytdorp Fault, situated immediately in front of the coast, may have last moved here during the late Pleistocene, resulting in a scarp that localized deposition of the coastal sand dunes now forming the Tamala Limestone. The length of coast shown here, referred to as Section 1 of the Zuytdorp Cliffs, is 85 km. See also Figures 117–120.

Figure 413. Tumblagooda Sandstone (on the left) folded into a small anticline, and faulted against Proterozoic gneissic rocks (on the right), along a thrust fault, the Hardabut Fault, that dips to the left (west) at about 30 degrees.

Figure 414. Aerial view looking south over the Murchison River near Hardabut Pool, where the Tumblagooda Sandstone is folded into a small anticline and thrust against Proterozoic gneissic rocks along the Hardabut Fault.

Figure 415. Aerial view looking southwest over the Murchison River gorge at The Loop, a large incised meander. The river cut down into the Tumblagooda Sandstone, following Cenozoic uplift thought to have been associated with reverse movement along the Hardabut Fault. The width of the meander at the base of the photo is 2 km.

Figure 416. Vertical airphoto of the Murchison River gorge, showing the incised meander at The Loop, cut into the Ordovician Tumblagooda Sandstone. The width of the field of view is 8.9 km. Airphoto courtesy of Landgate, Western Australia.

Figure 417. Aerial view looking east over the Murchison River gorge, cut into the Ordovician Tumblagooda Sandstone some 18 km south of The Loop. Note the deep incisions following joints in the sandstone.

Figure 418. Joints in the Tumblagooda Sandstone east of The Loop, showing that each joint has opened between 10 and 20 cm.

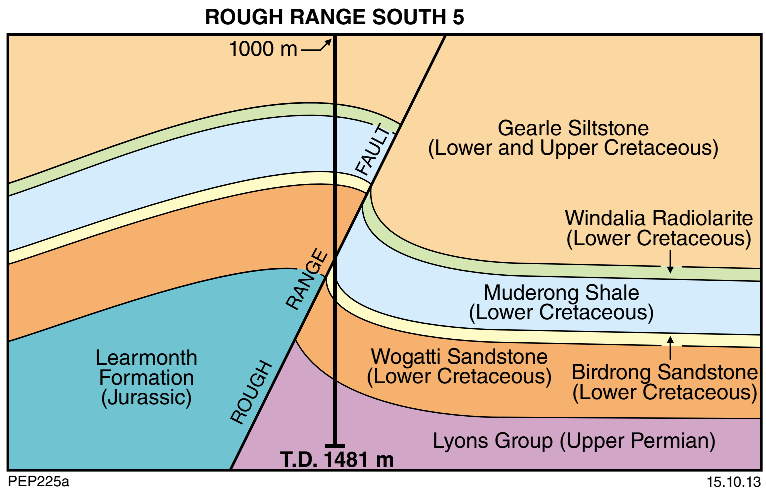

Figure 419. Diagram illustrating the section in Rough Range South no. 5 well, which drilled through the Rough Range Fault; it had normal movement during the Triassic and Jurassic, and reverse movement during the Cenozoic (after Playford, 1956).

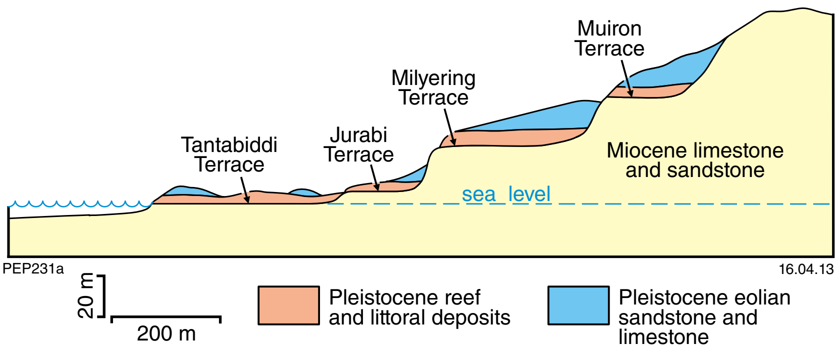

Figure 420. A series of terraces uplifted during the Pleistocene, on the west side of Cape Range Anticline in the Carnarvon Basin. After Van de Graaff et al., 1976.

Figure 421. View looking east from Kings Park over parts of Perth and the Swan River estuary towards the Darling Scarp, a fault-line scarp (photo was taken in 1955).

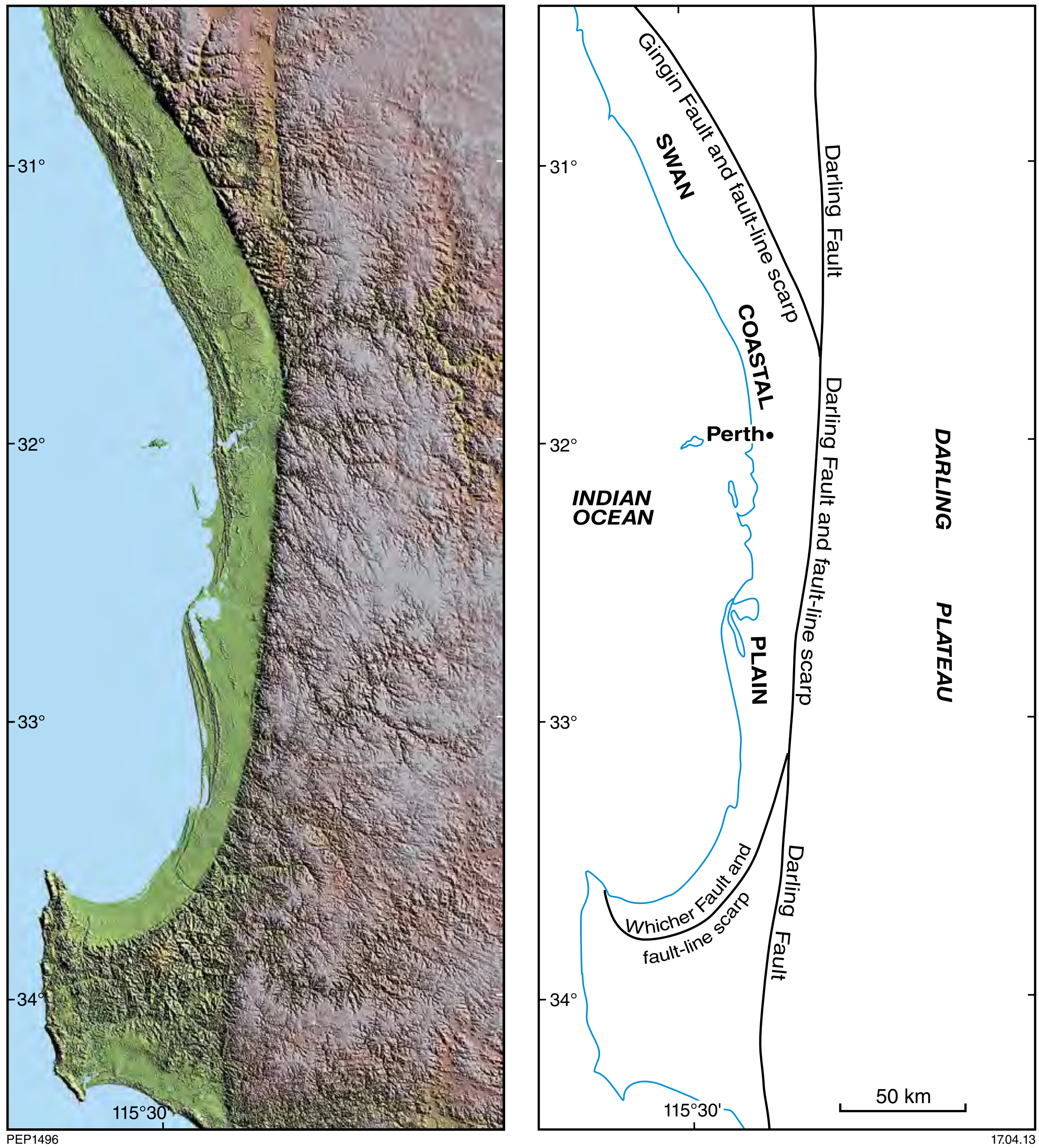

Figure 422. DEM image and diagram illustrating parts of the Darling, Gingin, and Whicher Faults, fault-line scarps, and the Darling Plateau. The Gingin and Whicher Faults and the intervening part of the Darling Fault may have last moved during the Pleistocene or early Holocene. The Darling Plateau is considered to have been planed down below Permo-Carboniferous ice sheets, and patches of that planed surface can be seen in places that have not been dissected by streams.

Figure 423. Small-scale, high-angle, reverse faults, dipping east and trending north–south, in the Pleistocene Tamala Limestone in a quarry near Jurien in the Perth Basin. Photo by Arthur Mory.

Faure Island

As previously discussed, Faure Island has been uplifted periodically during the Holocene, by about 10 m during the last 2400 years, and 14.5 m during about the last 3500 years. The Hoult Sandstone Member of the Peron Sandstone on the south coast of the island dips east at about 2º (Fig. 167) and that tilting must post-date the last interglacial period of about 130 000 years ago.

The overall structure of Faure Island is puzzling. It might be expected, based on the known anticlinal structure below Dirk Hartog Island and presumably also below Edel Land, Peron, and Nanga Peninsulas, that the Cenozoic structure below Faure Island is also anticlinal, with its axis trending north-northwest. Alternatively, it seems possible that the island could have formed above a domal structure that is still rising. However, both the anticlinal and domal hypotheses are difficult to reconcile with the observed easterly dip of 2º along the south coast of the island.

One of the most intriguing features of the structural geology of Faure Island is the presence of prominent polygonal (mainly pentagonal) jointing in indurated sandstone of the Peron Sandstone beside the south coast (Figs 424–427). There can be no doubt that these joints were formed very recently, long after induration of the quartz sandstone. The polygons are generally about 50–80 cm across, and when observed on 9 and 10 April 2002, some had clearly re-opened only a short time before, by as much as 1–2 mm. Many remained partly open, because there was insufficient time for any infilling of new sediment (Figs 425, 426). Prior to their recent opening the polygonal joints had been filled with sand that had become weakly cemented. Thin sandy clay had previously washed into depression along the joints, and this had fractured and opened very recently (Fig. 425). The cracks extended down as much as 2 m, dying out in or above the underlying Hoult Sandstone Member.

Even more remarkably, there was evidence that some other joints had recently been subject to compression, forcing sediment out of the cracks (Fig. 427). The reasons for this recent compression on the one hand and extension on the other are not readily apparent, although they could be associated with transpressional faulting, as previously mentioned. It also seems possible that the recent extensional opening of the joints was associated with a magnitude 2.8 earthquake that occurred on 6 April 2002, with its epicentre about 30 km east of Hamelin Pool.

The origin of the polygonal jointing is unclear, but it seems to point towards extension of the surface and near-surface part of the Peron Sandstone, perhaps supporting the hypothesis that the island is underlain by a domal structure that is still rising. It is also notable that similar pentagonal jointing has been observed beside the east shore of Hamelin Pool near Spaven Point, in well-cemented coquinite of the Hamelin Coquina.

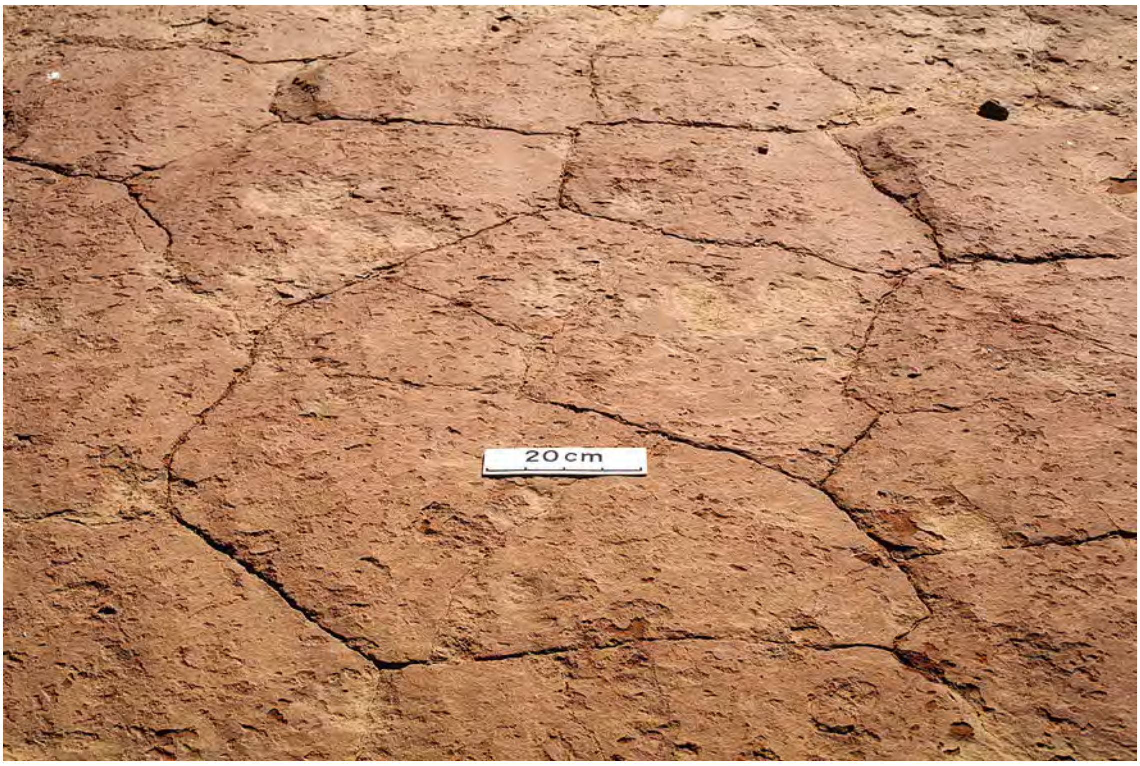

Figure 424. Polygonal jointing in Peron Sandstone near the south coast of Faure Island.

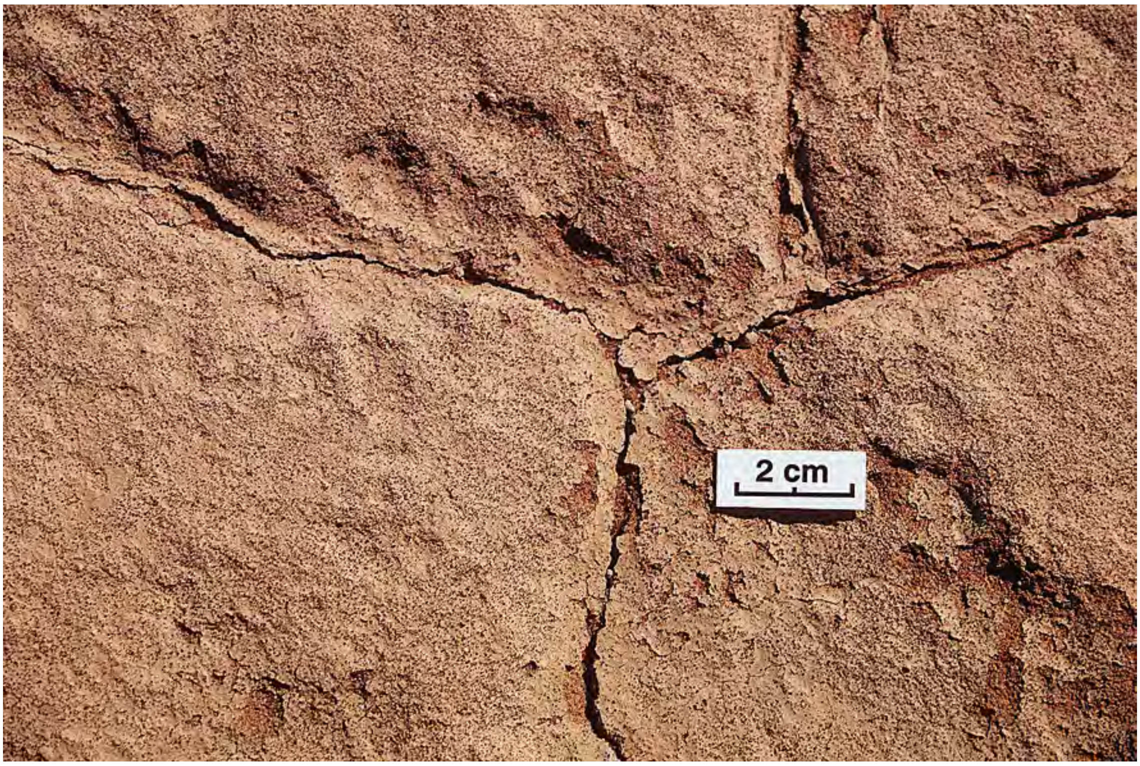

Figure 425. Photo taken on 10 April 2002 of pentagonal jointing in Peron Sandstone near the south coast of Faure Island, showing that sandy clay that had previously washed into depressions along the joints had opened by as much as 1 to 2 mm shortly before the photo was taken. It is possible that this opening was associated with a magnitude 2.8 earthquake in the Hamelin Pool area on 6 April 2002.

Figure 426. **Photo taken on 10 April 2002 of joints that had recently re-opened, in Peron Sandstone beside the south coast of Faure Island. The open joints extended down as much as 2 m, dying out in or above the Hoult Sandstone Member of the Peron Sandstone (in the lower right of the photo).**

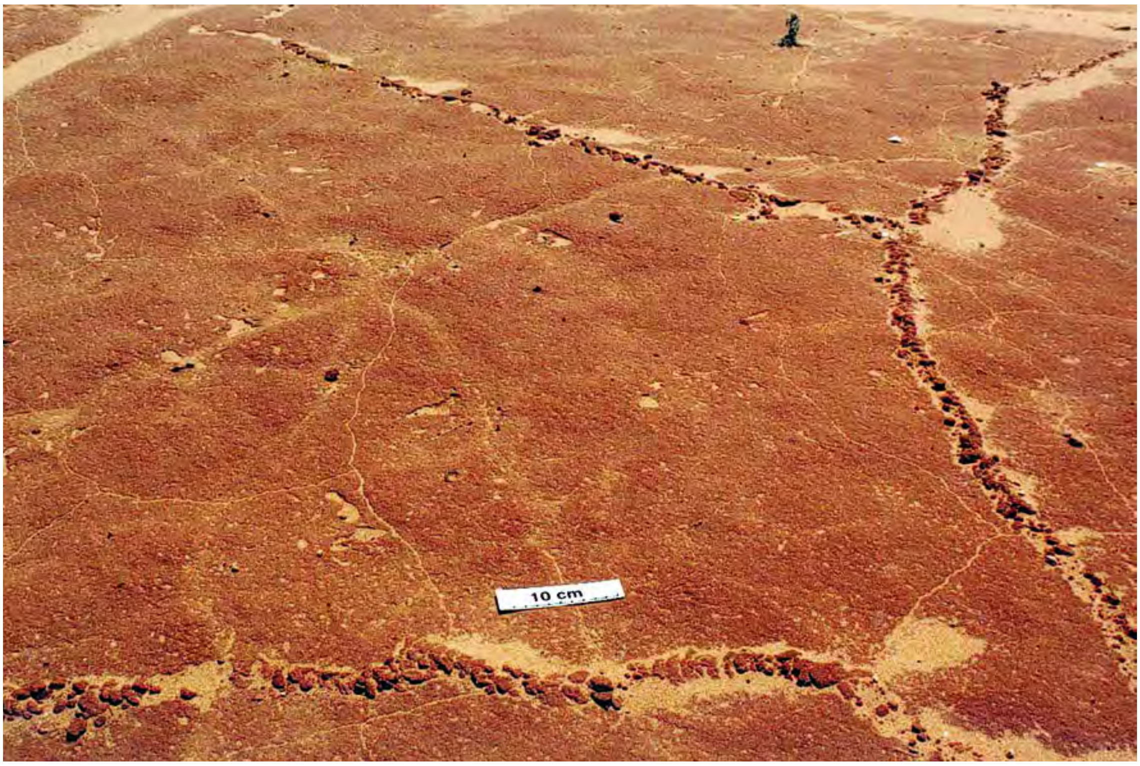

Figure 427. **Polygonal joints in the Peron Sandstone at another locality beside the south coast of Faure Island. Sandy mud (now lithified) had been extruded along some of the joints during the recent past, pointing to compression rather than the tension that is evidenced in Figures 425 and 426.**

Woodleigh Impact Structure

Although this Bulletin concentrates on the surface geology of the area, the subsurface Woodleigh Impact Structure east of Hamelin Pool needs to be mentioned, as it is one of the world's major meteoroid-impact structures (astroblemes). This subsurface feature is up to about 50 km in diameter, and is situated east of Hamelin Pool on Woodleigh Station (Mory et al., 2000, Glikson et al., 2005a, b, Carr et al., 2012; Fig. 428). It is interpreted to have been formed by the impact of a large meteoroid. The structure is entirely covered by flat-lying Cretaceous and Lower Jurassic strata, and is most likely to be of early Jurassic age (Carr et al., 2012). The impact origin has been interpreted from geophysics (seismic, gravity and aeromagnetic) and drilling that disclosed shock-metamorphosed granitic rock in the core of the structure.

Aeromagnetic survey

An aeromagnetic survey of the central part of the Shark Bay area was conducted by GPX Surveys for GSWA and GA in 2012; the data and survey operations report were published by GSWA in 2013 (GPX Surveys, 2012; Fig. 429).

A striking feature of the total-magnetic-intensity map is the presence of many narrow linear anomalies trending west-northwest to northwest, especially in the western part of the area. They are most likely caused by a swarm of igneous dykes underlying the Cenozoic and Cretaceous section, at depths ranging from perhaps a few hundreds to thousands of metres. The shallowest dykes are immediately west of Dirk Hartog Island. One of the dykes, in the northeast part of the image, is seen as a negative anomaly, which indicates emplacement during a reversal in the earth's magnetic field. It is likely that the red subcircular to elongate anomalies shown on this map reflect deep igneous intrusions.

These results were rather unexpected, although intrusive alkaline igneous rocks were already known from Edel 1 petroleum exploration bore (offshore, south of Shark Bay; Figure 147), and late Paleozoic and Cretaceous volcanic rocks are interpreted to occur elsewhere in the offshore area west of Shark Bay (Lockwood and D'Ercole, 2003).

Finely mottled, black, linear patterns of high-frequency anomalies can be seen over much of the total-magnetic-intensity map, in zones trending north–south, both onshore and offshore. They must reflect the presence of heavy-mineral-bearing sand dunes, some of which are now submerged and were formed when sea level was lower than it is today. Former shorelines, now submerged, can also be detected, for example east and north of Cape Peron and east and south of Faure Island (Fig. 429).

The fault-line scarp of the Zuytdorp Fault can also be seen clearly, by the abrupt truncation of the 'magnetic-dunes' pattern in the southwest part of the total-magnetic-intensity-map area (Fig. 429).

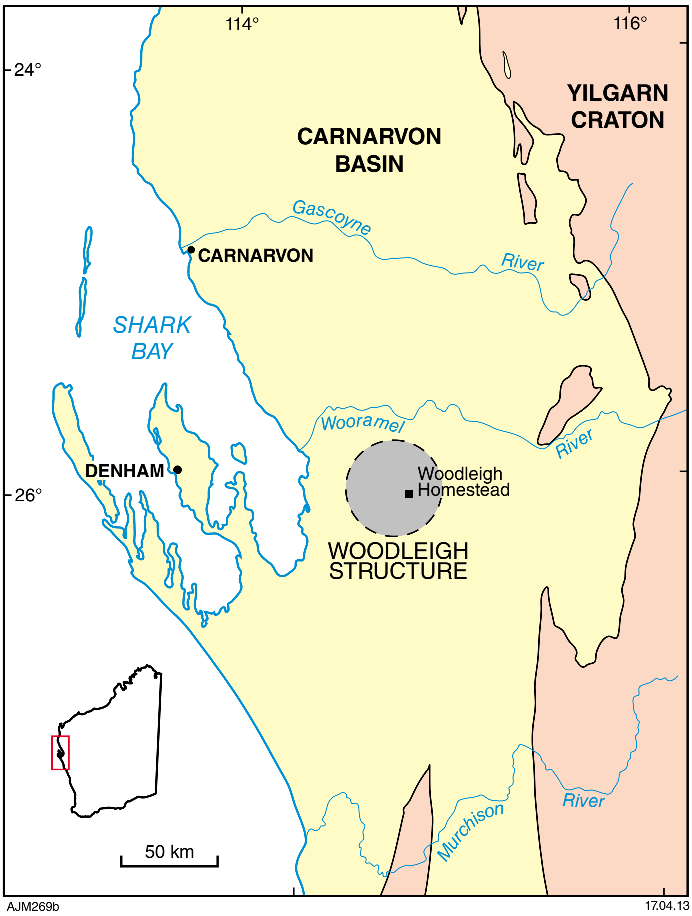

Figure 428. Diagram showing the subsurface location of the Woodleigh Impact Structure (from Mory et al., 2000, and Carr et al., 2012).

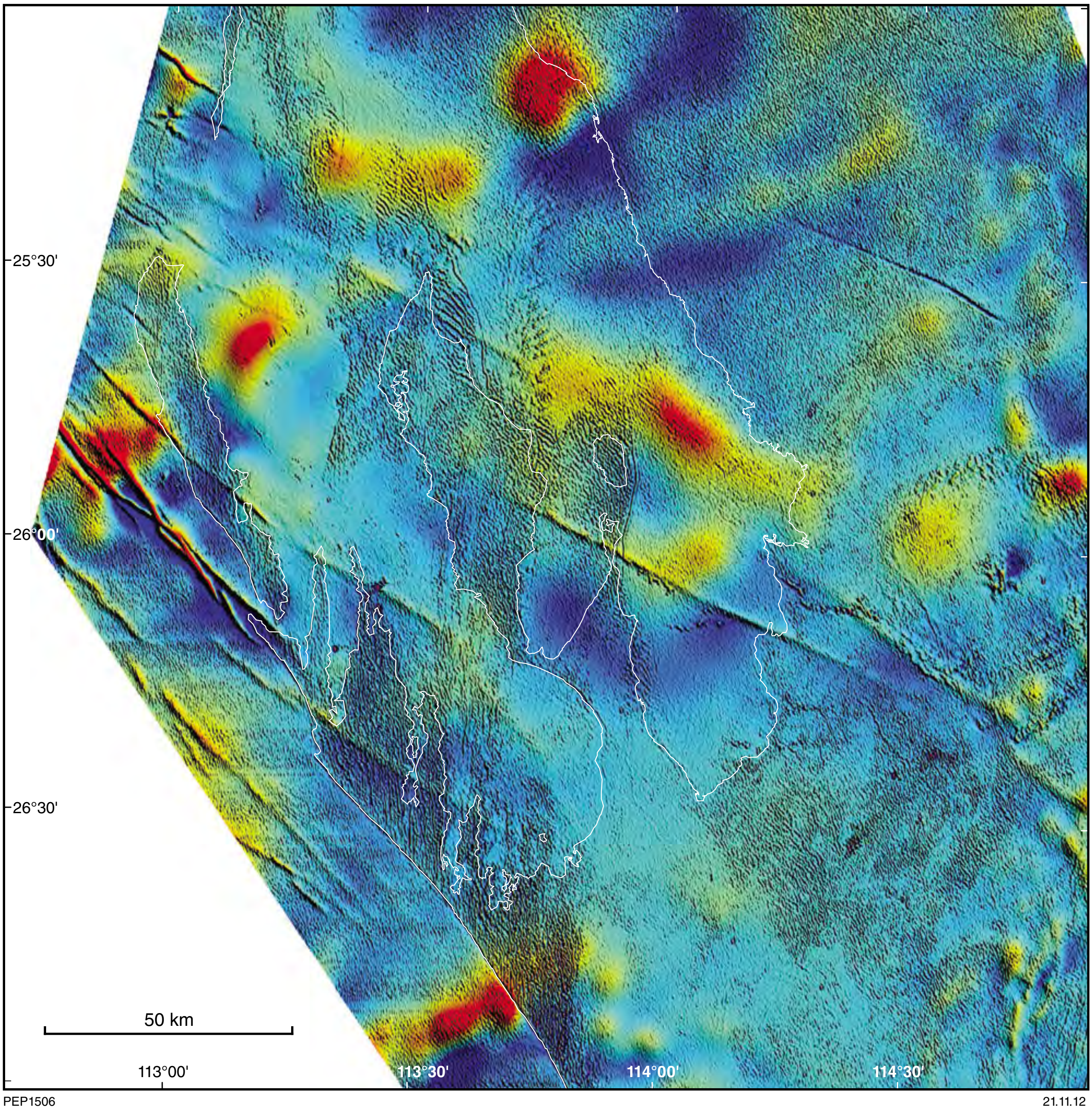

Figure 429. Aeromagnetic total-magnetic-intensity first-vertical-derivative image of the Shark Bay area, illuminated from the northeast. The linear features trending northwest to north-northwest are interpreted as igneous dykes in upper Paleozoic and perhaps Cretaceous rocks, below the Cenozoic succession. The red subcircular to elongate features probably represent igneous intrusions. Note the black speckled linear pattern, both onshore and offshore, elongate north–south and apparently caused by heavy mineral sand in sand dunes deposited when sea level was lower than at present. Note also the submerged shorelines (perhaps early Holocene) extending north–south, just east of Faure Island, Nanga Peninsula, and Cape Peron.

Economic geology

Mineral commodities that are being, or have been, exploited in the Shark Bay area are solar salt, gypsum, shell deposits, building stone, guano, pearls, pearl shell, and cultured pearls. Mineral-sand deposits known in the area (south of Hamelin Pool, outside the World Heritage Area) may be developed before long.

Solar salt

Solar salt is produced at Useless Loop and Useless Inlet on the northern side of Edel Land Peninsula (Figs 430–432), by the Shark Bay Salt joint-venture company.

The salt is precipitated from seawater by evaporation in a series of ponds, isolated from the open sea by bars constructed across Useless Inlet and Useless Loop. The salt is transported for loading onto ships along a causeway from Heirisson Prong to Slope Island and from there to a jetty (Fig. 432).

Salt production at Useless Loop commenced in 1965, and the first shipment was made to Japan in 1967. Cumulative production to 2011 amounted to 19 Mt, and current production is about 1 Mt/year.

Gypsum

High-quality gypsum fills birridas in low-lying interdune areas along Peron, Nanga, and Edel Land Peninsulas, and Dirk Hartog and Faure Islands (Figs 32, 67–71). The birridas are especially well developed between transverse dunes on Peron and Nanga Peninsulas and range in area from <100 m^2 to a maximum of 18 km^2 in a major birrida adjoining Cape Peron. The thickness of gypsum ranges from less than 1 m to 9 m (Butler, 1985). The gypsum must have been derived from seawater spray (aerosol) carried inland by winds, and subsequently concentrated by rainwater leaching.

Between 1968 and 1987, gypsum was produced by the Shark Bay Salt company from birrida deposits near Useless Loop, and exported from the loading jetty at Slope Island. This operation produced 2.4 Mt of gypsum, the largest production to date in Western Australia. Known remaining gypsum reserves are in birridas near Brown Inlet, Useless Loop, and Cape Peron (Flint and Abeysinghe, 2000).

The largest known undeveloped gypsum deposit in the Shark Bay area, with reserves of about 14 000 t, is in the largest birrida in the area, near Cape Peron (Fig. 433). This is a composite feature, formed by the coalescence of several birridas. It is approximately 9 km long, up to 3 m wide, and trends north–south (Jones, 1994; Butler, 1985). However, this deposit is situated within the Shark Bay World Heritage Area, so that is likely to remain undeveloped.

Mineral-sand deposits

Potentially economic heavy mineral sand deposits, held by Gunson Resources Limited, are known from an area between 5 and 60 km south of Hamelin Pool (Fig. 170). These deposits, here termed the Coburn heavy mineral sands, average 1.2% heavy minerals. Most occur within a belt of low parabolic and undulating dunes of the Nilemah Sand, but the northernmost deposit may be localized along a Neogene shoreline.

The company estimates that ore reserves of the Coburn mineral-sand deposits amount to 308 Mt, comprising ilmenite (46%), zircon (23%), rutile (7%), and leucoxene (5%) (Harley, 2004, 2008; Prospect Magazine; Department of Mines and Petroleum, September–November 2012). Environmental assessment concluded that mining can be allowed to proceed, subject to appropriate environment conditions (Environmental Protection Authority, 2005). The company recently agreed (subject to finance) to purchase Hamelin Station, on which some of the deposits occur (Gunson Resources Limited, 2012).

Shell deposits

Shell deposits, composed of uncemented or little-cemented accumulations of the bivalve *Fragum erugatum*, have been excavated for commercial purposes on the east coast of L'Haridon Bight and in small quarries beside the southeast coast of Hamelin Pool, near Flagpole Landing. The product is used for shell grit (in the poultry industry), surfacing grounds and tracks, and various decorative purposes.

Shell was used during the mid-1960s to construct large geometric patterns on Woodleigh Station, with the objective that they would be visible from space, as part of the NASA space program. They are still visible on Google Earth and orthophoto imagery, northwest of Woodleigh Homestead, around 268500E, 7101000N.

Building stone

Cemented coquinite of the Hamelin Coquina has been quarried periodically near Flagpole Landing (Figs 234, 235, 265, 434) and Carbla Point. A much smaller abandoned quarry is situated near Booldah Well.

The coquinite has been used to build station homesteads in the Hamelin Pool area (Fig. 435) and several buildings in Denham. It has also been used to build water tanks, the insides of which are lined with cement to prevent leakage (Fig. 436).

The coquinite blocks are relatively light to handle (Fig. 434) and have excellent insulation properties. They harden to some extent through exposure to the weather, but remain susceptible to the carving of graffiti.

Figure 430. Aerial view looking north over evaporite ponds at Useless Loop, with Bellefin Prong on the left and part of Heirisson Prong on the right.

Figure 431. Aerial view looking south over evaporite ponds in Useless Loop. A barrier across Useless Inlet can be seen in the upper middle distance. Useless Loop settlement is seen in the lower right.

Figure 432. Aerial view looking west over the salt-storage and ship-loading facilities at Slope Island and the causeway to Heirisson Prong. The evaporite ponds in Useless Loop are in the left middle distance.

Figure 433. Aerial view of the largest birrida in the Shark Bay area, 9 km long and up to 3 m wide, near Cape Peron. This birrida contains the largest known reserves of gypsum in the Shark Bay area.

Figure 434. The Flagpole quarry near Flagpole Landing, showing blocks of coquinite sawn by hand from the Hamelin Coquina. Photo taken in December 1954 (the person is Richard Chase).

Figure 435. Part of a wall of Hamelin Homestead, built with blocks of Hamelin Coquina from the Flagpole quarry.

Figure 436. The walls of buildings and a rainwater tank at Carbla Homestead, built with blocks of Hamelin Coquina from near Carbla Point, and lined with cement.

Guano

As discussed earlier, guano was stripped from the tops of many small islands in the Shark Bay area during the 1850s (Fig. 16). It had accumulated there over thousands of years, from the excrement of water birds. No significant reserves of guano remain in the area today.

Pearls, pearl shell, and cultured pearls

The pearling industry in Shark Bay began during the 1850s and continued, on a diminishing scale, into the 1930s. By the end of that period the numbers of pearl shells remaining in the area had greatly diminished. The pearl-shell populations may now have largely recovered, but there is no longer any market for the shells. However, a cultured-pearl farm is operating successfully near Monkey Mia.

Future research

Further research on the remarkable geoscientific features of the Shark Bay area is warranted. In particular, there is scope for more intensive studies of the Hamelin Pool stromatolites and on the structural geology and dune sands of the area. The tsunami deposits of Shark Bay and other coastal areas of the State warrant detailed study, especially because of the potential dangers of future tsunamis to people living in the coastal areas, and the implications for destruction of industrial infrastructure.

The extent of living and dead stromatolites needs to be mapped in some detail, and the causes for the deaths (or dormant states) of many submerged stromatolites and stromatolite reefs should be determined. Precise measurements are required to measure any elevation limitations for growth of the various stromatolite-building microbes.

Studies to date of the structural geology of the area have shown evidence of features that have developed in response to both regional compression and regional tension, and the relationships between those forces and their respective timings need to be clarified.

More detailed field studies of the tsunami boulder deposits are needed to more accurately quantify the size and ages of tsunamis that have affected the area, and to determine whether smaller boulder and sand deposits have resulted from tsunamis or intense tropical cyclones. Detailed examination and mapping of these intriguing deposits would more accurately define the runup limits of the tsunamis. Further radiocarbon datings are also needed to more closely define the timing of these deposits.

The dune systems in the Shark Bay area clearly warrant more detailed investigation. In particular there is a need for studies of the heavy-mineral assemblages in the various dune systems, along the lines of studies previously conducted in the Perth Basin. There would be an economic aspect involved in such studies, as most of the known mineral-sand deposits are hosted in dunes, and comparable deposits are expected to occur elsewhere in the area. There is also a need to determine the paleoclimates associated with deposition of the dunes, and the wind strengths that were involved.

Acknowledgements

Many people have generously assisted our work on this project over many years. Special thanks are due to the following: successive Directors of GSWA, Joe Lord, Alec Trendall, Phil Playford, Pietro Guj, David Blight, Tim Griffin, and Rick Rogerson, for their support and encouragement; other staff or former staff of GSWA: Roger Hocking, Arthur Mory, Don Flint, Franco Pirajno, Trevor Beardsmore, Kath Grey, Evert Van de Graaff, David Howard and John Brett (for their assistance and advice), Michael Prause, Suzanne Dowsett, and Joyce Peng (for drafting the diagrams), Murray Jones (for assistance in editing photos and designing the cover), Stewart Jefferys (for preparing the DEM images), Shaun Coldicutt and Kiaran Smith (for assistance in the field and for several photos provided by Shaun), Robin Bower, Tony Cockbain, and Sarah Martin (for editing the manuscript), Bec Hitchings (for preparing the text for publication); Daryl Johnstone and Richard Chase (for their participation in the early fieldwork); Tim Pietsch, Jon Olley, and Mat Cupper (for OSL dating); Alan Hogg and Fiona Petchey of the University of Waikato (for radiocarbon dating); Cheryl Cowell (President), councillors, and staff of the Shire of Shark Bay (for their assistance); Les Moss, past-President of the Shire (for his assistance); Brett Fitzgerald of the Department of Environment and Conservation (for allowing the use of a vehicle and facilitating fieldwork on Dirk Hartog Island); Pamela Reid and Erica Parke of the University of Miami (for advice on Hamelin Pool stromatolites); Glen Smith and Edward King of CSIRO (for supplying sea-surface temperature images); Malcolm Wallace of the University of Melbourne (for advice on diagenesis of the Hamelin Coquina); Tanya Whiteway of Geoscience Australia (for bathymetric information); Paul Hoffman (for a photo of Proterozoic stromatolites); Russell Lagdon of Chevron Australia (for facilitating a visit to Barrow Island and providing photos); George Kendrick and Shirley Slack-Smith of the Western Australian Museum (for paleontological and zoological advice); Sally Killoran, Sue Graham-Taylor, Dick Hoult, and staff of the Australian Wildlife Conservancy (for support at Faure Island); Tony Lamberto of the Department of Transport (for providing tide data from Hamelin Pool and Denham); Des Matthews (for a photo relating to the tidal range at Denham); Eric and John Lawson (for a photo taken on Nilemah Station); Craig Howson (for inviting participation in several voyages in the *True North* along the Kimberley coast) and Andy Lewis (for providing locality data for photos taken on one of those voyages); and Geoffrey Playford of the University of Queensland (for comments on a draft of this publication).

We also wish to express appreciation to the many station owners and managers in the area for their assistance and hospitality over many years, especially Brian and Mary Wake of Hamelin Station, Peter and Valmai Kopke of Carbla Station, Ross and Sue Lightfoot of Hamelin Station, and Kieren and Tory Wardle of Dirk Hartog Station. Generous assistance and advice were also provided by the following persons, now deceased: Adgee and Grace Cross of Hamelin Pool post office, Curley Williams of Dirk Hartog Station, Cecil Blood of Tamala Station, Tom and Lurley Pepper of Tamala and Peron Stations, and Mac Hoult of Denham.

References

Aires, T, Marbà, N, Cunha, RL, Kendrick, GA, Walker, DI, Serrão, EA, Duarte, C and Arnaud-Haond, S 2011, Evolutionary history of the seagrass genus *Posidonia*: Marine Ecology Progress Series, v. 421, p. 117–130.

Arakel, AV 1982, Genesis of calcrete in Quaternary soil profiles, Hutt and Leeman Lagoons, Western Australia: Journal of Sedimentary Research, v. 52, p. 109–125.

Attenborough, DF 1979, Life on Earth: William Collins and Sons Co., London, UK, 320p.

Awramik, SM and Vanyo, J 1986, Heliotropism in modern stromatolites: Science, v. 231, p. 1279–1281.

Bastian, LV 1994, The dune systems of the Swan Coastal Plain: subdivision based on mineral trends in the surface soils: Chemistry Centre Western Australia, Report of Investigation, no. 041, 45p.

Bastian, LV 1996, Residual soil mineralogy and dune subdivision, Swan Coastal Plain, Western Australia: Australian Journal of Earth Sciences, v. 43, p. 31–44.

Bastian, LV 2010, Comment on Hearty, PJ and O'Leary, MJ 2008, Carbonate eolianites, quartz sands, and Quaternary sealevel cycles, Western Australia: a chronostratigraphic approach: Quaternary Geochronology, v. 5, p. 76–77.

Batchelor, MT, Burne, RV, Henry, BI and Slatyer, T 2005, Statistical physics and stromatolite growth: new perspectives on an ancient dilemma: Physica A, v. 350, p. 6–11.

Bauld, J 1984, Microbial mats in marginal marine environments: Shark Bay, Western Australia, *in* Microbial mats: stromatolites *edited by* RW Castenholz, Y Cohen and HO Halvorson: Alan R Liss Inc., New York, USA, p. 39–58.

Bauld, J, Chambers, LA and Skyring, GW 1979, Primary productivity, sulfate reduction, and sulfur isotope fractionation in algal mats and sediments of Hamelin Pool, Shark Bay, Western Australia: Australian Journal of Marine and Freshwater Research, v. 30, p. 753–764.

Berry, PF and Playford, PE 1992, Territoriality in a subtropical kyphosid fish associated with macroalgal polygons on reef platforms at Rottnest Island, Western Australia: Journal of the Royal Society of Western Australia, v. 75, p. 67–73.

Berry, PF and Playford, PE 1997, The ecology of *Fragum erugatum* (Mollusca, Bivalvia, Cardiidae) in Shark Bay, Western Australia: Marine and Freshwater Research, v. 48, p. 415–420.

Bierwirth, PN, Lee, TJ and Burne, RV 1992, Shallow water mapping via the separation of depth and substrate components from multispectral data: an example from Useless Inlet, Shark Bay, Western Australia, *in* Proceedings: 6th Australasian Remote Sensing Conference, Wellington, New Zealand, 2–6 November 1992, v. 1, p. 99–109.

Bierwirth, PN, Lee, TJ and Burne, RV 1993, Shallow sea-floor reflectance and water depth derived by unmixing multispectral imagery: Photogrammetric Engineering and Remote Sensing, v. 59, p. 331–338.

Biggs, ER and Denman, PD 1978, Dampier Archipelago limesand and limestone: Geological Survey of Western Australia, Record 1978/6, p. 30.

Bowdler, S 1990, Archaeological research in the Shark Bay region, Western Australia: an introductory account, *in* Research in Shark Bay: report of the France–Australe bicentenary expedition committee *edited by* PF Berry, SD Bradshaw and BR Wilson: Western Australian Museum, Perth, Western Australia, p. 1–12.

Bowdler, S 1995, The excavation of two small rockshelters at Monkey Mia, Shark Bay, Western Australia: Australian Archaeology, v. 40, p. 1–13.

Brooke, B, Creasey, J and Sexton, M 2010, Broad-scale geomorphology and benthic habitats of the Perth coastal plain and Rottnest Shelf, Western Australia, identified in a merged topographic and bathymetric digital relief model: International Journal of Remote Sensing, v. 31, p. 6223–6237.

Brooke, BP, Harris, PT, Nichol, SL, Sexton, J, Hazelwood, M, Arthur, WC, Haese, RR, Heap, AD, Hazelwood, MC and Radke, LC 2012, Living on the edge — waterfront views, *in* Shaping a continent, building a nation: a geology of Australia *edited by* R Blewett: Geoscience Australia and ANU E Press, Canberra, p. 276–331.

Brown, RG and Woods, PJ 1974, Sedimentation and tidal-flat development, Nilemah Embayment, Shark Bay, Western Australia: American Association of Petroleum Geologists, Memoir 22, p. 316–340.

Bryant, EA 2001, Tsunami, the underrated hazard: Cambridge University Press, Melbourne, Victoria, 350p.

Bryant, EA 2008, Tsunami, the underrated hazard (2nd edition): Springer Praxis Books, Chichester, UK, 330p.

Bryant, EA, Walsh, G and Abbott, D 2007, Cosmogenic mega-tsunami in the Australia region: are they supported by Aboriginal and Maori legends?, *in* Myth and geology *edited by* L Piccardi and WB Masse: Geological Society, London, Special Publication 273, p. 203–214.

Burbidge, AA and George, AS 1978, The flora and fauna of Dirk Hartog Island: Journal of the Royal Society of Western Australia, v. 60, p. 71–90.

Burbidge, D and Cummins, PR 2007, Assessing the threat to Western Australia from tsunami generated by earthquakes along the Sunda Arc: Natural Hazards, v. 43 p. 319–331.

Burbidge, D, Cummins, PR, Mleckzo, R and Thio, HK 2008, A probabilistic tsunami hazard assessment for Western Australia: Pure and Applied Geophysics, v. 165 p. 2059–2088.

Bureau of Meteorology 2011, Tropical cyclone information for the Australian region, 1907 to 2006: Bureau of Meteorology, viewed 13 February 2013, <www.bom.gov.au>.

Burling, MC, Pattiaratchi, CB and Ivey, GN 2003, The tidal regime of Shark Bay, Western Australia: Estuarine, Coastal, and Shelf Science, v. 57, p. 725–735.

Burne, RV and Hunt, G (compilers) 1990, The geobiology of Hamelin Pool: research reports of the Baas Becking Geobiological Laboratory's Shark Bay project: Bureau of Mineral Resources, Geology and Geophysics, Record 1990/89, 288p.

Burne, RV and James, N 1986, Subtidal origin of club-shaped stromatolites, Shark Bay, *in* Sediments down-under: 12th International Sedimentological Congress, Canberra, Australian Capital Territory, 24–30 August 1986, Abstracts, p. 49.

Burne, RV, and Johnson, K 2012, Sea-level variation and the zonation of microbialites in Hamelin Pool, Shark Bay, Western Australia: Marine and Freshwater Research, v. 63, p. 994–1004.

Burne, RV and Moore, LS 1987, Miocrobialites: organosedimentary deposits of benthic microbial communities: Palaios, v. 2, p. 241–254.

Burns, BP, Anitori, R, Butterworth, P, Henneberger, R, Goh, F, Allen, MA, Ibañez-Peral, R, Bergquist, PL, Walter, MR and Neilan, BA 2009, Modern analogues and the early history of microbial life: Precambrian Research, v. 173, p. 10–18.

Butcher, BP, Van de Graaff, WJE and Hocking, RM 1984, Shark Bay – Edel, Western Australia: Geological Survey of Western Australia, 1:250 000 Geological Series Explanatory Notes, 21p.

Butler, RJ 1985, The Cape Peron gypsum deposits; report on 1985 drilling programme for Agnew Clough Ltd: Geological Survey of Western Australia, Statutory mineral exploration report, A16267 (unpublished).

Carr, LK, Korsch, RJ, Mory, AJ, Hocking, RM, Marshall, SK, Costelloe, RD, Holzschuh, J and Maher, JL 2012, Structural and stratigraphic architecture of Australia's frontier onshore sedimentary basins: the Western Officer and Southern Carnarvon Basins, Western Australia, *in* Extended abstracts: APPEA oil and gas conference and exhibition, Adelaide, South Australia, 13–16 May 2012, 5p.

Chen, B, Zhongyan, Stephenson, E and Finlayson, B, 2011, Morphodynamics of a boulder beach, Putuo Island, SE China coast: the role of storms and typhoon: Marine Geology, v. 283, p. 106–115.

Chen, M, Schliep, M, Willows, RD, Cai, Z-L, Neilan, BA and Scheer, H 2010, A red-shifted chlorophyll: Science, v. 329, p. 1318–1319.

Chivas, AR, Torgersen, T and Polach, HA 1990, Growth rates and Holocene development of stromatolites from Shark Bay, Western Australia: Australian Journal of Earth Sciences, v. 37, p. 113–121.

Cohen, KM and Gibbard, P 2011, Global chronostratigraphical correlation table for the last 2.7 million years: Subcommission on Quaternary Stratigraphy (International Commission on Stratigraphy), Cambridge, UK.

Courtney, J, Buchan, S, Cerveny RS, Bessemoulin, P, Peterson, TC, Rubiera Torres, JM, Beven, J, King, J, Trewin, B, and Rancourt, K, 2012, Documentation and verification of the world extreme wind gust record:113.3 m s–1 on Barrow Island, Australia, during passage of tropical cyclone Olivia: Australian Meteorological and Oceanographic Journal, v. 62, p. 1–9

Crowe, RWA 1975, The classification, genesis and evolution of sand dunes in the Great Sandy Desert: Geological Survey of Western Australia Annual Report for 1974, p. 46–49.

Dampier, W 1703, A voyage to New Holland etc in the year 1699: printed for James Knapton, at the Crown in St Paul's Church-yard, London, UK, 232p.

David, A 1995, The voyage of HMS Herald to Australia and the South-west Pacific 1852–1861 under the command of Captain Henry Mangles Denham: Miegunyah Press Series, Melbourne University Press, Carlton, Victoria, 521p.

Davies, GR 1970a, Carbonate bank sedimentation, eastern Shark Bay, Western Australia, *in* Carbonate sedimentation and environments, Shark Bay, Western Australia *edited by* BW Logan, GR Davies, JF Read and DE Cebulski: American Association of Petroleum Geologists, Memoir 13, p. 85–168.

Davies, GR 1970b, Algal-laminated sediments, Gladstone Embayment, Shark Bay, Western Australia, *in* Carbonate sedimentation and environments, Shark Bay, Western Australia *edited by* BW Logan, GR Davies, JF Read and DE Cebulski: American Association of Petroleum Geologists, Memoir 13, p. 169–205.

Davies, GR and Sherwin, MD 1997, Productive dolomitized coquina facies of the Lower Triassic Montney Formation, Western Canada Sedimentary Basin, *in* Sedimentary events, hydrocarbon systems: core conference guidebook *edited by* J Wood and B Martindale: Canadian Society of Petroleum Geologists and SEPM Joint Convention, Calgary, Canada, 5–6 June 1997, p. 257–276.

Denman, PD, Hocking, RM, Moore, PS, Williams, IR and Van de Graaff, WJE 1985, Wooramel, Western Australia (2nd edition): Geological Survey of Western Australia, 1:250 000 Geological Series Explanatory Notes, 23p.

Dominey-Howes, D 2007, Geological and historical records of tsunami in Australia: Marine Geology, v. 239, p 99–123

Donaldson, M 2010, Burrup rock art: ancient Aboriginal rock art of the Burrup Peninsula and Dampier Archipelago, Western Australia: Wildrocks Publications, Mount Lawley, Western Australia, 516p.

Edwards, H 1999, Shark Bay through four centuries, 1616 to 2000: a world heritage area: Scott Four Colour Print, Perth, Western Australia for Shark Bay Shire, 415p.

Environmental Protection Authority 2005, Coburn mineral sand project; Gunson Resources Limited, report and recommendations of the Environmental Protection Authority: Western Australia Environmental Protection Authority, Bulletin 1211, 175p.

Fichaut, B, and Suanez, S 2011, Quarrying, transport and deposition of cliff-top storm deposits during extreme events: Banneg Island, Brittany: Marine Geology, v. 283, p. 36–55.

Fischer, AG 1965, Fossils, early life, and atmospheric history: Proceedings of the National Academy of Sciences, v. 53, p 1205–1215.

Flannery, DT and Walter, MR 2011, Archean tufted microbial mats and the Great Oxidation Event: new insights into an ancient problem: Australian Journal of Earth Sciences, v. 59, p. 1–11.

Flint, DJ and Abeysinghe, A 2000, Geology and mineral resources of the Gascoyne region: Geological Survey of Western Australia, Record 2000/7, 29p.

Gibbard, P and Van Kolfschoten, T 2005, The Pleistocene and Holocene Series, *in* A geologic time scale 2004 *edited by* FM Gradstein, JG Ogg and AG Smith: Cambridge University Press, Cambridge, UK, p. 441–452.

Glikson, AY, Eggins, S, Golding, SD, Haines, PW, Iasky, RP, Mernagh, TP, Mory, AJ, Pirajno, F and Uysal, IT, 2005a, Microchemistry and microstructures of hydrothermally altered shock-metamorphosed basement gneiss, Woodleigh impact structure, Southern Carnarvon Basin, Western Australia: Australian Journal of Earth Sciences, v. 52, p. 555–573.

Glikson, AY, Mory, AJ, Iasky, RP, Pirajno, F, Golding, SD and Uysal, IT 2005b, Woodleigh, Southern Carnarvon Basin, Western Australia: history of discovery, Late Devonian age, and geophysical and morphometric evidence for a 120 km-diameter impact structure: Australian Journal of Earth Sciences, v. 52, p. 545–553.

Godard, P 1993, The first and last voyage of the Batavia: Abrolhos Publishing Company, Perth, Western Australia, 332p.

Godard, P and de Kerros, T 2002, Louis de Saint Aloüarn: lieutenant des vaisseaux du roy: un marin breton à la conquête des terres australes: Saint-Jacques-de-la-Lande, Portes du Larges, Rennes, France, 362p.

Goh, F, Leuko, S, Allen, MA, Bowman, JP, Kamekura, M, Neilan, BA and Burns, BP 2006, *Halococcus hamelinensis* sp. nov., a novel halophilic archaeon isolated from stromatolites in Shark Bay, Australia: International Journal of Systematic and Evolutionary Microbiology, v. 56, p. 1323–1329.

Golubic, S 1976, Organisms that build stromatolites, *in* Stromatolites (Developments in Sedimentology, v. 20) *edited by* MR Walter: Elsevier, Amsterdam, The Netherlands, p. 113–126.

Golubic, S 1982, Microbial ecology of algal mats and recent stromatolites in Shark Bay, Western Australia: National Geographic Society, Research Reports, v. 14, p. 277–286.

Golubic, S 1983, Stromatolites, fossil and recent, a case history, *in* Biomineralization and biological metal accumulation *edited by* P Westbroek and EW Jong: D Reidel Publishing, Dordrecht, The Netherlands, p. 313–326.

Golubic, S 1985, Microbial mats and modern stromatolites in Shark Bay, Western Australia, *in* Planetary Ecology *edited by* DE Caldwell, JA Brierley and CL Brierley: Van Nostrand Reinhold Co., New York, USA, p. 3–16.

Goto, K, Miyagi, K, Kawana, T and Imamura, F 2011, Emplacement and movement of boulders by known storm waves — field evidence from the Okinawa Islands, Japan: Marine Geology, v 283, p. 66–78.

GPX Surveys 2012, Airborne Geophysical Survey, Carnarvon Basin South, Western Australia, published by Geological Survey of Western Australia, 2013: www.dmp.wa.gov.au/documents/2438_GA_Carnarvon_Basin_South_Logistics_Report_ga.pdf.

Graham-Taylor, S 2012, Shark Bay pastoral voices: Western Australian Museum and Shire of Shark Bay, Denham, Western Australia, 376p.

Green, J 2007, Report on the 2006 Western Australian Museum, Department of Marine Archaeology, Cape Inscription National Heritage listing archaeological survey: Western Australian Museum, Department of Maritime Archaeology, Special Publication 10, 259p.

Grey, G 1841, Journals of two expeditions of discovery in north-west and western Australia during the years 1837, 38, and 39: T and W Boone, New Bond Street, London.

Grotzinger, JP and Rothman, DH 1996, An abiotic model for stromatolite morphogenesis: Nature, v. 383, p. 423–425.

Gunson Resources Limited 2012, Coburn Project — purchase of Hamelin Pastoral lease: Report to Australian Securities Exchange, 13 March 2012, 2p.

Hagan, GM and Logan, BW 1974a, Development of carbonate banks and hypersaline basins, Shark Bay, Western Australia: American Association of Petroleum Geologists, Memoir 22, p. 61–139.

Hagan, GM, and Logan, BW 1974b, History of Hutchison Embayment tidal flat, Western Australia, *in* Evolution and diagenesis of Quaternary carbonate sequences, Shark Bay, Western Australia *edited by* Logan, BW, Read, JF, Hagan, GM, Hoffman, P, Brown, RG, Woods, PJ and Gebelein, CD: American Association of Petroleum Geologists, Memoir 22, p. 283–315.

Haig, DW and Mory, AJ 2003, New record of siliceous, marine, later Eocene, from Kalbarri, Western Australia: Journal of the Royal Society of Western Australia, v. 86, p. 107–113.

Hall, AM 2011, Storm wave currents, boulder movement and shore platform development: a case study from East Lothian, Scotland: Marine Geology, v. 283, p. 98–105.

Hancock, DA 1989, A review of the Shark Bay pearling industry: Department of Fisheries, Western Australia, Fisheries Management Paper no. 27.

Harley, D 2004, Coburn mineral sand project bankable feasibility study progress report; Gunson Resources Limited: report to Australian Securities Exchange, 8 April 2004, 5p.

Harley, D 2008, Coburn Project — mineralogy, next CTIEC visit, and ore reserves; Gunson Resources Limited: report to Australian Securities Exchange, 18 April 2008, 3p.

Hearty, PJ 2003, Stratigraphy and timing of eolianite deposition on Rottnest Island, Western Australia: Quaternary Research, v. 60, p. 211–222.

Hearty, PJ and O'Leary, MJ 2008, Carbonate eolianites, quartz sands, and Quaternary sea-level cycles, Western Australia: a chronostratigraphic approach: Quaternary Geochronology v. 3, p. 26–55.

Hearty, PJ and O'Leary, MJ 2010, Reply to Bastian, LV's comment on Hearty, PJ and O'Leary, MJ 2008, carbonate eolianites, quartz sands, and Quaternary sealevel cycles, Western Australia: a chronostratigraphic approach: Quaternary Geochronology v. 3, p. 26–55: Quaternary Geochronology, v. 5, p. 78–81.

Heeres, JE 1899, The part borne by the Dutch in the discovery of Australia, 1606–1765: Lusac and Co., London, UK, and EJ Brill, Leiden, The Netherlands, 106p.

Hocking, RM 1990 Field guide for the Carnarvon Basin: Geological Survey of Western Australia, Record 1990/11, 74p.

Hocking, RM 2000, Geology of the southern Carnarvon Basin, Western Australia — a field guide: Geological Survey of Western Australia, Record 2000/10, 102p.

Hocking, RM, Moors, HT and Van de Graaff, WJE 1987, Geology of the Carnarvon Basin, Western Australia: Geological Survey of Western Australia, Bulletin 133, 289p.

Hodgkin, EF and Di Lolo, V 1958, The tides of south-western Australia: Journal of the Royal Society of Western Australia, v. 41, p. 42–54.

Hoffman, PF 1974, Shallow and deepwater stromatolites in an Early Proterozoic platform-to-basin facies change, Great Slave Lake, Northwest Territories: American Association of Petroleum Geologists, Bulletin 58, p. 856–867.

Hoffman, PF 1976, Stromatolite morphogenesis in Shark Bay, Western Australia, *in* Stromatolites (Developments in Sedimentology, v. 20) *edited by* MR Walter: Elsevier, Amsterdam, The Netherlands, p. 261–271.

Hordern, MC 1997, King of the Australian coast: the work of Phillip Parker King in the Mermaid and Bathurst: Melbourne University Press, Carlton, Victoria, 441p.

Iasky, RP and Mory, AJ 1999, Geology and petroleum potential of the Gascoyne Platform, Southern Carnarvon Basin, Western Australia: Geological Survey of Western Australia, Report 69, 46p.

Iasky, RP, D'Ercole, C., Ghori, KAR, Mory, AJ and Lockwood, AM 2003, Structure and petroleum prospectivity of the Gascoyne Platform, Western Australia: Geological Survey of Western Australia, Report 87, 56 p.

Imamura, F, Goto, K and Ohkubo, S 2008, A numerical model for the transport of a boulder by tsunami: Journal of Geophysical Research: Oceans, v. 113, no. C1, DOI: 10.1029/2007JC004170.

Izuno, G 2012, Holocene-recent paleosalinity reconstruction of Hamelin Pool, Western Australia, using bivalve morphology (*Fragum erugatum*); significance for stromatolite formation conditions: Journal of Geography, v. 121, p. 998–1009, and p. xiii (text in Japanese).

Jahnert, RJ and Collins, LB 2011, Significance of subtidal microbial deposits in Shark Bay, Australia: Marine Geology, v. 286, p. 106–111.

Jahnert, RJ and Collins, LB 2012, Characteristics, distribution, and morphogenesis of subtidal microbial systems in Shark Bay, Western Australia: Marine Geology, v. 303–306, p. 115–136.

Jahnert, R, de Paula, O, Collins, L, Strobach, E, and Pevzner, R 2012, Evolution of a coquina barrier in Shark Bay, Australia by GPR imaging: Architecture of a Holocene reservoir analog: Sedimentary Geology, v. 281, p. 59–74.

Johnstone, D and Playford, PE 1955, Geology of the Shark Bay – Murchison River area, Carnarvon Basin; West Australian Petroleum Pty Ltd: Geological Survey of Western Australia, open-file report, G775 A1 (unpublished).

Jones, DC 1994, Gypsum deposits of Western Australia: Geological Survey of Western Australia, Record 1993/5, 141p.

Jones, T, Middelmann, M and Corby, N 2005, Appendix E: On tsunami hazard in Western Australia, *in* Natural hazard risk in Perth, Western Australia *compiled by* T Jones, M Middelmann and N Corby: Geoscience Australia, Canberra, Australian Capital Territory, p. 345–352.

Keep, M, Hengesh, J and Whitney, B 2012, Natural seismicity and tectonic geomorphology reveal regional transpressive strain in northwestern Australia: Australian Journal of Earth Sciences, v. 59, p. 341–354.

Kendrick, GA, Walker, DI and McComb, AJ 1988, Changes in distribution of macro-algal epiphytes on stems of the seagrass Amphibolis antarctica along a salinity gradient in Shark Bay, Western Australia: Phycologia, v. 27, p. 201–208.

Kendrick, GW 1990, A Pleistocene molluscan fauna with *Anadara trapezia* (Deshayes) (Bivalvia: Arcoida) from the Dampier Limestone of Shark Bay, Western Australia, *in* Research in Shark Bay: report of the France–Australe bicentenary expedition committee *edited by* PF Berry, SD Bradshaw and BR Wilson: Western Australian Museum, Perth, Western Australia, p. 33–48.

Kendrick, GW, Wyrwoll, KH and Szabo, BJ 1991, Pliocene–Pleistocene coastal events and history along the western margin of Australia: Quaternary Science Reviews, v. 10, p. 419–439.

Kennard, JM and James, NP 1986, Thrombolites and stromatolites: two distinct types of microbial structures: Palaios, v. 1, p. 492–503.

Knight, J, and Burningham, H 2011, Boulder dynamics on an Atlantic-facing rock coastline, northwest Ireland: Marine Geology, v. 283, p. 56–65.

Lipar, M 2009, Pinnacle syngenetic karst in Nambung National Park, Western Australia: Acta Carsologica, v. 38, p. 41–50.

Lockwood, AM and D'Ercole, C 2003, Geophysical investigation of the Bernier Ridge and surrounding area, Southern Carnarvon Basin, Western Australia: Geological Survey of Western Australia, Report 89, 53 p.

Logan, BW 1959, Environments, foraminiferal facies, and sediments of Shark Bay, Western Australia: The University of Western Australia, Perth, Western Australia, PhD thesis, 287p (unpublished).

Logan, BW 1961, *Cryptozoon* and associate stromatolites from the Recent, Shark Bay, Western Australia: Journal of Geology, v. 69, p. 517–533.

Logan, BW 1968, Western Australia, *in* Quaternary shoreline research in Australia and New Zealand *edited by* ED Gill: Australian Journal of Science, v. 31, p. 110.

Logan, BW 1974, Inventory of diagenesis in Holocene–Recent carbonate sediments, Shark Bay, Western Australia, *in* Evolution and diagenesis of Quaternary carbonate sequences, Shark Bay, Western Australia *edited by* BW Logan, JF Read, GM Hagan, P Hoffman, RG Brown, PJ Woods and CD Gebelein: American Association of Petroleum Geologists, Memoir 22, p. 195–249.

Logan, BW and Cebulski, DE 1970, Sedimentary environments of Shark Bay, Western Australia, *in* Carbonate sedimentation and environments, Shark Bay, Western Australia *edited by* BW Logan, GR Davies, JF Read and DE Cebulski: American Association of Petroleum Geologists, Memoir 13, p. 1–37.

Logan, BW and Chase, RL 1961, The stratigraphy of the Moora Group, Western Australia: Journal of the Royal Society of Western Australia, v. 44, p. 14–31.

Logan, BW, Davies, GR, Read, JF and Cebulski, DE 1970a, Carbonate sedimentation and environments, Shark Bay, Western Australia: American Association of Petroleum Geologists, Memoir 13, 223p.

Logan, BW, Hoffman, P, and Gebelein, CD 1974a, Algal mats, cryptalgal fabrics and structures, Hamelin Pool, Western Australia, *in* Evolution and diagenesis of Quaternary carbonate sequences, Shark Bay, Western Australia *edited by* BW Logan, JF Read, GM Hagan, P Hoffman, RG Brown, PJ Woods and CD Gebelein: American Association of Petroleum Geologists, Memoir 22, p. 140–194.

Logan, BW, Read, JF and Davies, GR 1970b, History of carbonate sedimentation, Quaternary Epoch, Shark Bay, Western Australia, *in* Carbonate sedimentation and environments, Shark Bay, Western Australia *edited by* BW Logan, GR Davies, JF Read and DE Cebulski: American Association of Petroleum Geologists, Memoir 13, p 38–84.

Logan, BW, Read, JF, Hagan, GM, Hoffman, P, Brown, RG, Woods, PJ and Gebelein, CD 1974b, Evolution and diagenesis of Quaternary carbonate sequences, Shark Bay, Western Australia: American Association of Petroleum Geologists, Memoir 22, 358p.

Logan, BW, Rezak, R and Ginsburg, RN 1964, Classification and environmental significance of stromatolites: Journal of Geology, v. 72, p. 68–83.

Lorang, MS 2011, A wave-competence approach to distinguish between boulder and megaclast deposits due to storm waves versus tsunamis: Marine Geology, v. 283, p. 90–97.

Marsh, LM and Slack-Smith, SM 2010, Field guide to sea stingers: Western Australian Museum, Perth, 248p.

Mather, S 2011, Faure Island: a shorebird haven: Landscope, v. 26, no. 4, p. 32–38.

Mayer, W 2012, Early geological investigations of the Pleistocene Tamala Limestone, Western Australia: Geological Society, London, Special Publications, v. 301, p. 279–293.

McKenna, J, Jackson, DWT, and Cooper, AG 2011, In situ exhumation from bedrock of large rounded boulders at the Giant's Causeway, Northern Ireland: an alternative genesis for large shore boulders (mega-clasts): Marine Geology, v. 283, p. 25–35.

McNamara, KJ 1992, Stromatolites: Western Australian Museum, Perth, Western Australia, 25p.

McNamara, KJ 2009, Pinnacles: Western Australian Museum, Perth, Western Australia, 64p.

Meischner, D 1994, Stromatolites in Shark Bay, Western Australia: interglacial and subtidal origins, *in* Death Valley International Stromatolite Symposium, Laughlin, Nevada, USA *edited by* SM Awramik: Abstract with Program, p. 47.

Monty, CLV 1965, Recent algal stromatolites in the Windward Lagoon, Andros Island, Bahamas: Annales de la Société Géologique de Belgique, v. 90, p. 585–624.

Morse, K 1988, An archaeological survey of midden sites near the Zuytdorp wreck, Western Australia: Australian Institute for Maritime Archaeology Bulletin, v. 12, p. 37–40.

Morton, B 2000, The biology and functional morphology of *Fragum erugatum* (Bivalvia: Cardiidae) from Shark Bay, Western Australia: the significance of its relationship with entrained zooxanthellae: Journal of Zoology, v. 251, p. 39–52.

Mory, AJ 1994, Geology of the Hill River – Green Head 1:100 000 sheets: Geological Survey of Western Australia, 1:100 000 Geological Series Explanatory Notes, 30p.

Mory, AJ, Haig, DW, McLoughlin, S and Hocking, RM 2005, Geology of the northern Perth Basin, Western Australia — a field guide: Geological Survey of Western Australia, Record 2005/9, 71p.

Mory, AJ, Iasky, RP and Ghori, KAR 2003, A summary of the geological evolution and petroleum potential of the southern Carnarvon Basin, Western Australia: Geological Survey of Western Australia, Report 86, 26p.

Mory, AJ, Iasky, RP, Glikson, AY and Pirajno, F 2000, Woodleigh, Carnarvon Basin, Western Australia: a new 120 km diameter impact structure: Earth and Planetary Science Letters, v. 177, p. 119–128.

Moss, LR 1996, Hamelin Pool Common Management Plan: Shire of Shark Bay, 43 p.

Nandasena, NAK, Paris, R and Tanaka, N 2011, Reassessment of hydrodynamic equations: minimum flow velocity to initiate boulder transport by high energy events (storms, tsunamis): Marine Geology, v. 281, p. 70–84.

Newsome, D 2000, Origin of sandplains in Western Australia: a review of the debate and some recent findings: Australian Journal of Earth Sciences, v. 47, p. 695–706.

NHK 1987, The Miracle Planet: (Manga book, in Japanese) Shogakukan Publishing, Tokyo, Japan, 175p.

Nott, J 2003a, Tsunami or storm waves? — determining the origin of a spectacular field of wave-emplaced boulders using numerical storm surge and wave models and hydrodynamic transport equations: Journal of Coastal Research, v. 19, p. 348–356.

Nott, J 2003b, Waves, coastal boulder deposits, and the importance of pre-transport settings: Earth and Planetary Science Letters, v. 210, p. 269–276.

Nott, J 2004, The tsunami hypothesis — comparisons of the field evidence against the effects on the Western Australian coast of some of the most powerful storms on earth: Marine Geology, v. 208, p. 1–12.

Nott, J 2011, A 6000 year cyclone record from Western Australia: Quaternary Science Reviews, v. 30, p. 713–722.

Nott, J and Bryant, E 2003, Extreme marine inundations (tsunamis?) of coastal Western Australia: Journal of Geology, v. 111, p. 691–706.

O'Leary, MJ, Hearty, PJ and McCulloch, MT 2008, U-series evidence for widespread reef development in Shark Bay during the last interglacial: Palaeogeography, Palaeoclimatology, Palaeocology, v. 259, p. 424–435.

Paris R, Lavigne, F, Wassmer, P, and Sartohadi, J 2007, Coastal sedimentation associated with the December 26, 2004, tsunami in Lhok Nga, west Banda Ache (Sumatra, Indonesia): Marine Geology, v. 238, p. 93–106.

Paris, R, Naylor, LA, and Stephenson, WJ 2011, Boulders as a signature of storms on rock coasts: Marine Geology, v. 283, p. 1–11.

Pendal, PG 1994, Select Committee on Ancient Shipwrecks: State Law Publisher, Western Australia Legislative Assembly report, 44p.

Pietsch, T and Olley, J 2005a, Report on the optical dating of sediment samples from Perth and Womerangee, *supplied by* Brendan Brooke [collected by P Haines and B Brook]: Report to Geoscience Australia and the Geological Survey of Western Australia (unpublished).

Pietsch, T and Olley, J 2005b, Report on the optical dating of sediment samples from Rottnest Island, *supplied by* Brendan Brooke [collected by P Haines and PE Playford]: Report to Geoscience Australia and the Geological Survey of Western Australia (unpublished).

Pillans, B, Chappell, J and Naish, TR 1998, A review of the Milankovitch climatic beat: template for Plio–Pleistocene sea-level changes and sequence stratigraphy: Sedimentary Geology, v. 122, p. 5–21.

Playford, PE 1956, Notes on the tectonic history of the Rough Range Structure, based on a study of Rough Range South No. 5 Test; West Australian Petroleum Pty Ltd: Geological Survey of Western Australia, Statutory petroleum exploration report, S1366 A1 (unpublished).

Playford, PE 1959, The wreck of the Zuytdorp on the Western Australian coast in 1712: Journal and Proceedings of the Western Australian Historical Society, v. 5, part 5, p. 5–41.

Playford, PE 1972, Algal stromatolites in the Devonian of the Canning Basin, Western Australia: Annales de la Société Géologique de Belgique, v. 95, p. 401–402.

Playford, PE 1979, Stromatolite research in Western Australia: Journal of the Royal Society of Western Australia, v. 62, p. 13–20.

Playford, PE 1980a, Environmental controls on the morphology of modern stromatolites at Hamelin Pool, Western Australia: Geological Survey of Western Australia, Annual Report for 1979, p. 73–77.

Playford, PE 1980b, Australia's stromatolite stronghold: Natural History, v. 89, no. 10, p. 58–61.

Playford, PE 1988, Guidebook to the Geology of Rottnest Island: Geological Society of Australia and Geological Survey of Western Australia, Perth, Western Australia, 67 p.

Playford, PE 1990, Geology of the Shark Bay area, Western Australia, *in* Research in Shark Bay: report of the France–Australe bicentenary expedition committee *edited by* PF Berry, SD Bradshaw and BR Wilson: Western Australian Museum, Perth, Western Australia, p. 13–31.

Playford, PE 1993, Tourist access to stromatolites and shell deposits at Hamelin Pool: Department of Conservation and Land Management (Western Australia), Report, 31p (unpublished).

Playford, PE 1996, Carpet of silver, the wreck of the Zuytdorp: University of Western Australia Press, Nedlands, Western Australia, 260p.

Playford, PE 1997, Geology and hydrogeology of Rottnest Island, Western Australia, *in* Geology and hydrogeology of carbonate islands (Developments in Sedimentology, v. 54) *edited by* LH Vacher and TM Quinn: Elsevier, Amsterdam, The Netherlands, p. 783–810.

Playford, PE 1998, Voyage of Discovery to Terra Australis by Willem de Vlamingh in 1696–97: Western Australian Museum, Perth, Western Australia, 113p.

Playford, PE, 2003, Quaternary tectonism in the Carnarvon Basin Western Australia: Geological Society of Australia, Structural Geology and Tectonics Specialist Group, Abstracts v. 72, p. 89.

Playford, PE 2005, Hartog, Dirk (1580–1621), *in* Australian Dictionary of Biography, supplement 1580–1980, with a name index to the Australian dictionary of biography to 1980 *edited by* C Cunneen: Melbourne University Press, Melbourne, Victoria, p. 167–168.

Playford, PE 2012, Western Australia's mega-tsunami of 3000 years BP, in Unearthing our past and future — resourcing tomorrow: 34th International Geological Congress, Brisbane, Queensland, 5–10 August 2012, Congress handbook.

Playford, PE 2013, Recent mega-tsunamis in the Shark Bay, Pilbara, and Kimberley areas of Western Australia: Western Wildlife, v. 17, no.4, p. 1, 4, 5.

Playford, PE and Berry, PF 2002, Preliminary report on the geology of Faure Island; Geological Survey of Western Australia and Western Australian Museum: report to Australian Wildlife Conservancy (unpublished).

Playford, PE and Chase, RL 1955, Report on a geological reconnaissance of Dirk Hartog Island; West Australian Petroleum Pty Ltd; Geological Survey of Western Australia, Statutory petroleum exploration report, S776 A1 (unpublished).

Playford, PE and Cockbain, AE 1969, Algal stromatolites: deepwater forms in the Devonian of Western Australia: Science, v. 165, p. 1008–1010.

Playford, PE and Cockbain, AE 1976, Modern algal stromatolites at Hamelin Pool, a hypersaline barred basin in Shark Bay, Western Australia, *in* Stromatolites (Developments in Sedimentology, v. 20) *edited by* MR Walter: Elsevier, Amsterdam, The Netherlands, p. 389–411.

Playford, PE, Cockbain, AE, Druce, EC and Wray, JL1976a, Devonian stromatolites from the Canning Basin, Western Australia, *in* Stromatolites (Developments in Sedimentology, v. 20) *edited by* MR Walter: Elsevier, Amsterdam, The Netherlands, p. 543–564.

Playford, PE, Cockbain, AE and Lowe, GH 1976b, Geology of the Perth Basin, Western Australia: Geological Survey of Western Australia, Bulletin 124, 311p.

Playford, PE, Hocking, RM and Cockbain, AE 2009, Devonian reef complexes of the Canning Basin, Western Australia: Geological Survey of Western Australia Bulletin 145, 444p.

Playford, PE and Johnstone, MH 1959, Oil exploration in Australia: Bulletin of the American Association of Petroleum Geologists, v. 43, p. 397–433.

Prendergast, AL and Brown, N 2012, Far field impact and coastal sedimentation associated with the 2006 Java tsunami in West Australia: Post-tsunami Survey at Steep Point, Western Australia: Natural Hazards, v. 60, p. 69–79.

Price, DM, Brooke, BP and Woodroffe, CD 2001, Thermoluminescence dating of eolianites from Lord Howe Island and south-west Western Australia: Quaternary Science Reviews, v. 20, p. 841–846.

Read, JF 1974, Calcrete deposits and Quaternary sediments, Edel Province, Shark Bay, Western Australia, *in* Evolution and diagenesis of Quaternary carbonate sequences, Shark Bay, Western Australia *edited by* BW Logan, JF Read, GM Hagan, P Hoffman, RG Brown, PJ Woods and CD Gebelein: American Association of Petroleum Geologists, Memoir 22, p. 250–282.

Read, JF 1976, Calcretes and their distinction from stromatolites, *in* Stromatolites (Developments in Sedimentology, v. 20) *edited by* MR Walter: Elsevier, Amsterdam, The Netherlands, p 55–71.

Reid, RP, James, NP, Macintyre, IG, Dupraz, CP and Burne, RV 2003, Shark Bay stromatolites: microfabrics and reinterpretation of origins: Facies, v. 49, p. 299–324.

Richards, JD and Wilson, B 2008, A biological survey of Faure Island, Shark Bay World Heritage property, Western Australia: Records of the Western Australian Museum Supplement, no. 75, 75p.

Richmond, BM, Watt, S, Buckley, M, Jaffe, BE, Gelfenbaum, G and Morton, RA 2011, Recent storm and tsunami coarse-clast deposit characteristics, southeast Hawaii: Marine Geology, v. 283, p. 79–89.

Ride, WDL, Mees, GF, Douglas, AM, Royce, RD and Tyndale-Biscoe, CH 1962, The results of an expedition to Bernier and Dorre islands, Shark Bay, Western Australia: Department of Fisheries, Western Australia, Fauna Bulletin, no. 2, 129p.

Riding, R 1999, The term stromatolite: towards an essential definition: Lethaia, v. 32, p. 321–330.

Saint-Smith, EC 1912, A geological reconnaissance of a portion of the South-West Division of Western Australia: Geological Survey of Western Australia, Bulletin 44, 80p.

Saville-Kent, W 1897, The Naturalist in Australia: Chapman & Hall Ltd, London, UK, 302p.

Scheffers, SR, Scheffers, A, Kelletat, D and Bryant, EA 2008, The Holocene paleo-tsunami history of West Australia: Earth and Planetary Science Letters, v. 270, p. 137–146.

Scheffers, A, Kelletat, D, Haslett, S, Sander, S, Scheffers, SR and Brown, T 2010, Coastal boulder deposits in Galway Bay and the Aran Islands, western Ireland, Zeitschrift für Geomorphologie v. 54, Suppl. 3, p. 247–279.

Shulmeister, J, Goodwin, I, Renwick, J, Harle, K, Armand, L, McGlone, MS, Cook, E, Dodson, J, Hesse, PP, Mayewski, P and Curran, M 2004, The Southern Hemisphere westerlies in the Australasian sector during the last glaciation cycle: a synthesis: Quaternary International, v. 118–119, p. 23–53.

Siddall, M, Chappell, J and Potter, E-K 2006, Eustatic sea level during past interglacials, *in* The climate of past interglacials *edited by* F Sirocko, T Litt, M Claussen and M-F Sanchez-Goni: Elsevier, Amsterdam, The Netherlands, p. 75–92.

Skyring, GW and Bauld, J 1990, Microbial mats in Australian coastal environments: Advances in Microbial Ecology, v. 11, p. 461–498.

Smith, AJ, Massuel, S and Pollock, DW 2011, Geohydrology of the Tamala Limestone formation in the Perth region: origin and role of secondary porosity: CSIRO, Water for a Healthy Country National Research Flagship Report, 63p.

Stephenson, WJ and Naylor, LA 2011, Geological controls on boulder production in a rock coast setting: insights from South Wales, UK: Marine Geology, v. 283, p. 12–24.

Stirling, CH, Esat, TM, McCulloch, MT and Lambeck, K 1995, High-precision U-series dating of corals from Western Australia and implications for the timing and duration of the Last Interglacial: Earth and Planetary Science Letters, v. 135, p. 115–130.

Stirling, CH, Esat, TM, Lambeck, K and McCulloch, MT 1998, Timing and duration of the Last Interglacial: evidence for a restricted interval of widespread coral growth: Earth and Planetary Science Letters, v. 160, p. 745–762.

Szabo, BJ 1979 Uranium-series age of coral reef growth on Rottnest Island, Western Australia: Marine Geology, v. 29, p. M11–M15.

Tapsell, P, Newsome, D and Bastian, L 2003, Origin of yellow sand from Tamala Limestone on the Swan Coastal Plain, Western Australia: Australian Journal of Earth Sciences, v. 50, p. 331–342.

Van de Graaff, WJE 1980, Transportation patterns of Aboriginal artifacts in the Shark Bay area, Western Australia: Journal of the Royal Society of Western Australia, v. 63, p. 1–3.

Van de Graaff, WJE, Denman, PD and Hocking, RM 1976, Emerged Pleistocene marine terraces on Cape Range, Western Australia: Geological Survey of Western Australia, Annual Report for 1975, p. 62–70.

Van de Graaff, WJE, Hocking, RM and Butcher, BP 1983, Yaringa, Western Australia: Geological Survey of Western Australia, 1:250 000 Geological Series Explanatory Notes, 23p.

Veeh, HH, Schwebel, D, Van de Graaff, WJE, and Denman, PD, 1979, Uranium-series ages of coralline terrace deposits in Western Australia: Journal of the Geological Society of Australia, v. 26, p. 285–292.

Walter, MR and Bauld, J 1986, Subtidal stromatolites of Shark Bay, *in* Sediments down-under: 12th International Sedimentological Congress, Canberra, Australian Capital Territory, 24–30 August 1986, Abstracts, p. 315.

Wright, VP and Tucker, ME (editors) 1991, Calcretes (International Association of Sedimentologists Reprint Series, v. 2): Blackwell, Oxford, UK, 352p.

About the authors

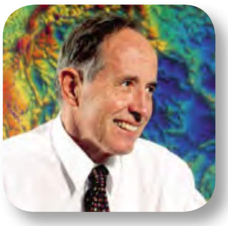

Phillip Playford was born in Western Australia. He was awarded BSc (Hons) and honorary DSc degrees by The University of Western Australia, and a PhD by Stanford University, which he attended with Fulbright and Hackett Scholarships. He has worked for the Western Australian and Federal Governments, and the petroleum-exploration industry, and is a former Director of GSWA and Assistant Director-General of Mines. His principal geological research has been in the Canning Basin (on Devonian reefs), Shark Bay, and the Perth Basin. Honours received include: Member of the Order of Australia (AM); Fellow of the Australian Academy of Technological Science and Engineering; Lewis G Weeks Gold Medal of the Australian Petroleum Production and Exploration Association; Medal and Honorary Member of the Royal Society of Western Australia; Gibb Maitland Medal and Fellow of the Geological Society of Australia; Special Commendation Award of the American Association Petroleum Geologists; Distinguished Honorary Member of the Petroleum Exploration Society of Australia; and Honorary Member of the National Trust (Western Australia). He is currently an Honorary Associate of GSWA and the Western Australian Museum.

Anthony (Tony) Cockbain was born in Warrington, England, and educated at the Boteler Grammar School and the University of Nottingham, where he obtained BSc (Hons) and PhD degrees. He has worked in universities (University of British Columbia Institute of Oceanography, University of Canterbury, New Zealand), geological surveys (Cyprus, Western Australia), and (briefly) in industry. In the Shark Bay study he mainly worked on the stromatolites of Hamelin Pool. After retiring as Assistant Director of GSWA in 1993, he became Editor of the Australian Journal of Earth Sciences, holding that position for 17 years on behalf of the Geological Society of Australia, for which he was awarded the Society's WR Browne Medal in 2010; he became Editor-in-Chief of the Journal of the Royal Society of Western Australia in 2012.

Patrick (Paddy) Berry was born in Johannesburg, South Africa, where he went to school at St John's College. He obtained BSc (Hons), MSc, and PhD degrees at the University of Natal. He worked at the Oceanographic Research Institute, Durban, as Research Officer, Principal Research Officer, and Acting Director. In 1980, he migrated to Perth with his family to become Director of Natural Science at the Western Australian Museum. He has published over 40 research papers, mainly in the field of marine ecology, and led the Western Australian Museum team on most of its tropical reef surveys of the Kimberley region, and Christmas and Cocos Islands. He retired in 2004, and remains an Honorary Associate of the Museum.

Anthony (Tony) Roberts was born in Wellington, New Zealand, and obtained a BSc (Hons) degree from The University of Queensland and a PhD from the Australian National University. He has conducted postdoctoral research at the University of Oxford, and as a Fulbright Fellow at Princeton University and the US National Institute of Standards and Technology. He is currently an Associate Professor of Mathematics at The University of Queensland. His research focuses on microstructure-property relationships in porous materials, fractals, and optimal bone implants. The analyses of Shark Bay tidal records presented in this Bulletin are mathematically analogous to a method of characterizing porous structure.

Peter Haines was born in the Northern Territory, and obtained BSc (Hons) and PhD degrees in geology from the University of Adelaide. He has worked for the Geological Surveys of the Northern Territory and Western Australia, and universities (South Australia, Adelaide, and Tasmania). His geological research has involved sedimentary basins ranging in age from Quaternary to Paleoproterozoic, and has included work on impact structures and ejecta horizons in the sedimentary record. He is a member of the Geological Society of Australia, Petroleum Exploration Society of Australia, American Geophysical Union, and the Meteoritical Society. He was presented with the Stillwell Award for best paper in the Australian Journal of Earth Sciences in 2001. Having joined GSWA in 2003, he currently works on Neoproterozoic to Phanerozoic basins and petroleum prospectivity as part of the Basins and Energy Geoscience group.

Brendan Brooke was born in New South Wales, and has a PhD in Geoscience from the University of Wollongong. His area of expertise is marine and coastal geomorphology, especially coastal sedimentary systems, Quaternary coastal evolution, and the influence of seabed geomorphology on the distribution of benthic habitats and communities. He has led a number of university- and government-based multidisciplinary teams focusing on strategic management of Australia's marine and coastal environments. Currently, he leads the Coastal Marine and Climate Change Group at Geoscience Australia, a team of marine and coastal scientists focused on the marine environmental-information needs of the Australian Government.

Index

Shark Bay is an area of major interest to geologists, historians, and members of the general public. The natural attributes of the area are of major international importance, hence its designation as a World Heritage Area.

Major features

Details of five decades of research on Shark Bay, focusing especially on:

- world-renowned stromatolites of Hamelin Pool
- complex sand dunes, delineated by Digital Elevation Modelling (DEM)
- mega-tsunamis that struck the Shark Bay and Pilbara areas in the recent past
- birrida evaporite pans, filled with gypsum
- coquinas and coquinites of the bivalve *Fragum erugatum*
- the high fault-line scarp of the Zuytdorp Cliffs, resulting from normal faulting along the Zuytdorp Fault during the Late Pleistocene and perhaps early Holocene
- recent thrust faulting along the Hardabut Fault
- elevated cormorant mangal deposits on Faure Island, pointing to recent uplift
- solar-salt, mineral sands, gypsum, and other economic commodities
- the human history of the area, beginning with the visit of Dirk Hartog in 1616 and followed by a succession of famous navigators
- more than 400 large-format colour photographs and diagrams, highlighting the area's unique geology and physiography.

The book will be of particular interest to:

- geoscientists worldwide
- geology, geography, science teachers and students
- academics and students studying earth sciences
- members of the public interested in Western Australian environments and landscapes, and the early history of this unique area.